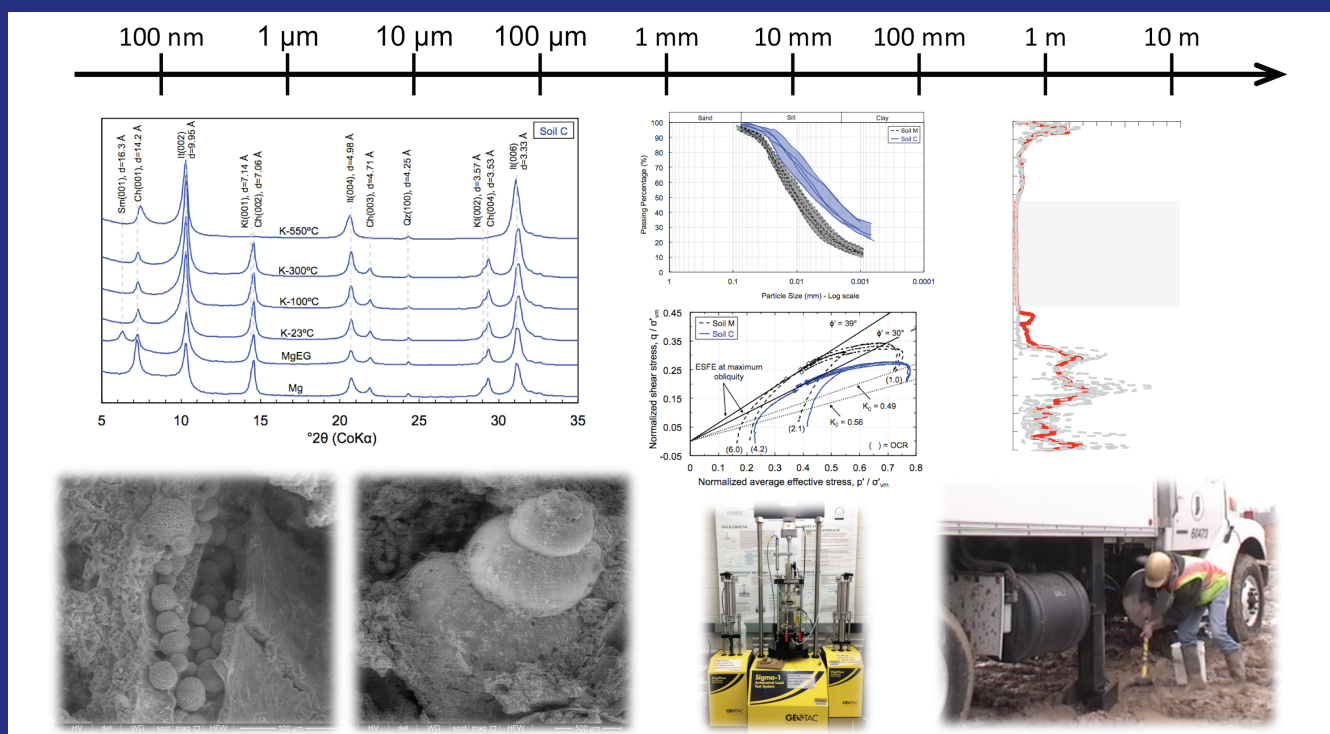


JOINT TRANSPORTATION RESEARCH PROGRAM

INDIANA DEPARTMENT OF TRANSPORTATION
AND PURDUE UNIVERSITY



Engineering Properties of Marls



Alain El Howayek

Marika Santagata

Antonio Bobet

Nayyar Zia Siddiki

RECOMMENDED CITATION

El Howayek, A., Santagata, M., Bobet, A., & Siddiki, N. Z. (2015). *Engineering properties of marls* (Joint Transportation Research Program Publication No. FHWA/IN/JTRP-2015/11). West Lafayette, IN: Purdue University. <http://dx.doi.org/10.5703/1288284315533>

AUTHORS

Alain El Howayek

Graduate Research Assistant
Lyles School of Civil Engineering
Purdue University

Marika Santagata, PhD

Associate Professor of Civil Engineering
Lyles School of Civil Engineering
Purdue University
(765) 494-0697
mks@purdue.edu
Corresponding Author

Antonio Bobet, PhD

Professor of Civil Engineering
Lyles School of Civil Engineering
Purdue University
(765) 494-5033
bobet@purdue.edu
Corresponding Author

Nayyar Zia Siddiki, PhD

Geotechnical Operations Manager
Indiana Department of Transportation

JOINT TRANSPORTATION RESEARCH PROGRAM

The Joint Transportation Research Program serves as a vehicle for INDOT collaboration with higher education institutions and industry in Indiana to facilitate innovation that results in continuous improvement in the planning, design, construction, operation, management and economic efficiency of the Indiana transportation infrastructure. https://engineering.purdue.edu/JTRP/index_html

Published reports of the Joint Transportation Research Program are available at <http://docs.lib.purdue.edu/jtrp/>.

NOTICE

The contents of this report reflect the views of the authors, who are responsible for the facts and the accuracy of the data presented herein. The contents do not necessarily reflect the official views and policies of the Indiana Department of Transportation or the Federal Highway Administration. The report does not constitute a standard, specification, or regulation.

COPYRIGHT

Copyright 2015 by Purdue University. All rights reserved.
Print ISBN: 978-1-62260-356-5
ePUB ISBN: 978-1-62260-357-2

1. Report No. FHWA/IN/JTRP-2015/11	2. Government Accession No.	3. Recipient's Catalog No.	
4. Title and Subtitle Engineering Properties of Marls		5. Report Date April 2015	
7. Author(s) Alain El Howayek, Maria C. Santagata, Antonio Bobet, Nayyar Zia-Siddiki		6. Performing Organization Code 8. Performing Organization Report No. FHWA/IN/JTRP-2015/11	
9. Performing Organization Name and Address Joint Transportation Research Program Purdue University 550 Stadium Mall Drive West Lafayette, IN 47907-2051		10. Work Unit No. 11. Contract or Grant No. SPR-3639	
12. Sponsoring Agency Name and Address Indiana Department of Transportation State Office Building 100 North Senate Avenue Indianapolis, IN 46204		13. Type of Report and Period Covered Final Report 14. Sponsoring Agency Code	
15. Supplementary Notes Prepared in cooperation with the Indiana Department of Transportation and Federal Highway Administration.			
16. Abstract <p>The term "marl" is used to designate soft, carbonate-rich, fine-grained soils, which pose concerns related to both settlement and stability. Despite the prevalence of marls in Indiana and the concerns associated with their behavior, very limited work has been done to study the engineering properties of these soils. This was the motivation for this research project, which involved two primary activities: a) the creation of a map and database of existing information on marl deposits in Indiana; and b) an in-depth characterization of the properties of a marl deposit in Daviess County, which was considered representative of similar deposits encountered in Indiana.</p> <p>The marl database was generated using ArcGIS 10.0 from information available at the INDOT, and involved mining data from over five thousand boreholes.</p> <p>The second part of the project involved field tests (seismic cone penetration tests, standard penetration tests, field vane shear tests), and laboratory experiments (index tests, incremental and constant rate of strain consolidation tests, and K_0-consolidated undrained triaxial tests) conducted on high quality Shelby tubes samples. Additionally, the mineralogy and the microstructure of the soil were studied in detail.</p> <p>The laboratory tests reveal that the deposit was not homogeneous as was initially anticipated, but was, instead, formed by two types of soils that repeat in horizontal thin layers. These two soils, referred to as 'soil M' and 'soil C', are both characterized by very high calcium carbonate contents but show distinct index and engineering properties, that may be ascribed to differences in mineralogy and composition. This stratification is not detected by the field tests.</p> <p>The consolidation tests show that the deposit has an OCR less than 2 and compressibility parameters markedly dependent on stress level, as typical of sensitive soils. K_0-consolidated undrained compression triaxial tests show that both soils exhibit normalized behavior, and that the relationship between strength and stress history is well described by the SHANSEP equation (although the SHANSEP parameters differ for the two soils).</p> <p>Comparison of the field data and laboratory results provides the means to validate published correlations for interpretation of the geotechnical properties of marls from field results. For the site examined, correlations to estimate shear wave velocity, stress history, and undrained strength from CPT results are identified. Implementation recommendations are provided for soil identification, sampling and specimen preparation, interpretation of filed data, and preliminary design.</p>			
17. Key Words marl, carbonatic soil, mineralogy, consolidation properties, undrained shear strength, SHANSEP		18. Distribution Statement No restrictions. This document is available to the public through the National Technical Information Service, Springfield, VA 22161.	
19. Security Classif. (of this report) Unclassified	20. Security Classif. (of this page) Unclassified	21. No. of Pages 105	22. Price

EXECUTIVE SUMMARY

ENGINEERING PROPERTIES OF MARLS

The term *marl* is used to designate soft, carbonate-rich, low-organic, gray-colored, fine-grained soils typically deposited under lakes or swamps, which are commonly encountered in the midwestern region of the United States. Such layers are typically characterized by low dry density, very high water content, and low shear strength, and they pose concerns related to excessive settlement, slope instability, and increased downdrag on deep foundations. Despite the prevalence of marls in Indiana and the concerns associated with their behavior, very limited work has been done to study the engineering properties of these soils. This was the motivation for this research project, which involved two primary activities: (1) the creation of a map and database of existing information on marl deposits in Indiana; and (2) the in-depth characterization of the properties of a marl deposit in Daviess County, Indiana, which was considered representative of similar deposits encountered throughout the state.

The database used for mapping marl deposits in Indiana was generated from information available at the Indiana Department of Transportation (INDOT) and involved mining data from over 5,000 boreholes. Through this effort, 325 borelogs were identified as containing marl. The data from these borelogs were compiled using ArcGIS 10.0. The resulting map preserves information on location, project DES number and description, borehole number and coordinates, marl layer thickness and depth, and percentage of CaCO_3 , and marl classification. It is easily accessible and can be expanded as more data becomes available.

The second part of the project involved field tests and laboratory experiments. The field testing program included (1) seismic cone penetration tests with pore pressure measurements (SCPTu); (2) standard penetration tests (SPTs) for soil profiling and collection of disturbed samples; (3) field vane shear tests; and (4) the installation of an open pipe piezometer. High-quality Shelby tubes samples were obtained for laboratory tests using mud rotary drilling and a fixed piston sampler. The laboratory testing program involved (1) assessment of the index properties (Atterberg limits, natural water content, LOI, CaCO_3 content, pH, salinity, specific gravity, and particle size distribution analysis) over the entire thickness of the deposit; (2) characterization of the stress history profile and measurement of the consolidation and creep properties of the soil through incremental and constant rate of strain consolidation tests; and (3) investigation of the undrained shear behavior, including derivation of the SHANSEP parameters through K_0 -consolidated undrained triaxial tests. Additionally, the mineralogy and the microstructure of the soil were studied in detail using state-of-the-art techniques, including X-ray diffraction (XRD), thermogravimetric analysis (TGA), and scanning electron microscopy (SEM) equipped with energy dispersive X-ray spectroscopy (EDX).

Examination in the laboratory of the soil samples revealed that the deposit is not homogenous as was initially anticipated, but is formed by two types of soils that repeat in horizontal thin layers. This stratification was not detected by the field tests. These two soils, referred to as “soil M” and “soil C,” are both characterized by very high calcium carbonate contents (over 50%, and close to 40%), but show distinct index properties (PL = 34.6 and 21.6; LL = 67.5 and 47.5; % clay = 20.2% and 36.9%; $G_s = 2.71$ and 2.79, for soils M and C, respectively). A characteristic specific to soil M, which is more prominent throughout the deposit, is the presence of shells. Additionally, this soil is characterized by a higher percentage of smectite minerals. Overall, the presence of these two soil types provided the opportunity to essentially study two types

of marls and explore, in particular, the effect of shells, mineral composition, and carbonate content on both index and engineering properties.

The consolidation tests showed that the deposit has an OCR less than 2, approximately constant with depth. The presence of the shells and/or the higher calcium carbonate content translated into a slightly higher preconsolidation stress in soil M versus soil C. Both soils exhibit S-shaped compression curves, with compressibility parameters markedly dependent on stress level. Soil C is characterized by a higher compression index relative to soil M, although for both soils the data fall within the range typical of soft clays. K_0 -consolidated tests performed varying the pre-shear effective stress showed that both soils exhibit normalized behavior with the relationship between undrained shear strength, OCR and effective stress being well described by the SHANSEP equation: $S_u/\sigma'_{vc} = S(\text{OCR})^m$. However, there was a significant difference in the SHANSEP parameters measured on the two soils ($S = 0.28$ and 0.34, and $m = 0.72$ and 0.85, for soils C and M, respectively). Consistent with this observation, the maximum obliquity friction angle for soil M ($\phi'_{mo} = 39^\circ$ [likely affected by the presence of shells]) exceeded that measured on soil C ($\phi'_{mo} = 30^\circ$), and the value of the normally consolidated K_0 was greater for soil C ($K_0 = 0.56$) relative to soil M ($K_0 = 0.49$). For both soils the cohesion intercept was found to be negligible.

Comparison of the field data and laboratory results provides the means to validate existing correlations for interpretation of the geotechnical properties of marls from field results. For the site examined it was found that, of the 13 relationships examined, only the one developed by Andrus, Monahan, Piratheepan, Ellis, and Holzer (2007) for soils with a Pleistocene geologic age provides a prediction of V_s from the CPT data consistent with the in situ seismic measurements. The preconsolidation stress of the deposit is best estimated from the CPT data using the correlation provided by Mayne (1995). The undrained shear strength, S_u , is best estimated from the CPT tip resistance data using the equation $S_u = (q_t - \sigma_{v0})/N_{kt}$, although for the same shear mode (triaxial compression) N_{kt} varies from 10 to 17 for soil M and soil C, respectively.

While the specific geotechnical data gathered for soils M and C are strictly applicable only to the site investigated, the work performed provides insights that have direct significance for construction on other marl deposits. In particular:

- While both the index and engineering properties of marls fell within the range typical of many other soft clays previously documented in the literature, the distinct properties exhibited by soils C and M identified in this project indicate that there is no “typical” marl, and that lessons from one deposit may not directly be extrapolated to others without consideration of index properties and mineralogical data. The data obtained as part of this project may be used as a guideline during the preliminary design stages, but any subsequent design stage will require the derivation of site-specific properties.
- The behavior of marls cannot be described solely by the CaCO_3 content, as the presence of shells and the mineralogy of the clay fraction play a critical role. For example, this research showed that the apparent inconsistency between Atterberg limits, carbonate content and clay content between soil M and soil C was explained by the higher smectite content of soil M.
- The fact that the soils examined exhibited normalized behavior indicates that the SHANSEP method can be effectively used for designing on marl deposits. This has significant practical value, as this method allows estimation

of the undrained shear strength profile as the vertical effective stress and stress history profiles of the site change, which is critical to the design of staged construction/preloading procedures commonly employed in marl deposits. The SHANSEP parameters derived in this project may be used for obtaining undrained strength profiles during the preliminary design stage on other marl deposits once anisotropy effects are accounted for. A SHANSEP laboratory testing program should be conducted for any subsequent stages of design.

- The field vane test was not successful in characterizing the strength profile of the marl deposit examined in this work. This is consistent with previous experiences in deposits characterized by the presence of shells and/or sand lenses documented in the literature. While it should be discouraged in these cases, its use continues to be recommended for measuring the undrained strength of soft homogeneous deposits with no shells or sand lenses, and thus it should be applicable to homogeneous marl deposits.
- This work has identified the correlations that provide the best estimates of shear wave velocity and preconsolidation

stress, and these are recommended for preliminary design. The former should be used when seismic measurements of V_s are not available. Laboratory measurements of σ'_p are required in latter stages of the design.

- For predicting the undrained strength from CPT results, the significant (70%) difference in the values of N_{kt} found to best match the data for soil M versus soil C demonstrates that no single value of N_{kt} can be recommended for marl deposits. The values derived for soil M and soil C may serve as guidelines during preliminary design, but a site-specific calibration should be conducted for accurate predictions of the undrained strength profile. Once this is done, the CPT can be used very effectively to examine spatial variability effects.
- The sampling and specimen preparation techniques used in this study (drilling using a mud rotary, sampling using a fixed piston sampler, extrusion using a piano wire, trimming using a wire saw) were found to generate samples of high-quality and reliable laboratory test data. Their use is advocated for sampling and testing in all marl deposits.

CONTENTS

1. INTRODUCTION: BACKGROUND AND PROBLEM STATEMENT	1
2. RESEARCH OBJECTIVES	1
3. ACTIVITIES	1
4. FINDINGS AND DELIVERABLES	2
4.1 Mapping of Marl in Indiana	2
4.2 Site Characterization and Field Testing Program	2
4.3 Index Properties, Mineralogy, and Microstructure	5
4.4 Engineering Properties	8
4.5 Integration of Laboratory and Field Data	11
5. CONCLUSIONS	13
6. IMPLEMENTATION RECOMMENDATIONS	13
6.1 Identification	13
6.2 Sampling and Specimen Preparation	13
6.3 Interpretation of Field Data and Design	13
6.4 Preliminary Design	14
REFERENCES	15
APPENDIX 1. MAPPING OF MARL IN INDIANA	19
A.1.1. INTRODUCTION	19
A.1.2. CLASSIFICATION OF MARLS BASED ON CALCIUM CARBONATE CONTENT	19
A.1.3. APPROACH	19
A.1.3.1 Data Collection	19
A.1.3.2 Data Input	19
A.1.3.3 Symbols	21
A.1.4. THE MARL MAP OF INDIANA	21
A.1.4.1 Overview	21
A.1.4.2 Using the Map	21
APPENDIX 2. SITE CHARACTERIZATION AND FIELD TESTING PROGRAM	25
A.2.1. INTRODUCTION	25
A.2.2. GEOGRAPHICAL LOCATION AND SOIL PROFILE	25
A.2.3. SAMPLING OPERATIONS	25
A.2.4. SAMPLING PROGRAM	28
A.2.5. FIELD TESTING PROGRAM	28
A.2.5.1 Seismic Cone Penetration Tests (SCPTu)	28
A.2.5.2 Standard Penetration Test (SPT)	28
A.2.5.3 Field Vane Shear Test	28
A.2.5.4 Open Pipe Piezometer and Field Hydraulic Conductivity Measurements	29
A.2.6. FIELD TESTS RESULTS	30
A.2.6.1 Seismic Cone Penetration Test (SCPTu)	30
A.2.6.2 Standard Penetration Test (SPT)	31
A.2.6.3 Field Vane Shear Test	31
APPENDIX 3. INDEX PROPERTIES, MINERALOGY, AND MICROSTRUCTURE	36
A.3.1. INTRODUCTION	36
A.3.2. DESCRIPTION OF SOILS WITHIN THE MARL DEPOSIT	36
A.3.3. INDEX PROPERTIES	36
A.3.3.1 Organic Content and Calcium Carbonate Content	36
A.3.3.2 Atterberg Limits, Natural Water Content, and Particle Size Distribution	37
A.3.3.3 Specific Gravity and Void Ratio	38
A.3.3.4 Total Unit Weight and Degree of Saturation	39
A.3.3.5 Salt Concentration and pH	40

A.3.4. MINERALOGY AND MICROSTRUCTURE.....	40
A.3.4.1 X-Ray Diffraction (XRD).....	41
A.3.4.2 Thermogravimetric Analysis (TGA).....	47
A.3.4.3 Scanning Electron Microscopy (SEM).....	50
A.3.4.4 Optical Light Microscopy (LM).....	51
APPENDIX 4. ENGINEERING PROPERTIES.....	56
A.4.1. INTRODUCTION.....	56
A.4.2. SAMPLE PREPARATION AND TESTING PROCEDURES.....	56
A.4.2.1 Sample Preparation.....	56
A.4.2.2 Testing Procedures.....	56
A.4.3. STRESS HISTORY AND CONSOLIDATION PROPERTIES.....	57
A.4.3.1 Introduction.....	57
A.4.3.2 Compression Curves.....	57
A.4.3.3 Stress History Profile.....	58
A.4.3.4 Compressibility.....	58
A.4.3.5 Coefficient of Consolidation and Permeability.....	60
A.4.3.6 Lateral Stress Ratio K_0	61
A.4.3.7 Creep Properties.....	62
A.4.3.8 Assessment of Sample Quality.....	63
A.4.4. UNDRAINED SHEAR BEHAVIOR.....	64
A.4.4.1 Introduction.....	64
A.4.4.2 General Undrained Shear Behavior.....	64
A.4.4.3 Young's Modulus.....	65
A.4.4.4 Undrained Strength Ratio.....	65
A.4.4.5 Effective Stress Failure Envelope.....	65
APPENDIX 5. INTEGRATION OF LABORATORY AND FIELD DATA.....	70
A.5.1. INTRODUCTION.....	70
A.5.2. FIELD VANE (FV) TEST.....	70
A.5.3. PIEZOCONE TEST (CPTu).....	71
A.5.3.1 Shear Wave Velocity.....	71
A.5.3.2 Preconsolidation Stress.....	73
A.5.3.3 Undrained Shear Strength.....	73
APPENDIX 6. SUMMARY OF BORING LOGS.....	76
APPENDIX 7. PIEZOCONE PENETRATION PROFILES.....	91
APPENDIX 8. FIELD VANE SHEAR TESTS.....	95

LIST OF TABLES

Tables	Page
Table 4.1 Classification of marls based on calcium carbonate content	2
Table 4.2 Summary of index properties	6
Table 4.3 Mineralogy of soils M and C (in order of predominance) as observed by XRD analysis (from randomly oriented powder and oriented aggregates)	7
Table 4.4 Summary of consolidation properties	10
Table 4.5 Summary of undrained shear properties	12
Table 6.1 Key index properties of soil M and soil C	14
Table 6.2 Key engineering properties of soil M and soil C	14
Table A.1.1 Classification of marls based on calcium carbonate content	19
Table A.2.1 Coordinates of borings, field vane, piezometer and piezocones	26
Table A.3.1 Summary of index properties	37
Table A.3.2 Location and depth of the XRD samples examined	43
Table A.3.3 The mineralogy of marl (in order of predominance) as observed by XRD analysis (from randomly oriented powder and oriented aggregates)	43
Table A.3.4 D-spacing of detected clay minerals for different treatment	47
Table A.3.5 Clay mineral composition of soil M and soil C	47
Table A.3.6 Mass loss during thermogravimetric analysis of soil M and soil C before and after treatment with Na-acetate	49
Table A.3.7 Semi-quantification of clay minerals present in soil M and soil C using TGA	52
Table A.4.1 Summary of tests location and index properties of soil M specimens	56
Table A.4.2 Summary of tests location and index properties of soil C specimens	57
Table A.4.3 Summary of consolidation data for the CRS consolidation, IL consolidation, and SHANSEP CK ₀ UTC(L) tests for soil M	58
Table A.4.4 Summary of consolidation data for the CRS consolidation, IL consolidation, and SHANSEP CK ₀ UTC(L) tests for soil C	59
Table A.4.5 Summary of consolidation properties	59
Table A.4.6 Typical values of the compression index C_c	62
Table A.4.7 Summary of consolidation data for the CRS consolidation, IL	62
Table A.4.8 Typical values of the coefficient of consolidation C_v	63
Table A.4.9 Values of C_e/C_c for natural soils	64
Table A.4.10 Summary of shear data from SHANSEP CK ₀ UTC(L) tests for soil M	66
Table A.4.11 Summary of shear data from SHANSEP CK ₀ UTC(L) tests for soil C	66
Table A.4.12 Summary of shear properties	66
Table A.5.1 CPT- V_s correlation equations	72

LIST OF FIGURES

Figures	Page
Figure 4.1 Indiana map showing the location of marl deposits using ArcMap	3
Figure 4.2 Map of Daviess County (Indiana) showing the site location	3
Figure 4.3 CPT results: (a) tip resistance, (b) skin friction, and (c) porewater pressure versus depth	4
Figure 4.4 Profiles of (a) field vane undrained shear strength and (b) soil sensitivity with depth	5
Figure 4.5 Plasticity chart with data for soils M and C: (a) USCS and (b) AASHTO	6
Figure 4.6 Results of particle size analyses on soils M and C	7
Figure 4.7 Results of consolidation tests: (a) ϵ - compression curves; (b) e - compression curves; (c) lateral stress ratio vs. σ'_v ; and (d) lateral stress ratio vs. OCR	9
Figure 4.8 Stress history profile: (a) preconsolidation stress and overburden stress; and (b) OCR with depth	9
Figure 4.9 Results of triaxial tests: (a) normalized shear stress vs. axial strain, (b) normalized change in excess pp, (c) p' - q stress path, and (d) normalized shear stress vs. OCR	11
Figure A.1.1 Data associated with each borehole	20
Figure A.1.2 Symbols associated with each layer	21
Figure A.1.3 Indiana map showing the location of marl deposits using ArcMap	22
Figure A.1.4 Setting the data source for each layer	23
Figure A.1.5 Points of the layer 'marl quantitative' are displayed. The information related to the circled borehole is displayed on the popup screen on the right. Two boreholes are listed in the top pane (circled) indicating that two boreholes overlap each other	23
Figure A.1.6 Modifying the symbols of a layer	24
Figure A.2.1 Map of Daviess County (Indiana) showing the site location	25
Figure A.2.2 Stratigraphy for the site	26
Figure A.2.3 Location of borings, piezometer, field vane, and piezocone tests (to scale)	26
Figure A.2.4 (a) Truck mounted drilling rig and (b) rig control panel	27
Figure A.2.5 Fixed piston sampler: (a) fixed piston and (b) piston mounted on Shelby tube	27
Figure A.2.6 Hollow stem auger: (a) drilling with continuous-flight augers, (b) auger flight and drive cap of the drilling rig and (c) cutter head	27
Figure A.2.7 Mud rotary: (a) T connection (b) rotary blades	27
Figure A.2.8 Quality of samples collected	29
Figure A.2.9 Generation of a surface shear wave using a hammer	30
Figure A.2.10 (a) Saturation of pressure transducer, (b) piezocone head, and (c) piezocone filter	30
Figure A.2.11 Standard penetration test (SPT)	30
Figure A.2.12 (a) Split-spoon sampler (b) plastic spring core catcher	30
Figure A.2.13 Field vane geometry	31
Figure A.2.14 (a) Force arm and sub mounted on the casing (b) ball bearing guide coupling	31
Figure A.2.15 Stages of the field vane shear test	32
Figure A.2.16 Details of installation of open pipe piezometer	32
Figure A.2.17 CPT results: (a) tip resistance, (b) skin friction, and (c) porewater pressure versus depth	33
Figure A.2.18 Shear wave arrival traces for CPT#4	33
Figure A.2.19 Shear wave arrival traces for CPT#5	34
Figure A.2.20 (a) Shear wave velocity, and (b) shear modulus profiles with depth	34
Figure A.2.21 Standard penetration resistance (N-values) with depth	35
Figure A.2.22 Results of field vane shear test (FV4) conducted at ~ 7.2 m (23.5 ft)	35

Figure A.2.23	Profiles of (a) field vane undrained shear strength and (b) soil sensitivity with depth	35
Figure A.3.1	Soil samples showing layers of soil M and soil C	36
Figure A.3.2	(a) Organic content and (b) calcium carbonate content profiles for marl	37
Figure A.3.3	Results of Atterberg limits for marl	38
Figure A.3.4	Plasticity chart with data from soils M and C: (a) USCS and (b) AASHTO	38
Figure A.3.5	Results of particle size analyses on soils M and C	39
Figure A.3.6	(a) Specific gravity and (b) void ratio profiles for marl	39
Figure A.3.7	(a) Total unit weight and (b) initial degree of saturation profiles for marl	40
Figure A.3.8	Salt concentration in (a) g/l of pore fluid and (b) g/kg of dry soil, and (c) pH profiles for marl	41
Figure A.3.9	Oriented clay aggregates of (a) soil M (showing cracking and peeling) and (b) soil C	42
Figure A.3.10	X-ray diffraction system (PANalytical B.V. diffractometer)	42
Figure A.3.11	XRD patterns (randomly oriented powder) of soil M. Mineral codes: Sm = smectite, Ch = chlorite, It = Illite, Kt = kaolinite, Qz = quartz, Dt = dolomite, Ct = calcite, K-Fr = K-feldspar, Pl = plagioclase feldspar, At = aragonite	43
Figure A.3.12	XRD patterns (randomly oriented powder) of soil C. Mineral codes: Sm = smectite, Ch = chlorite, It = Illite, Kt = kaolinite, Qz = quartz, Dt = dolomite, Ct = calcite, K-Fr = K-feldspar, Pl = plagioclase feldspar	44
Figure A.3.13	XRD patterns (randomly oriented powder) of shells collected from soil M. Mineral codes: At = aragonite, Qz = quartz, Ct = calcite	44
Figure A.3.14	XRD analysis of the three predominant minerals: calcite, dolomite, and quartz	45
Figure A.3.15	XRD patterns (oriented samples) of the clay fraction (<2 μm) of soil M. Mineral codes: Sm = smectite, Ch = chlorite, It = Illite, Kt = kaolinite, Qz = quartz	46
Figure A.3.16	XRD patterns (oriented samples) of the clay fraction (<2 μm) of soil C. Mineral codes: Sm = smectite, Ch = chlorite, It = Illite, Kt = kaolinite, Qz = quartz	46
Figure A.3.17	Normalized thermogravimetric analysis curves of soil M (black dashed line) and soil C (blue continuous line) (~50 mg samples, 20°C/min heating rate, 20 mL/min N ₂ purge)	48
Figure A.3.18	Thermogravimetric analysis curve of soil M (51.2 mg sample, 20°C/min heating rate, 20 mL/min N ₂ purge)	48
Figure A.3.19	Thermogravimetric analysis curve of soil C (53.6 mg sample, 20°C/min heating rate, 20 mL/min N ₂ purge)	49
Figure A.3.20	Normalized thermogravimetric analysis curves of shell aragonite, natural calcite, natural dolomite, and natural quartz (~50 mg samples, 20°C/min heating rate, 20 mL/min N ₂ purge)	50
Figure A.3.21	Normalized thermogravimetric analysis curves of natural calcite showing the effect of sample mass, heating rate, and N ₂ purge on decarbonation temperature	50
Figure A.3.22	Normalized thermogravimetric analysis curves of soil M subjected to different pre-treatment procedures, soil C, and shell aragonite (~50 mg samples, 20°C/min heating rate, 20 mL/min N ₂ purge)	51
Figure A.3.23	Thermogravimetric analysis curve of the clay fraction (<2 μm) of soil M treated with Na-acetate (49.9 mg sample, 20°C/min heating rate, 20 mL/min N ₂ purge)	51
Figure A.3.24	Thermogravimetric analysis curve of the clay fraction (<2 μm) of soil C treated with Na-acetate (50.7 mg sample, 20°C/min heating rate, 20 mL/min N ₂ purge)	52
Figure A.3.25	Scanning electron microscopy samples of (a) soil M and (b) soil C	52
Figure A.3.26	Scanning electron micrographs for soil M showing different types of microfossils and framboidal pyrite that are integrated into the soil matrix	53
Figure A.3.27	Scanning electron micrographs for soil C	53
Figure A.3.28	EDX analysis for soil C identifying the different chemical elements	54
Figure A.3.29	Microscopic images for the different types of microfossils collected from soil M	55
Figure A.3.30	Microscopic images for charophyte oospores collected from soil M	55
Figure A.4.1	(a) ϵ - compression curves and (b) e - compression curves from CRS consolidation and SHANSEP CK ₀ UTC(L) tests	60
Figure A.4.2	Stress history profile: (a) preconsolidation stress and overburden stress; and (b) OCR with depth	61

Figure A.4.3	Values of (a) compression index, and (b) compression ratio with depth	61
Figure A.4.4	Compression index versus initial void ratio	62
Figure A.4.5	Compression index versus natural water content	62
Figure A.4.6	Compression index versus liquid limit	62
Figure A.4.7	Coefficient of consolidation versus vertical effective stress from CRS and IL consolidation tests	63
Figure A.4.8	Void ratio versus permeability from CRS and IL consolidation tests	63
Figure A.4.9	C_k versus initial void ratio from CRS and IL consolidation tests	63
Figure A.4.10	Lateral stress ratio versus vertical effective stress from consolidation phase of SHANSEP $CK_0UTC(L)$ tests	64
Figure A.4.11	Lateral stress ratio versus overconsolidation ratio from consolidation phase of SHANSEP $CK_0UTC(L)$ tests	64
Figure A.4.12	Relationship between secondary compression index and compression index for marl.	64
Figure A.4.13	Evaluation of sample quality for marl specimens according to the criterion proposed by Lunne et al. (1997)	65
Figure A.4.14	Results for SHANSEP $CK_0UTC(L)$ tests of marl: (a) normalized shear stress, (b) norm. excess pore pressure, and (c) obliquity vs. axial strain	67
Figure A.4.15	Results for SHANSEP $CK_0UTC(L)$ tests of marl: (a) normalized shear stress, (b) norm. excess pore pressure, and (c) A-parameter vs axial strain	67
Figure A.4.16	Strain at failure versus OCR for marl	68
Figure A.4.17	Pore pressure parameter at failure versus OCR for marl	68
Figure A.4.18	Normalized undrained modulus degradation for SHANSEP	68
Figure A.4.19	Undrained strength ratio vs. OCR for SHANSEP $CK_0UTC(L)$ tests of marl	68
Figure A.4.20	Effective stress paths for SHANSEP $CK_0UTC(L)$ tests of marl	69
Figure A.4.21	Normalized effective stress paths for SHANSEP $CK_0UTC(L)$ tests of marl	69
Figure A.5.1	Index properties: (a) water content, (b) organic content, and (c) $CaCO_3$ content versus depth	70
Figure A.5.2	Field vane correction factor versus plasticity index derived from embankment failures	71
Figure A.5.3	(a) Undrained shear strength and (b) normalized undrained shear strength as obtained from field vane and laboratory SHANSEP $CK_0UTC(L)$ tests.	71
Figure A.5.4	Shear wave velocity as obtained from CPT correlations and seismic measurements from (a) all CPTs and (b) from CPT#4 and CPT#5.	72
Figure A.5.5	(a) Preconsolidation stress and (b) overconsolidation ratio as obtained from CPT correlations and laboratory tests.	73
Figure A.5.6	Empirical cone factor $N_{kt(TC)}$ derived from all CPTs for (a) soil M and (b) soil C	74
Figure A.5.7	(a) Undrained shear strength and (b) normalized undrained shear strength as obtained from CPT (using $N_{kt} = 10$) and laboratory SHANSEP $CK_0UTC(L)$ tests for soil M	74
Figure A.5.8	(a) Undrained shear strength and (b) normalized undrained shear strength as obtained from CPT (using $N_{kt} = 17$) and laboratory SHANSEP $CK_0UTC(L)$ tests for soil C	75
Figure A.7.1	CPT#1 results: (a) tip resistance, (b) skin friction, and (c) porewater pressure versus depth	91
Figure A.7.2	CPT#2 results: (a) tip resistance, (b) skin friction, and (c) porewater pressure versus depth	91
Figure A.7.3	CPT#3A results: (a) tip resistance, (b) skin friction, and (c) porewater pressure versus depth	92
Figure A.7.4	CPT#4 results: (a) tip resistance, (b) skin friction, and (c) porewater pressure versus depth	92
Figure A.7.5	CPT#5 results: (a) tip resistance, (b) skin friction, and (c) porewater pressure versus depth	93
Figure A.7.6	CPT#6 results: (a) tip resistance, (b) skin friction, and (c) porewater pressure versus depth	93
Figure A.7.7	CPT#7 results: (a) tip resistance, (b) skin friction, and (c) porewater pressure versus depth	94
Figure A.8.1	Results of field vane shear test (FV1) conducted at ~5.3 m (17.5 ft)	95
Figure A.8.2	Results of field vane shear test (FV2) conducted at ~5.9 m (19.5 ft)	95
Figure A.8.3	Results of field vane shear test (FV3) conducted at ~6.6 m (21.5 ft)	95

Figure A.8.4	Results of field vane shear test (FV4) conducted at ~7.2 m (23.5 ft)	95
Figure A.8.5	Results of field vane shear test (FV5) conducted at ~7.8 m (25.5 ft)	95
Figure A.8.6	Results of field vane shear test (FV6) conducted at ~8.4 m (27.5 ft)	95
Figure A.8.7	Results of field vane shear test (FV7) conducted at ~9.0 m (29.5 ft)	95
Figure A.8.8	Results of field vane shear test (FV8) conducted at ~9.6 m (31.5 ft)	95
Figure A.8.9	Results of field vane shear test (FV9) conducted at ~10.2 m (33.5 ft)	96
Figure A.8.10	Results of field vane shear test (FV10) conducted at 10.8 m (35.5 ft)	96
Figure A.8.11	Results of field vane shear test (FV11) conducted at 11.4 m (37.5 ft)	96

1. INTRODUCTION: BACKGROUND AND PROBLEM STATEMENT

The term *marl* is used to designate soft, carbonate-rich, low-organic, gray-colored, fine-grained soils that are typically deposited under lakes or swamps (IDOT, 1999; INDOT, 2010; MDOT, 2009). Marls are often characterized by the presence of shells, which contribute to the high calcium carbonate content. These soft fine-grained carbonatic soils are commonly encountered in the Midwest of the US, including the states of Illinois, Indiana, Michigan, and Ohio (IDOT, 1999; INDOT, 2010; MDOT, 2009; ODOT, 2010) as well as other places around the world such as Italy (Bozzano, Marcoccia, & Barbieri, 1999; Jamiolkowski, Lancellotta, & Lo Presti, 1995), England (Hawkins, Lawrence, & Privett, 1988), Greece (Anagnostopoulos, Kalteziotis, Tsiambaos, & Kavvadas, 1991; Tsiambaos, 1991), Spain (Lamas, Irigaray, & Chacon, 2002; Paaza, Lamas, Irigaray, & Chacon, 1998), India (Datta, Gulhati, & Rao, 1982), Saudi Arabia (Aiban, 1995), Jordan (Shaqour, Jarrar, Hencher, & Kuisi, 2008), and Iran (Hajimohammadi, Hosseini, & Cheshomi, 2010; Sadrekarimi, Zekri, & Majidpour, 2006). The properties of these soils, however, vary depending on their origin and geological history, as well as on the carbonate content, and type and quantity of the minerals present in the soil.

Deposits of marl are found in the State of Indiana with layers as thick as 20', at relatively shallow depths (10–15') below the ground surface. Such layers are typically characterized by low dry density, very high water content, and low shear strength, which makes them “problem soils.” They pose concerns related to excessive settlement, slope instability, and increased downdrag on deep foundations. When constructing on these soils, wick drains are commonly used to accelerate consolidation and/or preloading to improve the shear strength of the deposit, and in some cases, more costly solutions such as deep foundations are employed (Andromalos, Hegazy, & Jasperse, 2001). For instance, as part of the construction of the interstate I-69, the Indiana Department of Transportation (INDOT) constructed a bridge that passes over First Creek in Daviess Co., Indiana. The twin bridge structure has a total length of about 815 ft and six spans, with abutments and embankments heights of about 12 ft and 16 ft above the existing grade. A thick layer of marl was identified at this site and additional borings were conducted to better define the extent of these soils leading to additional costs. The bridge was constructed on a total of 208 steel H piles extending up to 120 ft to avoid the soft marl layer and rely on the frictional resistance of a sand layer beneath it and the end bearing from the bedrock.

Despite the prevalence of marls in Indiana and the issues associated with their behavior, very limited work has been done to study the engineering properties of these soils. This is causing uncertainties within the geotechnical engineering designers in terms of

extent of geotechnical explorations and expectations on short-term and long-term behavior of these materials. This necessarily creates additional costs as well as delays due to the additional field exploration needed. All this points towards the necessity of developing a fundamental knowledge of the behavior of marls and creating a database with expected properties and behavior.

The research performed was aimed at contributing to resolve these issues, by performing an in-depth study of the engineering properties, microstructure and mineralogy of a soft fine-grained carbonatic soil deposit in southwestern Indiana (Daviess Co.), which will aid in design and construction on these soils.

2. RESEARCH OBJECTIVES

Within the broad scope of developing an improved knowledge of the engineering properties, microstructure, and mineralogy of marls, the specific objectives of the work conducted as part of this research project were to:

- Identify marl deposits in the State of Indiana based on existing information, and compile this information in a format that could be easily accessible and expandable as additional sites were identified;
- Select a site where a marl layer of significant thickness (>15–20 ft) existed, and that was representative of similar deposits encountered in the state, conduct a field testing program and obtain samples for laboratory tests;
- Characterize the engineering properties (i.e., consolidation, creep and undrained shear strength behavior) of this deposit using state of the art approaches for conducting and interpreting tests to obtain a database of properties that could aid in future design and construction on these soft soils;
- Gain a fundamental understanding of the microstructure and mineralogy of marls (with specific emphasis on understanding the role played by the different forms of carbonate [i.e., shells vs. soil matrix] present in the soil), and understand the impact of these properties on soil behavior;
- Integrate the laboratory and field data to develop recommendations for the interpretation of geotechnical properties from field results.

3. ACTIVITIES

The research objectives outlined above were pursued through the following activities that are described in detail in Appendices 1 to 5:

- Mapping of marl deposits in Indiana; this portion of the work relied on information available from previous projects. Locations where marl deposits had been found were identified and a database and map were created using ArcGIS 10.0;
- Field program: a site characterized by a marl layer of significant thickness was selected in Daviess Co., Indiana. Seismic cone penetration tests with pore pressure measurements (SCPTu); standard penetration tests (SPTs) for soil profiling and collection of disturbed samples; and field vane shear tests to determine the

undrained shear strength and soil sensitivity were conducted as part of the in-situ testing program. Additionally, an open pipe piezometer was installed to locate the water table and conduct hydraulic conductivity measurements. High-quality Shelby tubes samples were obtained for laboratory tests.

- Assessment of the index properties: this portion of the experimental program consisted of performing index tests (Atterberg limits, natural water content, LOI, CaCO₃ content, pH, salinity, specific gravity, and particle size distribution analysis) on samples over the entire thickness of the deposit;
- Analysis of the mineralogy and the microstructure: X-ray diffraction (XRD), thermogravimetric analysis (TGA), scanning electron microscopy (SEM) equipped with energy dispersive X-ray spectroscopy (EDX), and optical light microscopy (LM) were performed on samples of the two main soil types identified in the marl layer;
- Assessment of the engineering properties: this portion of the experimental program included (i) incremental and constant rate of strain consolidation tests to derive the stress history, consolidation and creep properties; (ii) shear strength tests for derivation of the undrained shear strength profiles and the soil's SHANSEP parameters.
- Integration of field and lab results: this portion of the work focused on the analysis of the FV shear tests and the CPT data in conjunction with the laboratory results to develop site-specific correlations.

4. FINDINGS AND DELIVERABLES

4.1 Mapping of Marl in Indiana

Although marl deposits in Indiana are fairly widespread (as discussed in the introduction), the soil maps of Indiana rarely provide any information about these deposits. In addition, having an understanding of the occurrence of such deposits could prove very useful in detecting potential problems in future projects. Hence, the first outcome of this project was to develop a map of marl in Indiana. Details about the map development are provided in Appendix 1.

The database used for the mapping of marl was generated from information available at the INDOT. It consisted of data from more than five thousand boreholes, which was mined to identify the boreholes where marl was found. In total, 325 boreholes were identified to contain marl and their borelogs were used to develop the map using ArcGIS 10.0. Each data point on the map is associated with information displayed by clicking on the corresponding point. This information includes: project DES number and description; borehole number and coordinates; marl layer thickness and depth; percentage of CaCO₃; and marl classification. The latter is based on the INDOT classification system, which classifies fine-grained soils into five groups according to the calcium carbonate content (INDOT, 2010). The classification system keeps intact the INDOT classification system in specs section 903 (INDOT, 2014). Table 4.1 summarizes the five categories. The term soil in Table 4.1 is to be replaced by the classification of the soil obtained using INDOT

TABLE 4.1
Classification of marls based on calcium carbonate content.

Classification	Calcium Carbonate Content (%)
Soil* with trace marl	1% < %CaCO ₃ < 9%
Soil* with little marl	10% < %CaCO ₃ < 17%
Soil* with some marl	18% < %CaCO ₃ < 25%
Marly soil (A-8)	26% < %CaCO ₃ < 40%
Marl (A-8)	%CaCO ₃ > 40%

*Soils classified in accordance with INDOT specs 903.02 shall also include this classification.

specs section 903.02. For example, if a soil is classified as “silty loam” in accordance to 903.02 and the calcium carbonate content was in the range of 18–25%, then the soil would be denoted as “silty loam with some marl.”

Figure 4.1 shows the map of Indiana with data points corresponding to locations where marls were identified. Data from over five thousand boreholes across the state were examined. Of these, 325 boreholes indicated the presence of marls. (Note: 425 data points are plotted reflecting that marl was found at more than one depth.) Each of the different groups discussed above are represented as a layer and can be accessed via the Contents. The data points belonging to a particular layer can be made visible by checking the box next to the corresponding layer. Each data point on the map is associated with a set of information displayed by clicking on the corresponding point. Since the database from the I-69 project was more comprehensive, the data points are concentrated in this particular stretch. The rest of the locations are scattered with the majority located in the northern parts of Indiana. The majority of the boreholes with marl (CaCO₃ content >40%) were located along I-69. It is from one of the sites on this stretch that the field testing and soil sampling was performed for this research, as will be discussed in the next section.

4.2 Site Characterization and Field Testing Program

This section briefly describes the site selected for conducting field tests and obtaining samples for laboratory tests; and summarizes the site stratigraphy, and the results of the CPT and FV tests. The reader is referred to Appendix 2 for more details.

4.2.1 Geographical Location and Soil Profile

The site is located at the intersection of County Road 900 E and County Road 1650 N, Madison, Daviess County, Indiana, about 85 miles southwest of Indianapolis (see Figure 4.2). The selection of this site was based on the presence of marl deposits at shallow depths, the percentage of calcium carbonate present in the soil, as well as the accessibility to the site. The site is adjacent to a creek (First Creek), which controls the water table making it very close to the ground surface. The average ground elevation was determined as 150.84 m (494.88 ft), and the water table was located at 1.9 m (6.25 ft) below the ground surface. The average soil profile

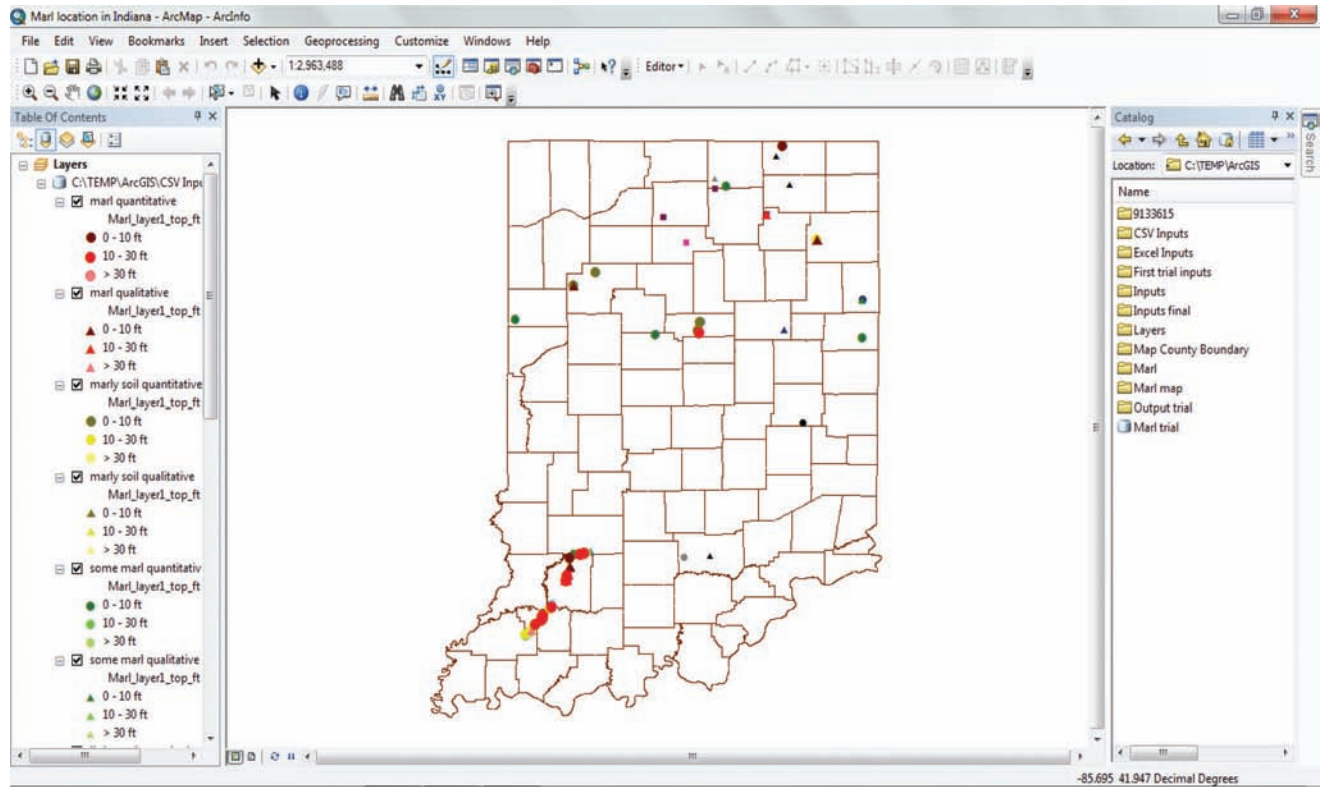


Figure 4.1 Indiana map showing the location of marl deposits using ArcMap.

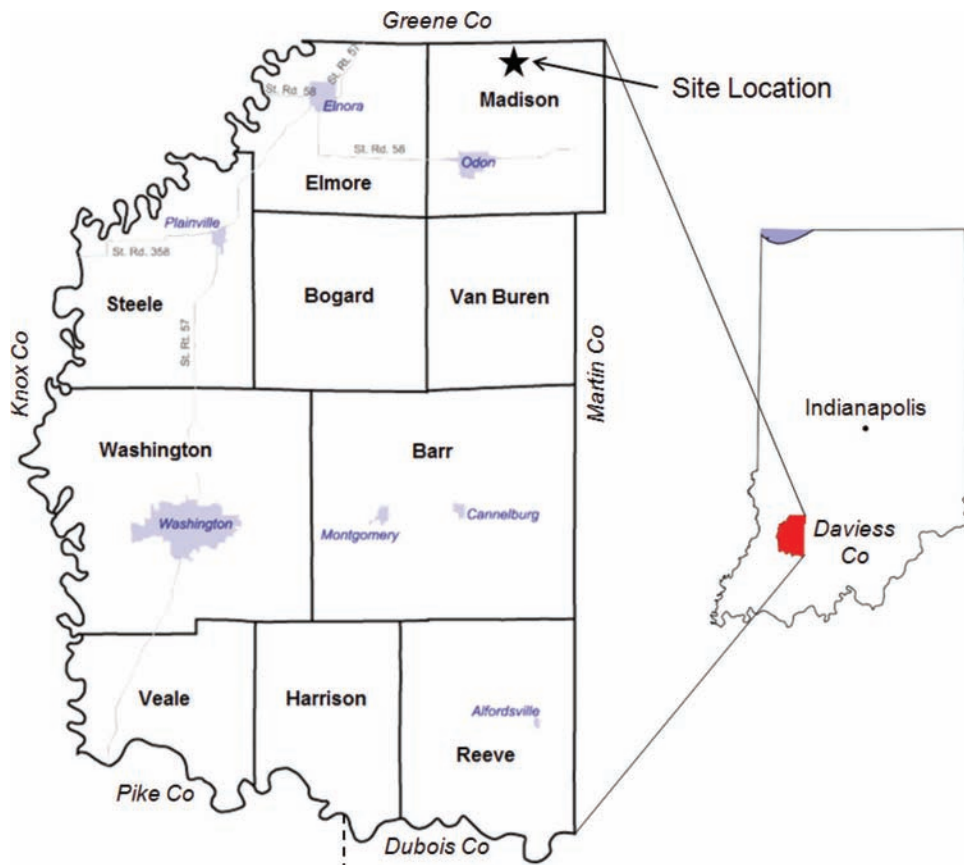


Figure 4.2 Map of Daviess County (Indiana) showing the site location.

comprises about 1.9 m (~6.25 ft) of silty sand underlain by 1.5 m (~4.75 ft) of clayey silt and 2.7 m (~9 ft) of clay. At a depth of 6.1 m (~20 ft) the marl layer starts and has a thickness of 4.3 m (~14 ft). A sand layer is encountered below the marl layer. The bedrock, mostly sandstone, is located at a depth of about 40 m (120 ft).

4.2.2 Sampling Operations

Four boreholes were drilled using mud rotary, from which continuous sampling was conducted up to a depth of 15.24 m (50 ft). A total of 53 Shelby tubes were pushed with a fixed piston sampler between 4.88 m (16 ft) and 11.58 m (38 ft) where marl was found. Tubes with modified geometry were used to reduce the shear-induced strains during sampling. The modified Shelby tubes are 76.2 cm (30 in) long and have a diameter of 76 mm (3 in) with sharp edge (tapered from the outside) and an inside clearance ratio (ICR) of zero. Standard penetration tests (SPTs) were performed in the layers both above and below the marl layer, and disturbed samples were collected from the split spoons and preserved in sealed containers and plastic bags. The purpose of conducting continuous sampling was to analyze the stratigraphy at the site. Field testing (CPT and FV) and sampling were performed in close proximity to each other in order to minimize the effect of spatial variability and facilitate the comparison between field and laboratory results. All the field work was done within an area of about 9 m × 7 m (30 ft × 23 ft).

4.2.3 Field Tests Results

One of the major tasks in this project was to conduct field tests that would complement the laboratory testing program. The in-situ testing program included:

(i) seven seismic cone penetration tests with pore pressure measurements (SCPTu); (ii) eleven field vane (FV) shear tests to determine the undrained shear strength and soil sensitivity profile; (iii) forty-six SPTs for soil profiling and collection of disturbed samples; and (iv) the installation of an open pipe piezometer to locate the water table. This section summarizes the results of the first two tests (i.e., SCPTu and FVT); the entire field testing program with details on the methods and results is discussed in detail in Appendix 2.

The tip resistance, the skin friction and the pore water pressure variation with depth obtained from the CPT tests are summarized in Figure 4.3. The figure shows the data for a total of seven CPTs (dashed gray lines) as well as the average values (continuous black line). High permeability layers, such as sand and silty sand layers, are characterized by a high tip resistance (q_t) and sleeve friction (f_s), and porewater pressure (u_2) close to the hydrostatic value (u_0). Low permeability layers, such as marl and soft clay layers, are characterized by low q_t and f_s , and high u_2 . The average CPT results show that there is a very soft layer ($q_t \sim 500$ kPa and $f_s \sim 7$ kPa) at a depth ranging between 4.9 m (16 ft) and 11.6 m (38 ft). This is the marl layer from which undisturbed Shelby tubes were obtained. The shear wave velocity profile was also determined through two SCPTu. The results show (see Figure 2.19 in Appendix 2) that the marl layer (between 4.9 m (16 ft) and 11.6 m (38 ft)) has an average shear wave velocity equal to 155 m/s. Based on this value of V_s , the average shear modulus of the deposit is estimated to be approximately 40 MPa.

The field vane (FV) is a widely used in-situ test for evaluating the undrained shear strength of soft soil deposits. The marl layer was tested every 0.6 m (2 ft)

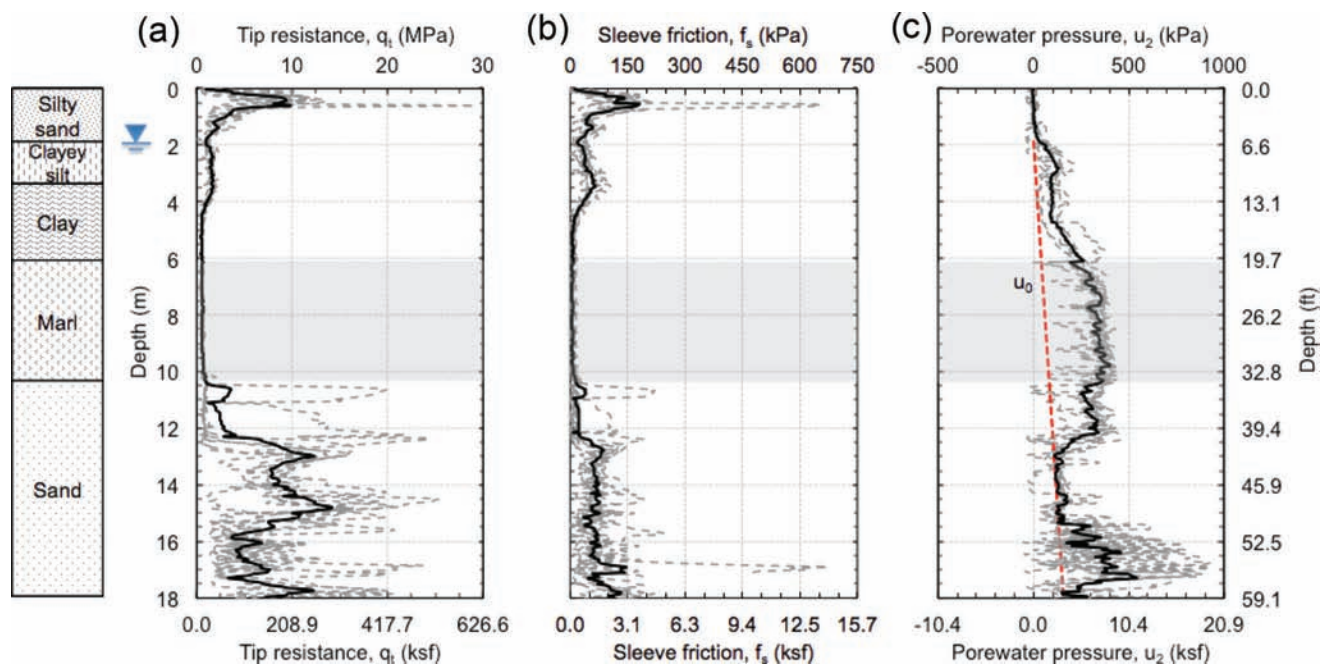


Figure 4.3 CPT results: (a) tip resistance, (b) skin friction, and (c) porewater pressure versus depth.

from 4.9 m (16 ft) to 11.6 m (38 ft) and the results are summarized in Figure 4.4(a). The peak and remolded strengths are computed from the FV using the relationship for both ends tapered vanes reported in ASTM D2573-08 (ASTM, 2008b). The peak undrained shear strength varies between 25 kPa and 50 kPa, which is typical for soft clays. Figure 4.4(b) shows the soil sensitivity with depth; this parameter is calculated from the ratio between the peak and the remolded undrained shear strength measurements. The figure shows that the sensitivity of the deposit is about 5.0. Thus the marl can be considered a sensitive soil.

4.3 Index Properties, Mineralogy, and Microstructure

From the interpretation of the field data collected, marl was identified at depths between 6.1 m (20 ft) and 10.4 m (34 ft). A full laboratory testing program was performed on Shelby tubes samples obtained from this layer. The program consisted of tests aimed at characterizing: (i) the index properties; (ii) the mineralogy and microstructure; and (iii) the consolidation, and (iv) shear strength behavior of this layer. Index properties, mineralogy and microstructure are summarized in this section, whereas the engineering properties are discussed in the following section.

Examination of the soil samples obtained from the marl layer revealed that the marl layer was not homogenous as was initially anticipated, but was formed by two types of soils with distinct properties that repeated in horizontal thin layers. These two soils were identified after starting the laboratory tests, and are herein referred to as “soil M” and “soil C.” This

denomination were selected based on the fact that soil M has relatively more silt, hence the letter “M”; whereas soil C has relatively more clay, hence the letter “C.” These two types of soils showed distinct index and engineering properties, which created the necessity to carefully characterize each soil separately and examine the fundamental difference(s) between them. Moreover, as discussed below, both soils are characterized by very high calcium carbonate contents (over 50%, and close to 40%). Soil M was found to be more prominent throughout the depth of the deposit.

4.3.1 Index Properties

Index tests were conducted on a total of 25 soil samples obtained from different depths to classify the soil present in the marl deposit and derive parameters that correlate with the engineering behavior. Index properties measured included organic content, calcium carbonate content, Atterberg limits, natural water content, particle size distribution, specific gravity, void ratio, total unit weight, degree of saturation, salt concentration, and pH. See Appendix 3 for a description of the methods used and a detailed presentation and discussion of the results. Key index properties for soils M and C are summarized in Table 4.2. The table shows that soil M is characterized by a lower specific gravity and unit weight, but has higher porosity, water content, silt content, and CaCO₃ content. In particular, the average CaCO₃ content exceeds 50% for soil M and is close to 40% for soil C. Based on these values the two soils would be classified based on the INDOT classification system as a marl and a marly soil, respectively.

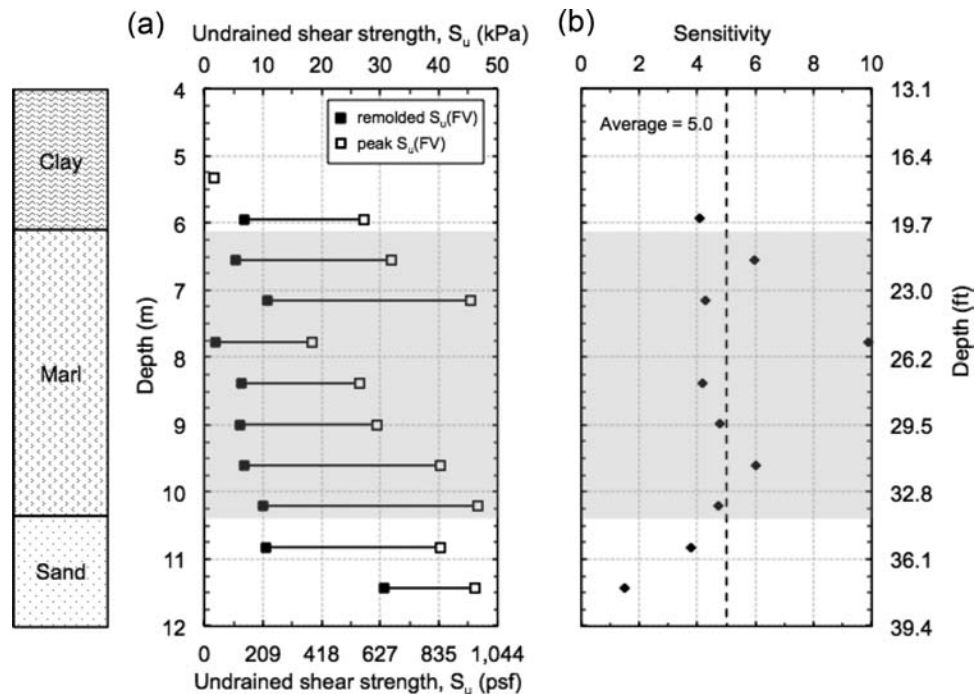


Figure 4.4 Profiles of (a) field vane undrained shear strength and (b) soil sensitivity with depth.

TABLE 4.2
Summary of index properties

	Soil M		Soil C	
	Range	Mean \pm SD*	Range	Mean \pm SD
Organic content (%)	2.0–4.3	3.1 \pm 0.6	1.7–3.0	2.5 \pm 0.4
CaCO ₃ content (%)	35.9–64.4	54.0 \pm 7.4	33.7–41.8	37.0 \pm 2.9
Water content, w _n (%)	50.5–68.5	60.9 \pm 6.0	36.6–52.2	42.1 \pm 5.2
Plastic limit, PL (%)	29.0–40.6	34.6 \pm 3.5	18.8–25.5	21.6 \pm 2.3
Liquid limit, LL (%)	61.7–78.8	67.5 \pm 5.2	40.1–52.4	47.5 \pm 4.2
Silt content (%)	72.0–82.0	77.6 \pm 3.0	54.0–66.0	61.0 \pm 5.5
Clay content (%)	15.0–23.0	18.3 \pm 2.8	33.0–45.0	38.3 \pm 5.3
Specific gravity, G _s	2.68–2.80	2.71 \pm 0.03	2.76–2.82	2.79 \pm 0.02
Void ratio, e	1.4–1.9	1.7 \pm 0.1	1.1–1.5	1.2 \pm 0.1
Total unit weight, γ_t (kN/m ³)	15.5–16.8	15.9 \pm 0.4	16.8–18.3	17.6 \pm 0.5
Degree of saturation, S _i (%)	95.3–99.8	97.9 \pm 1.4	93.2–99.0	97.4 \pm 1.9
Salt concentration (g/l)	2.1–3.8	3.0 \pm 0.5	2.2–5.1	3.6 \pm 1.2
Salt concentration (g/kg)	1.4–2.2	1.9 \pm 0.2	0.9–1.9	1.5 \pm 0.4
pH	7.5–7.9	7.8 \pm 0.1	7.6–7.9	7.8 \pm 0.1

*SD: Standard deviation.

A characteristic specific to soil M is the presence of shells, which, as discussed below, is responsible for a higher void ratio. Overall, the presence of these two soil types provides the opportunity to essentially study two types of marls, and explore, in particular, the effect of shells, mineral composition, and carbonate content on both index and engineering properties.

The liquid limit and the plasticity index of all the specimens from the marl layer are plotted on the plasticity chart in Figure 4.5. For the most part, Soil M plots below the A-line and is thus classified as an elastic silt (MH) according to the USCS or A-7-5 according to the AASHTO, whereas soil C plots above the A-line and is classified as a lean clay (CL) according to the USCS or A-7-6 according to the AASHTO. Based on the INDOT classification system in specs 903 (INDOT, 2014), soil M is classified as “marl (silty loam)” and soil C is classified as “marly soil (silty clay).”

Figure 4.6 shows the particle size distribution curves obtained from hydrometer tests. Both soils have a fine

fraction (less than 75 μm) greater than 96%. The small percentage of sand-size particles (greater than 75 μm) found in soil M (< 4%) consists mainly of shells. The figure shows that soil M and soil C fall on two distinct bands. The average percentage of clay size particles (less than 2 μm) is 18.3% \pm 2.8SD for soil M, which is lower than soil C (38.3% \pm 5.3SD).

The higher plasticity of soil M is not consistent with the typical trends reported in the literature of increasing LL and PI with higher clay content. It is also inconsistent with the data reported by Lamas et al. (2002) for other carbonatic fine-grained soils, which show that LL and PI decrease with increasing calcium carbonate. This difference can be ascribed to variations in the mineralogy of the clay fraction of the two soils, as both the type and amount of clay in a soil influence the Atterberg limits. The mineralogical analysis summarized in the next section shows that the smectite content in the bulk soil is about 10% for soil M and about 2% for soil C. The large difference in the smectite content

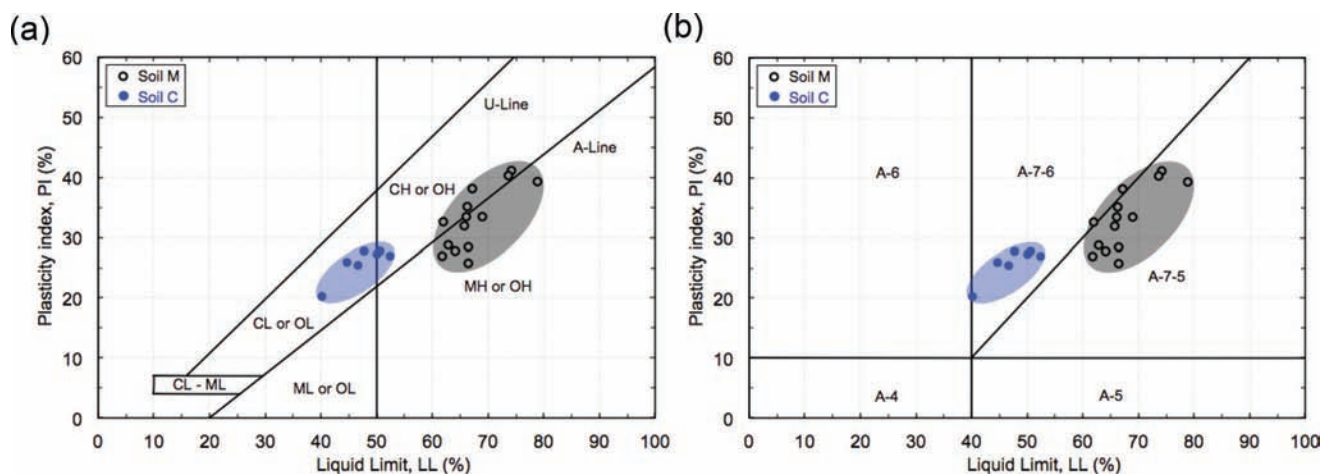


Figure 4.5 Plasticity chart with data for soils M and C: (a) USCS and (b) AASHTO.

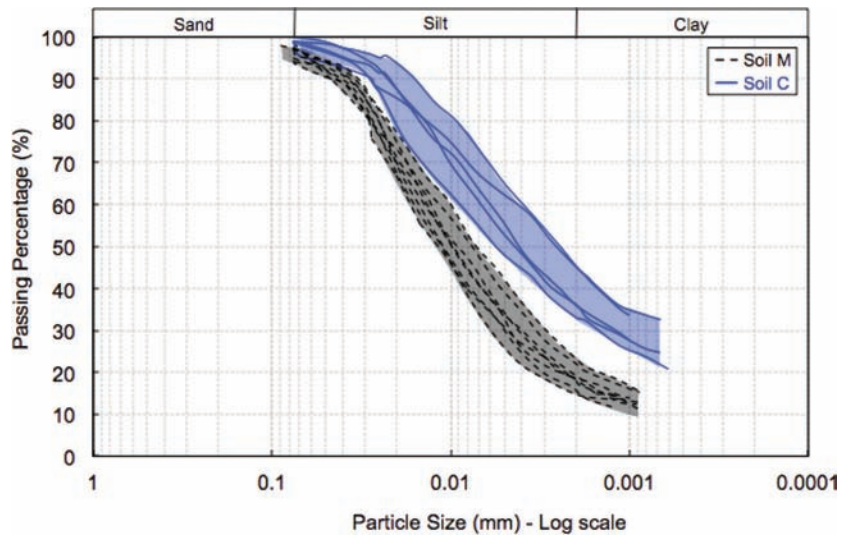


Figure 4.6 Results of particle size analyses on soils M and C.

between soil M and soil C may explain the discrepancy observed in the Atterberg limits, as soils rich in smectite have higher LL and PI, due to their higher water sorption capacity caused by the higher specific surface area (De Kimpe et al., 1979).

4.3.2 Mineralogy and Microstructure

The mineralogy and microstructure of the two soils identified in the marl deposit were investigated using a combination of several techniques that included: X-ray diffraction (XRD), thermogravimetric analysis (TGA), as well as electron microscopy equipped with energy-dispersive X-ray spectroscopy (EDXS), which can provide useful information on microstructure and chemical composition of individual particles. The detailed procedures, analyses, and results are provided in Appendix 3. The following summarizes the procedures and results obtained from these analyses, as well as the dominant mineralogical composition and the microstructure of the soils. In this portion of the work specific emphasis was placed on understanding the fundamental differences between soil M and soil C.

4.3.2.1 Mineral composition. The mineral composition was determined using XRD analysis on both randomly oriented powder and oriented aggregates. X-ray diffraction patterns were obtained using a PANalytical B.V. (Model X'Pert PRO diffractometer; Almelo,

Netherlands) diffractometer using Co radiation of 1.79 Å. A total of 5 specimens were obtained from different boreholes at various depths (3 specimens from soil M and 2 specimens from soil C) and analyzed using XRD. While no variations in mineral composition were observed with depth, the mineralogy varied significantly between soil M and soil C. The different minerals identified in the samples are shown in Table 4.3 in order of predominance (from largest to smallest).

All soil samples yielded similar results. The dominant non-clay mineral components are calcite, dolomite, and quartz. Soil M and soil C contain small quantities of feldspars. Aragonite (CaCO_3) is identified in soil M, which was found to be attributed to the presence of shells. This component is not identified in soil C due to the absence of shells. XRD patterns of oriented clay aggregate subjected to different treatments show that smectite and illite are the predominant clay minerals in soil M, while chlorite and kaolinite occur in smaller quantities. Soil C, on the other hand, is mainly composed of Illite and chlorite, while smectite and kaolinite are found in very small amounts.

The XRD analysis reveals the following differences between the matrix of soil M and that of soil C:

- Soil M is richer in carbonates than soil C, which is confirmed by the thermogravimetric analysis.
- Soil M has more calcite than soil C, which might be attributed to the presence of secondary calcite crystals that were precipitated more in soil M during the soil

TABLE 4.3 Mineralogy of soils M and C (in order of predominance) as observed by XRD analysis (from randomly oriented powder and oriented aggregates)

Soil type	Mineral type	Identified minerals
Soil M	Non-clay minerals	Calcite, quartz, dolomite, aragonite, plagioclase feldspar, K-feldspar
	Clay minerals	Smectite (50%), illite (27%), chlorite (12%), kaolinite (11%)
Soil C	Non-clay minerals	Quartz, dolomite, calcite, plagioclase feldspar, K-feldspar
	Clay minerals	Illite (62%), chlorite (30%), smectite (5%), kaolinite (3%)

deposition. This is confirmed by the calcite crystals identified with the scanning electron microscope (presented in the following subsection). These crystals are identified in soil M but are not found in soil C.

- Soil M has less dolomite than soil C.
- Aragonite is identified in soil M but is absent in soil C. This is expected due to the presence of shells in soil M and their absence in soil C.
- Soil M has a smaller clay content than soil C, which is consistent with the results of particle size analysis.
- The clay fraction of soil M is mainly composed of smectite and illite, whereas soil C is mainly composed of Illite and chlorite.

4.3.2.2 Microstructure. Scanning electron microscopy was employed to gain insight into the microstructure of the two types of marl. Each sample was allowed to dry at room temperature for ~1 week and then broken to create a free fractured face that was mounted on a sampler holder using graphite paste. All samples were imaged without coating. Images were obtained at the Purdue University's Life Science Microscopy facility with the FEI Quanta 3D FEG SEM using the low vacuum LVSED detector as well as the backscattered BSE detector (with 20kV, Spot 6.0, and 10mm WD). Magnifications ranged between 250x and 4000x. X-ray analysis (EDX) was done with an Oxford INCA Xstream-2 with Xmax80 detector (Oxford Instruments, Peabody, MA) using 20kV, 6.5 spot, 10mm WD, 50 μ m objective aperture, and P4. EDX was used to analyze the chemical composition of the objects of interest in the SEM.

Scanning electron micrographs for soil M and soil C are shown in Figure 3.25 and Figure 3.26 in Appendix 3, respectively. Based on the SEM analysis, different types of microfossils and shells of snails and bivalves are found in soil M as well as calcite crystals. These are part of the soil matrix and result in a higher calcite content in soil M, as reported in the XRD results. The micrographs also show the presence of 5–30 micron framboidal pyrite (iron sulfide), consisting of crystallites ranging from 0.5–3 microns. These different features were identified chemically using EDX. For soil C, the SEM observations confirm that there are no shells; however, iron sulfide was detected, although not in the framboidal form observed in soil M. This might be an indication of the different environmental conditions (e.g., presence of water, temperature) in which the soil was deposited. In general, soil M shows a more open microstructure compared with soil C, which is consistent with the higher void ratio reported earlier (soil M: $e \sim 1.7$; soil C: $e \sim 1.2$).

Charophyte oospores were also found in soil M. These are pond-dwelling algae that live in still or slow-moving water with calcium carbonate. The absence of both shells and charophytes in soil C might be an indication of the absence of life when soil C was deposited.

4.4 Engineering Properties

This section provides a summary of the results of the consolidation tests and the triaxial tests conducted on

undisturbed samples of marl. In this study, a total of six CRS consolidation, two IL consolidation, and eleven triaxial tests were performed on marl samples obtained from different boreholes at various depths. Details on the equipment and methods used to perform these tests, as well as on the measured engineering properties are provided in Appendix 4.

4.4.1 Consolidation Testing Program

A total of 17 one-dimensional compression curves obtained from CRS consolidation tests and the K_0 -consolidation stage of triaxial tests performed on undisturbed samples of marl are presented in Figure 4.7, where the dashed black lines represent soil M and the continuous blue lines represent soil C. In general, both types of marl show similar compressibility properties that fall in the range of soft clays.

Figure 4.7(a, b) show the compression curves in the strain- and void ratio- effective stress space, respectively. All results show a consistent behavior (i.e., the compression curves are characterized by a clear break in correspondence to the preconsolidation stress σ'_p , and have an S-shape), which is evidence of the soil's high sensitivity. This S-shape is more pronounced for soil C.

Figure 4.8(a) and Figure 4.8(b) show the variation with depth of preconsolidation stress and overconsolidation ratio, respectively. Different symbol shapes are used to indicate different types of tests (square, triangle and circle for CRS consolidation, IL consolidation, and TX tests, respectively), while different colors are used to indicate the different types of marl (hollow black symbols correspond to soil M and solid blue circles correspond to soil C). In general, there is no clear difference between the results obtained from the different types of tests (CRS, IL, and TX). However, a clear difference can be observed between soil M and soil C. The preconsolidation stress for soil M shows an increasing trend with depth ranging between 120 and 193 kPa (mean $\sigma'_p = 148 \text{ kPa} \pm 21.3\text{SD}$). This trend was not observed for soil C due to the limited number of data points and the significant scatter; however, its average preconsolidation stress (mean $\sigma'_p = 104 \text{ kPa} \pm 11.7\text{SD}$) is lower than that of soil M. These stresses correspond to OCR values around $1.9 \pm 0.2\text{SD}$ for soil M and around $1.3 \pm 0.2\text{SD}$ for soil C. The higher values of OCR for soil M might be attributed to the natural cementation caused by the higher carbonate content present in soil M, as illustrated earlier by the mineralogical analysis.

Values of the lateral stress ratio (or coefficient of earth pressure) at rest, K_0 , were derived from the K_0 -consolidation stage of the triaxial tests. Figure 4.7(c) presents the variation of K_0 with vertical effective stress for each of the tests performed. The figure shows that K_0 decreases as the specimen is loaded, reaches a minimum and then increases again reaching a constant value in the normally consolidated region. This behavior is typical of structured soils. The normally consolidated value of K_0 for soil C (0.559) exceeds the average value (0.488). This is consistent with the friction

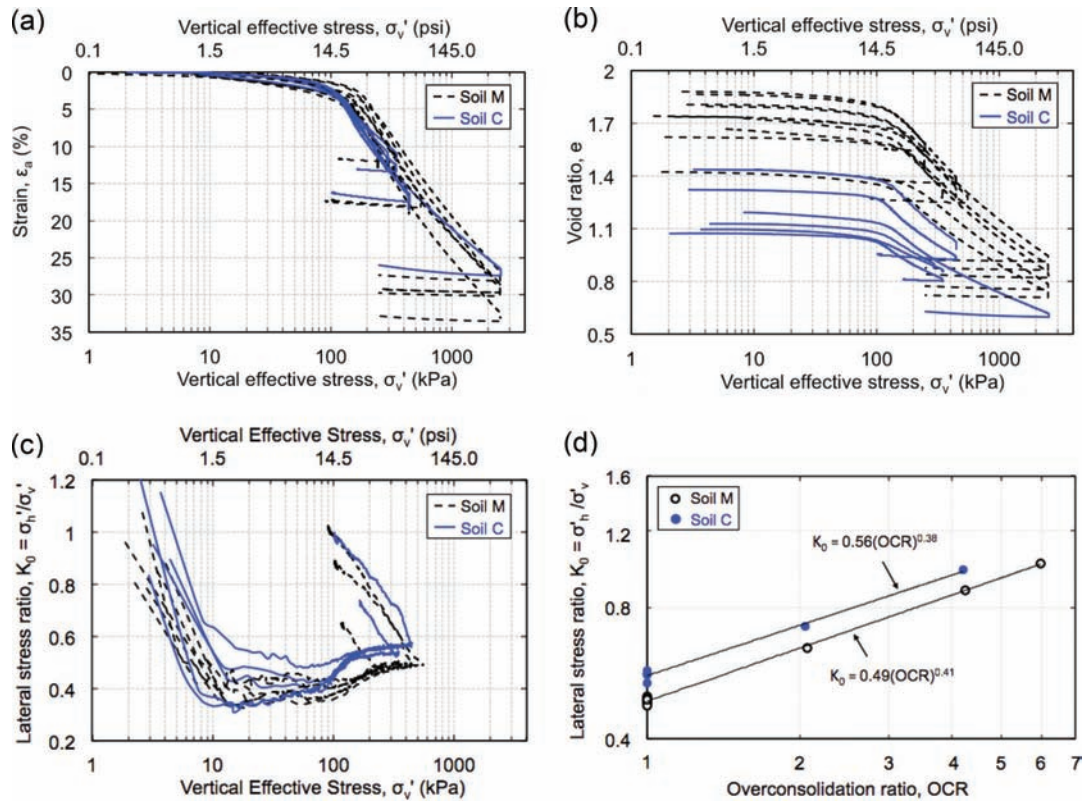


Figure 4.7 Results of consolidation tests: (a) ϵ -compression curves; (b) e -compression curves; (c) lateral stress ratio vs. σ'_v ; and (d) lateral stress ratio vs. OCR.

angle values measured on these two soils (see below). Upon unloading K_0 increases once again. From the data shown in Figure 4.7(c) it is possible to derive the

relationship between K_0 and OCR (see Figure 4.7(d)), which has similar form for both soils. Note that the values of K_0 shown in Figure 4.7(d) are obtained at the end of

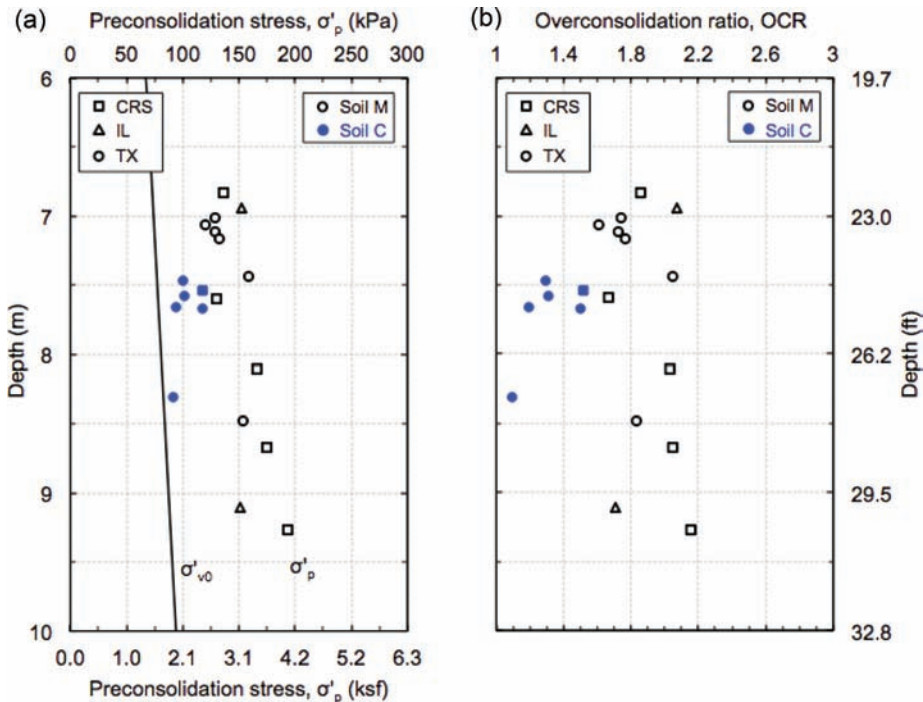


Figure 4.8 Stress history profile: (a) preconsolidation stress and overburden stress; and (b) OCR with depth.

the unloading phase and before shear. The relationship between K_0 and OCR has the following form:

$$K_0 = K_{0NC} (\text{OCR})^n$$

Where $K_{0NC} = 0.49$, $n = 0.41$, and $r^2 = 1.00$ for soil M; and $K_{0NC} = 0.56$; $n = 0.38$; and $r^2 = 0.99$ for soil C.

Key consolidation properties for soil M and soil C are summarized in Table 4.4. In addition to the parameters discussed above, Table 4.4 shows the ratio C_{ae}/C_c calculated for soil M and soil C using three IL consolidation tests. The ratio is equal to 0.041, which falls in the range of soils with relatively high creep rate (Mesri & Godlewski, 1977). Moreover, the quality of the soil samples was assessed by calculating $\delta e/e_0$ obtained from the consolidation (CRS and IL) tests, and the K_0 consolidation phase of triaxial tests. The average values are shown in Table 4.4 from soils M and C. All the data fall below 0.05, indicating that the samples can be designated as “excellent” to “good” based on the sample quality designation suggested by Lunne, Berre, and Strandvik (1997). This highlights the effectiveness of the techniques used in this study (i.e., drilling using mud rotary, sampling using fixed piston sampler, extrusion using a piano wire to debond the soil along the inside of the tube, trimming using wire saw) to obtain high-quality and reliable laboratory test data for soft soils. In general, despite some limited scatter, values of $\Delta e/e_0$ obtained from tests on soil M specimens (average $\Delta e/e_0 = 0.033 \pm 0.009\text{SD}$) are smaller than those obtained from tests performed on soil C (average $\Delta e/e_0 = 0.039 \pm 0.009\text{SD}$). This is in agreement with the fact that soil C is more sensitive (depicted by the strong S-shape compression curves), which makes it more susceptible to disturbance.

4.4.2 Shear Testing Program

A total of eleven K_0 -consolidated SHANSEP triaxial compression tests (CK₀UTC(L)) were performed on marl samples obtained from different boreholes at various depths. Six of these tests were sheared at OCR of 1, and five were sheared at OCR values varying between approximately 2 and 6. All undrained shear stages were conducted using an axial strain rate of 0.5%/hr.

TABLE 4.4
Summary of consolidation properties

	Soil M		Soil C	
	Range	Mean \pm SD*	Range	Mean \pm SD
Overburden stress, σ'_{v0} (kPa)	73.1–89.4	79.2 \pm 5.8	77.3–82.9	78.9 \pm 2.0
Preconsolidation stress, σ'_p (kPa)	120–193	148 \pm 21.3	91.0–118	104 \pm 11.7
Overconsolidation ratio, OCR	1.6–2.2	1.9 \pm 0.2	1.1–1.5	1.3 \pm 0.2
Virgin compression index, C_c	0.56–0.81	0.71 \pm 0.08	0.34–0.67	0.52 \pm 0.13
Maximum virgin compression ratio, CR_{max}	0.23–0.29	0.26 \pm 0.02	0.16–0.28	0.23 \pm 0.05
Normally consolidated lateral stress ratio, K_{0NC}	0.475–0.499	0.488 \pm 0.009	0.537–0.573	0.559 \pm 0.013
$K_0 = K_{0NC} (\text{OCR})^n$	$K_{0NC} = 0.49$; $n = 0.41$		$K_{0NC} = 0.56$; $n = 0.38$	
C_{ae}/C_c	0.041		0.041	
$\Delta e/e_0$	0.016–0.049	0.033 \pm 0.009	0.024–0.050	0.039 \pm 0.009

*SD: Standard deviation.

The triaxial tests results are summarized in Figure 4.9(a–d) (black for soil M and blue for soil C). Figure 4.9(a) shows the normalized shear stress—strain curves. It can be observed that for the same value of OCR, the marl with higher CaCO_3 content (soil M) has higher normalized undrained shear strength than the marl with lower CaCO_3 content (e.g., for OCR = 1, $q_f/\sigma'_{vc} \sim 0.34$ vs. 0.28). This might be attributed to the shear reinforcement provided by the shells as well as the cementation caused by the higher carbonate content present in soil M.

Figure 4.9(b) presents the effective stress paths normalized by the maximum vertical consolidation stress (σ'_{vm}) for SHANSEP CK₀UTC(L) tests conducted on NC and OC marl. The MIT stress path convention was used where the shear stress is calculated as $q = (\sigma'_v - \sigma'_h) / 2$ and the average effective stress is calculated as $p' = (\sigma'_v + \sigma'_h) / 2$. The results show that the effective stress paths approach a common failure envelope at large strains. The p' - q effective stress failure envelope (ESFE) is defined by a linear regression through the shear stress and average effective stress at maximum obliquity represented with hollow black diamonds for soil M and solid blue diamonds for soil C. The linear regression on the data yields a friction angle at maximum obliquity (ϕ'_{mo}) of 39° for soil M and 30° for soil C and a negligible cohesion intercept ($c' \sim 0$) for both soils. As mentioned earlier, the higher friction angle measured on soil M might be attributed to the shear reinforcement provided by the shells as well as the cementation caused by the higher carbonate content present in soil M.

Figure 4.9(c) presents the change in normalized excess pore pressure, while Figure 4.9(d) illustrates the change in normalized shear stress with OCR. Overall, the triaxial data are repeatable and the results show that the soil exhibits normalized behavior. The SHANSEP parameters link stress history to undrained shear strength through the following equation:

$$S_u / \sigma'_{vc} = S (\text{OCR})^m$$

Where S_u is the undrained shear strength, σ'_{vc} is the vertical effective stress, OCR is the overconsolidation

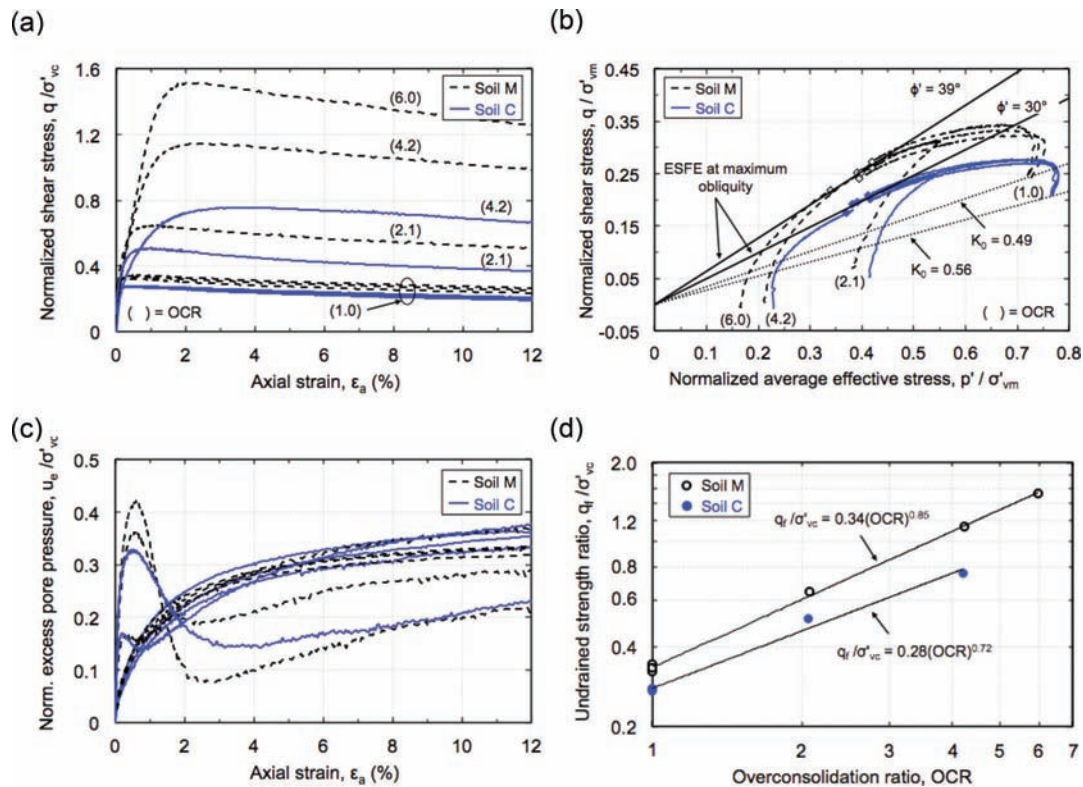


Figure 4.9 Results of triaxial tests: (a) normalized shear stress vs. axial strain, (b) normalized change in excess pp, (c) p' - q stress path, and (d) normalized shear stress vs. OCR.

ratio, and S and m are the two SHANSEP parameters ($S = 0.34$; $m = 0.85$; $r^2 = 1.00$ for soil M; and $S = 0.28$; $m = 0.72$; and $r^2 = 0.99$ for soil C). Although these values fall in the range of soft soils previously documented in the literature (e.g., BBC: $S = 0.28$ and $m = 0.70$ (Sheahan, 1991); Taipei clay: $S = 0.32$ and $m = 0.82$ (Chin, Chen, Hu, Yao & Chao, 2007)), it is important to note the significant difference between soils M and C.

This concept has significant practical value as it provides a useful framework for comparing and relating the behavioral characteristics of different cohesive soils and allows estimation of the undrained shear strength profile as the vertical effective stress and stress history profiles of the site change. Thus, the SHANSEP method is ideally suited for the design of staged construction/preloading procedures (Ladd, 1991), which are commonly employed in marl deposits.

Key undrained shear properties for soil M and soil C are summarized in Table 4.5.

4.5 Integration of Laboratory and Field Data

As mentioned earlier, eleven field vane tests and seven piezocone tests (two with seismic measurements) were performed at the marl site in close proximity to where the laboratory samples were collected. This provided the opportunity to compare field and lab predictions of key geotechnical properties such as shear wave velocity, undrained strength, and preconsolidation

stress. This part of the analysis is described in Appendix 5 which is organized in two sections: (i) analysis of field vane tests and (ii) analysis of piezocone tests. The field vane data ($S_{u(FV)}$) were corrected using Bjerrum's factor μ and compared with the reference strength values obtained from the laboratory SHANSEP $CK_0UTC(L)$ tests. In general, there is a large variation in the $S_{u(FV)}$ with depth, which might be caused by the presence of shells in soil M, which is known to cause a large increase in $S_{u(FV)}$ (Ladd & DeGroot, 2003). While field vane test data generally provide reasonable strengths for preliminary design (Ladd, 1991) in soft deposits, their use is generally discouraged in presence of shells and/or sand lenses. As a result its use would be recommended only in marl deposits with no shells (e.g., deposits of soil C). Due to the limited thickness of the marl layer and the large variation in the field vane data, the discussion below covers only the CPT data.

The piezocone tests results were analyzed and marl specific correlations to estimate shear wave velocity, stress history, and undrained strength from the Piezocone penetration measurements are provided. This section presents a summary of the CPT correlations; the reader is referred to Appendix 5 for more details.

Due to its numerous advantages over other in-situ tests, the CPT has been increasingly used for conducting site investigations for exploring soft soils. Extensive work has been conducted to correlate soil parameters from CPT results. The main objective of the piezocone

TABLE 4.5
Summary of undrained shear properties

OCR		Soil M				Soil C		
		1.0*	2.1	4.2	6.0	1.0*	2.1	4.2
At peak	q/ σ'_{vc}	0.333	0.649	1.145	1.521	0.275	0.509	0.757
	p'/ σ'_{vc}	0.684	1.124	1.842	2.462	0.731	1.109	1.611
	ε_{af}	0.528	1.298	2.46	2.092	0.394	1.005	4.217
	ϕ'	29.2	35.3	38.4	38.1	22.13	27.3	28
	A_f	0.721	0.173	0.084	0.027	0.763	0.178	0.091
At maximum obliquity	q/ σ'_{vc}	0.258	0.522	1.070	1.306	0.202	0.394	0.738
	p'/ σ'_{vc}	0.411	0.808	1.692	2.025	0.407	0.783	1.562
	ε_a	10.42	10.26	7.17	1.11	11.71	8.81	6.45
	ϕ'	39.0	40.3	39.2	40.2	29.73	30.2	28.2
$E_{0.1}/\sigma'_{vc}$	129.9	435.8	493.1	548.3	107.7	418.9	443.8	
$E_{u, max}/\sigma'_{vc}$	36.5	78.1	91.9	148.4	34.3	79.6	37.3	
$S_u/\sigma'_{v0} = S(OCR)^m$		S = 0.34; m = 0.85				S = 0.28; m = 0.72		
ϕ'_{mo}		39°				30°		

*The data corresponds to the average of three NC tests.

testing program in this research was to investigate the current correlations reported in the literature and provide site-specific correlations for marls to be used for preliminary design. The CPT field data were examined to derive correlations for three major soil properties: shear wave velocity (V_s), preconsolidation stress (σ'_p), and undrained shear strength (S_u).

Shear Wave Velocity

Thirteen different existing correlations linking V_s to the CPT data were reviewed for this study (see Table 5.1 in Appendix 5). The correlations were analyzed for the seven CPTs and the derived V_s values were compared with the field seismic measurements of V_s . This investigation shows that all correlations tend to underestimate the V_s of the marl, except the one developed by Andrus, Monahan, Piratheepan, Ellis, and Holzer (2007) for all soils with a Pleistocene geologic age, which shows to be effective in predicting the V_s of marl deposits.

Preconsolidation Stress

Three different relations were used to examine the ability to predict the preconsolidation stress of the marl deposit investigated in this research from the CPT results by comparing the derived σ'_p values with the laboratory measurements of σ'_p presented earlier. This investigation shows that the σ'_p of marl can be best estimated using the correlation provided by Mayne (1995). The values of σ'_p obtained applying this correlation to the traces of each of the seven CPTs performed are shown in Figure 5-5 in Appendix 5. It is found that the correlation by Mayne (1995) is effective in capturing the values of the preconsolidation stress for soil M, while slightly overestimating σ'_p for soil C. This

might be due to the fact that soil M is more prominent, and thus controls the measured tip resistance.

Undrained Shear Strength (Triaxial Compression)

The undrained shear strength, S_u , can be estimated from the net tip resistance, $q_t - \sigma_{v0}$, by substituting the cone tip resistance, q_t , the total overburden stress, σ_{v0} , and the empirical cone factor, N_{kt} , at given depths into the following equation:

$$S_u = (q_t - \sigma_{v0}) / N_{kt}$$

The value of N_{kt} was backcalculated using the cone resistance measurements obtained at all seven CPTs, and the $CK_0UTC(L)$ SHANSEP profile as the reference undrained shear strength (Soil M: $S_u = \sigma'_{v0} \times 0.34 (1.9)^{0.85}$; and soil C: $S_u = \sigma'_{v0} \times 0.28 (1.3)^{0.72}$). This results into an average N_{kt} derived from all CPTs of 10 and 17 for soil M and soil C, respectively.

It is important to note the significant difference between soils M and C, which is mainly caused by the large difference in $S_{u(TC)}$ derived from the SHANSEP program. This large variation indicates that there is no unique N_{kt} value that can be applied for all marl deposits and that site-specific calibration should be conducted for CPT data to account for the presence/absence of both types of soils (M and C) and representative values should be selected depending on the prevalence of each. In addition, the reported N_{kt} values are used to derive the S_u in triaxial compression mode, which is not necessarily the only mode of failure experienced by the soil. For instance, when building an embankment, Ladd (1991) shows that the soil under the embankment experiences three different modes of failures: extension, direct simple shear and compression. Hence, higher values of N_{kt} should be used to derive the S_u in triaxial extension mode or direct simple shear mode.

Below is a summary of the three correlations that are found to better match the results for the marl deposit investigated:

Shear Wave Velocity

$$V_s = 2.93 q_t^{0.395} I_c^{0.912} D^{0.124}$$

where V_s = shear wave velocity (in m/s)

q_t = tip resistance (in kPa)

$$I_c = \text{soil behavior type index} = [(3.47 - \log Q)^2 + (1.22 + \log F)^2]^{0.5}$$

Q = normalized tip resistance = $(q_t - \sigma_{v0}) / \sigma'_{v0}$

F = normalized friction = $f_s / (q_t - \sigma_{v0}) * 100$

D = depth (in meters)

Preconsolidation Stress

$$\sigma'_p = 0.33 (q_t - \sigma_{v0})$$

where σ'_p = preconsolidation stress

q_t = tip resistance

σ_{v0} = total overburden stress

Undrained Shear Strength (Triaxial Compression)

$$S_{u(TC)} = (q_t - \sigma_{v0}) / N_{kt}$$

where S_u = undrained shear strength

q_t = tip resistance

σ_{v0} = total overburden stress

N_{kt} = empirical cone factor = 10 for soil M and 17 for soil C

(Note that N_{kt} should be selected with caution as discussed above.)

5. CONCLUSIONS

Deposits of marl are found in the state of Indiana with layers as thick as 20', at relatively shallow depths (10–15') below the ground surface. Such layers typically have low dry density, very high water content, and low shear strength, which makes them “problem soils” and poses concerns related to excessive settlement, slope instability, and increased downdrag on deep foundations. The overall scope of this project was to develop a fundamental knowledge of expected behavior of marls and create a database with expected properties and behavior. This was achieved by performing an in-depth study of the engineering properties, microstructure and mineralogy of a soft fine-grained carbonatic soil deposit in southwestern Indiana (Daviss County). The study yielded the following conclusions:

- The index and engineering properties of marls fall within the range typical of many other soft clays previously documented in the literature. However, the distinct properties exhibited by soils C and M identified in this project indicate that there is no “typical” marl, and that lessons from one deposit may not directly be extrapolated to others without consideration of index properties and mineralogical data. The data obtained as part of this project may be used as a guideline during the preliminary

design stages, but any subsequent design stage will require the derivation of site-specific properties.

- The behavior of marl cannot be described solely by the CaCO_3 content; the presence of shells as well as the type and quantity of minerals present in the soil should be investigated since they have significant impact on the index and engineering behavior of the marl.
- This research showed the importance of conducting mineralogical analysis to understand the fundamental soil behavior and resolve the discrepancy observed in the Atterberg limits. Despite its higher carbonate content and its lower clay content, soil M has higher LL and PI. This is not consistent with the typical trends reported in the literature of increasing LL and PI with higher clay content and lower carbonate content. This difference can be ascribed to the higher smectite content for soil M.
- The piezocone tests results were analyzed and correlations to estimate shear wave velocity, stress history, and undrained strength that provided the best match to the laboratory results were identified (see section 4.5). The former should be used when seismic measurements of V_s are not available. Laboratory measurements of σ'_p and S_u are required in latter stages of the design.
- The sampling and specimen preparation techniques used in this study (drilling using mud rotary, sampling using fixed piston sampler, extrusion using a piano wire, trimming using wire saw) were found to generate samples of high-quality and reliable laboratory test data. Their use is advocated for sampling and testing in all marl deposits.

6. IMPLEMENTATION RECOMMENDATIONS

6.1 Identification and Mapping

This study validates the previous method used for the identification of marly soils and marls found in the INDOT classification system in specs section 903 (INDOT, 2014).

Mapping of marl deposits in the State of Indiana was conducted based on information available at INDOT (refer to section 4.1). It consisted of data from more than five thousand boreholes, which were mined to identify the boreholes where marl was found. In total, 325 boreholes were identified to contain marl and their borelogs were used to develop the map using ArcGIS 10.0 (see Figure 4.1). The map was compiled in a format that could be easily accessible and expandable as additional information becomes available.

6.2 Sampling and Specimen Preparation

In order to obtain high-quality samples and reliable laboratory test data, it is recommended to use: (1) mud rotary for drilling; (2) fixed piston sampler for sampling; (3) piano wire for extruding the sample; and (4) wire saw for trimming the sample. These techniques minimize disturbance, which is a critical issue for marls due to their high sensitivity.

6.3 Interpretation of Field Data and Design

The fact that the soils examined exhibit normalized behavior indicates that the SHANSEP method can be

TABLE 6.1
Key index properties of soil M and soil C

	Soil M		Soil C	
	Range	Mean	Range	Mean
CaCO ₃ content (%)	36–64	54	34–42	37
Plastic limit, PL (%)	29–41	35	19–26	22
Liquid limit, LL (%)	62–79	68	40–52	48
Dry unit weight, γ_d (pcf)*	59–70	63	70–85	78
Comment	Presence of shells		No shells	
INDOT classification	Marl (silty loam)		Marly soil (silty clay)	

*Dry unit weight of soil in natural conditions (\neq maximum dry unit weight).

effectively used for designing on marl deposits. This has significant practical value, as this method allows estimation of the undrained shear strength profile as the vertical effective stress and stress history profiles of the site change, which is critical to the design of staged construction/preloading procedures commonly employed in marl deposits. The SHANSEP parameters derived in this project under *triaxial compression (TC) mode of shear* may be used for obtaining TC undrained strength profiles during the preliminary design stage on other marl deposits. A SHANSEP laboratory testing program should be conducted for any subsequent stages of design.

The field vane test was not successful in characterizing the strength profile of the marl deposit examined in this work. This is consistent with previous experiences in deposits characterized by the presence of shells and/or sand lenses documented in the literature. While its use should be discouraged in these cases, this test is still recommended for measuring the undrained strength of soft homogeneous deposits with no shells or sand lenses, and thus it should be applicable to homogeneous marl deposits.

The shear wave velocity, V_s , can be best estimated from the CPT data using the correlation provided by Andrus et al. (2007) for all soils with a Pleistocene geologic age. Note that all other correlations investigated in this study tend to underestimate the V_s of marl.

TABLE 6.2
Key engineering properties of soil M and soil C

	Soil M		Soil C	
	Range	Mean	Range	Mean
Virgin compression index, C_c^*	0.56–0.81	0.71	0.34–0.67	0.52
NC lateral stress ratio, K_{0NC}	0.48–0.50	0.49	0.54–0.57	0.56
$K_0 = K_{0NC}$ (OCR) ^a	$K_{0NC} = 0.49$; $n = 0.41$		$K_{0NC} = 0.56$; $n = 0.38$	
C_{ae}/C_c	0.041		0.041	
$S_u/\sigma'_{v0} = S$ (OCR) ^m	$S = 0.34$; $m = 0.85$		$S = 0.28$; $m = 0.72$	
ϕ'_{mo}	39°		30°	

* C_c are measured between $1.5 \sigma'_p$ and $2 \sigma'_p$.

The preconsolidation stress of marl can be best estimated from the CPT data using the correlation provided by Mayne (1995).

The undrained shear strength, S_u , under *triaxial compression mode of shear* can be estimated from the CPT data using the equation: $S_{u(TC)} = (q_t - \sigma_{v0}) / N_{kt}$ with N_{kt} equals 10 and 17 for soil M and soil C, respectively.

Significant variation in the S_u values indicates that no single value of N_{kt} has general applicability for all marl deposits to predict S_u from CPT data. The values derived above for soil M and soil C may serve as guidelines during preliminary design, but site-specific calibration should be conducted for final design.

6.4 Preliminary Design

The marl deposit investigated in this research was formed by two types of soils (soil M and soil C), with distinct properties. This indicates that, as discussed in the conclusions, there are no “typical” properties that can be assumed to be valid for all marls, and that lessons from one deposit may not directly be extrapolated to others without consideration of index properties and mineralogical data. The data obtained as part of this project may be used as a guideline during the preliminary design stages, but any subsequent design stage will require the derivation of site-specific properties. For the purpose of preliminary design for soils with similar index properties, soil M and soil C can be identified based on calcium carbonate content, Atterberg limits, total unit weight, and presence/absence of shells using Table 6.1.

Note that the focus of this project was on the behavior of in-situ marl deposits, which is relevant for construction of embankments, design of foundations and retaining systems, settlement calculations, etc. With regard to the use of this soil as an embankment or subgrade material, it is recommended that the same conventional approaches and testing methodologies (e.g., density, water content limit, plasticity index, etc.) employed for other soft soils should be used also for this soil.

The key engineering properties of soil M and soil C derived in this research are summarized in Table 6.2. Note that these properties can be used only in

preliminary design for soils with similar properties, and laboratory measurements are required in latter stages of the design. The higher friction angle measured for soil M might be attributed to the shear reinforcement provided by the shells as well as the cementation caused by the higher carbonate content. This may not directly be extrapolated to other similar soils where derivation of site-specific properties is required.

REFERENCES

- AASHTO. (2008). *Standard method of test for determination of organic content in soils by loss on ignition* (Standard T 267-86). Washington, DC: American Association of State Highway and Transportation Officials.
- Abdulhadi, N. O. (2009). *An experimental investigation into the stress-dependent mechanical behavior of cohesive soil with application to wellbore instability* (Dissertation). Cambridge: Massachusetts Institute of Technology. Retrieved from <http://hdl.handle.net/1721.1/54841>
- Aiban, S. A. (1995). Strength and compressibility of Abqaiq marl, Saudi Arabia. *Engineering Geology*, 39, 203–215.
- Alpan, I. (1967). The empirical evaluation of the coefficient K0 and K0R. *Soils and Foundations*, 7(1), 31–40.
- Alt & Witzig. (2010). *I-69 extension, Section A.3—US 50 to US 231, Segment 12—I-69 mainline roadway, CR 1400N to CR 700E, Daviess County* (Geotechnical engineering report prepared for Indiana Department of Transportation). Indianapolis, IN: Indiana Department of Transportation.
- Anagnostopoulos, A. G., Kalteziotis, N., Tsiambaos, G. K., & Kavvadas, M. (1991). Geotechnical properties of the Corinth Canal marls. *Geotechnical and Geological Engineering*, 9, 1–26.
- Andromalos, K., Hegazy, Y., & Jasperse, B. (2001). Stabilization of soft soils by soil mixing. In J. L. Hanson & R. J. Termaat (Eds.), *Soft ground technology* (pp. 194–205). Noordwijkerhout, the Netherlands: ASCE.
- Andrus, R. D., Mohanan, N. P., Piratheepan, P., Ellis, B. S., & Holzer, T. L. (2007). Predicting shear-wave velocity from cone penetration resistance. In K. Pitilakis (Ed.), *Proceedings of the 4th International Conference on Earthquake Geotechnical Engineering, Thessaloniki, Greece, 25–28 June 2007* (Paper No. 1454). New York, NY: Springer.
- ASTM. (2007). Standard test method for particle-size analysis of soils (ASTM D422-63). In *Annual book of ASTM standards*. West Conshohocken, PA: ASTM International.
- ASTM. (2008a). Standard practice for sampling of soil using the hydraulically operated stationary piston sampler (ASTM D6519-08). In *Annual book of ASTM standards*. West Conshohocken, PA: ASTM International.
- ASTM. (2008b). Standard test method for field vane shear test in cohesive soil (ASTM D2573-08). In *Annual book of ASTM standards*. West Conshohocken, PA: ASTM International.
- ASTM. (2010). Standard test methods for liquid limit, plastic limit, and plasticity index of soils (ASTM D4318-10). In *Annual book of ASTM standards*. West Conshohocken, PA: ASTM International.
- ASTM. (2011). Standard test method for standard penetration test (SPT) and split-barrel sampling of soils (ASTM D1586-11). In *Annual book of ASTM standards*. West Conshohocken, PA: ASTM International.
- ASTM. (2013). Standard test method for pH of soils (ASTM D4972-13). In *Annual book of ASTM standards*. West Conshohocken, PA: ASTM International.
- ASTM. (2014a). Standard test methods for specific gravity of soil solids by water pycnometer (ASTM D854-14). In *Annual book of ASTM standards*. West Conshohocken, PA: ASTM International.
- ASTM. (2014b). Standard test methods for downhole seismic testing (ASTM D7400-14). In *Annual book of ASTM standards*. West Conshohocken, PA: ASTM International.
- ASTM. (2014c). Standard test method for compositional analysis by thermogravimetry (ASTM E1131-08). In *Annual book of ASTM standards*. West Conshohocken, PA: ASTM International.
- Azzouz, A. S., Krizek, R. J., & Corotis, R. B. (1976). Regression analysis of soil compressibility. *Soils and Foundations*, 16(2), 19–29.
- Baldi, G., Bellotti, R., Ghionna, V. N., Jamiolkowski, M., & LoPresti, D. C. F. (1989). Modulus of sands from CPTs and DMTs. *Proceedings of the 12th international conference on soil mechanics and foundation engineering* (pp. 165–170). Boca Raton, FL: CRC Press.
- Baligh, M. M., Azzouz, A., & Chin, C. T. (1987). Disturbances due to “ideal” tube sampling. *Journal of Geotechnical Engineering*, 113(7), 739–757.
- Barnhisel, R. I. & Bertsch, P. M. (1989). Chlorites and hydroxy-interlayered vermiculite and smectite. In J. B. Dixon & S. B. Weed (Eds.), *Minerals in soil environments* (pp. 729-788). Madison, WI: Soil Science Society of America.
- Becker, D. E., Crooks, J. H. A., Been, K., & Jefferies, M. G. (1987). Work as a criterion for determining in situ and yield stresses in clays. *Canadian Geotechnical Journal*, 24(4), 549–564
- Berman, D. R. (1993). *Characterization of the engineering properties of Boston blue clay at the MIT campus* (Master’s thesis). Cambridge: Massachusetts Institute of Technology.
- Bish, D. L., & Duffy, C. J. (1990). Thermogravimetric Analysis of Minerals. In J. W. Stucki, D. L. Bish, & F. A. Mumpton (Eds.), *Thermal analysis in clay science* (pp. 96-157). Boulder, CO: Clay Minerals Society Workshop Lectures.
- Bjerrum, L. (1954). Geotechnical properties of Norwegian marine clays. *Geotechnique*, 4(2), 49–69.
- Bjerrum, L. (1972). Embankments on soft ground. In *Performance of earth and earth-supported structures: Vol. 2* (pp. 1–54). New York, NY: American Society of Civil Engineers.
- Bozzano, F., Marcoccia, S., & Barbieri, M. (1999). The role of calcium carbonate in the compressibility of Pliocene lacustrine deposits. *Quarterly Journal of Engineering Geology*, 32, 271–289.
- Brindley, G. W., & Brown, G. (1980). *Crystal structures of clay minerals and their X-ray identification*. London, UK: Mineralogical Society.
- Brindley, G. W., & Lemaître, J. (1987). Thermal, oxidation and reduction reactions of clay minerals. In A. C. D. Newman (Ed.), *Chemistry of clays and clay minerals* (Mineralogical Society Monograph No. 6; pp. 319–370). London, UK: Mineralogical Society.
- Black, D. K., & Lee, K. L. (1973). Saturating laboratory samples by back pressure. *Journal of the Soil Mechanics and Foundations Division, ASCE* 1, 75–93.
- Bowles, J. W. (1979). *Physical and geotechnical properties of soils*. New York, NY: McGraw-Hill.

- Burghignoli, A., Miliziano, S., & Soccodato, F. M. (2010). Cementation effects in two lacustrine clayey soils. *Geotech Geol Eng* 28, 815–833.
- Casagrande, A. (1936). The determination of the pre-consolidation load and its practical significance. *Proceedings of the 1st International Conference on Soil Mechanics and Foundation Engineering: Vol. 3* (pp. 60–64). Cambridge, MA: Harvard University.
- Chen, B. S.-Y., & Mayne, P. W. (1996). Statistical relationships between piezocone measurements and stress history of clays. *Canadian Geotechnical Journal*, 33(3), 488–498.
- Chin, C.-T., Chen, J.-R., Hu, I.-C., Yao, D. T. C., & Chao, H.-C. (2007). Engineering characteristics of Taipei clay. In T. S. Tan et al. (Eds.), *Proceedings international workshop on characterization and engineering properties of natural soils ("Natural soils 2006")*: Vol. 3 (pp. 1755–1804). London, UK: Taylor & Francis.
- Clayton, C. R. I., Siddique, A., & Hopper, R. J. (1998). Effects of sampler design on tube sampling disturbance—Numerical and analytical investigations. *Geotechnique*, 48(6), 847–867.
- Datta, M., Gulhati, S. K., & Rao, G. V. (1982). Engineering behavior of carbonate soils of India and some observations on classification of such soils. In K. R. Demars & R. C. Chaney (Eds.), *Geotechnical properties, behavior and performance of calcareous soils* (pp. 113–140). West Conshohocken, PA: American Society for Testing and Materials.
- Defense Science Board. (2000). *Report of the Defense Science Board Task Force on national imagery and mapping agency*. Washington, DC: Defense Science Board.
- De Kimpe, C. R., Laverdiere, M. R., & Martel, Y. A. (1979). Surface area and exchange capacity of clay in relation to the mineralogical composition of gleysolic soils. *Canadian Journal of Soil Science*, 59(4), 341–347.
- Doner, H. E., & Grossl, P. R. (2002). Carbonates and evaporites. In J. B. Dixon & D. G. Schulze (Eds.), *Soil mineralogy with environmental applications* (pp. 199–228). Madison, WI: Soil Science Society of America.
- Doner, H. E., & Lynn, W. C. (1989). Carbonate, halide, sulfate, and sulfide minerals. In J. B. Dixon & S. B. Weed (Eds.), *Minerals in soil environments* (pp. 279–330). Madison, WI: Soil Science Society of America.
- Drees, L. R., Wilding, L. P., Smeck, N. E. & Senkayi, A. L. (1989). Silica in soils: Quartz and disordered silica polymorphs. In J. B. Dixon & S. B. Weed (Eds.), *Minerals in soil environments* (pp. 913–974). Madison, WI: Soil Science Society of America.
- Earnest, C. M. (1980). *Perkin-Elmer Thermal Analysis Application Study: Vol. 30. The application of differential thermal analysis and thermogravimetry to the study of kaolinite clay minerals*. Waltham, MA: Perkin-Elmer.
- Earth Exploration. (2010). *I-69 extension, Section A.3—US 50 to US 231, Segment 13—I-69 mainline roadway & access roads CR 700E to US 231, Daviess and Greene Counties* (Geotechnical engineering report prepared for Indiana Department of Transportation). Indianapolis, IN: Indiana Department of Transportation.
- Egashira, K., Miyazaki, M., Yamada, S., Yamashita, D., Isoda, M., Abe, T., & Inabe, V. (1999). Clay mineralogical composition of the Quaternary sediments collected in the North Coast of Ariake Bay, and the relation to depositional environment and weathering in the terrestrial condition. *Nendo Kagaku*, 39(2), 65–75.
- Fanning, D. S., Keramidas, V. Z., & El-Desoky, M. A. (1989). Micas. In J. B. Dixon & S. B. Weed (Eds.), *Minerals in soil environments* (pp. 551–634). Madison, WI: Soil Science Society of America.
- Fernandez, S. C. (1994). *Characterization of the engineering properties of Mexico City clay* (Master's thesis). Cambridge: Massachusetts Institute of Technology.
- Germaine, J. T., & Germaine, A. V. (2009). *Geotechnical laboratory measurements for engineers*. Hoboken, NJ: John Wiley and Sons, Inc.
- Germaine, J. T., & Ladd, C. C. (1988). State-of-the-art paper: Triaxial testing of saturated cohesive soils. In R. T. Donaghe, R. C. Chaney, & M. L. Silver (Eds.), *Advanced Triaxial Testing of Soil and Rock* (STP 977) (pp. 421–459). Philadelphia, PA: American Society for Testing and Materials. <http://dx.doi.org/10.1520/STP29091S>
- Hajimohammadi, A., Hosseini, S. M. M. M., & Cheshomi, A. (2010). Seismic piezocone interpretation for shear wave velocity (V_s) determination in the Persian Gulf. *Environmental Earth Sciences*, 61, 813–820.
- Hawkins, A. B., Lawrence, M. S., & Privett, K. D. (1988). Implications of weathering on the engineering properties of the Fuller's Earth formation. *Geotechnique*, 38(4), 517–532.
- Hegazy, Y. A., & Mayne, P. W. (1995). Statistical correlations between V_s and cone penetration data for different soil types. In *Proceedings of the international symposium on cone penetration testing (CPT '95)*: Vol. 2. Swedish Geotechnical Society Report, 3(95), 173–178. Linköping, Sweden.
- Holtz, R., & Kovacs, W. (1981). *An introduction to geotechnical engineering*. New Jersey: Prentice-Hall.
- Huang, P., Bobet, A., & Santagata, M. (2012). Identification of low-organic-content soils: an engineering approach. *Geotechnical Testing Journal*, 35(4), 596–606.
- Hwang, J. (2006). *Effects of cement treatment on the 1-D consolidation behavior of a highly organic soil* (Doctoral dissertation). West Lafayette, IN: Purdue University. Retrieved from <http://docs.lib.purdue.edu/dissertations/AAI3304583/>
- IDOT. (1999). *Geotechnical manual*. Springfield, IL: Illinois Department of Transportation.
- INDOT. (2010). *Geotechnical manual*. Indianapolis, IN: Indiana Department of Transportation.
- INDOT. (2014). *Standard specifications*. Indianapolis, IN: Indiana Department of Transportation.
- Islam, A. K. M. E., & Lotse, G. (1986). Quantitative mineralogical analysis of some Bangladesh soils with X-ray, ion exchange and selective dissolution techniques. *Clay Minerals*, 21, 31–42.
- Jackson, M. L. (1985). *Soil chemical analysis: Advanced course*. Madison, WI: Author.
- Jamiolkowski, M., Lancellotta, R., & Lo Presti, D. C. F. (1995). Remarks on the stiffness at small strains of six Italian clays. In *Pre-failure Deformation of Geomaterials, Vol 2* (pp. 817–836). Rotterdam, The Netherlands: AA Balkema.
- Jung, C. M., Bobet, A., & Siddiki, N. Z. (2011). Simple method to identify marl soils. *Transportation Research Record*, 2232, 76–84.
- Koppula, S. D. (1981). Statistical estimation of compression index. *Geotechnical Testing Journal*, 4(2), 68–73.
- Ladd, C. C. (1991). Stability evaluation during staged construction: 22nd Terzaghi lecture. *Journal of Geotechnical Engineering*, 117(4), 537–615.
- Ladd, C. C., & DeGroot, D. J. (2003). Recommended practice for soft ground site characterization: Arthur Casagrande Lecture. In *Proceedings of the 12th Pan-American conference on soil mechanics and geotechnical engineering: Vol. 1* (pp. 3–57).

- Ladd, C. C., & Foott, R. (1974). New design procedure for stability of soft clays. *Journal of Geotechnical Engineering*, 100(7), 763–786.
- Ladd, C. C., Foott, R., Ishihara, K., Schlosser, F., & Poulos, H. G. (1977). Stress-deformation and strength characteristics: SOA Report. In *Proceedings of the 9th International Conference on Soil Mechanics and Foundation Engineering, Tokyo: Vol. 2* (pp. 421–494).
- Lamas, F., Irigaray, C., & Chacon, J. (2002). Geotechnical characterization of carbonate marls for the construction of impermeable dam cores. *Engineering Geology*, 66(3–4), 283–294. [http://dx.doi.org/10.1016/S0013-7952\(02\)00048-0](http://dx.doi.org/10.1016/S0013-7952(02)00048-0)
- Lefebvre, G., Ladd, C. C., & Paré, J. J. (1988). Comparison of field vane and laboratory undrained shear strength in soft sensitive clays. In A. F. Richards (Ed.), *Vane shear strength testing in soils: Field and laboratory studies* (pp. 233–246). Philadelphia, PA: ASTM International.
- Long, M., & Lunne, T. (2003). Stiffness of Onsøy clay. In H. Di Benedetto, T. Donah, H. Geoffroy, & C. Sauzéat (Eds.), *Deformation characteristics of geomaterials* (pp. 151–158). Lisse, The Netherlands: Swets & Zeitlinger.
- Lunne, T., Berre, T., & Strandvik, S. (1997). Sample disturbance effect in soft low plasticity Norwegian clay. In *Proceedings of the conference on recent developments in soil mechanics, Rio de Janeiro* (pp. 81–102).
- Malla, P. B. (2002). Vermiculites. In J. B. Dixon & D. G. Schulze (Eds.), *Soil mineralogy with environmental applications* (pp. 501–525). Madison, WI: Soil Science Society of America.
- Marques, J. J., Teixeira, W. G., Schulze, D. G., & Curi, N. (2002). Mineralogy of soils with unusually high exchangeable Al from the western Amazon region. *Clay Minerals*, 37, 651–661.
- Mayne, P. W. (1995). CPT determinations of overconsolidation ratio and lateral stresses in clean quartz sands. In *Proceedings of the international symposium on cone penetration testing (CPT '95): Vol. 2. Swedish Geotechnical Society Report*, 3(95), 215–220. Linköping, Sweden.
- Mayne, P. W., & Rix, G. (1995). Correlations between shear wave velocity and cone tip resistance in natural clays. *Soils and Foundations*, 35(2), 107–110.
- Mayne, P. W. (2005). Integrated ground behavior: In-situ and lab tests. In *Deformation characteristics of geomaterials* (pp. 155–177). London, UK: Taylor & Francis.
- Mayne, P. W. (2006). Overview papers: In-situ test calibrations for evaluating soil parameters. In T. S. Tan, K. K. Phoon, D. W. Hight, & S. Leroueil (Eds.), *Proceedings of the second international workshop on characterisation and engineering properties of natural soils: Vol. 3* (pp. 1602–1652). Boca Raton, FL: CRC Press.
- Mesri, G., & Godlewski, P. M. (1977). Time- and stress-compressibility interrelationship. *Journal of Geotechnical Engineering*, 103(5), 417–430.
- Mesri, G., & Castro, A. (1987). The Ca/Cc concept and K₀ during secondary compression. *Journal of Geotechnical Engineering*, 113(3), 230–247.
- MDOT. (2009). *Uniform field soil classification system (modified unified description)*. Lansing, MI: Michigan Department of Transportation.
- Nishida, Y. (1956). A brief note on compression index of soils. *Journal of Soil Mechanics and Foundations Division, ASCE*, 82(SM3), 1027-1–1027-14.
- Obura, P. A. (2008). *Effect of soil properties on bioavailability of aluminum and phosphorus in selected Kenyan and Brazilian acid soils* (Doctoral dissertation). West Lafayette, IN: Purdue University. Retrieved from <http://docs.lib.purdue.edu/dissertations/AAI3344101/>
- ODOT. (2010). *Specifications for geotechnical explorations*. Columbus, OH: Ohio Department of Transportation.
- Ohtsubo, M., Egashira, K., Tanaka, H., & Mishima, O. (2002). Clay minerals and geotechnical index properties of marine clays in East Asia. *Marine Georesources and Geotechnology*, 20(4), 223–235. <http://dx.doi.org/10.1080/03608860290051921>
- Paaza, E. A., Lamas, F., Irigaray, C., & Chacon, J. (1998). Engineering geological characterization of Neogene marls in the Southeastern Granada Basin, Spain. *Engineering Geology*, 50(1), 165–175. [http://dx.doi.org/10.1016/S0013-7952\(98\)00008-8](http://dx.doi.org/10.1016/S0013-7952(98)00008-8)
- Piratheepan, P. (2002). *Estimating shear-wave velocity from SPT and CPT data* (Master's thesis). Clemson, SC: Clemson University.
- Purdue University. (2014). Isee—Integrating spatial educational experiences [Website]. Retrieved from isee.purdue.edu
- Rich, C. I., & Barnhisel, R. I. (1977). Preparation of clay samples for X-ray diffraction analysis. In J. B. Dixon & S. B. Weed (Eds.), *Minerals in soil environments* (pp. 797–808). Madison, WI: Soil Science Society of America.
- Robertson, P. K. (2009). Interpretation of cone penetration tests—A unified approach. *Canadian Geotechnical Journal*, 46(11), 1337–1355.
- Sadrekarami, J., Zekri, A., & Majidpour, H. (2006). *Geotechnical features of Tabriz marl* (IAEG 2006 Paper No. 335). London, UK: The Geology Society of London.
- Santagata, M. C. (1998). *Factors affecting the initial stiffness and stiffness degradation of cohesive soils* (Doctoral dissertation). Cambridge: Massachusetts Institute of Technology.
- Santagata, M. C., Sinfield, J. V., & Germaine, J. T. (2006). Laboratory simulation of field sampling: Comparison with ideal sampling and field data. *Journal of Geotechnical and Geoenvironmental Engineering*, 132(3), 351–362.
- Schmertmann, J. H. (1955). The undisturbed consolidation of clay. *Transactions, ASCE* 120, 1201–1233.
- Schmidt, B. (1966). Earth pressures at rest related to stress history. *Canadian Geotechnical Journal*, 3(4), 239–242.
- Schulze, D. G. (1984). The influence of aluminum on iron oxides. VIII. Unit-cell dimensions of Al-substituted goethites and estimation of Al from them. *Clays and Clay Minerals*, 32(1), 36–44.
- Shaqour, F. M., Jarrar, G., Hencher, S., & Kuisi, M. (2008). Geotechnical and mineralogical characteristics of marl deposits in Jordan. *Environmental Geology*, 55(8), 1777–1783. <http://dx.doi.org/10.1007/s00254-007-1128-5>
- Sheahan, T. C. (1991). *An experimental study of the time-dependent undrained shear behavior of resedimented Boston blue clay using automated stress path triaxial equipment* (Doctoral dissertation). Cambridge: Massachusetts Institute of Technology.
- Sheahan, T. C., & Germaine, J. T. (1992). Computer automation of conventional triaxial equipment. *Geotechnical Testing Journal*, 15(4), 311–322.
- Shibuya, S., Hwang, S. C., & Mitachi, T. (1997). Elastic shear modulus of soft clays from shear wave velocity measurement. *Géotechnique*, 47(3), 593–601.
- Skempton, A. W., & Northey, R. D. (1952). The sensitivity of clays. *Géotechnique*, 3(1), 30–53.
- Sykora, D. E., & Stokoe, K. H. (1983). Correlations of in-situ measurements in sands of shear wave velocity. *Soil Dynamic Earthquake Engineering*, 20(1), 125–136.

- Tavenas, F. P., Leblond, P. J., & Leroueil, S. (1983). The permeability of natural soft clays, part II: Permeability characteristics. *Canadian Geotechnical Journal*, 20(4), 645–660.
- Taylor, D. W. (1948). *Fundamentals of soil mechanics*. New York, NY: John Wiley & Sons, Inc.
- Terzaghi, K., & Peck, R. B. (1967). *Soil mechanics in engineering practice*. New York, NY: John Wiley & Sons, Inc.
- Tsiambaos, G. (1991). Correlation of mineralogy and index properties with residual strength of Iraklion marls. *Engineering Geology*, 30, 357–369.
- Velde, B. (1992). *Introduction to clay minerals: Chemistry, origins, uses and environmental significance*. London, UK: Chapman & Hill
- Weiler, W. A., Jr. (1988). Small strain shear modulus of clay. In *Earthquake engineering and soil dynamics II—Recent advances in ground-motion evaluation: Vol. 20* (pp. 331–345). New York, NY: American Society of Civil Engineers.
- Weir, A. H., Ormerod, E. C., & El Mansey, I. M. I. (1975). Clay mineralogy of sediments of the western Nile delta. *Clay Minerals*, 10, 369–386. <http://dx.doi.org/10.1180/claymin.1975.010.5.04>
- Wissa, A. E. Z., Christian, J. T., Davis, E. H., & Heiberg, S. (1971). Consolidation at constant rate of strain. *Journal of Soil Mechanics and Foundation Division*, 97(10), 1393–1413.
- Zhu, L. (2009). *An integrated study of steam-induced property changes of clay minerals* (Doctoral dissertation). Bloomington: Indiana University.

APPENDIX 1: MAPPING OF MARL IN INDIANA

A.1.1. INTRODUCTION

As discussed in the Introduction, marl is found in many locations in Indiana. Although the presence of marl deposits in Indiana is fairly widespread, the soil maps of Indiana rarely provide any information about marls. Also, having an understanding of the occurrence of such deposits could prove to be very useful because the possibility of encountering marl deposits while performing a future project can be considered. This appendix presents the mapping of the marl deposits in Indiana based on archived INDOT projects.

From the database of previous projects, locations where marl deposits are found are identified. The boreholes where marl was identified are represented on a map as points with latitude and longitude coordinates. The symbols are used in such a manner that the location can be filtered based on the calcium carbonate content of the soil, depth of the deposit and the data that is known about the soil deposit.

The map was created on ArcGIS 10.0, developed by esri, which is a Geographic Information System (GIS). GIS can be used to view, understand and visualize data which can reveal trends and patterns associated with it. The coordinate system that is used for this map is World Geodetic System 1984 (WGS 84). The WGS 84 represents the National Imagery and Mapping Agency's (NIMA) best geodetic model of the earth. The coordinate origin of WGS 84, which is the earth's center of mass, is modeled with an error less than 2 cm (Defense Science Board, 2000).

In addition to this Introduction, the appendix has three more sections. Section A.1.2 presents the classification system used for marl that is based on calcium carbonate content. Section A.1.3 discusses the approach and the details regarding the data that is represented in the marl map. Section A.1.4 provides an overview of the map and how to operate the map in ArcGIS.

A.1.2. CLASSIFICATION OF MARLS BASED ON CALCIUM CARBONATE CONTENT

As discussed in the introduction, marls are fine grained soils with significant calcium carbonate content. The Indiana Department of Transportation (INDOT) classifies fine grained soils into five groups based on the calcium carbonate content (INDOT, 2010). The classification system keeps intact the INDOT classification system in specs section 903 (INDOT, 2014). Table A.1.1 summarizes the five categories.

The term "soil" in Table A.1.1 is to be replaced by the classification of the soil obtained using INDOT specs section 903.02. For example, if a soil is classified as "silty loam" in accordance to 903.02 and the calcium carbonate content was in the range of 18%–25%, then the soil would be denoted as "silty loam with some marl." This classification is used in the mapping of marls throughout Indiana, which is discussed in the following sections.

A.1.3. APPROACH

The approach followed in creating the map is discussed in this section. The data that was used in mapping was obtained from the data of various projects that were performed by INDOT. The data were then classified into soils of various categories based on the classification system explained in Section A.1.2 and also on the availability of quantitative data. The map is then populated with the data in such a manner that soils falling into a particular category and depth can be easy to locate and visualize. Also the data associated with each data point can also be viewed as a pop-up window.

A.1.3.1 Data Collection

The database used for the mapping of marl was provided by INDOT. It consisted of borehole data for previous projects

TABLE A.1.1
Classification of marls based on calcium carbonate content

Classification	Calcium Carbonate Content (%)
Soil* with trace marl	1% < %CaCO ₃ < 9%
Soil* with little marl	10% < %CaCO ₃ < 17%
Soil* with some marl	18% < %CaCO ₃ < 25%
Marly soil (A-8)	26% < %CaCO ₃ < 40%
Marl (A-8)	%CaCO ₃ > 40%

*Soils classified in accordance with INDOT specs 903.02 shall also include this classification.

undertaken by INDOT. The database, which consisted of data from more than five thousand boreholes, was mined to identify the boreholes where marl was found. In total 325 boreholes were identified to contain marl. The latitude and longitude of the boreholes were used for locating them on ArcGIS. The data associated with each borehole is discussed in the next section.

The data that were obtained included the I-69 project as well as a number of other projects. The boreholes data associated with the I-69 project contained more information especially regarding the location data. From other projects, a number of boreholes did not have the location data required for mapping. In these cases the DES numbers of the boreholes were used to approximate their location. This was done as follows: The mile marker and location description were obtained from the SPMS feature class of INDOT; an arcGIS map, with the mile marker information for roadways in Indiana, provided an approximate location of the project; with the approximate location known, the start and end points of the project were identified using the location description. Some of the projects extended over a large area, which made the identification of the exact location of the borehole uncertain. For such cases, the midpoint of the project location was used as the location of all the boreholes associated with the project and a comment was placed in the borehole data (comments associated with each borehole are explained later).

The boreholes where marl was encountered are separated into six classes; the first five: soil with trace marl, little marl, some marl, marly soil and marl, depending on the content of carbonate present in the soil. The sixth class consists of soils where marl was identified without providing any qualitative or quantitative information as to which classification they fit into. The first five classes are further divided into two, depending on whether laboratory testing data was present or not. The class with laboratory data on calcium carbonate content has been named as "quantitative." In summary, there are a total of eleven groups: marl quantitative, marl qualitative, marly soil quantitative, marly soil qualitative, some marl quantitative, some marl qualitative, little marl quantitative, little marl qualitative, trace marl quantitative, trace marl qualitative and marl visual classification. For example, "marly soil quantitative" is the group of data for which the soil, from the corresponding borehole, has been tested and determined to have calcium carbonate content between 26% and 40%. This group of data named "qualitative" corresponds to those boreholes that provide a marl classification without laboratory tests.

A.1.3.2 Data Input

Each group is represented in the map as a separate layer. The data corresponding to each layer is saved as a Comma Separated Value (CSV) file. These files are then input into the map to form layers. A layer containing the boundary of the state of Indiana and the counties is also added to the map. The sections "File assignments to layers" and "Adding or editing data to the map" provide details on how to save the files and how to make edits to the data for each layer.

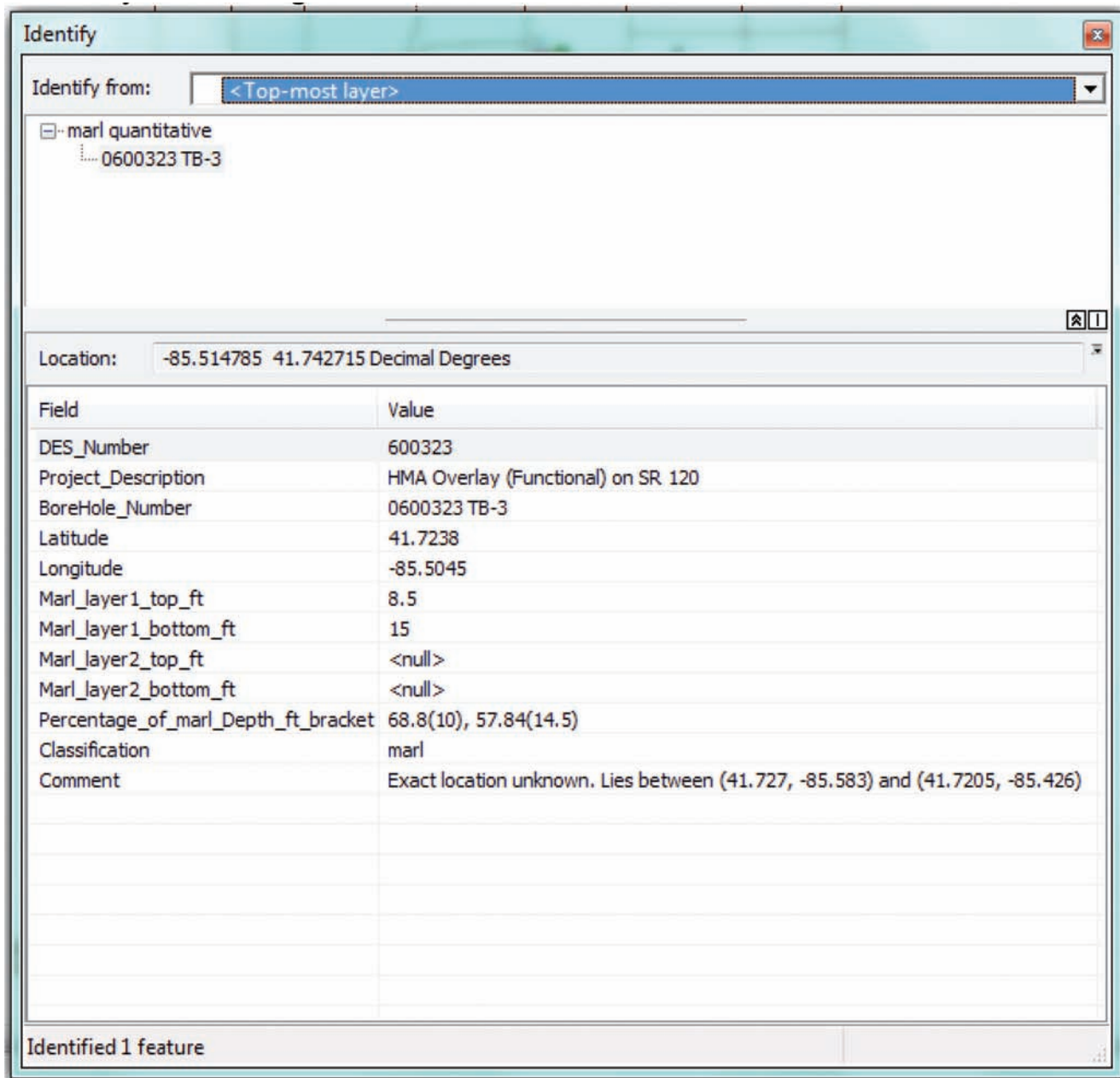


Figure A.1.1 Data associated with each borehole.

A.1.3.2.1 Data Associated with Each Borehole

Each point on the map represents a borehole where marl has been identified. Each borehole has information associated with it. The data associated with each borehole is discussed below using Figure A.1.1 as an illustrated example.

1. DES_Number: INDOT DES Number of the project.
2. Project_Description: Provides a brief description about the project (e.g., HMA Overlay (Functional) on SR 120).
3. BoreHole_Number: the borehole number that is selected.
4. Latitude & Longitude: in decimal degrees.
5. Marl_layer1_top_ft: Provides the depth (in feet) of the top of the first marl layer encountered in the borehole.
6. Marl_layer1_bottom_ft: Provides the depth (in feet) of the bottom of the first marl layer encountered in the borehole in feet.
7. Marl_layer2_top_ft: Provides the depth (in feet) of the top of the second marl layer encountered in the borehole (if any).
8. Marl_layer2_bottom_ft: Provides the depth (in feet) of the bottom of the second marl layer encountered in the borehole (if any).
9. Percentage_of_marl_Depth_ft_bracket: Provides the percentage of calcium carbonate content as determined from laboratory tests with the depth (in feet) of the tested layer in parenthesis. e.g., 68.8(10), 57.84(14.5) indicates that 68.8% and 57.84% calcium carbonate were obtained at depths of 10 and 14.5 ft respectively. This piece of information exists only for the layers with quantitative results.
10. Classification: Classifies the soil based on the marl content. In some cases soils are reported with a range in the classification (e.g., little to some marl indicates the marl content could lie anywhere between 10% and 25%).

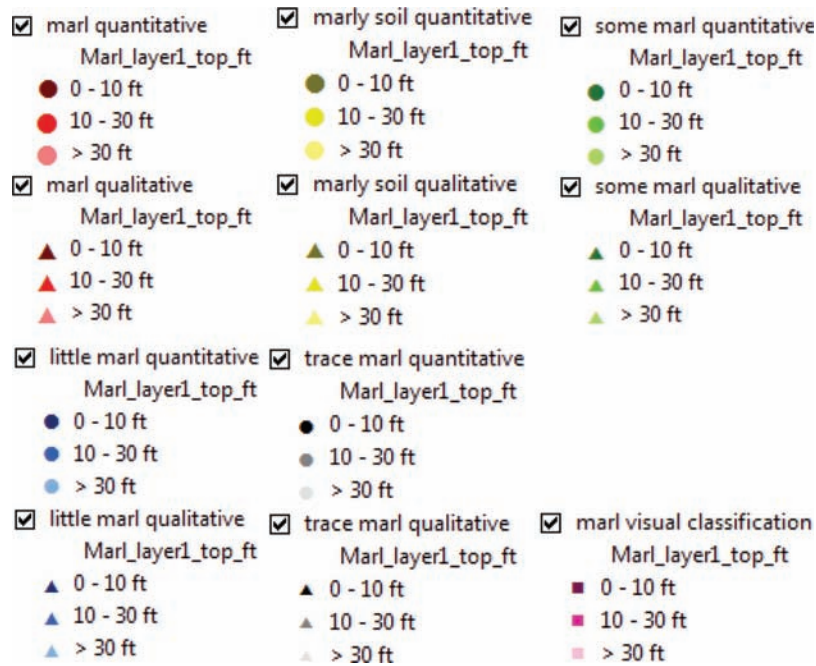


Figure A.1.2 Symbols associated with each layer.

11. Comment: Additional comments, if any.

Additional comments encompass the following scenarios:

1. The exact location of the borehole is unknown. In such case the midpoint of the project is used for representing the point shown on the map. The comment would indicate the start and end of the project.
2. The soil is classified visually. In such case the classification of marl is not known.
3. The marl encountered in the borehole exists as seams and thus the thickness of the marl layer is not significant.

A.1.3.3 Symbols

The symbols representing each borehole are selected in such a manner that the classification of the soil, the depth encountered and presence of laboratory results can be identified. The symbols used in the map are used to identify:

1. Whether a particular point has laboratory data or not. The points with quantitative data are represented by circles and the points with qualitative data by triangles. The locations, for which the classification is unknown (i.e., given by visual classification) are denoted by square symbols.
2. The classification of the soil based on the marl content. The variation in the marl content is distinguished by the size of the symbol and color. Larger symbols are used to represent higher marl content. The colors used to represent the various groups are: Red for marl, yellow for marly soil, green for some marl, blue for little marl and gray for trace marl.
3. The depth where marl has been identified. Each layer is divided into three groups based on the initial depth where marl was found: 0 – 10 ft, 10 – 30 ft and >30 ft. Depth is indicated in the map by color intensity. A darker color indicates that marl is found at shallower depth.

Figure A.1.2 represents the various symbols adopted, providing information about the presence of laboratory data,

classification of marl and the depth where marl is encountered. The eleven groups are distinguished by the color, shape and size of the symbol whereas the depth of the marl deposit is captured by the shade of the color.

A.1.4. THE MARL MAP OF INDIANA

A.1.4.1 Overview

Figure A.1.3 shows the map of Indiana with all the data points being represented (a total of 425 data points). Each of the eleven groups discussed in Section A.1.3.2 are represented as a layer and can be accessed under “Table Of Contents.” The data points belonging to a particular layer can be made visible by checking the box next to the corresponding layer. Each data point on the map is associated with a set of information displayed by clicking on the corresponding point. Since the database from the I-69 project was more comprehensive, the data points are concentrated in this particular stretch. The rest of the locations are scattered with the majority located in the northern parts of Indiana. The bulk of the boreholes with marl (Calcium carbonate content >40%) were located on the I-69 as well. It is from one of the sites on this stretch that the field testing and soil sampling was performed for this research, as will be discussed in Appendix 2.

A.1.4.2 Using the Map

A brief overview on how to operate the marl map is provided for those who are not familiar with the ArcGIS software.

A.1.4.2.1 File Assignment to Layers

This section discusses the procedure of inputting and assigning the data to layers in the GIS system. This information becomes important when any addition or modification is required on the existing data. While saving the files and the map, the following steps need to be performed to ensure that the files are assigned to the right layer:

1. The data that is used to generate the map is in comma-separated value (CSV) format, which can be opened with

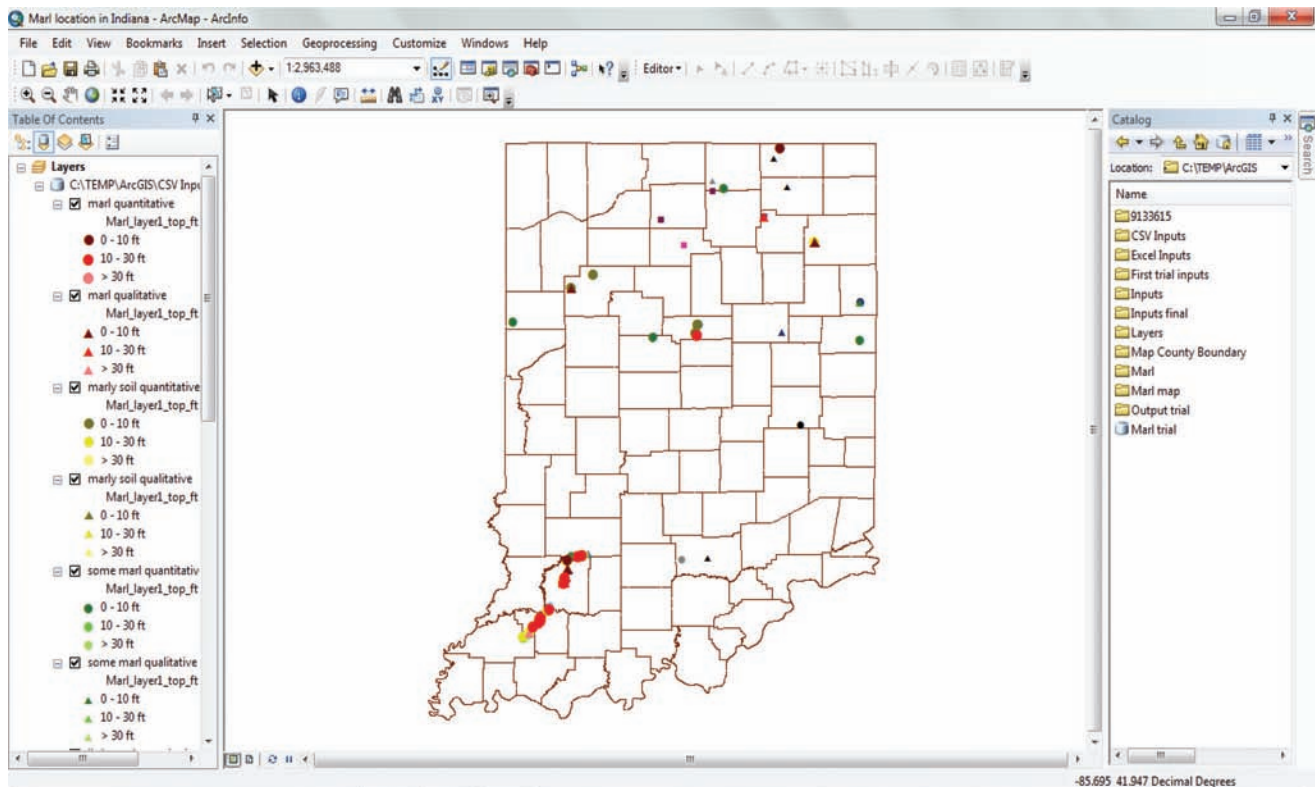


Figure A.1.3 Indiana map showing the location of marl deposits using ArcMap.

1. Excel. There are eleven such files in total; any modification to the data must be performed on the corresponding CSV file. These files must be then saved in the folder C:\TEMP\ArcGIS\CSV Inputs.
2. Save the map “Marl location in Indiana.mxd” in the folder C:\TEMP\ArcGIS\Marl map.
3. Open the map using ArcGIS Map 10.
4. The layers are listed in the table of contents on the left pane as shown in Figure A.1.4. Double click on one of the layers (e.g., top layer highlighted in blue in Figure A.1.4) to open the Layer Properties. Go to Layer Properties\Source\Set Data Source and select the corresponding CSV file for the layer. Repeat the procedure for other layers, as needed. This step is done to ensure whether the right file is assigned to each layer.

A.1.4.2.2 Operating the Map

Some of the important actions that might be required to operate the marl map are listed below:

1. To view the location of soils with a particular classification, check the box adjacent to the description to be displayed. Multiple boxes may be checked. An unchecked box means that this information is not displayed.
2. To view the data associated with a particular point on the map, select the  (Identify) icon on the top toolbar. Direct the pointer to the desired point and click on it. A popup window with the data associated with the point selected emerges, as shown in Figure A.1.5.
3. To add a new layer to the map, click on the  (Add Data) icon on the top toolbar and select the layer from the popup.

4. To modify the symbols of a layer, double click on the layer name in the “Table Of Contents” to open the “Layer Properties.” Go to Layer Properties\Symbology\ Quantities\ Graduated Colors to display the following popup screen. Double click on the symbol in the “symbol” list to open a “Symbol Selector” screen. Select the required shape, color and size of symbol. Figure A.1.6 shows the “Layer Properties” and the “Symbol Selector” screens.
5. For more help regarding the operation of arcGIS use the help menu on the toolbar.

A.1.4.2.3 Adding or Editing Data to the Map

In case where new data have to be added or when existing data need to be modified to include new information, the following must be done:

1. Open the CSV file associated with the corresponding layer.
2. Add points or make changes as required to the CSV file following the same format as the other data points. Save and close the file.
3. Toggle off the layer in the map and then toggle it on again to refresh the map. The edits made should now be included in the map.

If the layer doesn’t get updated, remove the corresponding layer and add the CSV file using the  (Add Data) icon. Right click on the file, in the “Table Of Contents,” and click “Add XY data.” Click “OK” to create a new layer.

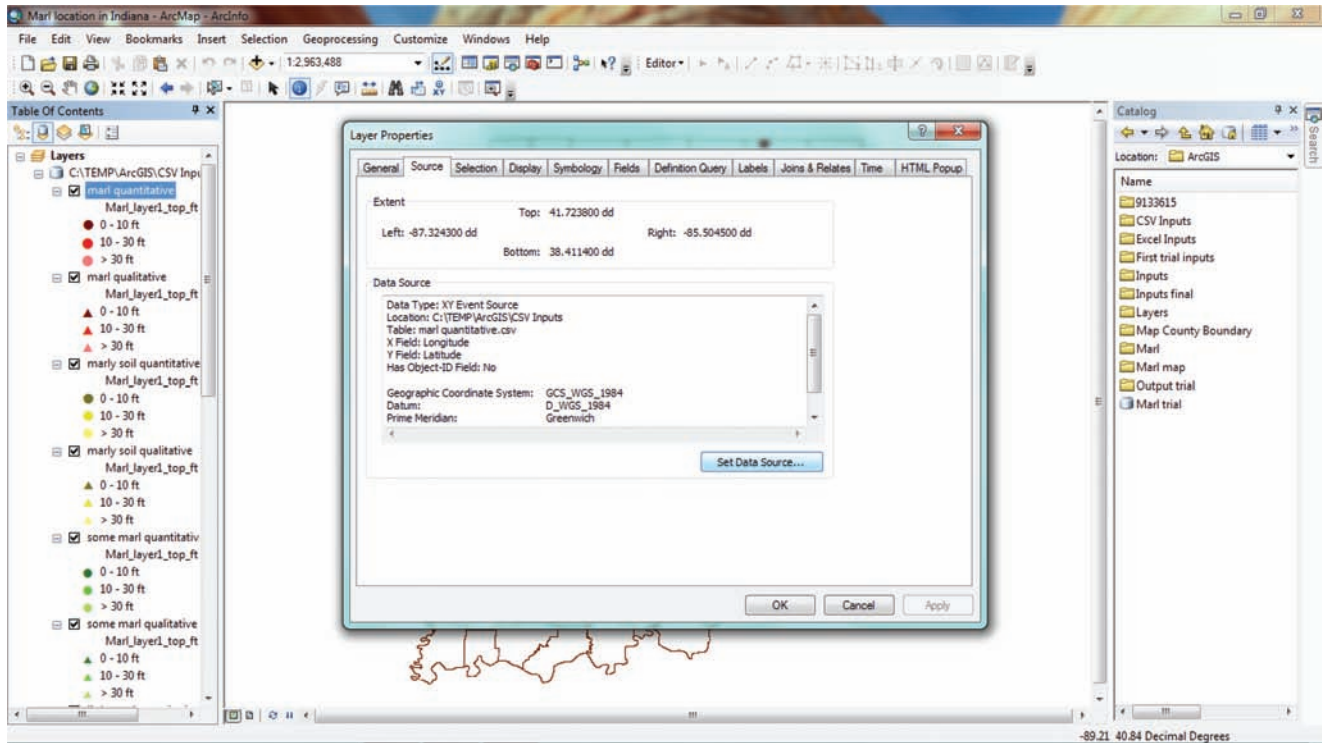


Figure A.1.4 Setting the data source for each layer.

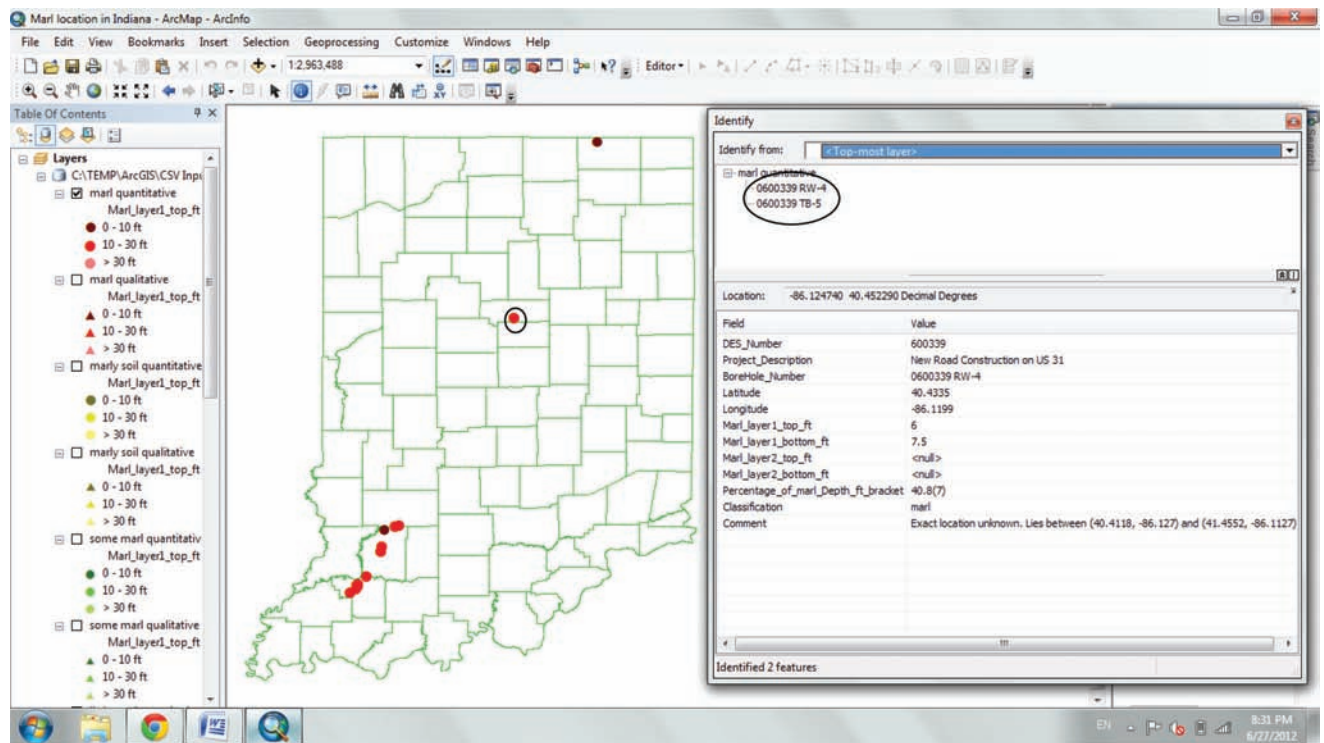


Figure A.1.5 Points of the layer “marl quantitative” are displayed. The information related to the circled borehole is displayed on the popup screen on the right. Two boreholes are listed in the top pane (circled) indicating that two boreholes overlap each other.

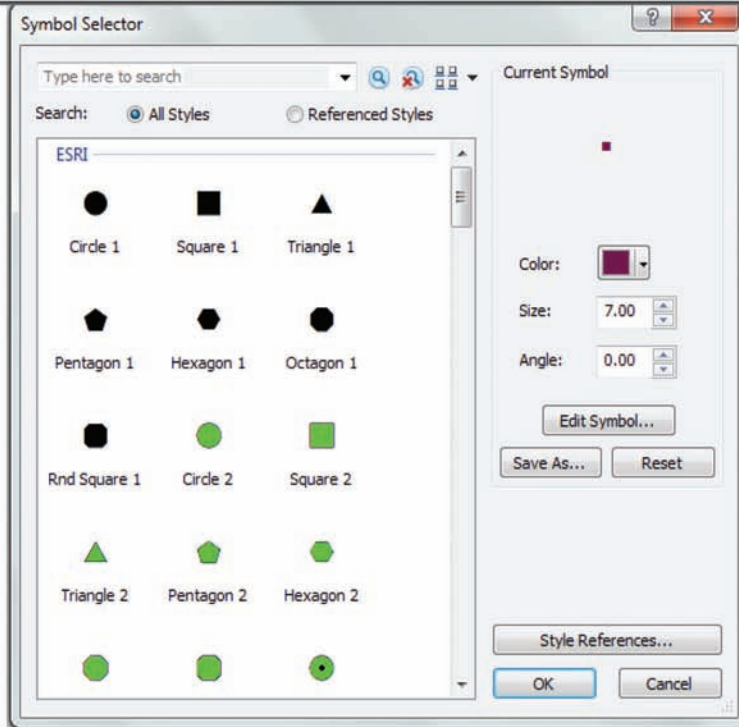
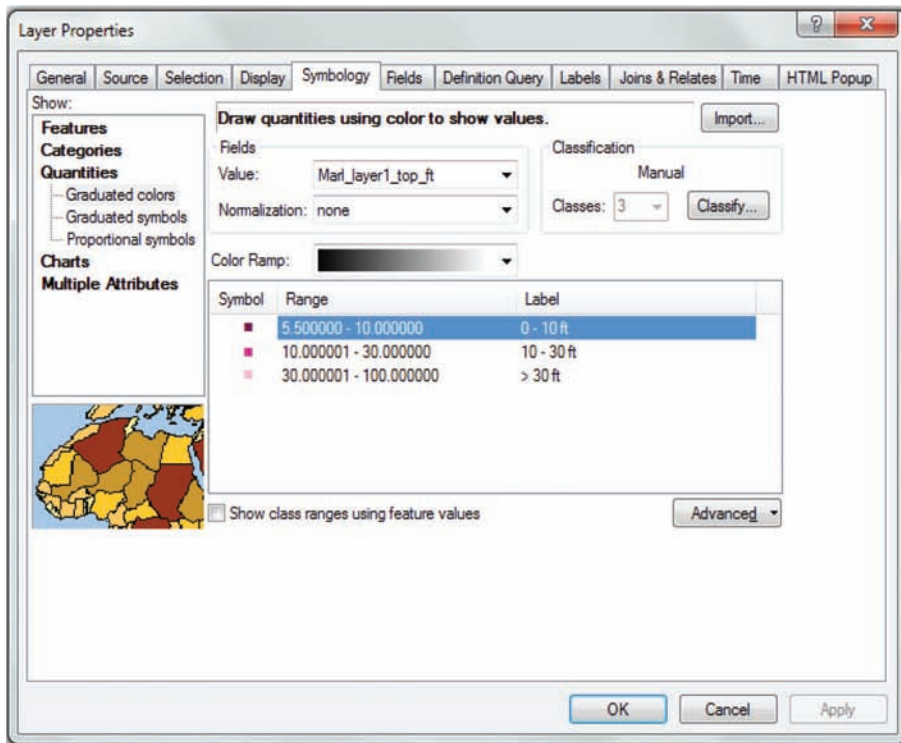


Figure A.1.6 Modifying the symbols of a layer.

APPENDIX 2: SITE CHARACTERIZATION AND FIELD TESTING PROGRAM

A.2.1. INTRODUCTION

Deposits of marl are encountered in the State of Indiana with layers as thick as 20', at relatively shallow depths (10–15') below the ground surface (Alt & Witzig, 2010; Earth Exploration, 2010). A site was selected in southwestern Indiana along the interstate I-69. The choice was based on the presence of marl deposits at shallow depths, the percentage of calcium carbonate present in the soil, as well as the ease of accessibility. This appendix provides the site characteristics and describes the field testing programs that were conducted as part of this research effort. Section A.2.2 describes the geographical location and soil profile, while Section A.2.3 deals with the sampling operations. An assessment of the quality of samples is briefly presented in Section A.2.4. The appendix concludes with a description of the field testing program (Section A.2.5) and of the field tests results (Section A.2.6).

A.2.2. GEOGRAPHICAL LOCATION AND SOIL PROFILE

The site is located at the intersection of County Road 900 E and County Road 1650 N, Madison, Daviess, Indiana about 85 miles southwest of Indianapolis (see Figure A.2.1).

The site is adjacent to a creek (First Creek), which controls the water table making it very close to the ground surface. The Integrating Spatial Educational Experiences (Purdue University, 2014) developed by the Agronomy department at Purdue University describes the site as “frequently flooded site” and this was confirmed on December 1, 2011 where the creek flooded and the water table was measured at only 1.37 m (4.5 ft) from the ground surface. The average ground elevation where sampling and in-situ tests were conducted was determined using a leveler as 150.84 m (494.88 ft). Figure A.2.2 illustrates the average soil profile determined based on observations made in the field as well

as examination of the samples used for the laboratory tests, which comprises about 1.9 m (~6.25 ft) of silty sand underlain by 1.5 m (~4.75 ft) of clayey silt and 2.7 m (~9 ft) of clay. At a depth of 6.1 m (~20 ft) the marl layer starts and extends by 4.3 m (~14 ft). A sand layer is encountered below the marl layer. The bedrock, mostly sandstone, was located at a depth of about 40 m (120 ft). The water table was located at 1.9 m (6.25 ft) below the ground surface using a 50.8 mm (2 in) diameter open pipe piezometer (see Section A.2.5.4).

A.2.3. SAMPLING OPERATIONS

A total of five boreholes were performed to collect undisturbed marl samples. Four boreholes were drilled using mud rotary, while the fifth was drilled using a hollow stem auger (see more details below). The first represents the best practice for sampling in soft soil (Ladd & DeGroot, 2003), while the latter was carried out as an example of the sampling practice that is routinely used in Indiana. Comparison of laboratory test results on samples obtained using these two methods provides an opportunity to explore the effect of the drilling method on sample disturbance. Figure A.2.3 shows the location of the borings with MR# denoting the borehole drilled using mud rotary and HSA# denoting the borehole drilled using hollow stem auger. The figure also shows the locations where field vane shear tests (FV#) and cone penetration tests (CPT#) were performed (see more details in Section A.2.5). Field testing and sampling were performed in close proximity to each other in order to minimize the effects of spatial variability and facilitate the comparison between field and laboratory results (the site is about 9 m × 7 m (30 ft × 23 ft)). Table A.2.1 summarizes the location of all the borings, field vane, piezometer and piezocones that were conducted in this research. Boring logs are attached in Appendix 6.

Continuous sampling was conducted from the ground surface to a depth of 15.24 m (50 ft). From 0 to 4.88 m (16 ft), a standard penetration test SPT was done and disturbed samples were collected from the split spoons and preserved in sealed containers and plastic bags. SPT plastic spring core

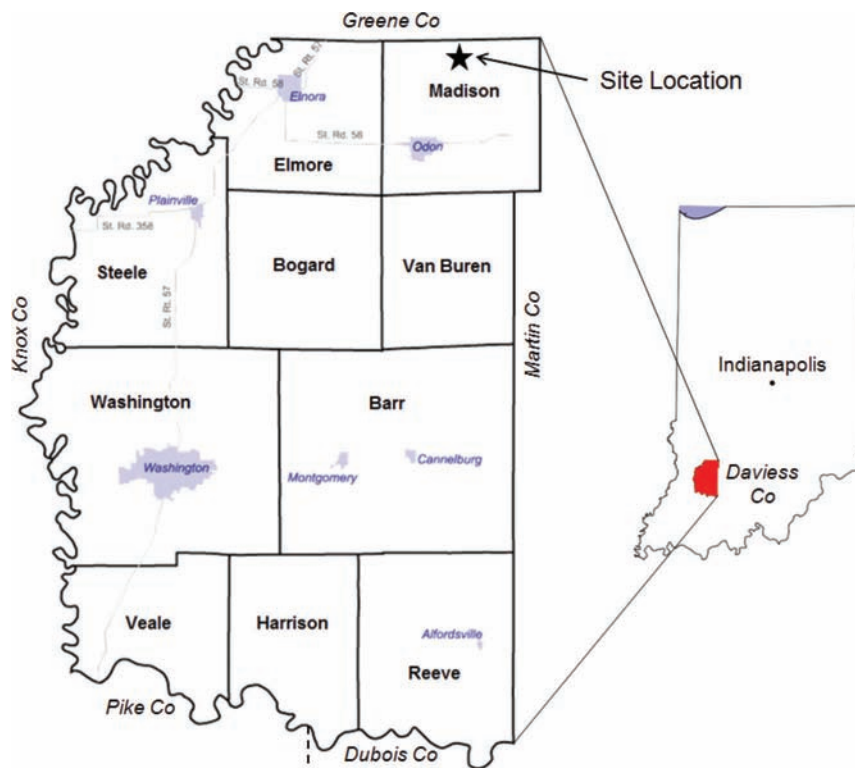


Figure A.2.1 Map of Daviess County (Indiana) showing the site location

TABLE A.2.1
Coordinates of borings, field vane, piezometer and piezocones

Boring no.	Latitude	Longitude
MR#1	38.898745	-86.990570
MR#2	38.898745	-86.990615
MR#3	38.898770	-86.990610
MR#4	38.898785	-86.990600
FV#1*	38.898770	-86.990570
HSA#1	38.898795	-86.990570
CPT#1	38.898770	-86.990595
CPT#2	38.898805	-86.990605
CPT#3†	38.898745	-86.990640
CPT#3A	38.898745	-86.990665
CPT#4	38.898759	-86.990640
CPT#5	38.898770	-86.990645
CPT#6	38.898781	-86.990635
CPT#7	38.898777	-86.990650

*FV#1 was also used to install an open pipe piezometer.

†CPT#3 was directly aborted due to the presence of some gravel below the piezocone.

catchers were used to retain the samples during retrieval. Shelby tubes were pushed between 4.88 m (16 ft) and 11.58 m (38 ft) where marl was found. For the last 3.66 m (12 ft) below the marl layer, the SPT was again performed and samples were collected and preserved in sealed containers and plastic bags. The purpose of conducting continuous sampling was to analyze the stratigraphy at the site and characterize the soil that is present above and below the marl layer. Figure A.2.4 shows the truck mounted drilling rig that was used to carry out the sampling and in-situ tests.

All the Shelby tubes were pushed with a fixed piston sampler to minimize sample disturbance. For very soft soils, it is very hard to collect undisturbed soil samples because they tend to fall out of the sampler. Under such conditions fixed piston sampler should be used which consists of a thin wall tube (i.e., Shelby tube) with a piston (shown in Figure A.2.5). The piston is first positioned at the bottom end of the thin wall tube and the sampler is lowered to the bottom of the borehole. The thin wall tube is pushed into the soil, past the piston. When the Shelby tube is filled, both tube and piston are pulled up. During the sampling process, the soil is in direct contact with the piston head, which, through a rubber packing (see Figure A.2.5(a)), applies a vacuum, keeping the

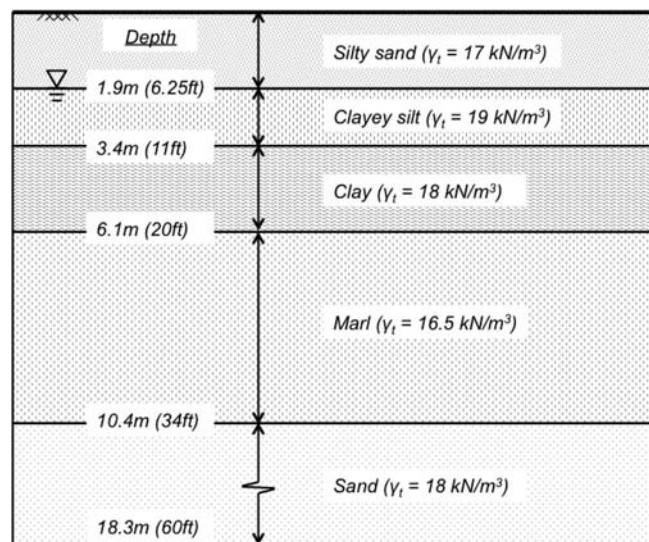


Figure A.2.2 Stratigraphy for the site.

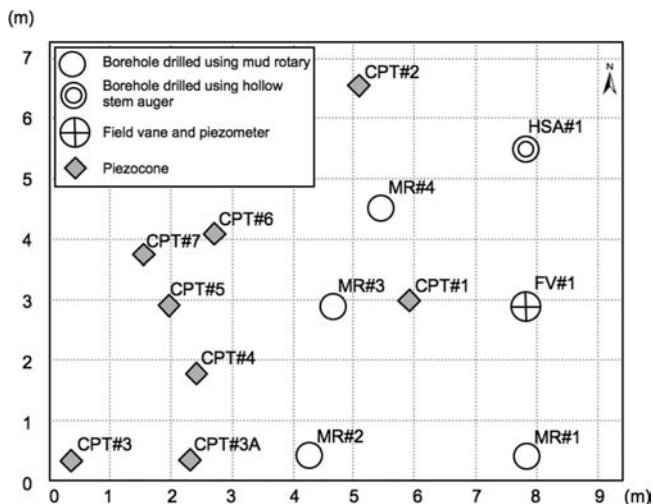


Figure A.2.3 Location of borings, piezometer, field vane, and piezocone tests (to scale).

sample from falling out of the sampler. Moreover, tubes with modified geometry were used to reduce the shear-induced strains during sampling. The modified Shelby tubes are 76.2 cm (30 in) long and have a diameter of 76 mm (3 in) with sharp edge (tapered from the outside) and an inside clearance ratio (ICR) of zero. Baligh, Azzouz, and Chin (1987) showed that during tube sampling, the soil at the centerline experiences shear in compression ahead of the tube, shear in extension while entering the tube and compression again when moving upward within the tube. The strain amplitude is dependent on the geometry of the tube increasing as the diameter to thickness ratio decreases. It is also affected by the geometry of cutting, and can be minimized using Shelby tubes with an ICR equal to zero because it prevents lateral expansion of the soil once inside the tube (e.g., Clayton, Siddique, & Hopper, 1998).

Two methods were used for advancing the borehole: (1) hollow stem auger and (2) mud rotary. In both cases the power for drilling is delivered by the truck mounted drilling rig (Figure A.2.4). Four boreholes were drilled with mud rotary whereas the fifth one was drilled using a hollow stem auger. For the first method, hollow stem augers with diameter equal to 82.55 mm (3.25 in) and length of 1.52 m (5 ft) were used. A cutter head (Figure A.2.6(c)) is attached to the tip of the auger (also referred to as "lead auger") while the other end is connected to the drive cap of the drilling rig (Figure A.2.6(b)). During the drilling operation (Figure A.2.6(a)), section after section of auger (1.52 m (5 ft) each) is added and the hole extends downward. A center bit is attached to the bottom of the auger by means of a center rod which helps keep the inside of the hollow augers clean, and loose soil from the bottom of the hole is brought to the surface by the flights of the augers. When soil samples are needed, the center rod is raised with the auger in place and the center bit is replaced by the sampler. Drilling mud (bentonite slurry) was used at all time to avoid heave of the soil at the bottom of the borehole caused by the upward water flow. The second method of advancing boreholes is mud rotary. In this method, the soil is drilled by means of rotary blades, also referred to as drilling bits, (Figure A.2.7(b)) attached to a drilling rod. Drilling mud (a slurry of water and bentonite) is forced down the drilling rods and the return flow forces the soil cuttings to rise in the drill hole and overflow at the top of the casing through a T connection (Figure A.2.7(a)). When soil samples are needed, the drilling rod is raised and the rotary blade is replaced by the sampler.

The first 4.27 m (14 ft) of soil was drilled the same way for all the five boreholes. Hollow stem augers (82.55 mm (3.25 in) diameter) were used to form the casing for the borehole. Three augers were inserted (1.52 m (5 ft) each) until reaching a depth of 4.27 m (14 ft) (0.3 m (1 ft) was left above the ground surface). At a depth of 4.88 m (16 ft), the fixed piston was positioned at the



Figure A.2.4 (a) Truck mounted drilling rig and (b) rig control panel.

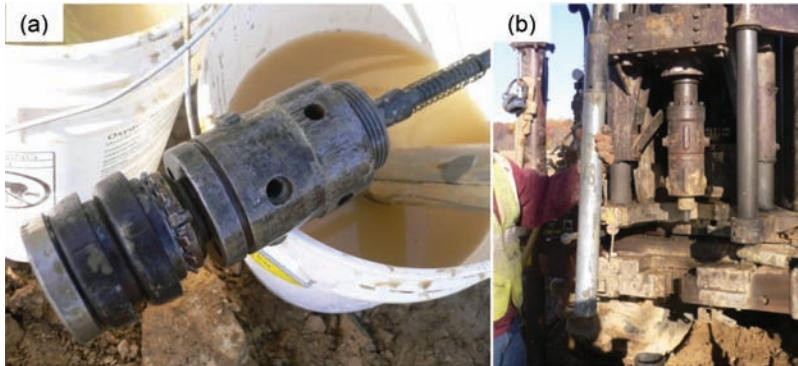


Figure A.2.5 Fixed piston sampler: (a) fixed piston and (b) piston mounted on Shelby tube.



Figure A.2.6 Hollow stem auger: (a) drilling with continuous-flight augers, (b) auger flight and drive cap of the drilling rig and (c) cutter head.

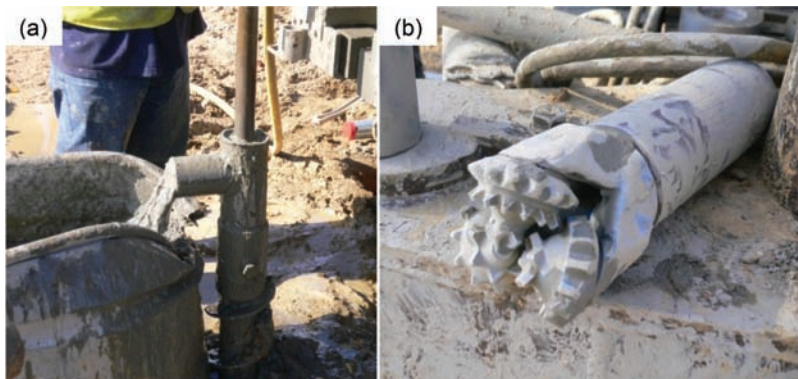


Figure A.2.7 Mud rotary: (a) T connection (b) rotary blades.

bottom end of the Shelby tube and then inserted in the borehole (see Figure A.2.5). Once the desired sampling depth was reached, the sampling tube was advanced ahead of the piston followed by a waiting period of ten minutes; which is necessary to improve sample recovery for soft saturated clays as reported by ASTM D6519-08 (ASTM, 2008a). The tube was then rotated several times to ensure shearing along the bottom surface, and the sampler was retracted, initially at a very slow rate to allow the sample to break from the ground; this is also consistent with ASTM D6519-08 (ASTM, 2008a). The tubes were then waxed and sealed with plastic caps and duct tape at both ends and transported in vertical position to Purdue's geotechnical laboratory. They were stored vertically in a humid room at a constant temperature of 10°C and 100% relative humidity to prevent soil drying.

A.2.4. SAMPLING PROGRAM

A total of 53 Shelby tubes (ST) (76.2 cm (30 in) long and 76 mm (3in) in diameter) were obtained from the sampling operations for depths ranging between 4.9 m (16 ft) and 11.6 m (38 ft). The soil samples retrieved are ~61 cm (24 in) long since the fixed piston occupies the first top 15.2 cm (6 in) of the ST. Figure A.2.8 summarizes the samples collected in each boring. Different symbols are used to indicate differences in the sampling operations. Specifically, ellipses denote ST with machined edges (i.e., zero inside clearance ratio (ICR—see Section A.2.3)), while dashed ellipses identify the two samples obtained using the two non-machined tubes, which were pushed at depths between 4.3 m (14 ft) and 4.9 m (16 ft) [MR#3 ST1] and between 9.1 m (30 ft) and 9.8 m (32 ft) [MR#4 ST8]. These samples were obtained in order to examine the effect of the ICR on sample disturbance. Finally, a double ellipse is used for the single sample [MR#4 ST7], which was pushed without a fixed piston. Note that this procedure resulted in zero recovery, demonstrating the importance of using a fixed piston when sampling soft soils.

Figure A.2.8 also provides an indication of the degree of disturbance of all ST, based on the degree of recovery, and observations made during sampling and transportation (a quantitative assessment of disturbance was also performed from the results of laboratory tests and is presented in Section A.4.3.8). Specifically, as described in the legend of the table, different colors are used to indicate different degrees of recovery (green, yellow and red for full, incomplete and no recovery, respectively), whereas samples that incurred disturbance during sampling due to problems with the piston (fixed piston was stuck because of the usage of the wrong screw) or during transportation (ST was bent because of the wire that was used to fix it during transportation) are identified with the colors brown and blue.

The table also shows the location of the split spoon (disturbed) samples (SS), which were collected from the soil above and below the marl layer. Between 0 and 4.9 m (16 ft), a total of 30 SS samples were obtained from MR#1, MR#2, HAS#1 and FV#1. From 11.6 m (38 ft) to 15 m (50 ft), a total of 16 SS samples were obtained from MR#1, MR#2, and MR#4. 1 SS sample was obtained from 10.4 m (34 ft) to 11 m (36 ft) [MR#1 SS8]. The locations of the vane shear tests conducted in boring FV#1 are included in the last column of Figure A.2.8 and are denoted by hexagons.

A.2.5. FIELD TESTING PROGRAM

One of the major tasks in this project was to conduct field tests that would complement the laboratory testing program. The in-situ testing program included: seismic cone penetration tests with pore pressure measurements (SCPTu), standard penetration tests (SPT) for soil profiling and collection of disturbed samples, and field vane (FV) shear tests to determine the undrained shear strength and soil sensitivity profile. Additionally, an open pipe piezometer was installed to locate the water table and conduct field hydraulic conductivity measurements.

A.2.5.1 Seismic Cone Penetration Tests (SCPTu)

A total of seven CPTs were conducted at the site for profiling the stratigraphy, and deriving tip resistance, skin friction, shear wave profiles with depth and measuring pore pressure dissipation. Three CPTs (CPT#1, CPT#2 and CPT#7) were conducted continuously up to a depth of 18.3 m (60 ft) at a constant rate of 20 mm/sec. Two CPTs (CPT#4 and CPT#5) were used to obtain the shear wave profiles with depth. At one-meter intervals, a surface shear wave was generated using a hammer (see Figure A.2.9) and the shear wave arrival times were recorded by a geophone in the cone. The last two CPTs (CPT#3A and CPT#6) were performed to conduct porewater dissipation tests. For each hole, four dissipation tests were conducted in the marl layer (increments of 1.5m (5ft)). Figure A.2.10 shows the assembly of the penetrometer before running the CPT; silicone gel was used for saturating the pressure transducer.

A.2.5.2 Standard Penetration Test (SPT)

SPTs were performed in the soil above and below the marl layer and were used for soil profiling, as described in Section A.2.3 (see Figure A.2.11). Disturbed samples retrieved from the split spoons were collected and preserved in sealed containers and plastic bags for index testing. All the samples were stored in a humid room at a constant temperature of 10°C and 100% relative humidity. Plastic spring core catchers were used to retain the sample during retrieval (Figure A.2.12). In order to have continuous sampling with 609.6 mm (2 ft) long split spoons, the sample tube was driven 609.6 mm (2 ft) into the ground and the number of blows needed for the tube to penetrate each 152.4 mm (6 in) was recorded. Thus, consistent with ASTM D1586-11 (ASTM, 2011), four intervals are obtained but only the top three are used to calculate the standard penetration resistance (N-value).

A.2.5.3 Field Vane Shear Test

In addition to the CPT, the field vane (FV) shear test is commonly used to determine the undrained shear strength of soft soil deposits. A separate borehole was drilled for the field vane shear test. Hollow stem augers (107.95 mm (4.25 in) diameter) were used to form the casing for the borehole. Note that an auger diameter larger than the one used for the other tests described in Section A.2.3 was utilized so that the vane shear blades could fit in the borehole. Figure A.2.13 shows the geometry of the field vane (both ends tapered) as well as the minimum and maximum dimensions required by ASTM D2573-08 (ASTM, 2008b). Three augers were inserted (1.52 m (5 ft) each) to form the casing until reaching a depth of 4.27 m (14 ft) (0.3 m (1 ft) was left above the ground surface, which is needed to install the sub and the force arm of the vane shear, see Figure A.2.14(a)). Drilling mud (bentonite slurry) was used at all time to avoid heave of the soil at the bottom of the borehole caused by the upward water flow. Ball bearing guide couplings, shown in Figure A.2.14(b), were used every 3 m (10 ft) to keep the drilling rod and vane in the center of the borehole. Figure A.2.15 summarizes the steps that were followed during the test. At a depth of 4.88 m (16 ft), the vane shear was inserted 0.6 m (2 ft) into the undisturbed soil; this is consistent with ASTM D2573-08 (ASTM, 2008b), in which it is recommended that the depth of penetration be at least 5 times the hole diameter, $5 \times 0.11 \text{ m} = 0.54 \text{ m}$ ($5 \times 4.25 \text{ in} = 21.25 \text{ in}$); also consistent with ASTM D2573-08 (ASTM, 2008b), the vane shear test was conducted by rotating the vane at 0.1 °/sec to obtain the peak strength. Ten full revolutions were then performed at high rate to free the vane; an additional test was conducted to determine the remolded undrained shear strength, which was used later to calculate the soil's sensitivity. Following the second measurement, the center rod was raised and the vane replaced by a split spoon sampler to collect the disturbed soil at the depth of the test. The marl layer was tested every 0.61 m (2 ft) from 4.88 m (16 ft) to 11.58 m (38 ft).

Depth		MR#1	MR#2	MR#3	MR#4	HSA#1	FV#1
(m)	(ft)						
0.6	2	SS1	SS1	-	-	SS1	SS1
1.2	4	SS2	SS2	-	-	SS2	SS2
1.8	6	SS3	SS3	-	-	SS3	SS3
2.4	8	-	SS4	-	-	SS4	SS4
3.0	10	SS4	SS5	-	-	SS5	SS5
3.7	12	SS5	SS6	-	-	SS6	SS6
4.3	14	SS6	SS7	-	-	SS7	SS7
4.9	16	SS7	SS8	ST1	-	SS8	FV0
5.5	18	ST1	ST1	ST2	ST1	ST1	FV1
6.1	20	ST2	ST2	ST3	ST2	ST2	FV2
6.7	22	ST3	ST3	ST4	ST3	ST3	FV3
7.3	24	-	ST4	ST5	ST4	ST4	FV4
7.9	26	ST4	ST5	-	ST5	ST5	FV5
8.5	28	ST5	ST6	ST6	ST6	-	FV6
9.1	30	ST6	ST7	ST7	ST7	ST6	FV7
9.8	32	ST7	ST8	ST8	ST8	ST7	FV8
10.4	34	ST8	ST9	ST9	ST9	ST8	FV9
11.0	36	SS8	ST10	ST10	ST10	ST9	FV10
11.6	38	ST9	-	ST11	ST11	ST10	FV11
12.2	40	SS9	ST11	-	ST12	-	-
12.8	42	SS10	SS9	-	SS1	-	-
13.4	44	SS11	SS10	-	SS2	-	-
14.0	46	SS12	SS11	-	SS3	-	-
14.6	48	SS13	SS12	-	SS4	-	-
		SS14	SS13	-	SS5	-	-

SS	Split spoon	●	Undisturbed - full recovery
ST	Shelby tube	●	Undisturbed - incomplete recovery
ST	Shelby tube (not machined)	●	No recovery
FV	Field vane shear test	●	Disturbed (fixed piston stuck)
○	Fixed piston was not used	●	Disturbed (ST bent during transportation)

Figure A.2.8 Quality of samples collected.

A.2.5.4 Open Pipe Piezometer and Field Hydraulic Conductivity Measurements

At the end of the field vane shear test, a 50.8 mm (2 in) diameter open pipe piezometer was installed with the perforated pipe located at the bottom of the marl layer between 9.1 m (30 ft) to 10.7 m (35 ft). Figure A.2.16 shows all the details about the

pipe installation, sand filter and bentonite sealant. The water was pumped twice from the tube and the water level was measured at different time intervals while rising in the tube to measure the hydraulic conductivity. A final reading was taken when the water level stabilized (after two weeks) to locate the ground water table. It was found to be located 1.9m (6.25ft) below the ground surface.



Figure A.2.9 Generation of a surface shear wave using a hammer.



Figure A.2.11 Standard penetration test (SPT).

A.2.6. FIELD TESTS RESULTS

The following section presents the basic results for the field tests described in Section A.2.5. Further analysis of the field results is provided in Appendix 5, which deals with integration of laboratory and field data.

A.2.6.1 Seismic Cone Penetration Test (SCPTu)

A.2.6.1.1 Seismic Piezocone Tests

The tip resistance, the skin friction and the pore water pressure variation with depth are summarized in Figure A.2.17. The figure shows the data for the seven CPTs (dashed gray lines) as well as the average values (continuous black line). Refer to Appendix 7 for the Piezocone penetration profiles obtained at different locations. High permeability layers, such as sand and silty sand layers, are characterized by a high tip resistance (q_t) and sleeve friction (f_s), and Porewater pressure (u_2) close to the hydrostatic value (u_0). Low permeability layers, such as marl and clay layers, are characterized by a low q_t and f_s , and a high u_2 . The average CPT results show that there is a very soft layer ($q_t \sim 500$ kPa and $f_s \sim 7$ kPa) at a depth ranging between 4.9 m (16 ft) and 11.6 m (38 ft) from which undisturbed Shelby tubes were obtained.

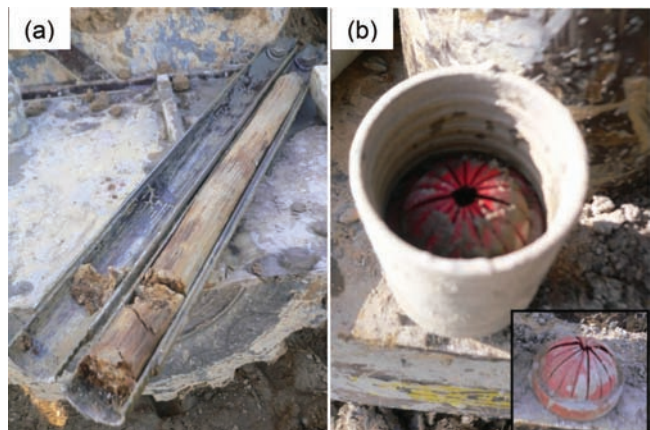


Figure A.2.12 (a) Split-spoon sampler (b) plastic spring core catcher.

A.2.6.1.2 Shear Wave Tests

Two CPTs (#4 and #5) were performed to derive the shear wave profiles with depth. At one-meter intervals, a shear wave was generated at the surface and the shear wave arrival times were recorded by a geophone located in the piezocone. Figure A.2.18 and Figure A.2.19 show the shear wave arrival traces for CPT#4

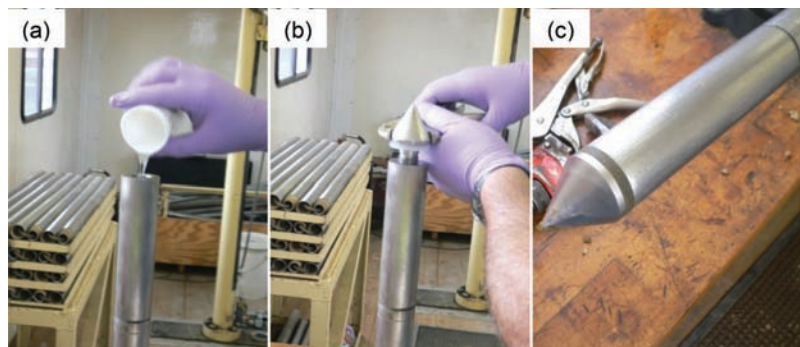


Figure A.2.10 (a) Saturation of pressure transducer, (b) piezocone head, and (c) piezocone filter.

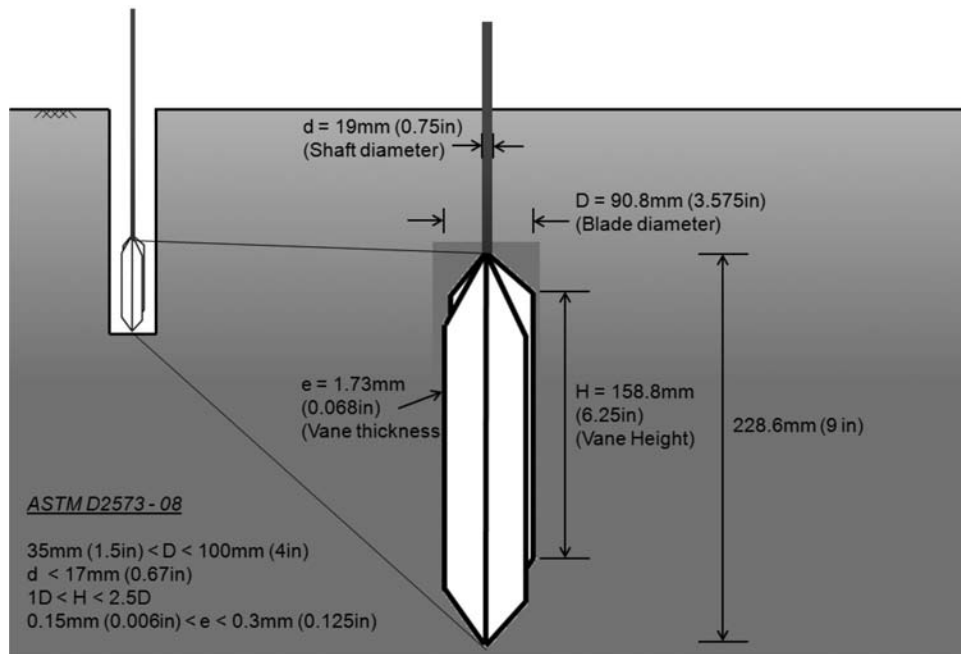


Figure A.2.13 Field vane geometry.

and CPT#5, respectively. The shear wave velocity was calculated from the arrival times as described in ASTM D7400-14 (ASTM, 2014b), and the shear modulus was derived using the relation $G_{max} = \rho V_s^2$; where G_{max} is the shear modulus, ρ is the density of the soil (shown in Figure A.2.2.), and V_s is the shear wave velocity. The resulting profiles are shown in Figure A.2.20. The figure shows that the marl layer (between 4.9 m (16 ft) and 11.6 m (38 ft)) has an average shear wave velocity equal to 155 m/s and an average shear modulus equal to 40 MPa. These are values typical of soft clays (e.g., Boston Blue Clay (Weiler, 1988), Bothkennar clay (Shibuya, Hwang, & Mitachi, 1997), and Onsoy clay (Long & Lunne, 2003)).

A.2.6.2 Standard Penetration Test (SPT)

SPTs were performed on the soil above and below the marl layer for soil profiling. Figure A.2.21 summarizes the values of the standard penetration resistance (N-values) obtained as a function of depth based on ASTM D1586-11 (ASTM, 2011). The figure shows the SPT N-values obtained from five boreholes (hollow black diamonds) as well as the average values (continuous red line). The top silty sand layer (described in Figure A.2.2) has N-values ranging between 5 and 15; N-values decrease to 0–5 for the clayey silt layer and clay layer below. For the sand layer beneath marl, N-values range between 5 and 25.

A.2.6.3 Field Vane Shear Test

The field vane (FV) is widely used in-situ test for evaluating the undrained shear strength of soft soil deposits. Figure A.2.22 shows the curves of shear stress versus rotation for the test conducted at a depth between 6.7 m (22 ft) and 7.3 m (24 ft). The figure shows two curves: one for the first measurement from which the peak undisturbed shear strength is derived (presented in hollow squares); the second used to obtain the remolded shear strength (presented in solid squares). The peak and remolded strengths are computed using the relationship for both ends tapered vanes

reported in ASTM D2573-08 (ASTM, 2008b):

$$S_u(FV) = \frac{12T_{max}}{\pi D^2 \left(\frac{D}{\cos(i_T)} + \frac{D}{\cos(i_B)} + 6H \right)}$$

where $S_u(FV)$ is the undrained shear strength from the vane (peak or remolded); T_{max} is the maximum value of measured torque; D is the vane diameter; H is the height of vane; and i_T and i_B are the angle of taper at vane top and bottom respectively (Figure A.2.22). The marl layer was tested every 0.6 m (2 ft) from 4.9 m (16 ft) to 11.6 m (38 ft). The data of undisturbed shear strength and remolded strength are summarized in Figure A.2.23(a). Refer to Appendix 8 for the complete results of all field vane tests conducted at various depths. Note that results of FV tests are not corrected for strain rate and anisotropy effects (Bjerrum, 1972); refer to Section A.5.2 for such correction.

Figure A.2.23(a) shows that the undrained shear strength varies between 25 kPa and 50 kPa, which is typical for soft clays. The sensitivity with depth is shown in Figure A.2.23(b); this parameter is calculated as the ratio between the undisturbed and the remolded undrained shear strength. The figure shows that the sensitivity value of marl is about 5.0 on average, with the exception of one test (FV5) conducted at depth ~7.8 m (25.5 ft); it is believed that the lower



Figure A.2.14 (a) Force arm and sub mounted on the casing (b) ball bearing guide coupling.

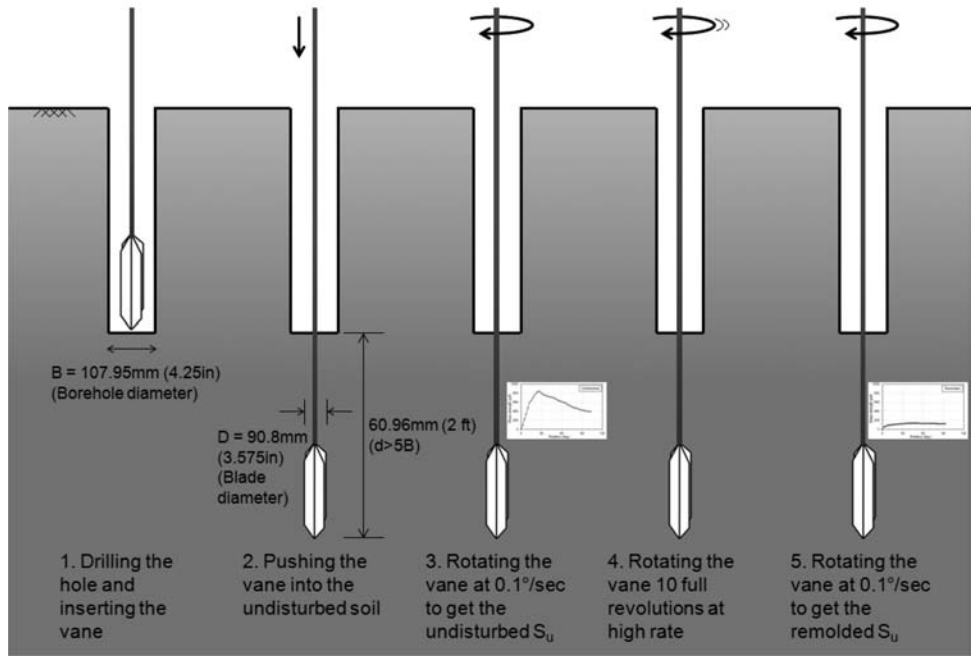


Figure A.2.15 Stages of the field vane shear test.

$S_u(FV) \sim 18$ kPa and the higher sensitivity ~ 10 at this depth are caused by the presence of a more sensitive soil within the marl layer (further discussion about this is presented in Section A.5.2). Thus the marl deposit can be considered a “sensitive” soil based on the

sensitivity scale reported by Skempton and Nortey (1952) or a “very sensitive” soil based on Bjerrum (1954). Note that field vane test is not applicable for sandy soils and the last two tests conducted in the bottom sand layer should be regarded with caution.

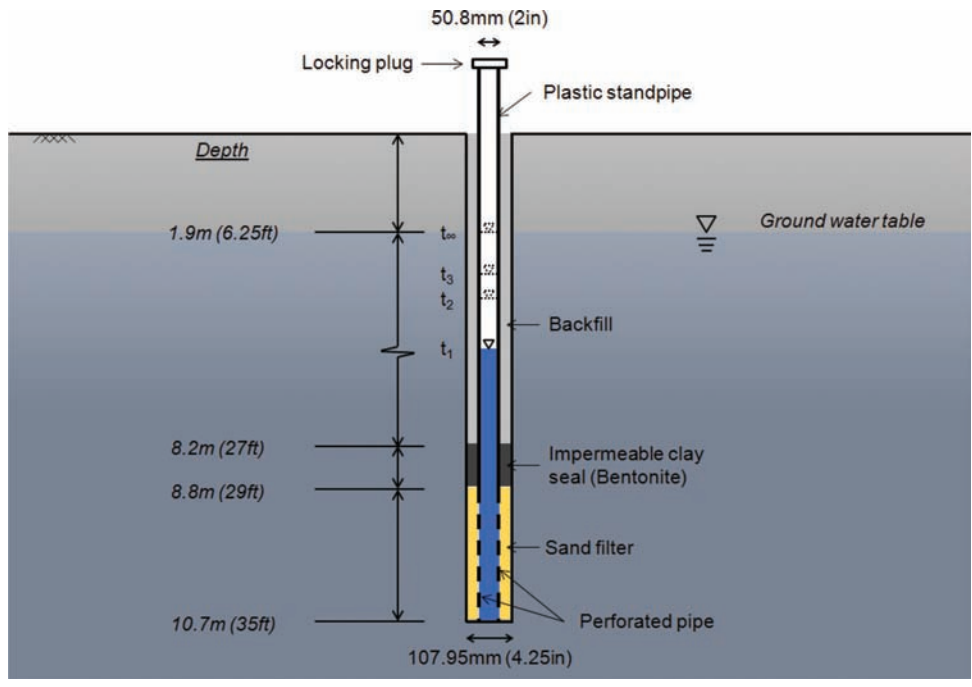


Figure A.2.16 Details of installation of open pipe piezometer.

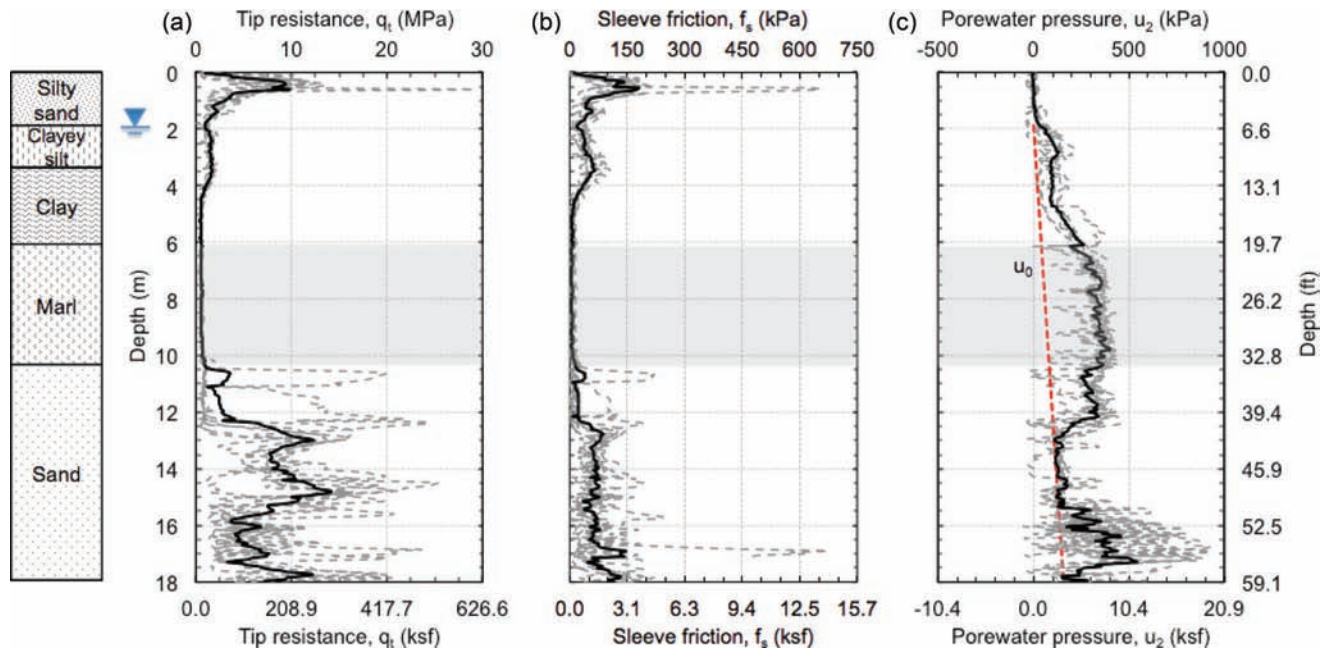


Figure A.2.17 CPT results: (a) tip resistance, (b) skin friction, and (c) porewater pressure versus depth.

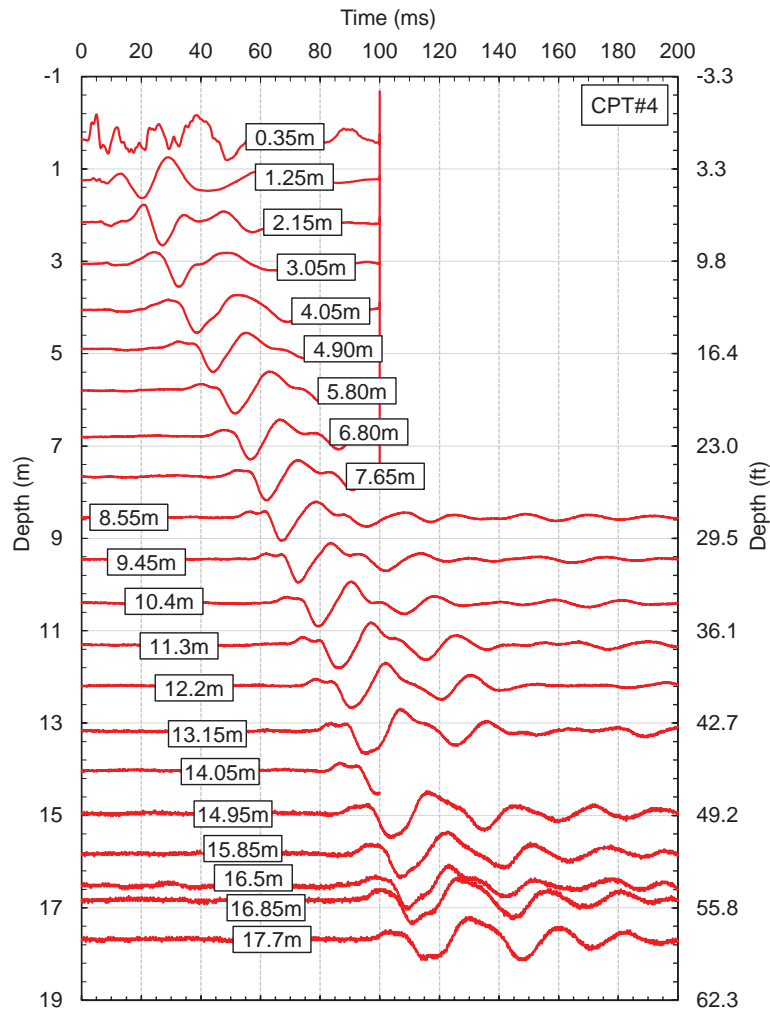


Figure A.2.18 Shear wave arrival traces for CPT#4.

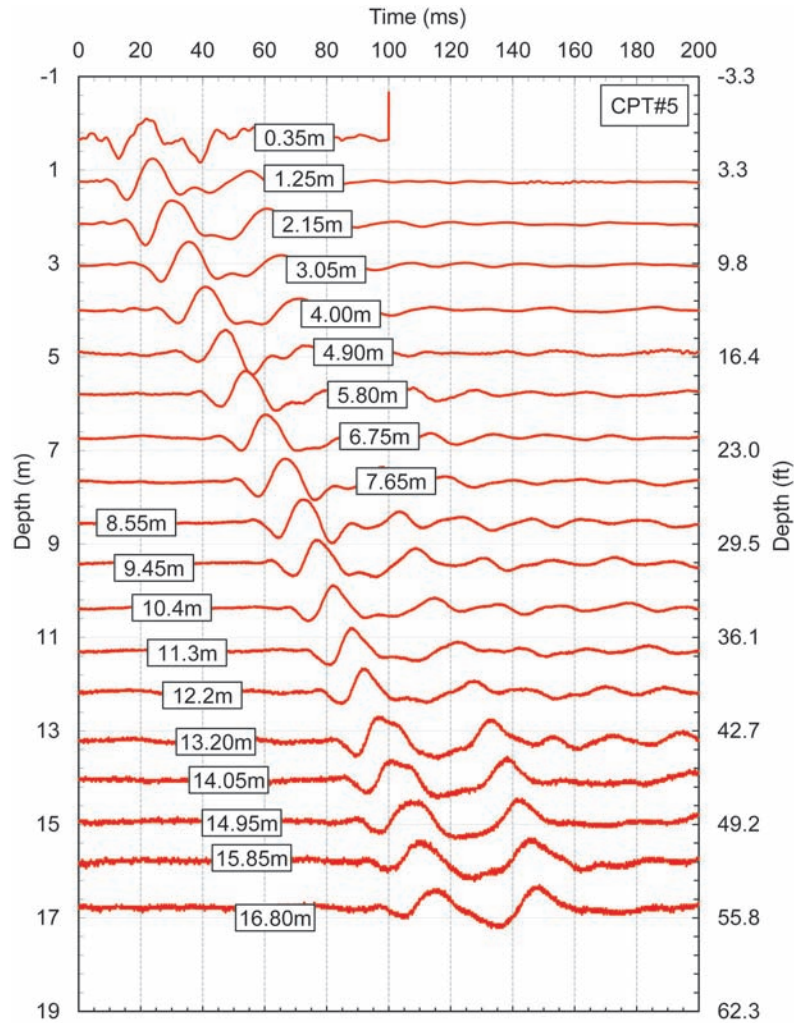


Figure A.2.19 Shear wave arrival traces for CPT#5.

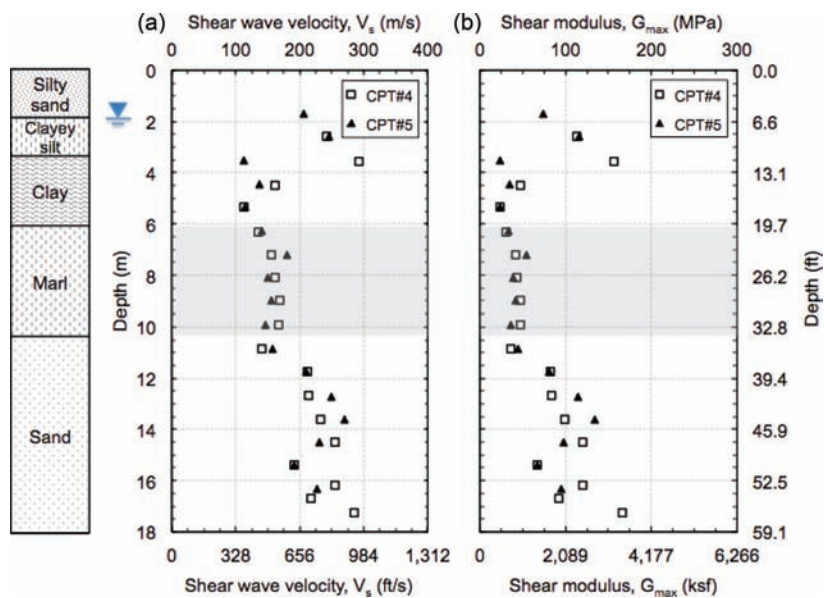


Figure A.2.20 (a) Shear wave velocity, and (b) shear modulus profiles with depth.

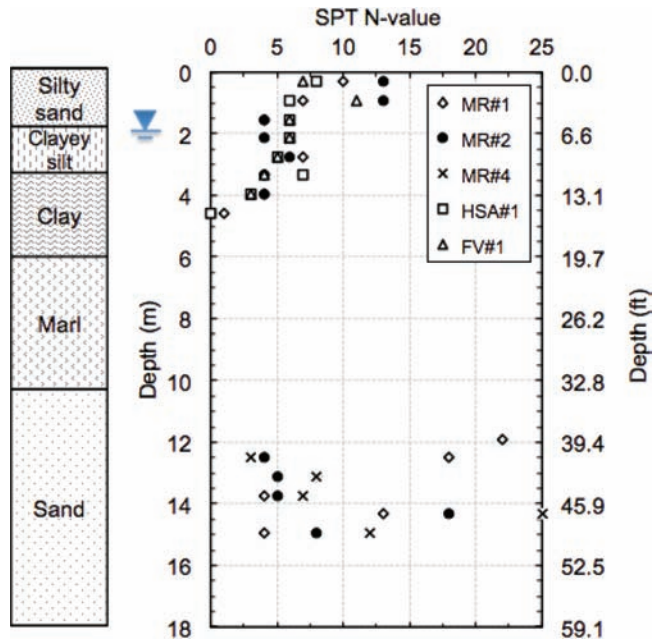


Figure A.2.21 Standard penetration resistance (N-values) with depth.

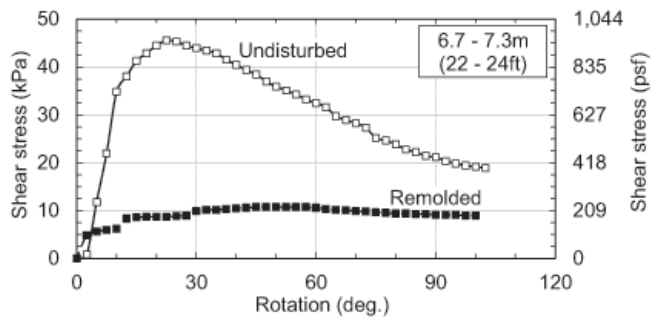


Figure A.2.22 Results of field vane shear test (FV4) conducted at ~7.2 m (23.5 ft).

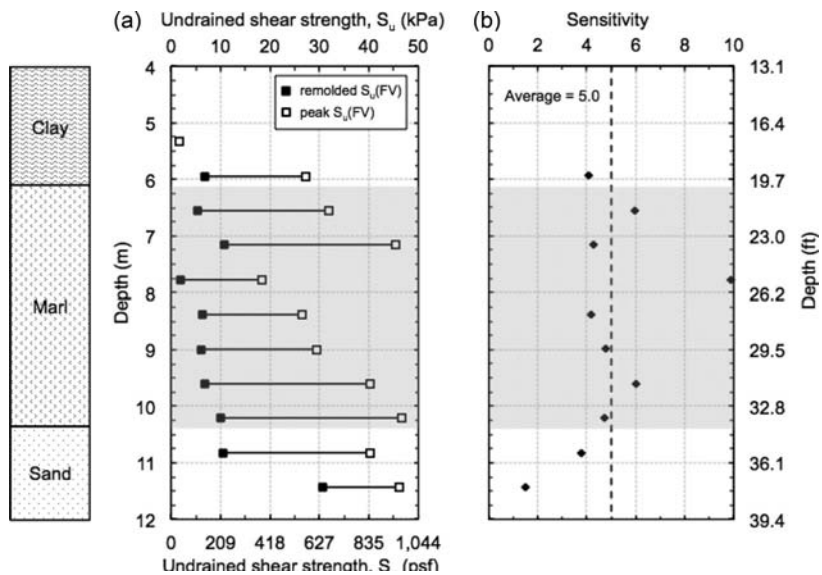


Figure A.2.23 Profiles of (a) field vane undrained shear strength and (b) soil sensitivity with depth.

APPENDIX 3: INDEX PROPERTIES, MINERALOGY, AND MICROSTRUCTURE

A.3.1. INTRODUCTION

From the interpretation of the field data collected, marl can be identified at depths between 6.1 m (20 ft) and 10.4 m (34 ft). A full laboratory testing program was performed on Shelby tubes samples obtained from this layer. The program consisted of: (i) index tests; (ii) mineralogy and microstructure; (iii) consolidation tests; and (iv) shear strength tests. The first two are presented in this appendix whereas the last two are discussed in APPENDIX 4. The soil samples obtained from the marl layer were not homogenous as was initially anticipated, but were composed of two types of soils. A brief description of these two soils is provided in Section A.3.2. Section A.3.3 presents and discusses the various index tests performed for this investigation. Section A.3.4 provides a detailed evaluation of the results from mineralogical analysis and microstructure.

A.3.2. DESCRIPTION OF SOILS WITHIN THE MARL DEPOSIT

The marl layer was not homogenous as was initially anticipated but was composed of two types of soils of varying properties that are repeated in horizontal thin layers. These two soils were identified after starting the laboratory tests and are herein referred to as “soil M” and “soil C.” The former is more prominent and characterized by a lower specific gravity and unit weight, but higher porosity, water content, silt content, and CaCO_3 content and by the presence of shells. The names for the soils were selected based on the fact that soil M has relatively more silt, hence the letter “M”; whereas soil C has relatively more clay, hence the letter “C” (as reported in Section A.3.3.2).

Although the field exploration showed the presence of a very soft layer between 6.1 m (20 ft) and 10.4 m (34 ft), it failed to detect the presence of the two types of soils (i.e., soil M and soil C). A more detailed description of the two soils is presented in Section A.3.3.

Figure A.3.1 shows soil samples composed from both soil M and soil C, with a clear difference between the color, texture and presence of shells. Soil C was found in thin layers of thicknesses ranging between a fraction of an inch (<2.54 cm) and few inches, whereas soil M was found in thicker layers and it formed the majority of the marl deposit. These two types of soils show different engineering behavior, which posed the necessity to carefully characterize each soil separately and try to examine the fundamental difference(s) between them. A special effort has been made to conduct tests on specimens with only one type of soil.

A.3.3. INDEX PROPERTIES

A range of index tests were conducted to classify the soil present in the marl deposit and to derive parameters that would aid the interpretation of the engineering tests. Index properties measured include organic content, calcium carbonate content, Atterberg limits, natural water content, grain size distribution, specific gravity, void ratio, total unit weight, degree of saturation, salt concentration, and pH. In most cases the index tests were performed on trimmings from engineering tests. Table A.3.1 presents a summary of all index properties for soil M and soil C. The following subsections will discuss the results of the various index tests in greater detail.

A.3.3.1 Organic Content and Calcium Carbonate Content

The organic content and calcium carbonate content were determined using the “sequential” loss on ignition (LOI) method proposed by Jung, Bobet, and Siddiki (2011). This method consists of heating the soil up to 455°C for six hours, in accordance with AASHTO T267-86 (AASHTO, 2008); the corresponding mass loss is used to estimate the organic content. The soil is then heated up to 800°C for six hours and the corresponding mass loss is used to determine the calcium carbonate content. The measurement is based on the fact that calcium carbonate decomposes into calcium oxide (CaO) and carbon dioxide (CO_2) in the range of 650°C to 800°C. The reduction in mass due to the release of CO_2 can be used to infer the calcium carbonate content. Note that the value obtained with the above method is not the percentage of calcium carbonate (CaCO_3), but the percentage of calcium carbonate equivalent (C.C.E.). This is due to the fact that other types of carbonates might be present in the soil such as dolomite ($\text{CaMg}(\text{CO}_3)_2$), as illustrated by the mineralogical analysis (Section A.3.4.1.3), which also decomposes in the range of 650°C to 800°C. In other words, the CaCO_3 presented in this thesis represents the amount of all carbonates in terms of C.C.E.

Figure A.3.2(a) and Figure A.3.2(b) show the organic content and the calcium carbonate content profiles for the marl deposit, respectively. Hollow black circles correspond to soil M whereas solid blue circles correspond to soil C. Low values of organic content were measured for all the soils tested. The LOI generally falls below 4% (Figure A.3.2(a)), with no clear difference between soil M and soil C. Huang, Bobet, and Santagata (2012) reported that the LOI often overestimates the true organic content when applied to soils with organic content matter content less than ~10%. Hence, the low values of LOI (<4%) obtained in this study did not warrant further testing to refine the organic content.

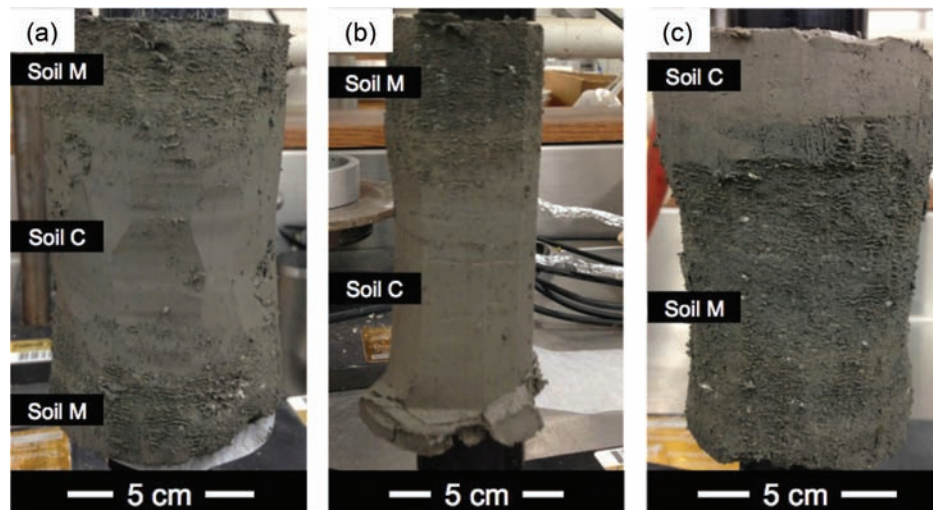


Figure A.3.1 Soil samples showing layers of soil M and soil C.

TABLE A.3.1
Summary of index properties

	Soil M		Soil C	
	Range	Mean \pm SD	Range	Mean \pm SD
Organic content (%)	2.0 – 4.3	3.1 \pm 0.6	1.7 – 3.0	2.5 \pm 0.4
CaCO ₃ content (%)	35.9 – 64.4	54.0 \pm 7.4	33.7 – 41.8	37.0 \pm 2.9
Water content, w _n (%)	50.5 – 68.5	60.9 \pm 6.0	36.6 – 52.2	42.1 \pm 5.2
Plastic limit, PL (%)	29.0 – 40.6	34.6 \pm 3.5	18.8 – 25.5	21.6 \pm 2.3
Liquid limit, LL (%)	61.7 – 78.8	67.5 \pm 5.2	40.1 – 52.4	47.5 \pm 4.2
Silt content (%)	72.0 – 82.0	77.6 \pm 3.0	54.0 – 66.0	61.0 \pm 5.5
Clay content (%)	15.0 – 23.0	18.3 \pm 2.8	33.0 – 45.0	38.3 \pm 5.3
Specific gravity, G _s	2.68 – 2.80	2.71 \pm 0.03	2.76 – 2.82	2.79 \pm 0.02
Void ratio, e	1.4 – 1.9	1.7 \pm 0.1	1.1 – 1.5	1.2 \pm 0.1
Total unit weight, γ_t (kN/m ³)	15.5 – 16.8	15.9 \pm 0.4	16.8 – 18.3	17.6 \pm 0.5
Degree of saturation, S _i (%)	95.3 – 99.8	97.9 \pm 1.4	93.2 – 99.0	97.4 \pm 1.9
Salt concentration (g/l)	2.1 – 3.8	3.0 \pm 0.5	2.2 – 5.1	3.6 \pm 1.2
Salt concentration (g/kg)	1.4 – 2.2	1.9 \pm 0.2	0.9 – 1.9	1.5 \pm 0.4
pH	7.5 – 7.9	7.8 \pm 0.1	7.6 – 7.9	7.8 \pm 0.1

All specimens have relatively high calcium carbonate content ranging between 35% and 65%, which is typical for marl soils. The calcium carbonate content was the basis for distinguishing between soil M and soil C. As shown in Figure A.3.2(b), soil C has an average calcium carbonate content of 37.0% \pm 2.9SD, while soil M has an average calcium carbonate content of 54.0% \pm 7.4SD. The higher calcium carbonate content in soil M could be partially caused by the presence of shells; which are composed of aragonite (CaCO₃) as well as the higher carbonate content present in the soil matrix of soil M, as illustrated by the mineralogical analysis (Section A.3.4.1.3).

A.3.3.2 Atterberg Limits, Natural Water Content, and Particle Size Distribution

Atterberg limit tests were performed in accordance with ASTM D4318-10 (ASTM, 2010). The only deviation from the standard is the order of performing the determination of the blow counts at various

water contents: while the standard suggests a dry to wet procedure (i.e., water is added to the soil before each blow count determination), a wet to dry procedure (using a fan to dry the soil) is instead recommended. It is acknowledged that the two procedures may cause slight differences in the results of liquid limit; however, the use of the latter procedure is reported to generate more repeatable data (Germaine & Germaine, 2009). Most of the tests were performed on trimmings from engineering tests.

The natural water contents are calculated, at the end of each engineering test, for the entire test specimen based on phase relationships, which use the initial wet mass and the final mass of solids. Water contents were also measured from the trimmings of each engineering test as part of the procedure for Atterberg limits testing. During the trimming process, sufficient trimmings were immediately collected for water content determination prior to storage of the soil for subsequent Atterberg limit tests in order to avoid soil drying. There was no significant difference between the water contents measured from the trimmings of the engineering tests and those calculated at the end of the test.

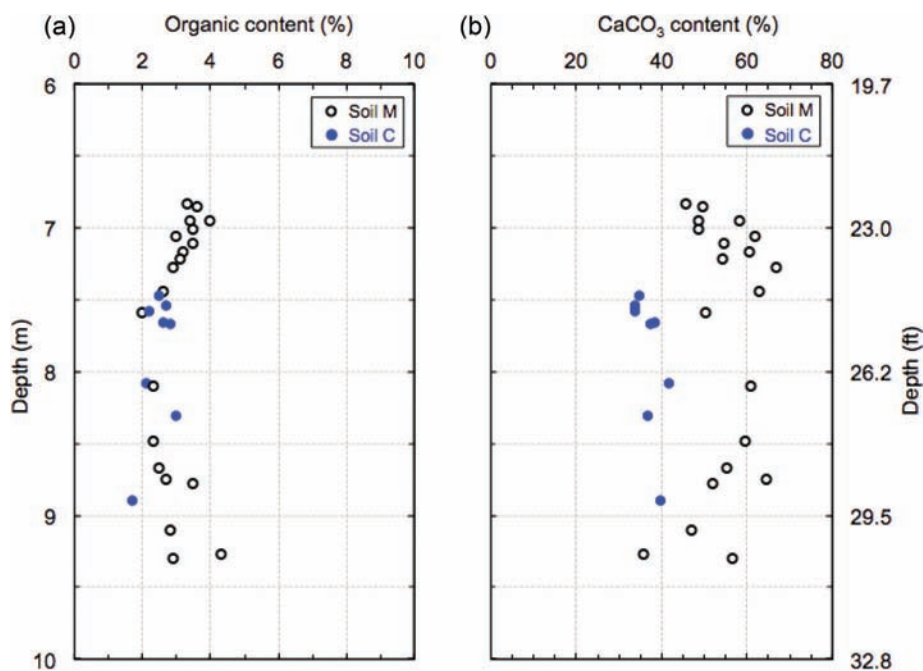


Figure A.3.2 (a) Organic content and (b) calcium carbonate content profiles for marl.

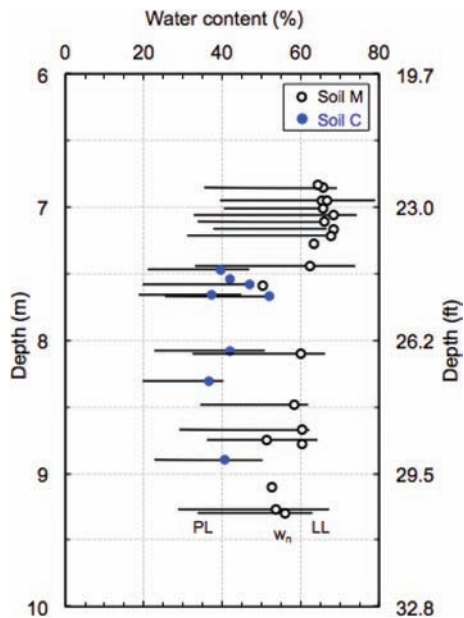


Figure A.3.3 Results of Atterberg limits for marl.

Figure A.3.3 plots depth versus plastic limit (PL), natural water content (w_n), and liquid limit (LL). The water contents are shown as data points (hollow black circles correspond to soil M and solid blue circles correspond to soil C) and the Atterberg limits are represented by lines (plastic limit represented by the left end of the line; liquid limit represented by the right end of the line). The data in Figure A.3.3 show the following:

1. In general, soil M has a natural water content higher than soil C. The average water content is $60.9\% \pm 6.0\text{SD}$ for soil M and $42.1\% \pm 5.2\text{SD}$ for soil C.
2. The Atterberg limits for soil M are consistently higher than the ones for soil C (soil M: mean PL = $34.6\% \pm 3.5\text{SD}$ and mean LL = $67.5\% \pm 5.2\text{SD}$; soil C: mean PL = $21.6\% \pm 2.3\text{SD}$ and mean LL = $47.5\% \pm 4.2\text{SD}$)
3. Marl has liquidity index (LI) values typically close to one (mean LI = $0.8 \pm 0.1\text{SD}$), which is evidence of the soil's high sensitivity, with no clear difference between soil M and soil C.
4. There is no clear variation of Atterberg limits or water contents with depth.

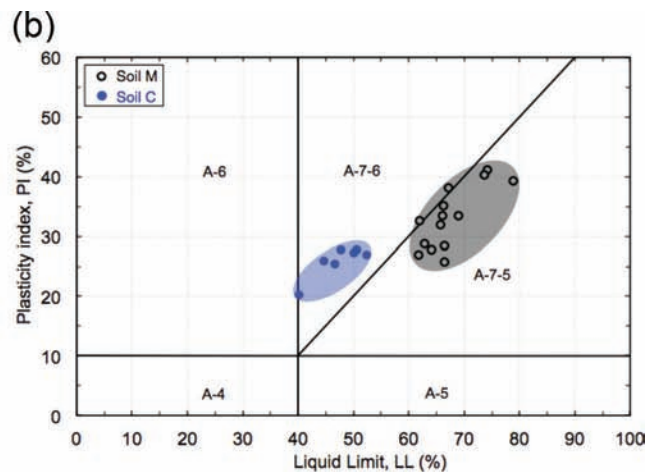
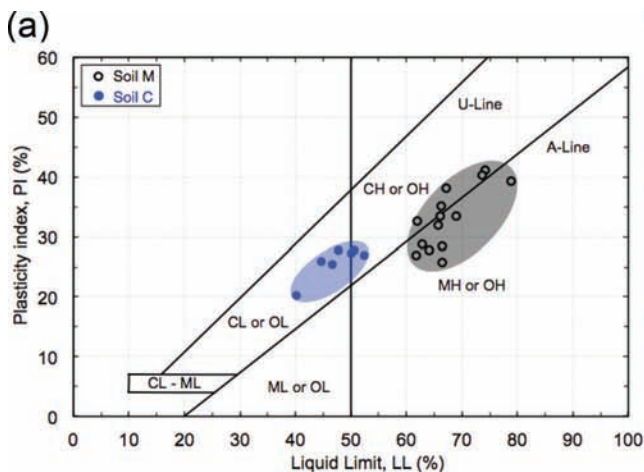


Figure A.3.4 Plasticity chart with data from soils M and C: (a) USCS and (b) AASHTO.

The liquid limit and the plasticity index of all the specimens tested from the marl layer are plotted on the plasticity chart in Figure A.3.4. For the most part, soil M plots below the A-line and is classified as elastic silt (MH) according to the USCS or A-7-5 according to the AASHTO, whereas soil C plots above the A-line and is classified as a lean clay (CL) according to the USCS or A-7-6 according to the AASHTO. Based on the INDOT classification system in specs 903 (INDOT, 2014), soil M is classified as "marl (silty loam)" and soil C is classified as "marly soil (silty clay)."

Figure A.3.5 shows the particle size distribution for marl from hydrometer tests performed in accordance with ASTM D422-63 (ASTM, 2007). Both soils have a fine fraction (less than $75 \mu\text{m}$) greater 96%. The small percentage of sand size particles (greater than $75 \mu\text{m}$) found in soil M ($<4\%$) consists mainly of shells. The figure shows that the distributions for soil M and soil C fall on two distinct bands. The average percentage of clay size particles (less than $2 \mu\text{m}$) is $18.3\% \pm 2.8\text{SD}$ for soil M, which is lower than soil C ($38.3\% \pm 5.3\text{SD}$).

The higher plasticity of soil M is not consistent with the typical trends reported in the literature of increasing LL and PI with higher clay content. It is also inconsistent with the data reported by Lamas, Irigaray, and Chacon (2002) for other carbonatic fine grained soils which show that LL and PI decrease with increasing calcium carbonate. This difference can be addressed by understanding the clay mineralogy as well as the role played by the shells on the interaction between soil and water. In particular, an investigation into the mineralogy of the soil could be important to distinguish between the two sources of calcium carbonate: the shells and the soil matrix (see Section A.3.4.1 and Section A.3.4.2).

A.3.3.3 Specific Gravity and Void Ratio

Specific gravity tests were performed based on ASTM D854-14 (ASTM, 2014a) on trimmings from engineering tests. The void ratio was calculated for the entire test specimen based on phase relationships.

Figure A.3.6 shows the variation with depth of specific gravity (G_s) and void ratio (e) for marl. For most part, soil M shows a specific gravity value lower than soil C (Figure A.3.6(a)). The average specific gravity for soil M is $2.71\% \pm 0.03\text{SD}$, while for soil C it is $2.79\% \pm 0.02\text{SD}$.

The initial void ratio for soil M show a decreasing trend with depth (Figure A.3.6(b)) ranging between 1.4 and 1.9 (mean $e = 1.7 \pm 0.1\text{SD}$), which is expected due to the increase in confinement. This trend was not observed for soil C due to the limited number of data points and the significant scatter; however, its average void ratio (mean $e = 1.2 \pm 0.1\text{SD}$) is lower than that of soil M.

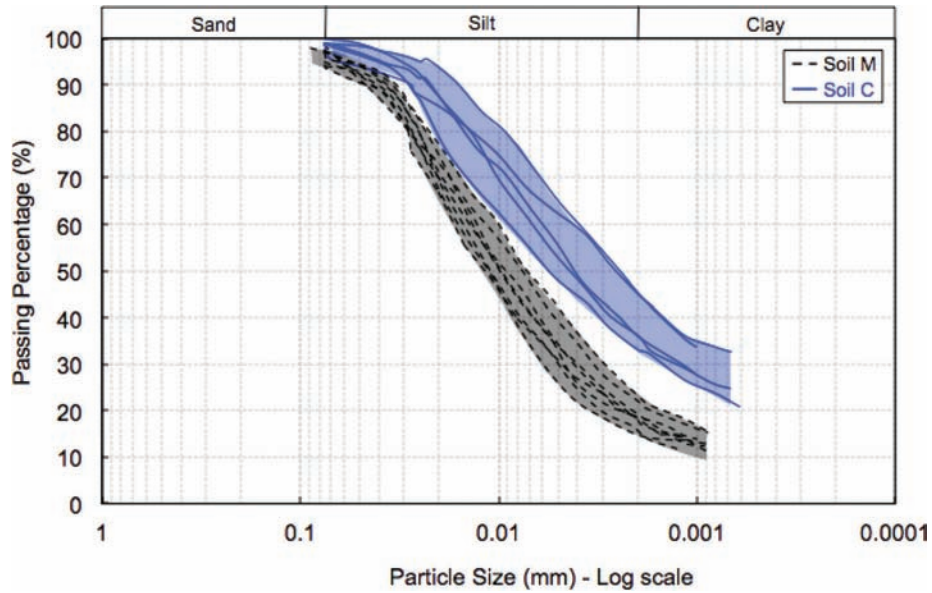


Figure A.3.5 Results of particle size analyses on soils M and C.

A.3.3.4 Total Unit Weight and Degree of Saturation

The total unit weight (γ_t) of the marl layer was measured for specimens used for laboratory consolidation and triaxial test programs. At the end of each engineering test, the initial degree of saturation (S_i) is calculated for the entire test specimen based on phase relationships, which use the initial mass and volume of the test specimen.

Figure A.3.7 shows the variation with depth of the total unit weight (γ_t), and the initial degree of saturation (S_i). Again a clear difference can be observed between soil M and soil C. As shown in Figure A.3.7(a), the values of the total unit weight for soil M increase with depth ($\gamma_t = 15.5\text{--}16.8 \text{ kN/m}^3$; mean $\gamma_t = 15.9 \text{ kN/m}^3 \pm 0.4\text{SD}$) and are at the low end of the range typically reported for fine grained soils (Germaine & Germaine, 2009), while the

values for soil C are higher ($\gamma_t = 16.8\text{--}18.3 \text{ kN/m}^3$; mean $\gamma_t = 17.6 \text{ kN/m}^3 \pm 0.5\text{SD}$). This is in agreement with the observation of a lower void ratio for soil C than for soil M. In general, S_i was greater than 95% (Figure A.3.7(b)) with an average of $97.7\% \pm 1.6\text{SD}$ indicating that the in situ marl deposit can be treated as fully saturated.

The average values of total unit weight for soil M and soil C are consistent with the average natural water contents determined from phase relationships at the end of each engineering test. For soil M, the average natural water content was $60.9\% \pm 6.0\text{SD}$ (Figure A.3.3), which translates into a total unit weight of 15.9 kN/m^3 . For soil C, the average natural water content was $42.1\% \pm 5.2\text{SD}$ (Figure A.3.3), which translates into a total unit weight of 17.7 kN/m^3 . These calculations used a degree of saturation of 98% and a specific gravity of 2.71 and 2.79 for soil M and soil C, respectively.

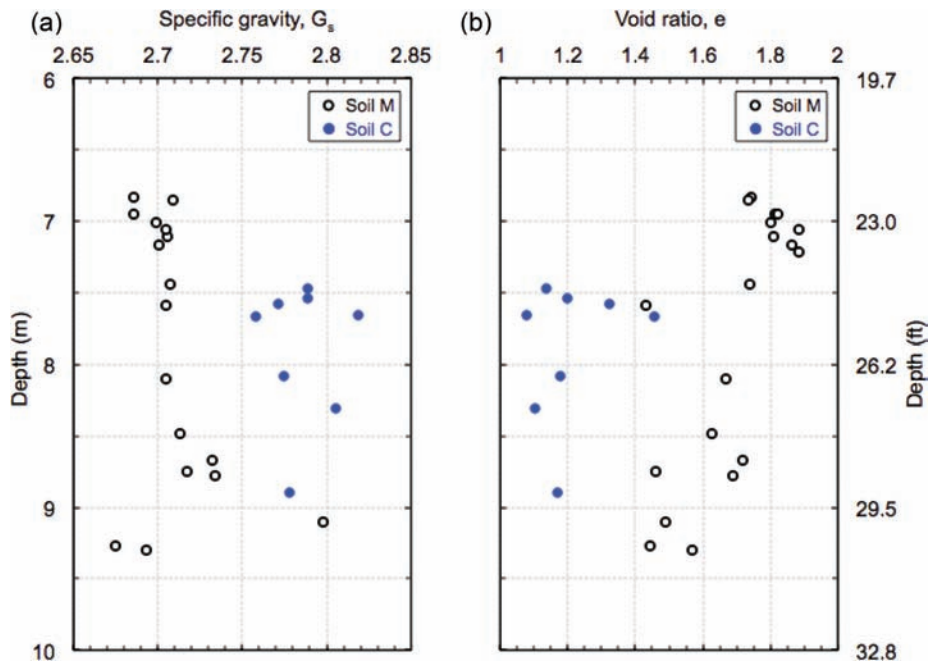


Figure A.3.6 (a) Specific gravity and (b) void ratio profiles for marl.

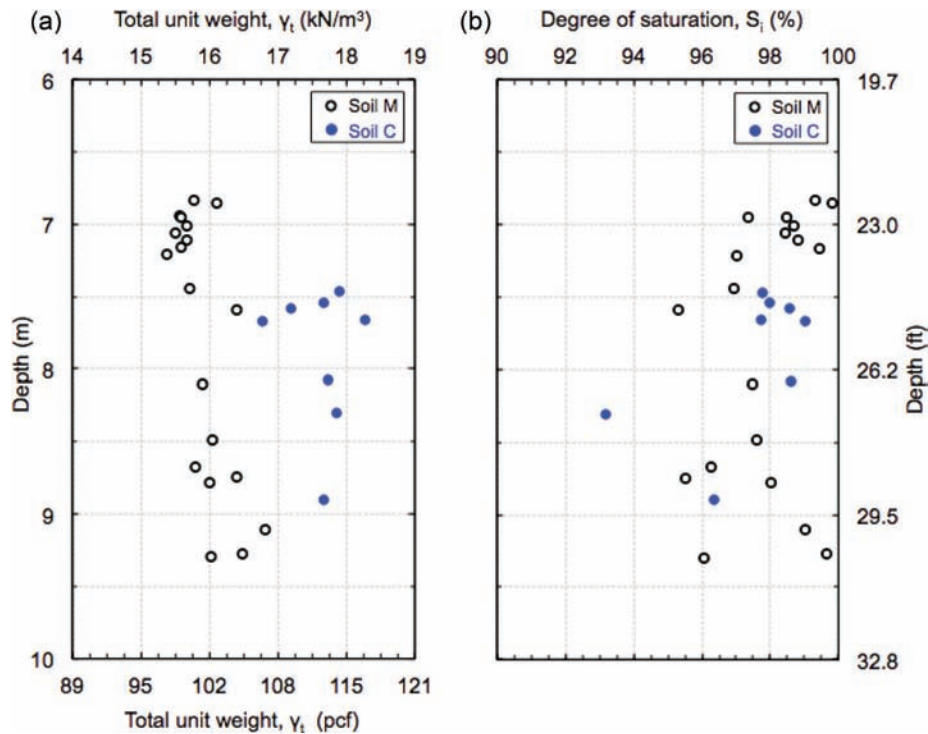


Figure A.3.7 (a) Total unit weight and (b) initial degree of saturation profiles for marl.

A.3.3.5 Salt Concentration and pH

The pH analysis was performed in general accordance with ASTM D4972-13 (ASTM, 2013) on trimmings from engineering tests. Each sample was tested using a distilled water solution and a dilute salt solution of 0.01 M calcium chloride (CaCl_2). The premise of using a salt solution is to minimize the effect of natural salts in the soil on the pH measurements (Germaine & Germaine, 2009). For each soil, two 10 gr air dried samples were prepared for pH measurements. One of the samples were mixed with 10 mL of water and the other with 10 mL of the 0.01 M CaCl_2 solution and the mixture was shaken with a reciprocating shaker (~228 excursions per minute) for 20 minutes. The samples were then placed in a centrifuge and ran at about 2500 rpm for 20 minutes.

The clear supernatant liquid was decanted from the centrifuge tube into a 10 ml glass beaker and the pH was measured while the extract was being mixed using a magnetic jar mixer. All measurements were performed at room temperature (21 to 25°C) with an Accumet™ Excel XL50 pH/mV/Temperature/ISE/Conductivity Meter. This device has the ability to account for temperature changes (i.e., Automatic temperature correction). Calibration of the measuring system was done every 8 hours using the buffer solutions with pH values of 4, 7, and 10.

The salt concentration was measured following the procedure provided by Germaine and Germaine (2009). The method estimates the soluble salts present in the soil pore fluid from the measurement of the electrical conductivity of the supernatant liquid. All tests were conducted on wet samples from trimmings of the engineering tests. The test should not be performed on dried material, because drying will transport salts to the boundaries of the specimen, making it difficult to obtain representative samples (Germaine & Germaine, 2009). An equivalent of 13 g dry mass of the soil was mixed with 15 ml of distilled water and the mixture was shaken with a reciprocating shaker (~228 excursions per minute) for 20 minutes. The samples were then placed in a centrifuge and ran at about 2500 rpm for 20 minutes.

The electrical conductivity (EC) of the supernatant liquid was measured at room temperature (21 to 25°C) with an Accumet™ Excel XL50 pH/mV/Temperature/ISE/Conductivity Meter. Calibration of the measuring system was done every 8 hours using the

buffer solution of KCl (single point calibration). The soluble salt concentration present in the supernatant was estimated from the measured EC using a sodium chloride (NaCl) calibration curve. The salt concentration is then corrected to account for the difference between the water content of the soil in the centrifuge tube and the natural water content w_n .

Figure A.3.8 plots depth versus salt concentration and pH. The salt concentration is expressed as equivalent NaCl concentration both in grams per liter of pore fluid and grams per kilogram of dry soil. The pH values obtained using a distilled water solution and a dilute salt solution of 0.01 M calcium chloride (CaCl_2) yielded very similar results and the data points shown in Figure A.3.8 correspond to the average values.

In general, there is no clear variation of salt concentration or pH with depth. The pH remains neutral, ranging from 7.5 to 7.9 (mean pH = $7.8 \pm 0.1\text{SD}$), through the marl deposit, with no clear difference between soil M and soil C.

The salt concentration shows some scatter in the data with values ranging from 2.1 g/l to 5.1 g/l and a collective average value equals to $3.2 \text{ g/l} \pm 0.8\text{SD}$; significantly lower than that of seawater (35 g/l). These values are very close to the ones obtained by Fernandez (1994) on Mexico City Clay: pH ranges from 7.2 to 9.1 and salinity ranges from 1 g/l to 6 g/l. However, when comparing the salt concentration in grams per kilogram of dry soil, soil M has slightly higher values than soil C (soil M: mean salt concentration = $1.9 \text{ g/kg} \pm 0.2\text{SD}$ and soil C: mean salt concentration = $1.5 \text{ g/kg} \pm 0.4\text{SD}$), which might be due to the fact that soil M has higher water content.

A.3.4. MINERALOGY AND MICROSTRUCTURE

The mineralogy and microstructure of marl was investigated using a combination of several techniques that include X-ray diffraction (XRD), thermogravimetric analysis (TGA), as well as electron microscopy equipped with energy-dispersive X-ray spectroscopy (EDXS), which can provide useful information on microstructure and chemical composition of individual particles. The following subsections summarize the procedures and results obtained from these techniques, as well as the dominant mineralogical composition of marl and how their mineralogy may affect their engineering

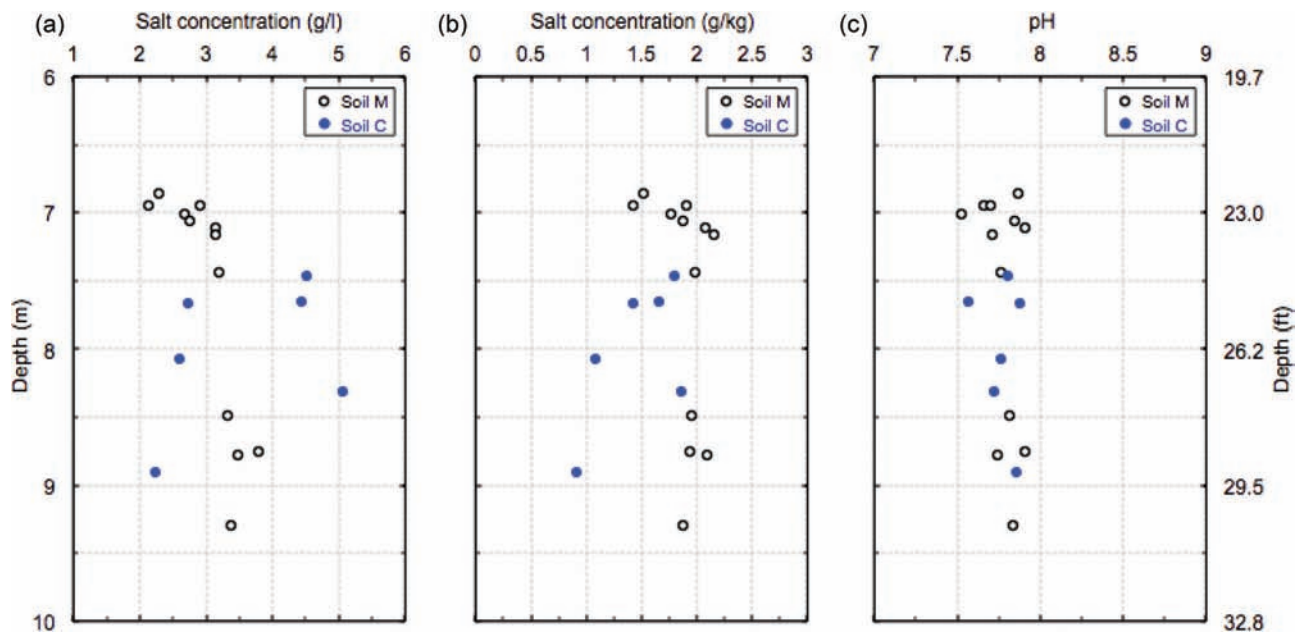


Figure A.3.8 Salt concentration in (a) g/l of pore fluid and (b) g/kg of dry soil, and (c) pH profiles for marl.

properties. A specific emphasis was placed on understanding the fundamental differences between soil M and soil C.

A.3.4.1 X-Ray Diffraction (XRD)

X-ray diffraction (XRD) is generally used to study crystalline minerals, including the minerals in soil environments. There are two common methods used to conduct XRD tests: the random powder method and the oriented aggregates method. The former requires a random orientation of the particles and is typically used to identify the non-clay minerals found in the soil (e.g., quartz, feldspars, and carbonates), while the latter requires all platy particles to have preferred orientation in the XRD samples and is generally used to identify clay minerals.

A.3.4.1.1 Sample Preparation for XRD

Randomly oriented powder. Self-supporting powder mounts of air-dried bulk soil samples were prepared as described by Schulze (1984). First, the sample was grinded using mortar and pestle to break up large aggregates. Then, about 300 mg of material was mounted into an Aluminum sample holder (15 × 20 mm sample area) and gently pressed against a glass slide attached to an unglazed paper to minimize preferred orientation. The sample holder is flipped over and the glass slide and the paper are removed. Samples prepared using this method had a flat surface that looked smooth and homogenous to the naked eye.

Oriented aggregates. With the presence of sand- and silt-size particles in the soil sample, it is usually hard to identify clay minerals (especially for peaks with higher order n) since their corresponding peaks are masked by the relatively high intensity ones from the larger size particles (e.g., quartz). Thus, it is critical to separate the coarse fraction (i.e., particle size >2 μm) before running the XRD analysis.

Oriented aggregates were prepared by depositing the clay fraction (<2 μm) of the soil on 32 mm (1.27 inch) diameter alumina porous disks with 1 bar air entry value. Obura (2008) showed that the mass of clay needed to obtain 95% of the theoretical diffraction at $35^\circ 2\theta$ is $\sim 11 \text{ mg/cm}^2$. Therefore 88 mg of clay was needed to cover each porous disk that has an average surface of 8 cm^2 . Determination of the optimum amount of clay is essential to ensure that the relative intensities of the diffraction

peaks are representative of the right amount of the different minerals in the sample (Rich & Barnhisel, 1977).

The procedures described by Jackson (1985) were followed for sample pretreatment and clay fractionation. In summary, sufficient amount of air-dried bulk soil ($\sim 3 \text{ g}$ for soil M and $\sim 1 \text{ g}$ for soil C) was weighed out and placed into 50 mL conical-bottom centrifuge tubes. The amount of soil needed was estimated based on the particle size analysis (Section A.3.3.2) and the carbonate content (Section A.3.3.1), in order to provide $\sim 350 \text{ mg}$ of clay. Carbonates were removed by adding $\sim 25 \text{ mL}$ of pH 5 1 M sodium acetate (NaOAc) to the tubes and heating to about 100°C in a water bath for 20 min, followed by centrifuging and discarding the clear supernatant. This process was repeated 5 times to ensure a complete removal of carbonates (no vigorous bubbling was observed). About 25 mL of 1 M sodium chloride (NaCl) was added and the samples were shaken overnight on a reciprocating shaker (~ 228 excursions per minute). The samples were then centrifuge washed 3 times with $\sim 25 \text{ mL}$ of 1 M NaCl to saturate the exchange complex with Na^+ ions. Saturating the soil with lower valence ions (i.e., Na^+) results in an increase of the double layer thickness, which facilitates the clay dispersion. Sufficient deionized water was added to the samples to bring the suspension level up to 7 cm from the bottom of the centrifuge tube. The suspensions were then shaken thoroughly and centrifuged at 5000 rpm for 7 minutes (time calculated to extract the clay fraction by sedimentation according to Stoke's law). This step was repeated 5 times while decanting the supernatant into a beaker.

The clay suspensions collected were divided into two portions containing 88 mg of clay each, and saturated with either K^+ by adding 1 M KCl or Mg^{2+} by adding 0.5 M MgCl_2 . The suspensions were then poured onto the porous disks under suction and repeatedly washing with either KCl or MgCl_2 , followed by washing off the excess salts with deionized water. (Note that all the excess salt should be completely removed since it might crystallize and affect the diffraction pattern). The samples were then covered at an angle with watch glass and allowed to dry slowly (2-3 days) at room temperature before XRD analysis. Because of the inherent nature of the clay fraction in soil M to crack and peel on drying (as shown in Figure A.3.9), oriented aggregates of the clay fraction of soil M had to be repeated with much slower drying rate (6-7 days) by completely covering with watch glass and once the soil started to dry (~ 24 hours), the disks samples were covered with clean disks to avoid cracking and peeling.

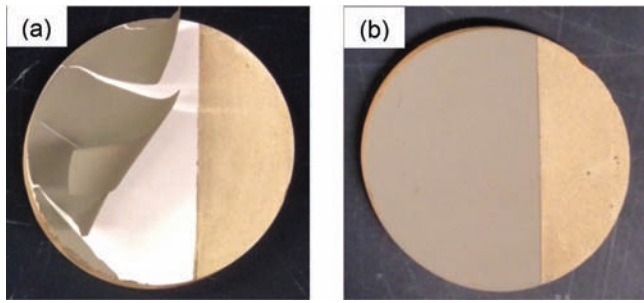


Figure A.3.9 Oriented clay aggregates of (a) soil M (showing cracking and peeling) and (b) soil C.

A.3.4.1.2 X-Ray Diffraction Analysis

The Mg saturated samples were scanned at room temperature before and after solvating with ethylene glycol (EG) in a sealed desiccator heated at 60°C for about 24 hours. The K saturated samples were scanned at room temperature and after successive heating to 100, 300, and 550°C for 2 hours (Note that samples should not be heated longer than 2 hours because chlorite slowly dehydroxylises between 300°C and 550°C resulting in false interpretation). Diffractograms were obtained using a PANalytical X'Pert PRO MPD x-ray diffraction system (PANalytical, Almelo, The Netherlands) equipped with a PW3050/60 θ - θ goniometer and uses Co-K α ($\lambda = 1.79 \text{ \AA}$) radiation generated at 45 KeV and 40 mA. Figure A.3.10 shows the different components of the diffractometer used in this research. The incident beam optics consisted of an Fe beta filter, 0.04 radian Soller slit, a programmable divergence slit, and a beam mask set to illuminate a $15 \times 20 \text{ mm}$ sample area. A fixed, 1° anti-scatter slit was used at diffraction angles smaller than $12^\circ 2\theta$. The diffracted beam optics consisted of a programmable diffracted beam anti-scatter slit, a 0.04 radian Soller slit, and a PW3015/20 X'Celerator detector configured for an active length of $2.12^\circ 2\theta$. The XRD data were obtained by step-scanning the sample (powder mounts or oriented clay aggregates) from 2.1 to $80^\circ 2\theta$ at 0.05° steps using a counting time of 60 sec per step. The data were analyzed with the

X'Pert High Score Plus software package (PANalytical, Almelo, The Netherlands) and were converted to a fixed 1° divergence slit prior to phase analysis and plotting.

A.3.4.1.3 Results and Discussion

The mineral composition of marl was identified using XRD analysis on both randomly oriented powder and oriented aggregates. A total of 5 specimens were obtained from different boreholes at various depths (3 specimens from soil M and 2 specimens from soil C) and analyzed using XRD. Table A.3.2 presents basic information about the XRD samples examined.

The XRD patterns (randomly oriented powder and oriented aggregates) of soil M specimens (TX112, TX114, and SEM1) were almost identical, hence the results of only one specimen (i.e., TX114) is presented in this section. Similarly, the two specimens from soil C (TX102 and TX103) have similar mineral composition and the results of only one specimen (i.e., TX102) is presented. There is no variation of mineral composition with depth, however it varies significantly between soil M and soil C, which might be one of the fundamental reasons of the differences observed in the geotechnical index and engineering properties. The different minerals identified in the samples are shown in Table A.3.3 in order of predominance (from largest to smallest).

Non-clay minerals All soil samples yielded similar results and indicate that the dominant non-clay mineral components are calcite, dolomite, and quartz. Figure A.3.11 and Figure A.3.12 show the XRD patterns for a randomly oriented powder sample obtained from soil M and soil C, respectively. Each peak in the figures is labeled with the mineral name, the Miller index (hkl), and the d-spacing. Quartz is identified by distinctive peaks at 4.26 \AA , 3.35 \AA , 2.46 \AA , 2.13 \AA , and 1.98 \AA ; with the strongest peak observed at 3.35 \AA (101). The carbonate minerals, calcite and dolomite, are found prominently in the bulk samples with the strongest (104) peak observed at 3.03 \AA and 2.89 \AA , respectively. Calcite is also identified from 3.85 \AA , 2.84 \AA , 2.49 \AA , 2.28 \AA , and 2.09 \AA peak; whereas dolomite is identified from 4.03 \AA , 3.70 \AA , 2.56 \AA , 2.19 \AA , and 2.02 \AA peak.

Soil M and soil C contain small quantities of feldspars; K-feldspar is identified by a small peak at 3.24 \AA and plagioclase

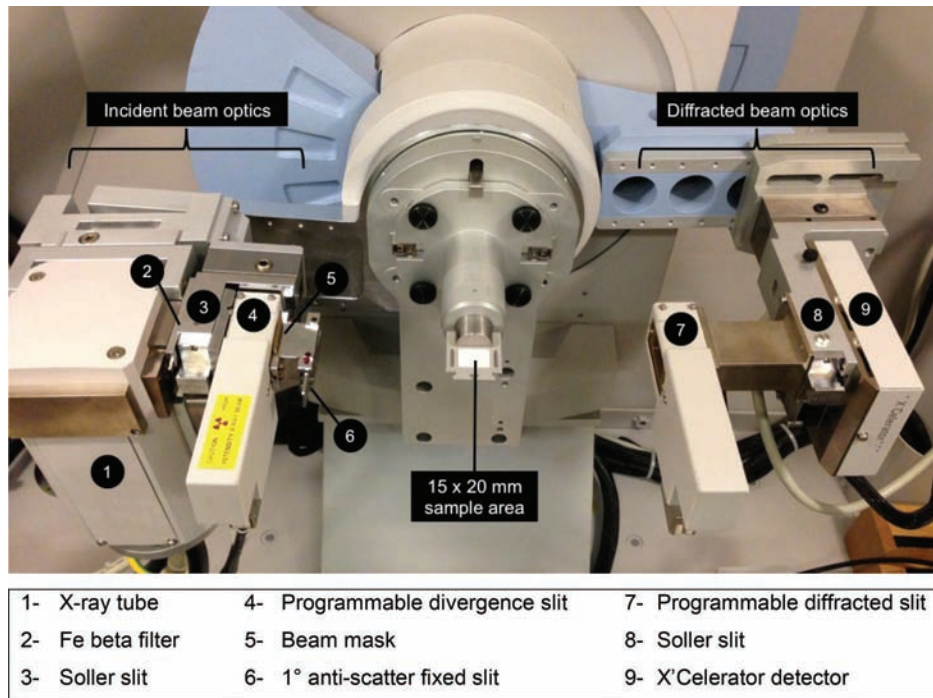


Figure A.3.10 X-ray diffraction system (PANalytical B.V. diffractometer).

TABLE A.3.2
Location and depth of the XRD samples examined

Specimen Number	Sample Location	Depth	Soil Type
TX112	MR#3-ST5	7.16 m (23.5 ft)	Soil M
TX114	MR#4-ST5	7.44 m (24.4 ft)	Soil M
SEM1	MR#4-ST4	7.28 m (23.9 ft)	Soil M
TX102	MR#3-ST6	8.31 m (27.2 ft)	Soil C
TX103	MR#1-ST4	7.47 m (24.5 ft)	Soil C

feldspar is identified by a peak at 3.19 Å. The latter peak is differentiated from the (012) magnesite peak by conducting XRD analysis on randomly oriented powder samples prepared with soil M and soil C treated with pH 5 1 M sodium acetate (NaOAc) to remove carbonates (including magnesite). XRD pattern for both soils show that the 3.19 Å peak persists even after treatment. Thus, it is concluded that this peak corresponds to plagioclase feldspar.

In addition, the XRD pattern for soil C shows a few additional peaks at lower angles, indicating the presence of clay minerals (e.g., smectite, chlorite, vermiculite, illite, and/or kaolinite). These peaks can be hardly identified in the pattern for soil M most likely due to its lower clay content (~20% compared to ~37% for soil C). Identification of the clay minerals in soil M and soil C were achieved by conducting XRD analysis on oriented aggregates obtained from <2 µm fractions and the results are discussed in the next subsection entitled “clay minerals.”

Aragonite (CaCO₃) is identified in soil M by a peak at 2.71 Å, which might be attributed to the presence of shells in soil M. This peak is not identified in soil C due to the absence of shells in this soil. To support this hypothesis, XRD analysis was conducted on

randomly oriented powder samples prepared using shells collected from soil M. Aliquots of soil M was placed in deionized water for several days to soften the sediment enough to pass through a 0.075 mm sieve (ASTM #200). Shells were hand-picked from the retained fraction and repeatedly washed with deionized water to remove all the soil that adhered to the shell surface. The shells were then broken and the soil that was lodged within the shell was removed with small spatula and washed repeatedly with deionized water. The recovered shells were air-dried and randomly oriented powder samples were prepared according to the procedure described in Section A.3.4.1.1. A total of three samples were scanned using X-ray, and the patterns were identical. Figure A.3.13 shows the typical XRD pattern for the shells. Aragonite is the predominant mineral and is identified by distinctive peaks at 4.21 Å, 3.39 Å, 3.27 Å, 2.87 Å, 2.70 Å, 2.48 Å, 2.41 Å, 2.37 Å, 2.33 Å, 2.19 Å, 2.11 Å, and 1.98 Å; with the strongest peak observed at 3.39 Å (111). This principal peak could not be identified in the pattern of soil M (Figure A.3.11) as because of the principal peak of quartz (3.35 Å) of about the same position. However, the second largest peak of aragonite was observed at 2.70 Å. Note that the aragonite (012) peak observed in soil M at 2.71 Å is very small and this is because the calcite (104) peak is so robust that is typically much larger than the aragonite peaks.

The XRD patterns shown in Figure A.3.11 and Figure A.3.12 reveal the following differences between the matrix of soil M and that of soil C:

1. Soil M has more carbonates than soil C, which is confirmed by the thermogravimetric analysis presented in Section A.3.4.2.
2. Soil M has more calcite than soil C, which might be attributed to the presence of secondary calcite crystals that were precipitated more in soil M during the soil deposition. This is confirmed by the calcite crystals identified with the

TABLE A.3.3
The mineralogy of marl (in order of predominance) as observed by XRD analysis (from randomly oriented powder and oriented aggregates)

Soil Type	Mineral Type	Identified Minerals
Soil M	Non-clay minerals Clay minerals	Calcite, quartz, dolomite, aragonite, plagioclase feldspar, K-feldspar Smectite, illite, chlorite, kaolinite
Soil C	Non-clay minerals Clay minerals	Quartz, dolomite, calcite, plagioclase feldspar, K-feldspar Illite, chlorite, smectite, kaolinite

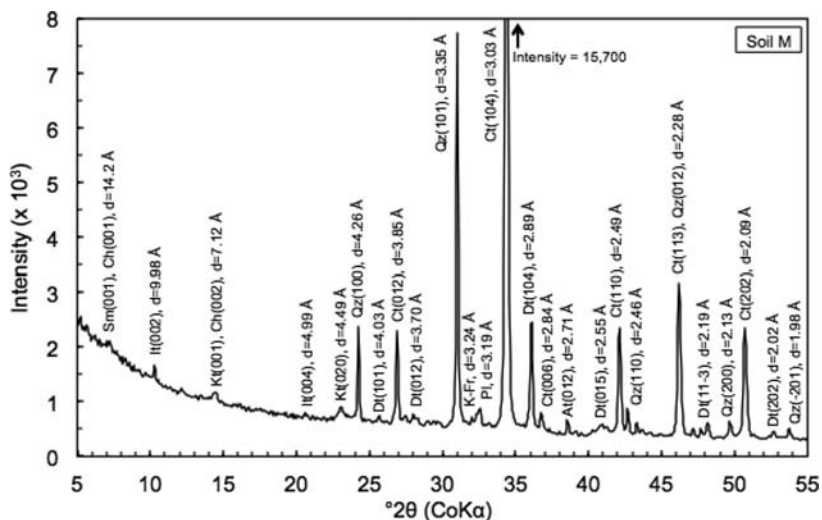


Figure A.3.11 XRD patterns (randomly oriented powder) of soil M. Mineral codes: Sm = smectite, Ch = chlorite, It = Illite, Kt = kaolinite, Qz = quartz, Dt = dolomite, Ct = calcite, K-Fr = K-feldspar, Pl = plagioclase feldspar, At = aragonite.

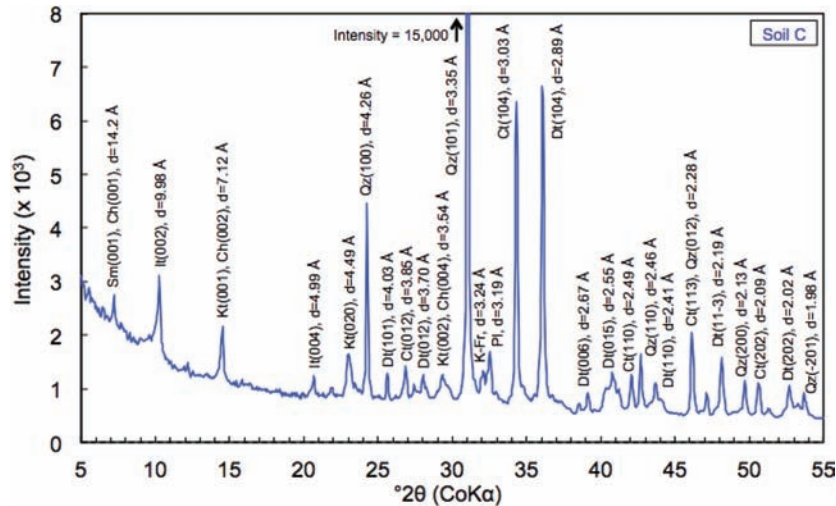


Figure A.3.12 XRD patterns (randomly oriented powder) of soil C. Mineral codes: Sm = smectite, Ch = chlorite, It = Illite, Kt = kaolinite, Qz = quartz, Dt = dolomite, Ct = calcite, K-Fr = K-feldspar, Pl = plagioclase feldspar.

scanning electron microscope (presented in Section A.3.4.3). These crystals are identified in soil M but are not found in soil C.

- Soil M has less dolomite than soil C, as shown by the relative peak intensities in the XRD patterns. This is in agreement with the observation made during the removal of carbonates for oriented aggregate samples preparation. It was observed that soil C reacts much slower with acid addition than soil M, and fizzing is observed for much longer time in soil C despite the fact that it has lower carbonate content. Doner and Grossl (2002) reported that dolomite reacts slower with acid addition than calcite. Hence, it can be concluded that soil C has more dolomite than soil M.
- Aragonite is identified in soil M but is absent in soil C. This is expected due to the presence of shells in soil M and their absence in soil C.
- Soil M has less clay content than soil C as presented earlier in the results of particle size analysis (Section A.3.3.2).

The three predominant minerals calcite, dolomite and quartz were each analyzed separately using XRD analysis on randomly

oriented powder samples prepared using pure minerals. The premise of analyzing these pure minerals is to better identify the minerals found in the marl deposit and to compare them to the shell aragonite. Figure A.3.14 shows the results from the XRD patterns for a randomly oriented powder sample obtained from each pure mineral. The table also includes the source from which the mineral was obtained as well as a photo. TGA was also conducted on these three minerals and the results are discussed in Section A.3.4.2.

Clay minerals Figure A.3.15 and Figure A.3.16 summarize the XRD patterns of oriented clay aggregate subjected to different treatments for soil M and soil C, respectively. Each figure shows six patterns: Mg²⁺-saturated (Mg), ethylene glycol-solvated sample (MgEG), K⁺-saturated sample x-rayed after air-drying at room temperature (K-23°C), K⁺-saturated sample x-rayed after heating at 100°C for 2 hours (K-100°C), 300°C for 2 hours (K-300°C), and 550°C for 2 hours (K-550°C). All XRD patterns are corrected for position shifts using corundum as a standard (corundum disks were used as sample holders). These results show that smectite, illite, chlorite, and kaolinite are present in both soils (M and C), but with different proportions.

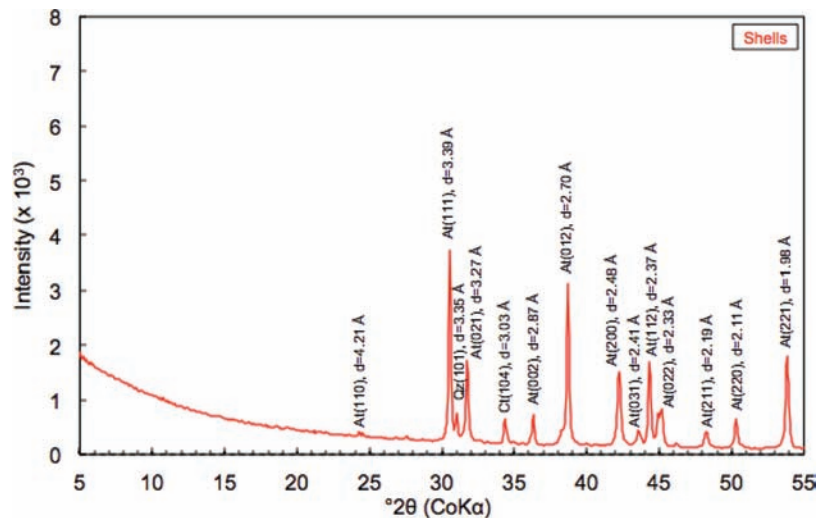


Figure A.3.13 XRD patterns (randomly oriented powder) of shells collected from soil M. Mineral codes: At = aragonite, Qz = quartz, Ct = calcite.

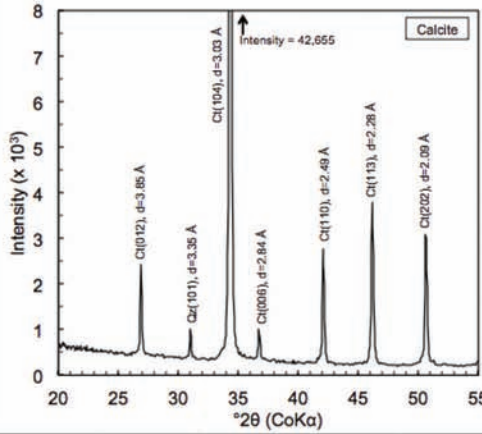
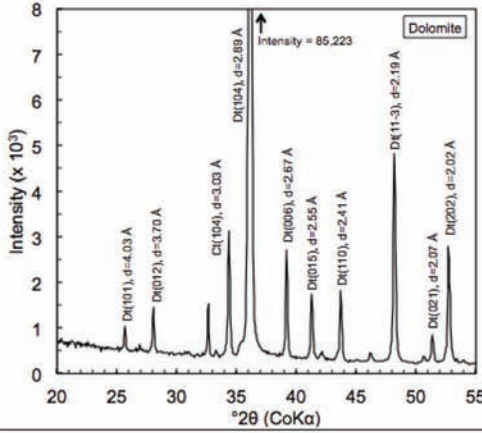
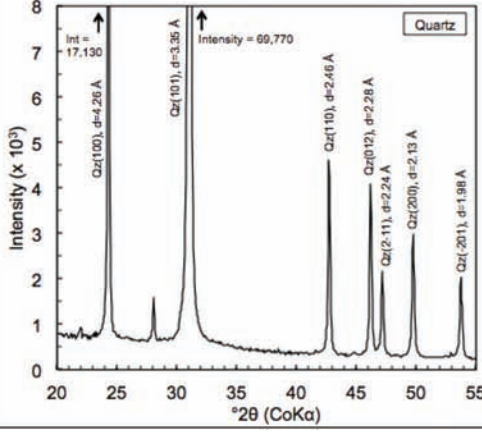
Name	Source	Photo	XRD patterns (randomly oriented powder)
Calcite	Chisos Mountain, Brewster County, Texas (Ward's Natural Science Establishment, Inc., Rochester, N.Y.)		
Dolomite	Thornwood, New York (Ward's Natural Science Establishment, Inc., Rochester, N.Y.)		
Quartz	Commission of the European Communities, Community Bureau of Reference BCR, Reference material Nr. 66 (#0788)		

Figure A.3.14 XRD analysis of the three predominant minerals: calcite, dolomite, and quartz.

As shown in Figure A.3.15, smectite and illite are the predominant minerals in soil M, while chlorite and kaolinite occur in smaller quantities. Smectite is identified by a strong peak at $\sim 14.2 \text{ \AA}$ in the sample saturated with Mg^{2+} , which shifts to 16.9 \AA when solvated with ethylene glycol (EG), and collapses to $\sim 11 \text{ \AA}$ and $\sim 10 \text{ \AA}$ with K^+ saturation and heating at 100°C and 550°C , respectively. The smectite probably has appreciable hydroxy-interlayering because it does not collapse completely to

$\sim 10 \text{ \AA}$ upon K^+ saturation and heating up to 100°C (Marques, Teixeira, Schulze, & Curi, 2002).

Illite is identified by peaks at 9.96 \AA , 4.98 \AA , and 3.33 \AA that do not change position with K^+ or Mg^{2+} saturation, or with ethylene glycol solvation and persist in K^+ -saturated samples heated up to 550°C . The pattern also shows an increase in the (002) peak at 9.96 \AA with K^+ saturation and heating to 550°C , which is attributed to the collapse of smectite. The sharp peaks

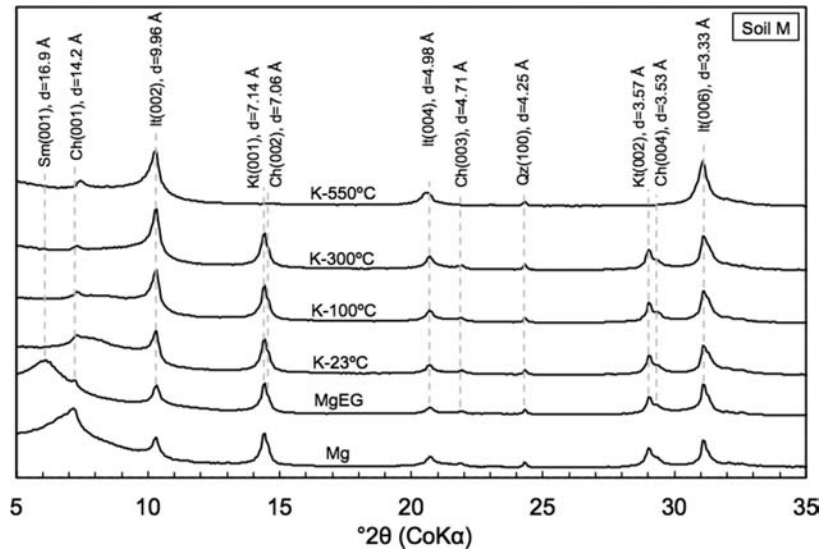


Figure A.3.15 XRD patterns (oriented samples) of the clay fraction (<2 μm) of soil M. Mineral codes: Sm = smectite, Ch = chlorite, It = Illite, Kt = kaolinite, Qz = quartz.

of illite indicate that illite of all the samples are well crystallized (Brindley & Brown, 1980).

Chlorite is also found in soil M and is identified by peaks at 14.2 Å, 7.06 Å, 4.71 Å, and 3.53 Å. Chlorites are differentiated from vermiculites in that, unlike vermiculite which expands to 14 Å with ethylene glycol and collapses to 10 Å when saturated with K⁺ (Malla, 2002), chlorite maintains a 14.2 Å basal spacing with glycolation and 550°C heat treatment. When chlorite is heated to temperatures as high as 550°C, the peak intensity of the 001 reflection (14.2 Å) increases, and at the same time, the peak intensities of higher-order (00l) reflections decrease in intensity (Barnhisel & Bertsch, 1989).

The MgEG pattern in Figure A.3.15 also shows the presence of some kaolinite, which is identified by peaks at 7.14 Å and 3.57 Å. All kaolinite are found to be unaffected on glycolation and 300°C heat treatment. On heating to 550°C, kaolinite tends to lose its crystalline character causing the two peaks at 7.14 Å and 3.57 Å to disappear.

Soil C, on the other hand, is mainly composed of Illite and chlorite (Figure A.3.16), while smectite and kaolinite are found in very small amount. Illite, chlorite, and kaolinite present in soil C are identified at d-spacing values similar to the ones found in soil M, hence the reader is referred to the description provided above. However, the relative peak intensities are different between the two soils indicating the difference in the mineral proportions.

Soil C also contains small amount of smectite that is identified by a peak at ~14.2 Å in the sample saturated with Mg²⁺, which shifts to 16.3 Å when solvated with ethylene glycol (EG), and collapses to 9.95 Å with K⁺ saturation. The peak disappears completely and the 9.95 Å peak becomes stronger (Figure A.3.16), indicating the collapse of smectite into illite. The charge on these smectite layers is quite high and there is very little hydroxy-interlayering because collapse is complete at 23°C (Marques et al., 2002).

Fine quartz in the <2 μm fraction can be identified by its (100) peak observed at 4.25 Å presented in both soil M and soil C.

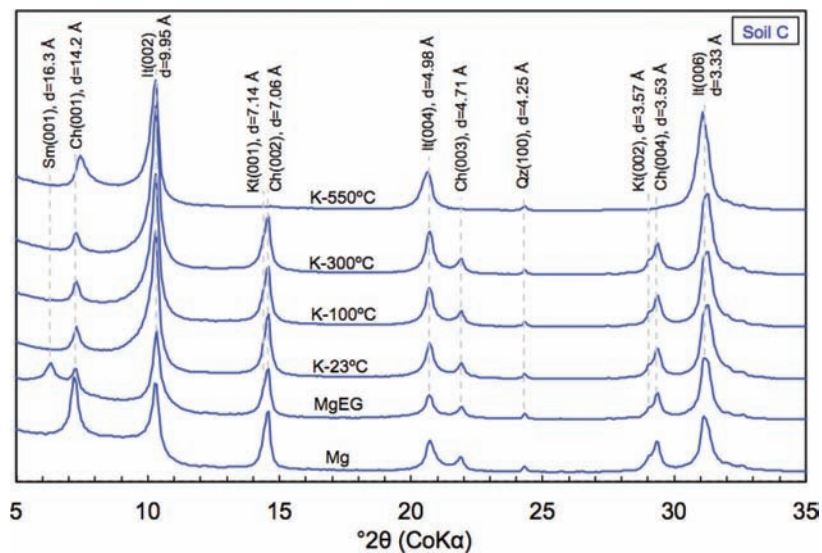


Figure A.3.16 XRD patterns (oriented samples) of the clay fraction (<2 μm) of soil C. Mineral codes: Sm = smectite, Ch = chlorite, It = Illite, Kt = kaolinite, Qz = quartz.

However, this peak is very weak, indicating that quartz is present in negligible amount in the clay fraction.

A.3.4.1.4 Semi-Quantitative Analysis Using XRD

A semi-quantitative mineralogical composition in the clay fractions was determined based on relative peak intensities. The peak intensities were calculated by multiplying the maximum peak height with the full width at half maximum (FWHM). These two parameters were estimated from the XRD patterns after subtracting the baseline and correcting for position shifts using corundum as a standard (corundum disks were used as sample holders). The intensities for the different patterns were also adjusted (normalized) by simple proportion to equalize the $\sim 7 \text{ \AA}$ peak area, using the $\sim 7 \text{ \AA}$ peak area for the K-300°C pattern as the basis for comparison (Islam & Lotse, 1986; Weir, Ormerod, & El Mansey, 1975). Note that the $\sim 7 \text{ \AA}$ peak area was almost the same for all patterns and only slight adjustment was needed. The peak intensities at each d-spacing were represented with the characters a to e in Table A.3.4.

Islam and Lotse (1986) and Egashira et al. (1999) estimated the peak intensity ratios of the respective clay minerals to illite when the minerals are present in an equal amount in the soil: $\text{Sm}(001)/\text{It}(002) = 3.0$; $\text{Ch}(002)/\text{It}(002) = 1.5$; $\text{Ch}(001)/\text{It}(002) = 1.0$; $\text{Kt}(001)/\text{It}(002) = 2.0$. The following equations were formulated to estimate the relative weight equivalent to the peak intensities for the respective clay minerals:

Smectite:	$W_{\text{Sm}} = 1/3 [a \times d/(d+3e)]$
Illite:	$W_{\text{It}} = b$
Chlorite:	$W_{\text{Ch}} = a \times 3e/(d+3e)$
Kaolinite:	$W_{\text{Kt}} = c/2 - W_{\text{Ch}}$

The percentage of the clay minerals was calculated by dividing the relative weight of each clay mineral (W_i) by the total of the relative weight of the clay minerals (ΣW_i). The results for both soils (M and C) are summarized in Table A.3.5.

The large difference in the smectite content between soil M and soil C can be used to explain the discrepancy observed in the Atterberg limits results (Section A.3.3.2). Soil M has lower clay content than soil C (20% vs. 37%) yet higher LL and PI, which is not consistent with the typical trends reported in the literature of increasing LL and PI with higher clay content. However, both the type and amount of clay in a soil influence the Atterberg limits. Generally, soils rich in smectite have higher LL and PI, which is attributed to the higher water sorption capacity caused by the higher specific surface area (De Kimpe, Laverdiere, & Martel, 1979). The smectite content

TABLE A.3.4
D-spacing of detected clay minerals for different treatment (modified after Ohtsubo, Egashira, Tanaka, & Mishima, 2002)

Treatment	d-spacing (Å)	Minerals Indicated	Peak Intensity
Mg air-dried	1.4-1.5	Sm, Ch	a
	1.0	It	b
	0.7	Kt, Ch	c
Mg glycol	1.7	Sm	d
	1.4	Ch	e

Mineral codes: Sm = smectite, Ch = chlorite, It = Illite, Kt = kaolinite.

in bulk soil is calculated by multiplying the smectite content in the clay fraction with its percentage. Hence, the smectite content in bulk soil is about 10% for soil M and about 2% for soil C.

A.3.4.2 Thermogravimetric Analysis (TGA)

Thermogravimetric analysis (TGA) is used primarily to characterize the hydration status of some materials and study their thermal stability at elevated temperatures (up to 1,000°C). In the context of this research, the results of TGA are useful to complement the XRD data in detecting the different minerals present in marl deposit and understand the fundamental differences between soil M and soil C. The standard testing procedure for this test is summarized in ASTM E1131-08 (ASTM, 2014c). TGA was performed in the Soil Chemistry laboratory of Purdue University's Agronomy Department. Air-dried samples were ground into powder using a mortar and a pestle, and $\sim 50 \text{ mg}$ were loosely loaded into a 70 μL aluminum oxide (Al_2O_3) ceramic crucibles. The crucibles were placed in the thermogravimetric analyzer (Model—TGA/SDTA851e, Mettler Toledo, OH, USA) and gradually heated from 25°C to 1,000°C at a rate of 20°C/min. During the test, dry nitrogen (N_2) was used as the purge gas at a flow rate of 20 mL/min. The purpose of employing a flowing gas in the TGA analyzer is to purge the thermobalance of any gas emitted from the sample during the experiment, thus minimizing its interaction with the sample powder (Bish & Duffy, 1990). Results were normalized so that all final masses (at 1,000°C) are equal to 10 mg, and first derivatives were calculated digitally from the raw TGA data.

TGA was used to analyze the thermal reactions of the same 5 samples analyzed using XRD (see Table A.3.2). All samples were tested twice for repeatability. A total of ten TGA curves were obtained and are presented in Figure A.3.17, where the dashed black lines represent soil M and the continuous blue lines represent soil C. The TGA curves for both samples show a major mass-loss event at temperatures $>700^\circ\text{C}$, which likely reflects the breakdown of carbonates. As expected, soil M has a greater mass loss compared with soil C due to its higher carbonate content. In addition, within the same soil type, samples with higher CaCO_3 content result in higher mass losses: SEM1 > TX114 > TX112 and TX102 > TX103.

In order to better detect the mass-loss events, the derivative mass-loss curve, also known as the derivative TGA (DTG) curve, was computed for soil M (TX114) and soil C (TX102), and plotted with the corresponding TGA curve in Figure A.3.18 and Figure A.3.19, respectively. The results for soil M and soil C show four distinctive mass loss stages when the samples were heated from 25°C to 1,000°C, with the fourth being the largest. The four mass loss events were observed at 25–200°C, 200–300°C, 400–600°C, and $>600^\circ\text{C}$, resulting in a total mass loss of $\sim 32\%$ for soil M and $\sim 20\%$ for soil C. A mass loss plateau is reached at $\sim 880^\circ\text{C}$ and $\sim 840^\circ\text{C}$ for soil M and soil C, respectively. Table A.3.6 summarizes the percentage mass loss at various temperature ranges. The mass losses at temperatures $<200^\circ\text{C}$ are due to the loss of the adsorbed water on clay surfaces, whereas the ones at 200 to 300°C are due to the removal of interlayer bound water in the clay structure (dehydration of smectite and illite, as reported by Velde (1992)). The third mass loss event (400 to 600°C) is related to the dehydroxylation of kaolinite and illite (Brindley & Lemaitre, 1987; Fanning, Keramidias, & El-Desoky,

TABLE A.3.5
Clay mineral composition of soil M and soil C

Mineral	Soil M	Soil C
Smectite	50%	5%
Illite	27%	62%
Chlorite	12%	30%
Kaolinite	11%	3%

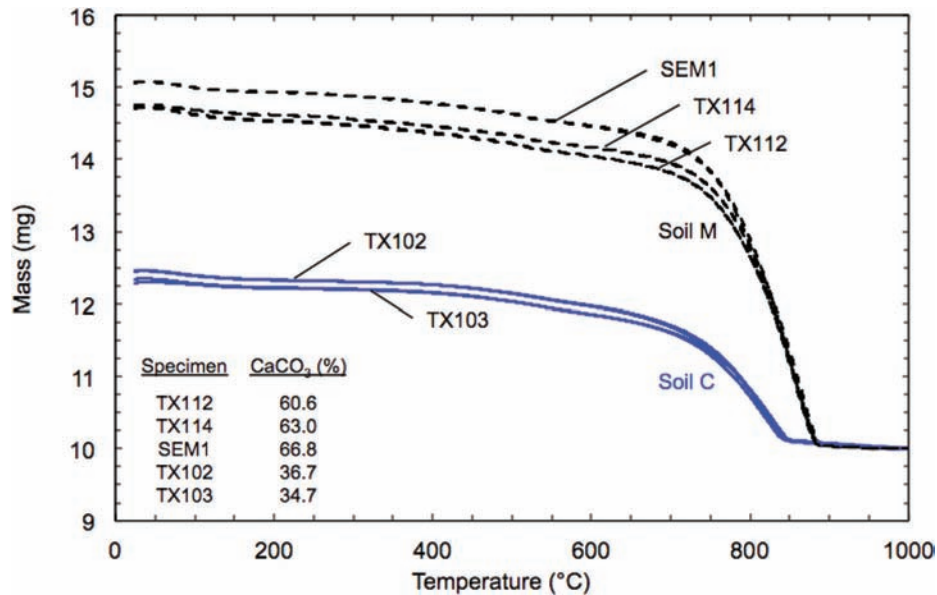


Figure A.3.17 Normalized thermogravimetric analysis curves of soil M (black dashed line) and soil C (blue continuous line) (~50 mg samples, 20°C/min heating rate, 20 mL/min N₂ purge).

1989; Velde, 1992), the presence of which was detected through XRD analyses, and the fourth large mass loss at temperatures >600°C is due to a combination of carbonate breakdown and dehydroxylation of chlorite and smectite (Bish & Duffy, 1990; Velde, 1992; Zhu, 2009). Note that the majority of the mass loss occurs at temperatures >600°C, which is expected due the elevated carbonate content present in marl.

A.3.4.2.1 Effect of Carbonates on TGA Curves

As an attempt to identify the different amounts of carbonate minerals present in marl (calcite, dolomite, aragonite for soil M; calcite, dolomite for soil C), the shell aragonite as well as the three different pure minerals (calcite, dolomite, and

quartz) described in Section A.3.4.1 were analyzed using TGA. The normalized results are summarized in Figure A.3.20. As expected, the TGA curve for quartz does not show any mass loss since quartz mineral is known to be an inert material and very stable even when heated to moderately high temperatures (Drees, Wilding, Smeck, & Senkayi, 1989). All three carbonates (calcite, dolomite, and shell aragonite) decompose around the same temperature range (700–900°C), which makes the distinction between them using TGA curves almost impossible. However, a comparison between the relative abundance of calcite and dolomite in soil M and soil C can be still made. Figure A.3.20 shows that shell aragonite and dolomite decarbonate at almost the same temperature, whereas calcite decarbonates at slightly higher temperature. Similar observation was reported by Doner and Lynn (1989) and Bish and

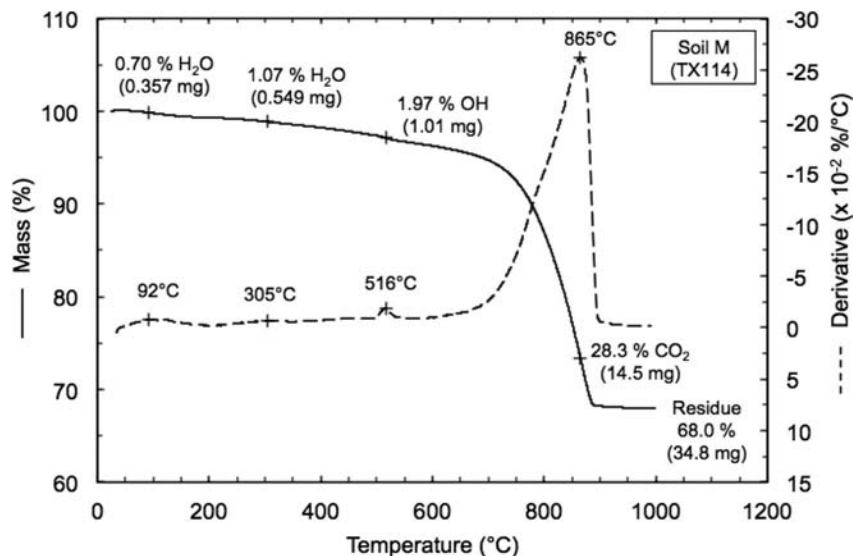


Figure A.3.18 Thermogravimetric analysis curve of soil M (51.2 mg sample, 20°C/min heating rate, 20 mL/min N₂ purge).

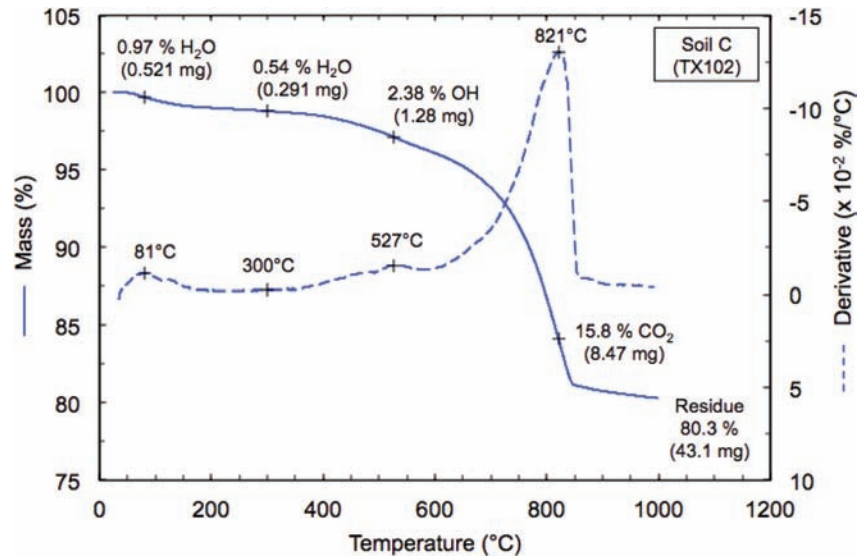


Figure A.3.19 Thermogravimetric analysis curve of soil C (51.2 mg sample, 20°C/min heating rate, 20 mL/min N₂ purge).

TABLE A.3.6
Mass loss during thermogravimetric analysis of soil M and soil C before and after treatment with Na-acetate

Sample	Percentage Mass Loss at				Total
	25–200°C	200–300°C	400–600°C	>600°C	
Soil M	0.70	1.07	1.97	28.3	32.0
Soil C	0.97	0.54	2.38	15.8	19.7

Duffy (1990) but at different reaction temperatures, which is mainly caused by the differences in the testing conditions. Great care must be taken in comparing data obtained in different laboratories on different samples due to the number of instrument- and sample-related factors that can affect TGA results. This is illustrated in Figure A.3.21, which presents normalized thermogravimetric analysis curves of natural calcite heated at different testing conditions. The figure shows that generally, the reaction temperatures shift to higher values with (i) larger sample mass (curve 3 to 4); (ii) higher heating rate (curve 2 to 3); and (iii) lower N₂ purge rate (curve 1 to 2). TGA curve 1 was obtained using the same sample mass, heating rate, and N₂ purge employed by Bish and Duffy (1990), which led to similar decarbonation temperature.

Since the decarbonation temperature of calcite is higher than that of dolomite (as reported above), it would be expected that the decarbonation temperature shifts to a higher value with an increase in calcite content. As shown in Figure A.3.18 and Figure A.3.19, the carbonate breakdown for soil M occurs at relatively higher temperatures compared with soil C (soil M: DTG_{max} ~865°C; soil C: DTG_{max} ~821°C). In addition, the mass loss plateau for soil M is reached at higher temperature (~880°C) compared to soil C (~840°C). These observations lead to the conclusion that soil M contains relatively more calcite than soil C, whereas the latter is richer in dolomite. This is in agreement with the XRD results.

In order to study the effect of shells on the TGA curves, soil M was subjected to different pre-treatment procedures and the following samples were examined using TGA:

1. soil M in its natural state;
2. soil M without shells; this was achieved carefully wet sieving the soil on the #200 (75 μm) sieve to remove the shells;

3. soil M without all carbonates; this was achieved removing the shells through wet sieving and treating the soil passing the #200 (75 μm) sieve with Na-acetate. The premise of testing this sample is to assess the effectiveness of Na-acetate treatment in removing carbonates.

Figure A.3.22 shows the TGA curves of the three samples described above. TGA curves for soil C (natural state) and shell aragonite are included for comparison. This investigation leads to the following conclusions:

1. Shell aragonite contributes to a small portion of the carbonates present in soil M; the carbonates minerals present in this soil are mostly calcite and dolomite.
2. Even after removing the shells from soil M, the TGA curve (“Soil M—no shells”) still shows a mass loss event that is about twice that of soil C. This indicates that the presence of shells is not the only difference between soil M and soil C but there is also a difference between the soil matrix; the total calcite/dolomite content in soil M is larger than the one in soil C.
3. The complete disappearance of the mass loss event corresponding to the carbonates breakdown (700–900°C) indicates that the Na-acetate treatment was effective in removing the carbonates present in the soil.

A.3.4.2.2 Semi-Quantitative Analysis Using TGA

Additional analyses were conducted on samples prepared with the clay fraction (<2 μm) of soil M and soil C treated with pH 5 1 M sodium acetate (NaOAc) to remove carbonates. The TGA and DTG curves for soil M and soil C are shown in Figure A.3.23 and Figure A.3.24, respectively. The premise of testing treated samples of marl using TGA is to identify the mass losses that correspond to the clay portion. This is expected to complement the XRD results presented in Section A.3.4.1 and aid in understanding the fundamental differences between soil M and soil C that might be influencing their engineering behavior. Earnest (1980) reported that quantitative analysis using TGA ideally requires that the components of a mixture do not have overlapping mass losses. This is not the case for marl, since it is composed of kaolinite and illite that dehydroxylize at the same temperature range (450–600°C) as well as chlorite and smectite (>600°C). However the clay mineral composition obtained in the semi-quantitative

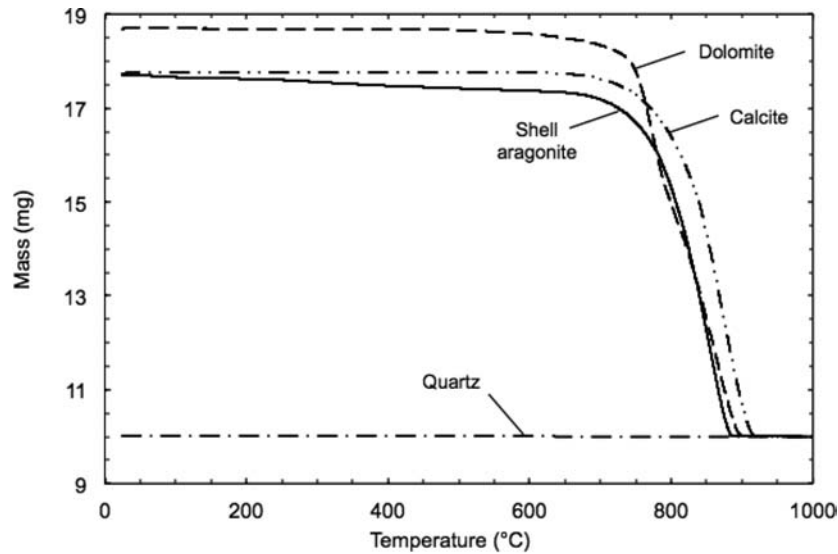


Figure A.3.20 Normalized thermogravimetric analysis curves of shell aragonite, natural calcite, natural dolomite, and natural quartz (~50 mg samples, 20°C/min heating rate, 20 mL/min N₂ purge).

analysis using XRD (Section A.3.4.1.4) can be used to estimate the expected mass loss in each temperature range.

From the semi-quantitative analysis using XRD data (Section A.3.4.1.4), the clay fraction (<2 μm) of soil M contains about 50% smectite, 27% illite, 12% chlorite, and 11% kaolinite; whereas that of soil C contains about 5% smectite, 62% illite, 30% chlorite, and 3% kaolinite. These numbers can be used to estimate the percentage mass losses for the 450–600°C range (dehydroxylation of kaolinite and illite) and >600°C (dehydroxylation of chlorite and smectite). Table A.3.7 summarizes the ideal hydroxyl (OH) water loss (wt. %) due to the dehydroxylation of each mineral as well as the expected mass loss (wt. %) calculated based on each mineral fraction estimated using XRD. The total expected mass loss (at temperature >450°C) is 6.1% for soil M and 6.7% for soil C. These numbers are generally in good agreement with the observed mass losses recorded using TGA: 7.3% for soil M (temperature >450°C in Figure A.3.23) and 5.7% for soil C (temperature >450°C in Figure A.3.24).

A.3.4.3 Scanning Electron Microscopy (SEM)

Scanning electron microscopy was employed to gain insight into the microstructure of the previously mentioned two types of marl and observe the main difference(s) between them. The sample was allowed to dry at room temperature for ~1 week and then broken to reveal a free fractured face that was mounted using graphite paste (Figure A.3.25). All samples were imaged without coating. Images were obtained in Purdue University’s Life Science Microscopy facility with the FEI Quanta 3D FEG SEM using the low vacuum LVSED detector as well as the backscattered BSE detector. Parameters were 20kV, Spot 6.0, and 10mm WD. Magnifications ranged between 250x and 4000x. Energy dispersive X-ray spectroscopy (EDX) was conducted with an Oxford INCA Xstream-2 with Xmax80 detector (Oxford Instruments, Peabody, MA) using parameters of 20kV, 6.5 spot, 10mm WD, 50μm objective aperture, and P4. EDX was applied to analyze the chemical composition of the objects of interest present in the samples.

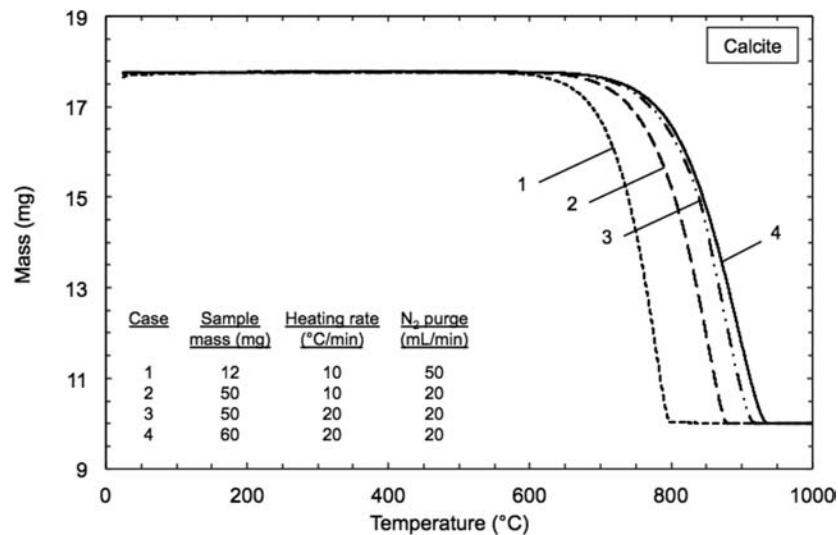


Figure A.3.21 Normalized thermogravimetric analysis curves of natural calcite showing the effect of sample mass, heating rate, and N₂ purge on decarbonation temperature.

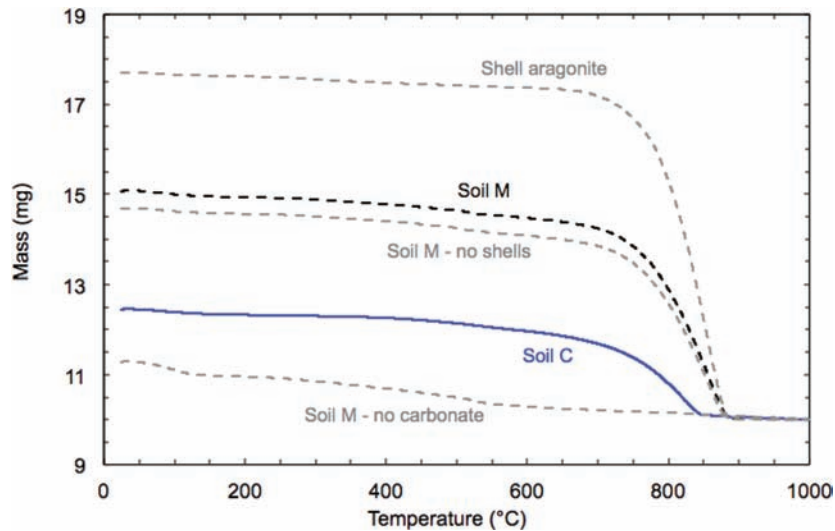


Figure A.3.22 Normalized thermogravimetric analysis curves of soil M subjected to different pre-treatment procedures, soil C, and shell aragonite (~50 mg samples, 20°C/min heating rate, 20 mL/min N₂ purge).

Figure A.3.26 shows the scanning electron micrographs for soil M. The length in micrometers (µm) of each scale bar is given below the micrographs. The figures illustrate different types of microfossils and shells of snails (Figure A.3.26(a)) and bivalves (Figure A.3.26(b)) that are integrated into the soil matrix. Figure A.3.26 (c) shows the presence of calcite crystals as part of the soil matrix resulting in a higher calcite content in soil M as reported in the XRD results. The micrographs also show the presence of 5–30 micron framboidal pyrite (iron sulfide), consisting of crystallites ranging from 0.5–3 microns (Figure A.3.26 (d-f)). These different features were identified chemically using EDX.

Figure A.3.27 shows the scanning electron micrographs of soil C. It is clear that this soil does not have shells as described earlier; however, iron sulfide was detected, although not in the framboidal form observed in soil M. This might be an indication of the different environmental conditions (e.g., presence of water, temperature) in which the soil was deposited. In general, soil M shows a more open microstructure compared with soil C, which is

consistent with the higher void ratio reported in Section A.3.3.3 (soil M: $e \sim 1.7$; soil C: $e \sim 1.2$).

EDX was applied to map the distribution of chemical elements in the samples. This is a powerful tool that can aid in identifying the objects of interest in the SEM and detecting any trace minerals or metals that are present in the soil. For example, Figure A.3.28 shows how EDX was used to map the chemical elements in soil C. It can be seen that iron (Fe) and sulfur (S) are detected where the SEM analysis showed the existence of iron sulfide, whereas the soil matrix in the background has silicon (Si), oxygen (O), aluminum (Al) and calcium (Ca).

A.3.4.4 Optical Light Microscopy (LM)

Shells found in soil M were collected and analyzed using an optical light microscope. Six major species were identified, as summarized in Figure A.3.29. Identifying the different type of

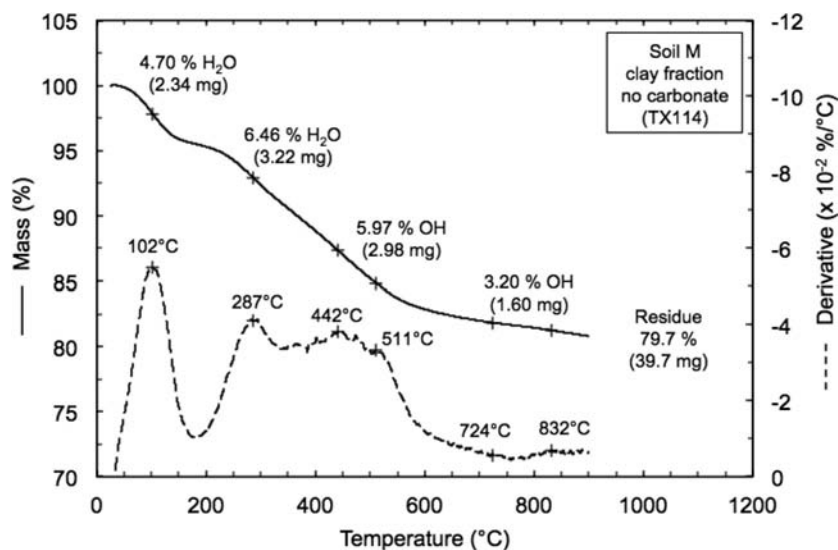


Figure A.3.23 Thermogravimetric analysis curve of the clay fraction (<2 µm) of soil M treated with Na-acetate (49.9 mg sample, 20°C/min heating rate, 20 mL/min N₂ purge).

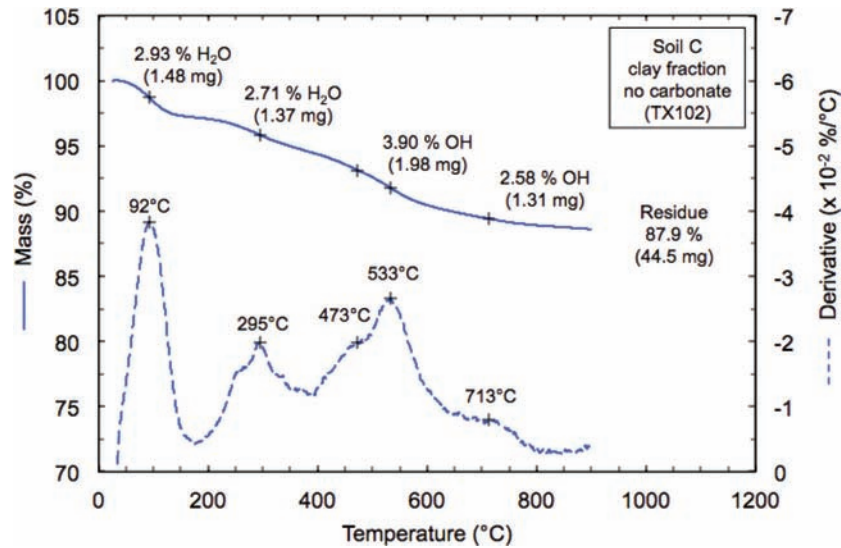


Figure A.3.24 Thermogravimetric analysis curve of the clay fraction ($<2\ \mu\text{m}$) of soil C treated with Na-acetate (50.7 mg sample, $20^{\circ}\text{C}/\text{min}$ heating rate, $20\ \text{mL}/\text{min}$ N_2 purge).

TABLE A.3.7
Semi-quantification of clay minerals present in soil M and soil C using TGA

Sample	Mineral	Ideal OH loss (%)	Dehydroxylation temp. ($^{\circ}\text{C}$)	References*	Mineral fraction from XRD (%)	Expected mass loss [†] (%)
Soil M	Kaolinite	14	450–550 $^{\circ}\text{C}$	[1], [2]	11	1.5
	Illite	5	500–600 $^{\circ}\text{C}$	[3], [2]	27	1.4
	Chlorite	10	$>600^{\circ}\text{C}$	[4], [2]	12	1.2
	Smectite	4	$>600^{\circ}\text{C}$	[4], [2]	50	2.0
Soil C	Kaolinite	14	450–550 $^{\circ}\text{C}$	[1], [2]	3	0.4
	Illite	5	500–600 $^{\circ}\text{C}$	[3], [2]	62	3.1
	Chlorite	10	$>600^{\circ}\text{C}$	[4], [2]	30	3.0
	Smectite	4	$>600^{\circ}\text{C}$	[4], [2]	5	0.2

*[1] Brindley & Lemaitre (1987); [2] Velde (1992); [3] Fanning et al. (1989); [4] Bish & Duffy (1990).

[†]Expected mass loss = (mineral fraction from XRD) \times (ideal OH loss) / 100.

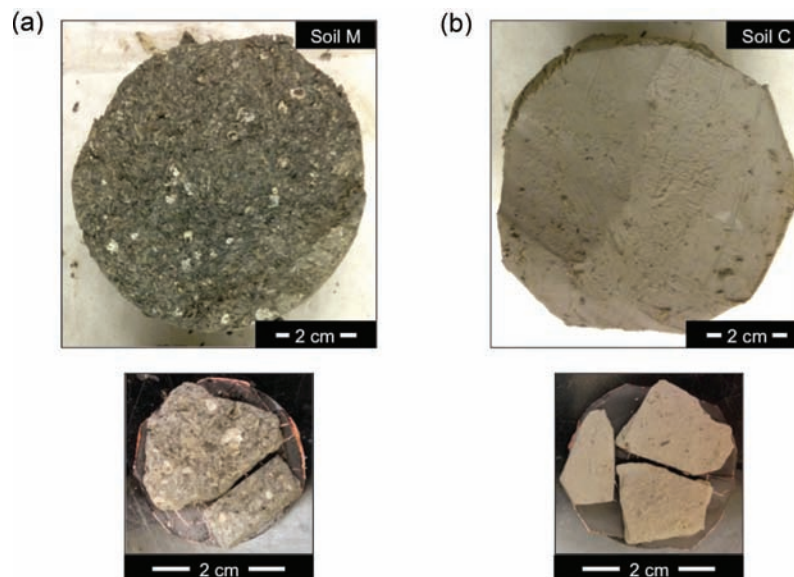


Figure A.3.25 Scanning electron microscopy samples of (a) soil M and (b) soil C.

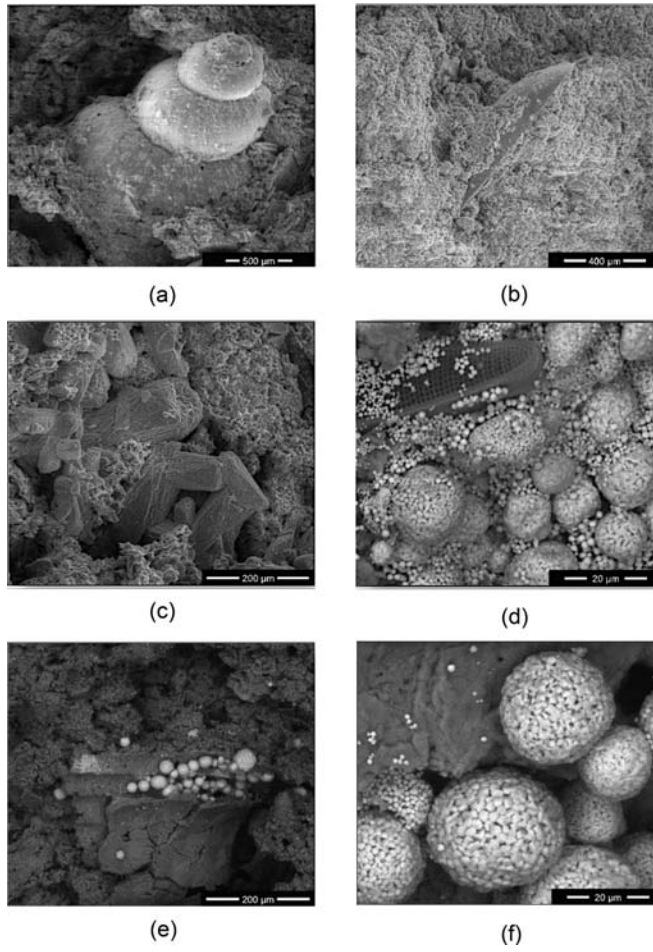


Figure A.3.26 Scanning electron micrographs for soil M showing different types of microfossils and framboidal pyrite that are integrated into the soil matrix.

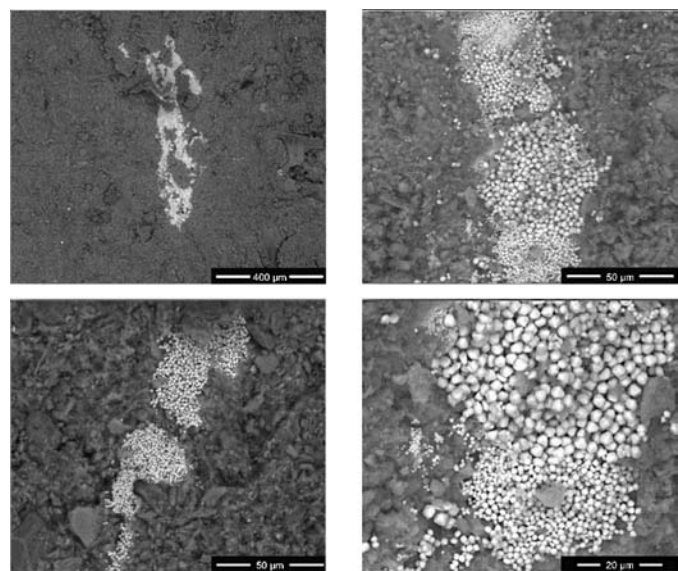


Figure A.3.27 Scanning electron micrographs for soil C.

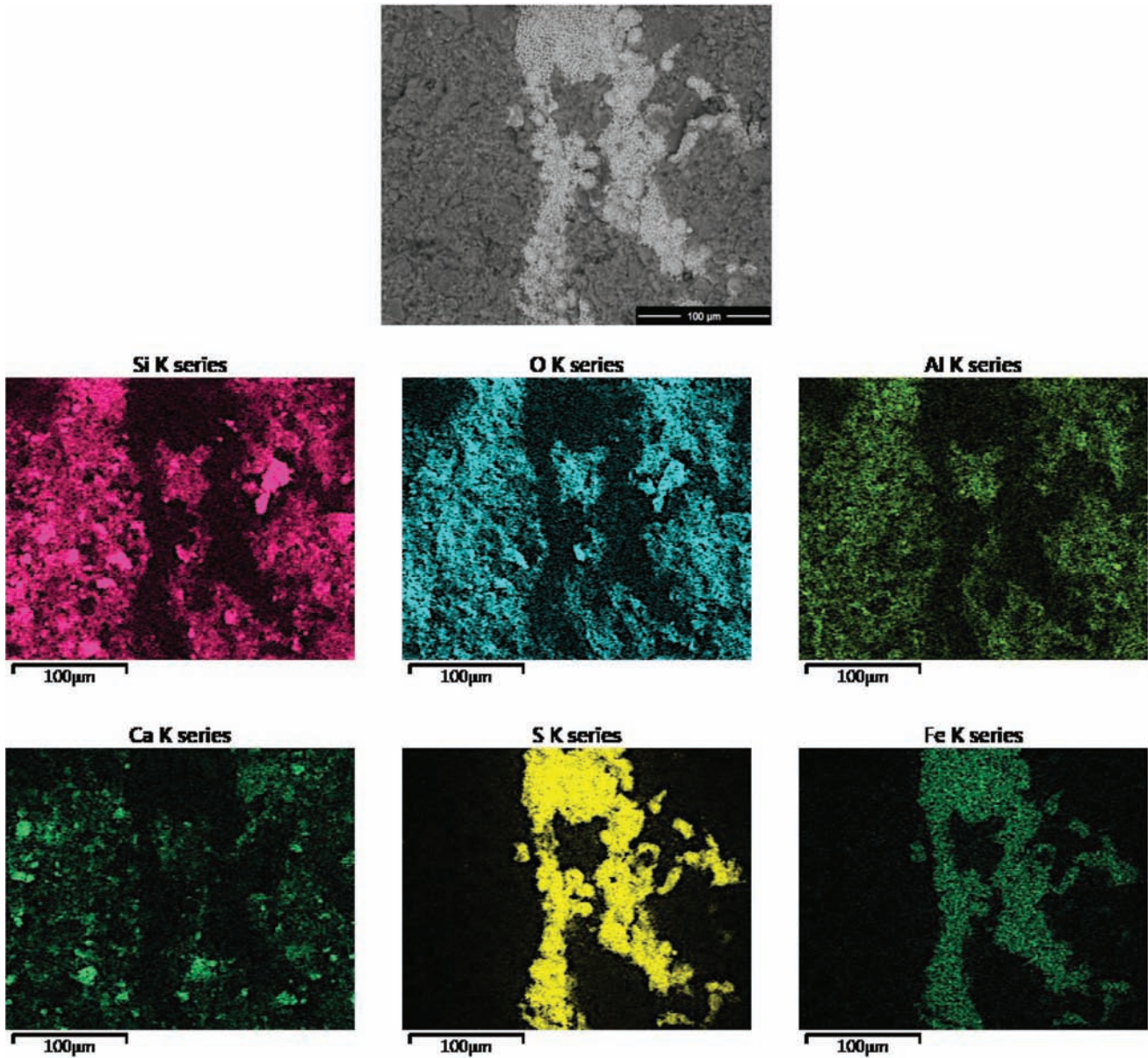


Figure A.3.28 EDX analysis for soil C identifying the different chemical elements.

species allows a better understanding of the geology of the site and the environmental conditions (e.g., presence of water, salinity, temperature) in which the soil was formed. There is also a possibility of estimating the age of the deposit using carbon dating.

Charophyte oospores were also found in soil M (see Figure A.3.30). These are pond-dwelling algae that live in still or slow-moving water with calcium carbonate. The absence of both shells and charophytes in soil C might be an indication of the absence of life when soil C was deposited.



Figure A.3.29 Microscopic images for the different types of microfossils collected from soil M.

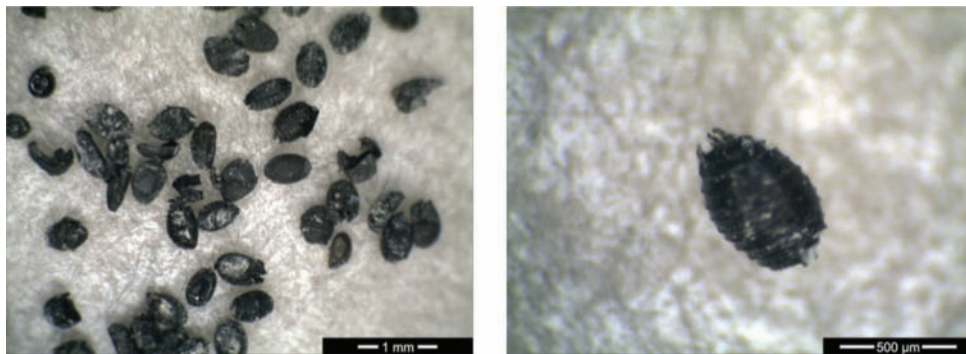


Figure A.3.30 Microscopic images for charophyte oospores collected from soil M.

APPENDIX 4: ENGINEERING PROPERTIES

A.4.1. INTRODUCTION

This appendix provides a detailed evaluation of results from consolidation tests and triaxial tests, conducted on undisturbed samples of marl. The consolidation tests, performed using constant rate of strain (CRS) and incremental loading (IL), were used to derive the stress history, consolidation and creep properties, whereas the shear strength tests were used to derive the undrained shear strength profiles and the soil's SHANSEP parameters. Section A.4.2 summarizes the sample preparation and testing procedures used during consolidation and shear tests. The stress history and consolidation properties are summarized in Section A.4.3, while the undrained shear behavior is presented in Section A.4.4.

In this study, a total of six CRS consolidation, two IL consolidation, and eleven triaxial tests were performed on marl samples obtained from different boreholes at various depths. Table A.4.1 and Table A.4.2 present a summary of the tests location, and index properties of soil M and soil C specimens, respectively. The index properties include: the carbonate content (CaCO_3), the natural water content (w_n), the plastic limit (PL), the liquid limit (LL), the clay content, the specific gravity (G_s), the in situ void ratio (e_0), the in situ degree of saturation (S_i), the total unit weight (γ_t), the salt concentration, and the pH.

A.4.2. SAMPLE PREPARATION AND TESTING PROCEDURES

A.4.2.1 Sample Preparation

Specimens were prepared for all the engineering tests using the following procedure. The Shelby tube was cut above and below

the selected specimens using a horizontal band saw with lengths appropriate for each consolidation or shear test to reduce disturbance due to extrusion. The remaining segments of the tube were resealed with wax and plastic caps and stored in the humid room for later use. The specimen was extruded following the method described by Ladd and DeGroot (2003). In summary, a piano wire was penetrated through the soil along the inside of the tube with the help of a thin hypodermic tube. The wire was used to debond the soil by rotating the tube 3–4 times. The specimen was then gently pushed by hand out of the tube. The resulting specimen, ~7.4 cm (~2.9 in) diameter, was trimmed in different manners and dimensions depending on the specific type of test (see Section A.4.2.2).

A.4.2.2 Testing Procedures

The general procedures of consolidation and triaxial tests include specimen setting up, saturation, consolidation, and undrained shearing (for triaxial test only). Since most of these steps are controlled by a computer and the techniques are well published (e.g., Germaine & Germaine, 2009; Hwang, 2006; and Sheahan & Germaine, 1992), only a brief summary is provided.

CRS and IL consolidation tests were performed using computer controlled CRS apparatuses available at Purdue University's Bechtel geotechnical laboratory, which are based on the original apparatus developed by Wissa, Christian, Davis, & Heiberg (1971). All tests were conducted under single drainage conditions with measurements of the excess pore-water pressure at the base of the specimens. The extruded specimen described in Section A.4.2.1 was trimmed into a stainless steel confining ring (6.35 cm (2.5 in) diameter and 2.54 cm (1 in) height). Trimming was conducted by advancing the ring in small increments while trimming the soil ahead of the ring using a thin spatula to reduce

TABLE A.4.1
Summary of tests location and index properties of soil M specimens

Test #/Depth (m)	Boring Sample	CaCO_3 (%)	w_n (%)	PL (%)	LL (%)	Clay (%)	G_s	e_0	S_i (%)	γ_t (kN/m^3)	Salt conc (g/l)	pH
CRS103 6.83	MR#2 ST4	45.5	64.4	—	—	—	2.686	1.74	99	15.77	—	—
CRS105 9.27	MR#1 ST7	35.9	53.7	29.0	67.1	—	2.675	1.44	100	16.49	—	—
CRS106 8.10	MR#3 ST6	60.9	60.2	32.6	66.0	18	2.705	1.67	97	15.89	—	—
CRS108 8.67	MR#2 ST7	55.4	60.5	29.4	62.0	—	2.732	1.72	96	15.80	—	—
CRS110 7.59	MR#1 ST4	50.2	50.5	—	—	—	2.705	1.43	95	16.4	—	—
IL101 6.95	MR#2 ST4	48.8	66.6	—	—	—	2.686	1.82	98	15.56	2.14	7.66
IL103 9.11	MR#3 ST7	46.9	52.7	—	—	—	2.798	1.49	99	16.81	—	—
TX107 8.48	MR#3 ST6	59.6	58.4	34.7	61.7	16	2.713	1.63	98	16.1	3.33	7.82
TX108 7.01	MR#2 ST4	48.5	65.7	40.6	66.4	23	2.699	1.80	99	15.7	2.68	7.53
TX109 7.11	MR#2 ST4	54.6	65.9	33.8	65.7	22	2.706	1.81	99	15.7	3.15	7.91
TX111 7.06	MR#3 ST5	61.8	68.5	33.1	74.2	19	2.705	1.89	98	15.5	2.74	7.85
TX112 7.16	MR#3 ST5	60.6	68.5	37.9	66.4	18	2.701	1.86	99	15.6	3.15	7.71
TX114 7.44	MR#4 ST5	63	62.2	33.4	73.7	15	2.707	1.74	97	15.7	3.19	7.77

TABLE A.4.2
Summary of tests location and index properties of soil C specimens

Test # Depth (m)	Boring Sample	CaCO ₃ (%)	w _n (%)	PL (%)	LL (%)	Clay (%)	G _s	e ₀	S _i (%)	γ _t (kN/m ³)	Salt conc (g/l)	pH
CRS109 7.54	MR#1 ST4	33.9	42.1	—	—	—	2.789	1.20	98	17.66	—	—
TX102 8.31	MR#3 ST6	36.7	36.6	19.9	40.1	36	2.805	1.11	93	17.86	5.07	7.72
TX103 7.47	MR#1 ST4	34.7	39.7	21.3	46.7	45	2.789	1.14	98	17.90	4.51	7.80
TX105 7.67	MR#1 ST4	37.4	52.2	25.5	52.4	33	2.758	1.46	99	16.77	2.73	7.88
TX115 7.58	MR#4 ST5	33.7	47.0	20.0	47.7	45	2.771	1.32	99	17.20	—	—
TX116 7.66	MR#4 ST5	38.4	37.3	18.8	44.7	36	2.819	1.08	98	18.28	4.44	7.57

disturbance caused by the ring advancement. The top and bottom ends of the specimen were cut with a wire saw and flattened with a razor-sharp stainless steel straight edge. Porous stones and filter papers were used at each end of the specimens. The specimen was backpressure saturated at constant volume to 200 kPa (29 psi) for a period of 24 hours. The saturation pressure and time were chosen based on the work reported by Black and Lee (1973), and they were also confirmed by satisfactory Skempton's pore-pressure parameters ($B = \Delta u / \Delta \sigma_{\text{cell}}$) measured in the triaxial tests. For CRS tests, consolidation was performed by imposing a constant rate of displacement equivalent to a strain rate varying between 1%/hr and 2%/hr. For IL tests, the consolidation was performed by doubling the applied load (i.e., load increment ratio (LIR) equals to one), and each load increment was maintained for 24 hours. An IL consolidation test can take several weeks to complete compared with the CRS consolidation test, which can be completed in much shorter period of time and results in a continuous compression curve. However, IL consolidation tests were still needed in order to derive the creep properties of marl.

Triaxial tests were K_0 consolidated tests sheared under undrained conditions in compression loading ($CK_0UTC(L)$). The tests were performed using computer controlled triaxial apparatuses available at Purdue University's Bechtel geotechnical laboratory. The triaxial cell features an internal load cell to measure the axial load, eliminating the need to correct for the piston friction and uplift force caused by the cell pressure. Soil specimens were all trimmed using a wire saw into a cylindrical shape (3.8 cm (1.5 in) diameter and 7.6 cm (3 in) height). The top and bottom of the specimen were trimmed using a razor-sharp stainless steel straight edge. Porous stones and filter papers were used at each end of the specimens. Vertical filter drains (eight 6-mm wide filter strips) were used to provide lateral drainage and two thin membranes (i.e., non-lubricated prophylactics) were used to enclose the specimen and isolate it from the cell fluid. Silicon oil was used for the cell fluid for two main reasons: (i) prevent membrane leakage, and (ii) provide a non-conductive medium for the submerged load cell and its connections. Data were corrected for the change in the specimen area during deformation, membranes resistance, and filter drains resistance (Germaine & Ladd, 1988). The specimens were all backpressure saturated to 200 kPa for 24 hours before consolidation, which resulted in an average B value of $0.99 \pm 0.01SD$ for 11 triaxial tests. For all the triaxial tests, SHANSEP procedures were followed. After backpressure, the specimens were K_0 consolidated to stresses higher than $2\sigma'_p$, at a strain rate varying between 0.5%/hr and 2%/hr. The specimens were allowed to creep for a period of 24 hours to dissipate the excess pore pressure. They were either sheared normally consolidated ($OCR = 1$) or swelled to the desired OCR , where they were sheared following a second creep stage. All undrained shear stages were conducted using a strain rate of 0.5%/hr.

A.4.3. STRESS HISTORY AND CONSOLIDATION PROPERTIES

A.4.3.1 Introduction

This section provides a detailed evaluation of results from consolidation tests conducted on undisturbed samples of marl (soil M and soil C). The evaluation includes development of the stress history profile; determination of the compressibility properties, coefficient of consolidation, and permeability; estimation of the lateral stress ratio (K_0); and determination of the creep properties.

The consolidation data for marl were obtained from the CRS consolidation tests, the IL consolidation tests, and the consolidation phase of SHANSEP triaxial tests. The stress history profile and the compressibility properties were determined based on the compression curves from all tests. In addition, the lateral stress ratio was estimated from the K_0 consolidated triaxial tests. The CRS and IL consolidation tests provided information about the coefficient of consolidation and the permeability of the marl deposit. The IL consolidation tests were used to determine the creep properties.

The consolidation data for the CRS consolidation, IL consolidation, and SHANSEP $CK_0UTC(L)$ tests for soil M and soil C are summarized in Table A.4.3 and Table A.4.4, respectively. The tables give the tests location, the in situ phase data (w_n , e_0 , and S_i), the overburden stress (σ'_{v0}), the preconsolidation stress (σ'_p), the overconsolidation ratio (OCR), the maximum virgin compression ratio (CR_{max}), the normally consolidated lateral stress ratio (K_{0NC}), and the consolidation strain rate (%/hr).

Table A.4.5 presents a summary of all consolidation properties for soil M and soil C. The following subsections will discuss the results of the various consolidation properties in greater detail.

A.4.3.2 Compression Curves

A total of 17 one-dimensional compression curves obtained from CRS consolidation tests and triaxial tests performed on undisturbed samples of marl are presented in Figure A.4.1, where the dashed black lines represent soil M and the continuous blue lines represent soil C. In general, both types of marl show similar compressibility properties that fall in the range of soft clays. Figure A.4.1(a) shows the compression curves in the strain-effective stress plane, whereas Figure A.4.1(b) shows the compression curves in the void ratio-effective stress plane. All results show a consistent behavior (i.e., the compression curves are characterized by a clear break at the preconsolidation stress σ'_p and have an

TABLE A.4.3

Summary of consolidation data for the CRS consolidation, IL consolidation, and SHANSEP CK₀UTC(L) tests for soil M

Test #Depth (m)	BoringSample	In situ			Stress history (kPa)				Strain rate (%/hr)
		w _n (%)	e ₀	S _i (%)	σ' _{v0}	σ' _p	OCR	CR _{max} K _{0NC}	
CRS103 6.83	MR#2 ST4	64.4	1.74	99	73.1	136	1.86	0.28	1.0
CRS105 9.27	MR#1 ST7	53.7	1.44	100	89.4	193	2.16	0.23	1.0
CRS106 8.10	MR#3 ST6	60.2	1.67	97	81.6	166	2.03	0.25	1.0
CRS108 8.67	MR#2 ST7	60.5	1.72	96	85.4	175	2.05	0.26	1.0
CRS110 7.59	MR#1 ST4	50.5	1.43	95	78.2	130	1.66	0.24	2.0
IL101 6.95	MR#2 ST4	66.6	1.82	98	73.8	153	2.07	0.29	—
IL103 9.11	MR#3 ST7	52.7	1.49	99	88.3	151	1.71	0.24	—
TX107 8.48	MR#3 ST6	58.4	1.63	98	84.1	154	1.83	0.28 0.499	2.0
TX108 7.01	MR#2 ST4	65.7	1.80	99	74.3	129	1.74	0.27 0.483	2.0
TX109 7.11	MR#2 ST4	65.9	1.81	99	75.0	129	1.72	0.27 0.486	2.0
TX111 7.06	MR#3 ST5	68.5	1.89	98	74.6	120	1.61	0.27 0.475	0.5
TX112 7.16	MR#3 ST5	68.5	1.86	99	75.3	133	1.77	0.28 0.495	0.5
TX114 7.44	MR#4 ST5	62.2	1.74	97	77.2	158	2.05	0.26 0.491	0.5

S-shape), which is evidence of the soil's high sensitivity. This S-shape is more pronounced for soil C and the compression curves are characterized by a larger decrease in the virgin compression ratio (CR) along the virgin compression line (VCL) compared with soil M.

A.4.3.3 Stress History Profile

When building on soft soils, it is essential to develop a reliable stress history profile, which is most useful for: (i) estimation of long term consolidation settlements that are highly affected by the amount of precompression ($\sigma'_p - \sigma'_{v0}$); and (ii) estimation of the undrained shear strength of marl, which is directly related to the vertical effective stress and OCR via the SHANSEP equation (see Section A.4.4).

Figure A.4.2 presents the stress history for the marl deposit. Overburden stress (σ'_{v0}), preconsolidation stress (σ'_p), and OCR are tabulated for all tests in Table A.4.3 and Table A.4.4. The overburden (effective) stress (σ'_{v0}) profile was calculated by subtracting the pore water pressure (u_0) from the total overburden stress (σ_{v0}). The total overburden stresses were calculated based on the soil profiles and estimated unit weights shown in Figure A.2.2. The pore water pressure profile was calculated based on hydrostatic water pressures with water table located at 1.9 m (6.25 ft) below the ground surface, as reported in Section A.2.2. The preconsolidation stress was estimated using the strain energy technique proposed by Becker, Crooks, Been, & Jefferies (1987), which is based on the work per unit volume. This method is less subjective and less empirical compared with other methods proposed in the literature (e.g., Casagrande (1936) and Schmertmann (1955)) and can be easily computerized.

Figure A.4.2(a) and Figure A.4.2(b) show the variation with depth of preconsolidation stress and overconsolidation ratio,

respectively. Different symbol shapes are used to indicate different types of tests (square, triangle and circle for CRS consolidation, IL consolidation, and TX tests, respectively), while different colors are used to indicate the different types of marl (hollow black symbols correspond to soil M and solid blue circles correspond to soil C). In general, there is no clear difference between the results obtained from the different types of tests (CRS, IL, and TX). However, a clear difference can be observed between soil M and soil C. The preconsolidation stress for soil M shows an increasing trend with depth ranging between 120 and 193 kPa (mean $\sigma'_p = 148 \text{ kPa} \pm 21.3\text{SD}$). This trend was not observed for soil C due to the limited number of data points and the significant scatter; however, its average preconsolidation stress (mean $\sigma'_p = 104 \text{ kPa} \pm 11.7\text{SD}$) is lower than that of soil M. These stresses correspond to OCR ($= \sigma'_p/\sigma'_{v0}$) values around $1.9 \pm 0.2\text{SD}$ for soil M and around $1.3 \pm 0.2\text{SD}$ for soil C (see Figure A.4.2(b)). The higher values of OCR for soil M might be attributed to the natural cementation caused by the higher carbonate content present in soil M, as illustrated by the mineralogical analysis (Section A.3.4.1.3).

A.4.3.4 Compressibility

The virgin compression index (C_c) and compression ratio ($\text{CR} = C_c/(1+e_0)$) were obtained for each CRS consolidation, IL consolidation, and triaxial test. In order to obtain comparable results that are not influenced by the S-shape observed in the compression curves (see Section A.4.3.2), the maximum values of C_c and CR were derived from the consolidation curves between 2 σ'_p and 3 σ'_p , and their variation with depth is presented in Figure A.4.3. The maximum compression ratio for all tests is reported in Table A.4.3 and Table A.4.4.

TABLE A.4.4
Summary of consolidation data for the CRS consolidation, IL consolidation, and SHANSEP CK₀UTC(L) tests for soil C

Test #Depth (m)	BoringSample	In situ			Stress history (kPa)				Strain rate (%/hr)
		w _n (%)	e ₀	S _i (%)	σ'v ₀	σ'p	OCR	CR _{max} K _{0NC}	
CRS109 7.54	MR#1 ST4	42.1	1.20	98	77.8	118	1.52	0.24	2.0
TX102 8.31	MR#3 ST6	36.6	1.11	93	82.9	91	1.10	0.16 0.563	1.0
TX103 7.47	MR#1 ST4	39.7	1.14	98	77.3	100	1.29	0.20 0.560	2.0
TX105 7.67	MR#1 ST4	52.2	1.46	99	78.7	118	1.50	0.28 0.573	2.0
TX115 7.58	MR#4 ST5	47.0	1.32	99	78.1	102	1.31	0.28 0.562	0.5
TX116 7.66	MR#4 ST5	37.3	1.08	98	78.6	94	1.20	0.24 0.537	0.5

In general, there is no clear difference between the results obtained from the different types of tests (CRS, IL, and TX). However, a clear difference can be observed between soil M and soil C. As shown in Figure A.4.3(a), the compression index for soil M shows a decreasing trend with depth ranging between 0.56 and 0.81 (mean C_c = 0.71 ± 0.08SD), which is expected since the initial void ratio (e₀) also decreases with depth (Section A.3.3.3). This is consistent with the trends reported in the literature relating C_c and e₀ (see discussion below). This trend was not observed for soil C due to the limited number of data points and the significant scatter; however, its average compression index (mean C_c = 0.52 ± 0.13SD) is lower than that of soil M. Given the values of C_c as high as 0.8, marl can be classified as highly compressible. As a reference, typical values of the compression index for other soils obtained from the literature are presented in Table A.4.6.

Figure A.4.3(b) plots the variation of compression ratio with depth. Since the values of CR are obtained by normalizing with the initial void ratio, it can be seen that the results are more uniform, with a collective average value of CR equals to 0.25 ± 0.03SD.

The virgin compression index (C_c) and compression ratio (CR) are necessary for settlement calculation. These parameters are found from consolidation tests conducted on undisturbed soil samples. Because of the time and expense involved in consolidation testing, several researchers (e.g., Nishida, 1956; Terzaghi & Peck, 1967) have investigated alternative ways to obtain the values of compressibility of clayey soils. The compression index can be related to the physical properties of soils, such as initial void ratio, natural water content, and liquid limit. Table A.4.7 summarizes some of the relationships reported in the literature.

As expected, these proposed relationships differ from each other since they are based on different types of soils. As an attempt to obtain correlations that are more applicable for the marl deposit, the compression index was plotted against the initial void ratio, natural water content, and liquid limit in Figure A.4.4, Figure A.4.5, and Figure A.4.6, respectively. Using linear regression analysis, the following equations for marl are proposed:

$$C_c = 0.451 (e_0 - 0.104) \quad (r^2 = 0.861)$$

$$C_c = 0.012 (w_n + 1) \quad (r^2 = 0.873)$$

$$C_c = 0.010 (LL + 6.8) \quad (r^2 = 0.602)$$

In general, the first two equations yield C_c values that are close to the ones proposed by Nishida (1956) (Table A.4.7). However, when soil M and soil C are considered separately, the regression analysis for soil C yields a correlation (C_c = 0.746 (e₀ - 0.52)) that is very close to the one proposed by Bowles (1979) for moderately sensitive soils with low plasticity; while the one for soil M (C_c = 0.51 (e₀ - 0.304)) is very close to the one proposed by Nishida (1956) for natural soils. This is in good agreement with the fact that soil C has relatively lower plasticity (CL) and higher sensitivity (depicted by the strong S-shape compression curves) compared with soil M.

Note that the coefficient of determination for the third equation (C_c vs LL) is relatively low (r² = 0.602), which might

TABLE A.4.5
Summary of consolidation properties

	Soil M		Soil C	
	Range	Mean ± SD	Range	Mean ± SD
Overburden stress, σ'v ₀ (kPa)	73.1 – 89.4	79.2 ± 5.8	77.3 – 82.9	78.9 ± 2.0
Preconsolidation stress, σ'p (kPa)	120 – 193	148 ± 21.3	91.0 – 118	104 ± 11.7
Overconsolidation ratio, OCR	1.6 – 2.2	1.9 ± 0.2	1.1 – 1.5	1.3 ± 0.2
Virgin compression index, C _c	0.56 – 0.81	0.71 ± 0.08	0.34 – 0.67	0.52 ± 0.13
Maximum virgin compression ratio, CR _{max}	0.23 – 0.29	0.26 ± 0.02	0.16 – 0.28	0.23 ± 0.05
Permeability change index, C _k	0.648 – 0.699	0.674 ± 0.022	0.529	0.529
Normally consolidated lateral stress ratio, K _{0NC}	0.475 – 0.499	0.488 ± 0.009	0.537 – 0.573	0.559 ± 0.013
K ₀ = K _{0NC} (OCR) ^a	K _{0NC} = 0.49; n = 0.41		K _{0NC} = 0.56; n = 0.38	
C _{ae} /C _c	0.041		0.041	
Δe/e ₀	0.016 – 0.049	0.033 ± 0.009	0.024 – 0.050	0.039 ± 0.009

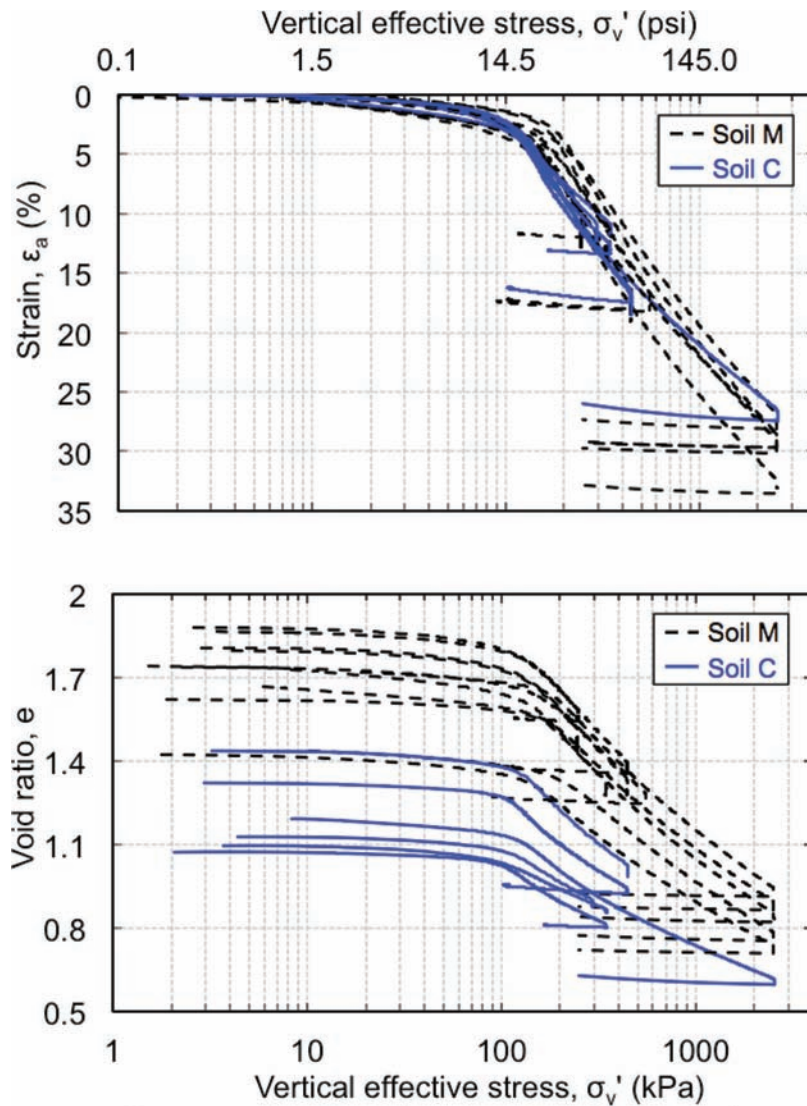


Figure A.4.1 (a) ϵ -compression curves and (b) e -compression curves from CRS consolidation and SHANSEP CK_0 UTC(L) tests.

be partially caused by the fundamental differences between the mineralogy of soil M and soil C, as illustrated by the mineralogical analysis (Section A.3.4.1.3).

A.4.3.5 Coefficient of Consolidation and Permeability

This section presents a summary of the coefficients of consolidation (C_v) and the permeability (k) of marl. The results presented are based on six CRS consolidation tests and two IL consolidation tests.

For the CRS consolidation tests, the values of k and C_v are calculated based on the CRS consolidation theory developed by Wissa et al. (1971). The permeability is first calculated from the excess pore pressure (u_e) recorded at the base of the specimen due to loading, and then C_v is calculated from the permeability and compressibility using the following equation:

$$C_v = k / (m_v \cdot \gamma_w)$$

where k is the permeability, $m_v (= \Delta \epsilon / \Delta \sigma'_v)$ is the coefficient of volume change, and γ_w is the unit weight of water.

For the IL consolidation tests, the values of C_v represent the average of the logarithm of time (Casagrande, 1936) and the

square root of time (Taylor, 1948) curve fitting methods. The logarithm of time method is based on similarity between theoretical and experimental curves when plotted versus log of time; it uses the time corresponding to 50% consolidation (t_{50}) to calculate C_v . For the square root of time, however, curves are plotted versus the square root of time and t_{90} corresponding to 90% consolidation is used for C_v calculation. The values of k are then calculated from C_v and m_v using the above equation.

Figure A.4.7 shows the coefficient of consolidation versus the vertical effective stress for the loading and unloading range obtained from CRS (denoted by lines) and IL (denoted by triangles) consolidation tests. The results show a decrease in C_v during loading followed by a slight increase in the normally consolidated region. For all tests, the results are characterized by an increasing value of C_{vNC} , similar trends were reported by Berman (1993) and Abdulhadi (2009). As a reference, typical values of the coefficient of consolidation for other soils obtained from the literature are presented in Table A.4.8.

The void ratio (e) versus the log of the permeability during loading is shown in Figure A.4.8. The decrease in permeability with compression is due to the reduction in the size of the macropores. As can be seen, there is an approximate linear relationship between the void ratio and $\log-k$. The slope of the

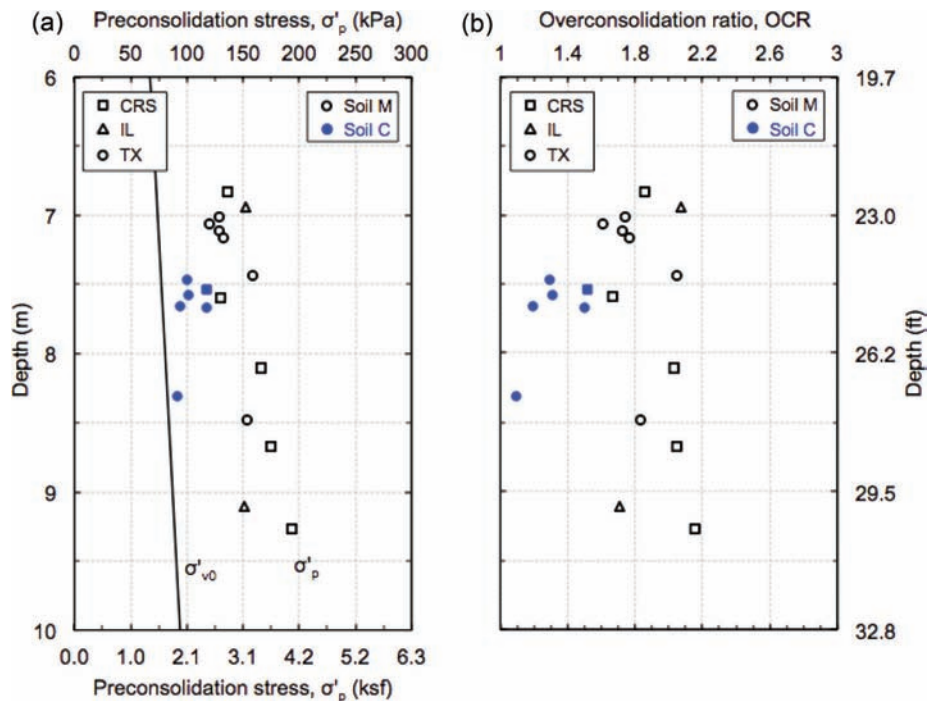


Figure A.4.2 Stress history profile: (a) preconsolidation stress and overburden stress; and (b) OCR with depth.

e-log k line is referred to as the permeability change index and denoted by C_k . In general, soil M has a C_k value higher than soil C. The average value of C_k is $0.674 \pm 0.022SD$ for soil M (five tests) and 0.529 for soil C (only one test available).

Tavenas, Leblond, and Leroueil (1983) examined the permeability of different natural soils and suggested that for clay and silt deposits $C_k/e_0 = 0.5$. Figure A.4.9 shows that the empirical correlation for marl deposits is $C_k/e_0 = 0.42$. This value is similar to the one reported by Berman (1993) for Boston blue clay.

A.4.3.6 Lateral Stress Ratio K_0

The lateral stress ratio $K_0 (= \sigma'_h/\sigma'_v)$ is an important soil parameter used in many geotechnical applications. For instance, it is necessary for the estimation of the in situ horizontal stresses (σ'_h). The consolidation phase of eleven SHANSEP CK₀U triaxial tests were used to develop a K_0 profile for the marl deposit.

Figure A.4.10 presents the variation of the lateral stress ratio K_0 with the vertical effective stress. The results show a decrease in K_0 during initial loading followed by an increase in the normally

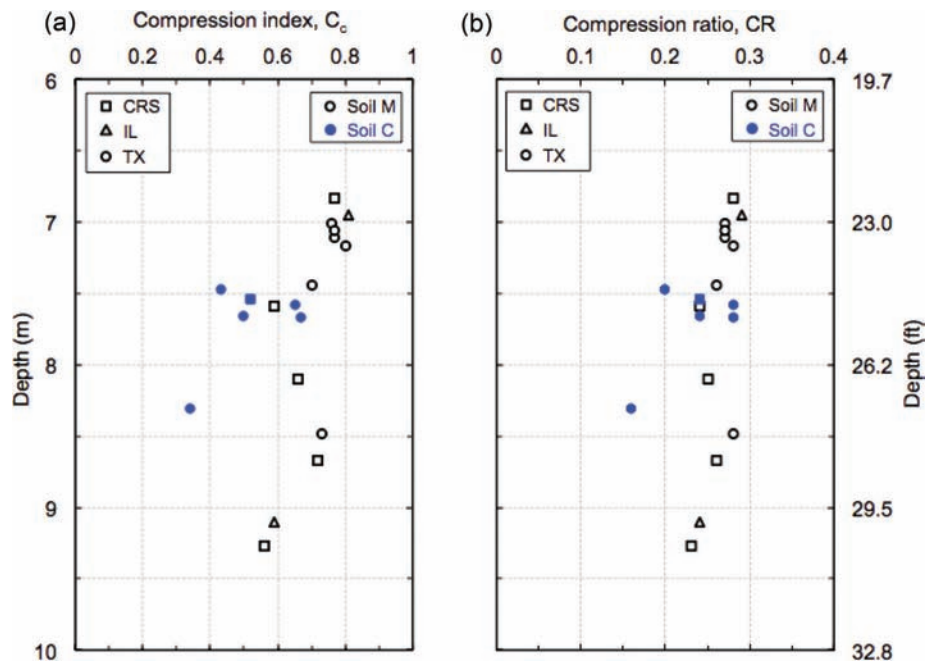


Figure A.4.3 Values of (a) compression index, and (b) compression ratio with depth.

TABLE A.4.6
Typical values of the compression index C_c (modified after Holtz & Kovacs, 1981)

Soil	C_c
San Francisco Bay Mud (CL)	0.4 to 1.2
San Francisco Old Bay clays (CH)	0.7 to 0.9
Vicksburg buckshot clay (CH)	0.5 to 0.6
Bangkok clay (CH)	0.4
Boston blue clay (CL)	0.3 to 0.5
Chicago silty clay (CL)	0.15 to 0.3

consolidated region until it reaches an approximately constant value, which is referred to as the normally consolidated value of K_0 (K_{0NC}). The figure shows that soil C has higher values of K_{0NC} ($0.559 \pm 0.013SD$ vs. $0.488 \pm 0.009SD$ for soil M).

Schmidt (1966) and Alpan (1967) developed an empirical equation that links OCR to K_0 as shown below:

$$K_0 = K_{0NC} (OCR)^n$$

where K_0 is the lateral stress ratio, K_{0NC} is the normally consolidated value of K_0 , OCR is the overconsolidation ratio, and n is a constant. This equation was used to estimate K_0 as a function of OCR for the marl deposit. To do so, five of the eleven triaxial tests were swelled to different OCR values (OCR = 2.1, 4.2, and 6.0) following K_0 conditions (i.e., the volumetric strain (ϵ_v) is always equal to the axial strain (ϵ_a)), hence maintaining a constant cross-sectional area at all time, and the overconsolidated lateral stress ratio was calculated (K_{0OC}). Figure A.4.11 plots the lateral stress ratio (overconsolidated and normally consolidated) versus OCR on a log-log plot. The data lie on two straight lines that can be represented by $K_{0NC} = 0.49$, $n = 0.41$, and $r^2 = 1.00$ for soil M; and $K_{0NC} = 0.56$, $n = 0.38$; and $r^2 = 0.99$ for soil C.

A.4.3.7 Creep Properties

Mesri and Godlewski (1977) developed the C_α/C_c concept of compressibility for the analysis of secondary settlement. The authors studied the compressibility of wide variety of natural soils and showed that for any one soil there is a unique relationship between the secondary compression index $C_{\alpha e} = \Delta e / \Delta \log t$ and the compression index $C_c = \Delta e / \Delta \log \sigma'_v$. This relationship holds true at all combinations of time, effective stress, and void ratio. For most soils, C_α/C_c varies between 0.02 and 0.08, with an average value of about 0.05. Typical values of C_α/C_c for natural soils are summarized in Table A.4.9.

According to the concept of compressibility, the secondary compression behavior of any one soil can be defined from the value of C_α/C_c and the end-of-primary (EOP) e - $\log \sigma'_v$ compression curve. This concept was adopted in this research and the ratio C_α/C_c was calculated for marl using three IL consolidation tests. Figure A.4.12 plots the secondary compression index $C_{\alpha e}$ versus the compression index C_c . These values were determined graphically from all

TABLE A.4.7
Summary of consolidation data for the CRS consolidation, IL

Equations	Applicability	References
$C_c = 0.54 (e_0 - 0.35)$	Natural soils ($S_t < 1.5$)	Nishida (1956)
$C_c = 0.01404 (w_n - 13.46)$	Natural soils ($S_t < 1.5$)	Nishida (1956)
$C_c = 0.4 (e_0 - 0.25)$	All natural soils	Azzouz, Krizek, & Corotis (1976)
$C_c = 0.01 (w_n - 5)$	All natural soils	Azzouz, Krizek, & Corotis (1976)
$C_c = 0.75 (e_0 - 0.50)$	Soils with low plasticity (moderately sensitive, $S_t < 5$)	Bowles (1979)
$C_c = 0.01 w_n$	Chicago & Alberta clays ($S_t < 1.5$)	Koppula (1981)
$C_c = 0.009 (LL - 10)$	Natural clays (moderately sensitive, $S_t < 5$)	Terzaghi & Peck (1967)

Note: S_t = Sensitivity of the soil

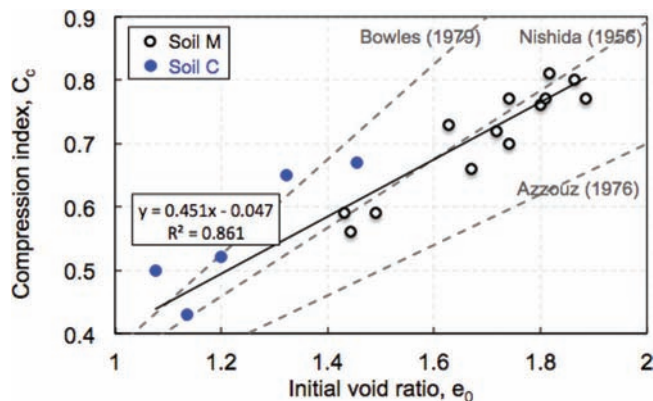


Figure A.4.4 Compression index versus initial void ratio.

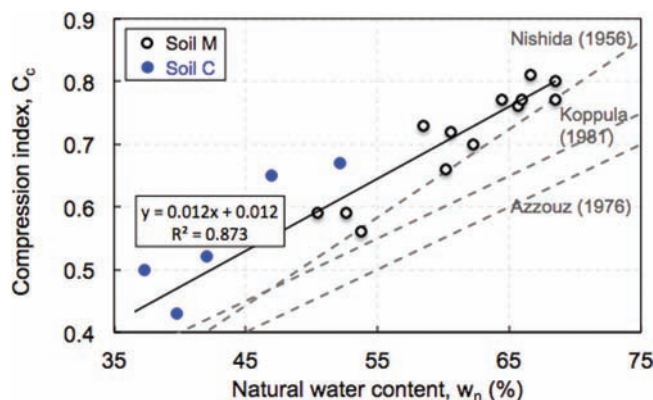


Figure A.4.5 Compression index versus natural water content.

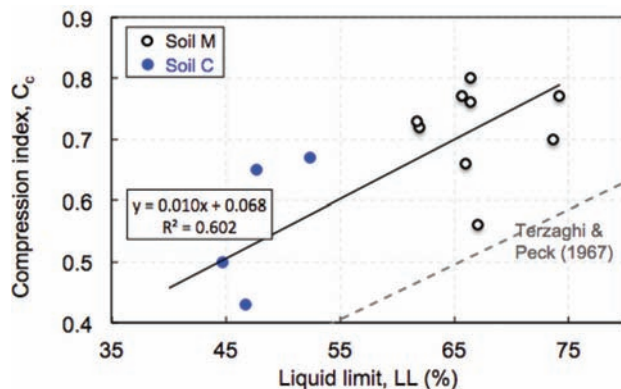


Figure A.4.6 Compression index versus liquid limit.

increments (both in the overconsolidated and normally consolidated range) according to the method proposed by Mesri and Castro (1987). The authors reported that near the preconsolidation stress σ'_p , the slope e versus $\log \sigma'_v$ (i.e., C_c , significantly increases with the increase in σ'_v). Therefore, care must be exercised in choosing the corresponding values of $C_{\alpha e}$ and C_c . The value of C_c is not simply the slope of the e - $\log \sigma'_v$ curve at the EOP consolidation, but it is the slope at the same void ratio at which $C_{\alpha e}$ was selected.

As shown in Figure A.4.12, the results lie on straight line with a slope ($C_{\alpha e}/C_c$) equals to 0.041 with a coefficient of determination r^2 equals to 0.99.

A.4.3.8 Assessment of Sample Quality

Sample disturbance is the most significant issue affecting the quality and reliability of laboratory test data for soft soils. Santagata, Sinfield, and Germaine (2006) defined sampling disturbance as the alteration of the true in situ soil properties due to sampling operation. The authors stated that disturbance might result from drilling, sampler penetration, sample retrieval, transportation, storage, extrusion, and preparation for laboratory testing. There has been a large effort on quantifying this disturbance. For instance, Lunne, Berre, and Strandvik (1997) suggested that $\Delta e/e_0$ may be a good parameter for evaluating sample quality, where Δe is the change of the void ratio associated with reconsolidation of the soil to the in situ stresses and e_0 is the initial void ratio. According to the criterion proposed by Lunne et al. (1997) for evaluating sample disturbance, for OCR values between 1 and 2, the quality of soil specimen is considered to be “very good to excellent” if $\Delta e/e_0$ is less than 0.04; “good to fair” if $\Delta e/e_0$ is between 0.04 and 0.07; “poor” if $\Delta e/e_0$ is between 0.07 and 0.14; and “very poor” if $\Delta e/e_0$ is greater than 0.14. This evaluation method was employed to assess the quality of the specimens tested in this study.

Variations in $\Delta e/e_0$ obtained from the consolidation (CRS and IL) tests, and the K_0 consolidation phase of triaxial tests are shown in Figure A.4.13(a). All the data fall below 0.05, and are designated as “excellent” to “good” based on the sample quality designation suggested by Lunne et al. (1997). This highlights the effectiveness of the techniques used in this study (i.e., drilling using mud rotary, sampling using fixed piston sampler, extrusion using a piano wire to debond the soil along the inside of the tube, trimming using wire saw) to obtain high quality and reliable laboratory test data for soft soils.

A close-up view for the $\Delta e/e_0$ values is presented in Figure A.4.13(b). In general, despite some limited scatter, values of $\Delta e/e_0$ obtained from tests on soil M specimens (average $\Delta e/e_0 = 0.033 \pm 0.009SD$) are smaller than those obtained from tests performed on soil C (average $\Delta e/e_0 = 0.039 \pm 0.009SD$). This is in agreement with the fact that soil C is more sensitive (depicted by the strong S-shape compression curves), which makes it more susceptible to disturbance.

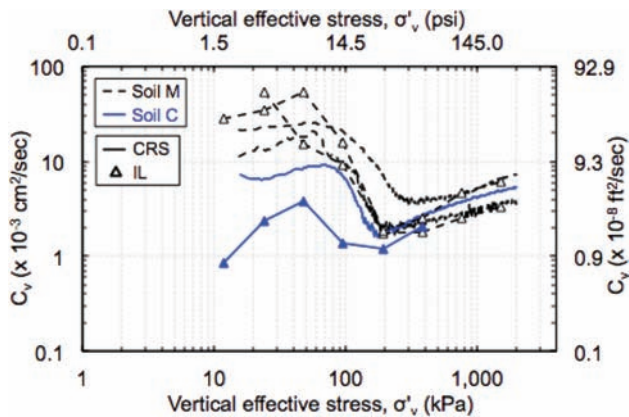


Figure A.4.7 Coefficient of consolidation versus vertical effective stress from CRS and IL consolidation tests.

TABLE A.4.8
Typical values of the coefficient of consolidation C_v (modified after Holtz & Kovacs, 1981)

Soil	C_v ($\times 10^{-4}$ cm ² /s)
Boston blue clay (CL)	40 ± 20
Chicago silty clay (CL)	8.5
San Francisco Bay Mud (CL)	2 to 4
Glacial lake clays (CL)	6.5 to 8.7
Mexico City clay (MH)	0.9 to 1.5

A distinction is also made between values of $\Delta e/e_0$ obtained from the K_0 consolidation phase of triaxial tests and those derived from IL and CRS consolidation tests. As shown in the figure, for the same type of soil, the values of the $\Delta e/e_0$ obtained from the K_0 consolidation phase of triaxial tests are generally smaller than those obtained from the consolidation tests. This might be attributed to (1) the additional disturbance imposed on the CRS/IL specimens while inserting the consolidation ring; and (2) the difference in diameter for these two types of specimens (6.35 cm (2.5 in) and 3.8 cm (1.5 in) for CRS/IL and triaxial specimens). Due to the fact that the soil in proximity to the wall of the Shelby tube is subjected to higher degree of disturbance (Santagata et al., 2006), smaller diameter specimens (i.e., triaxial specimens) are expected to be less disturbed, resulting in lower values of $\Delta e/e_0$.

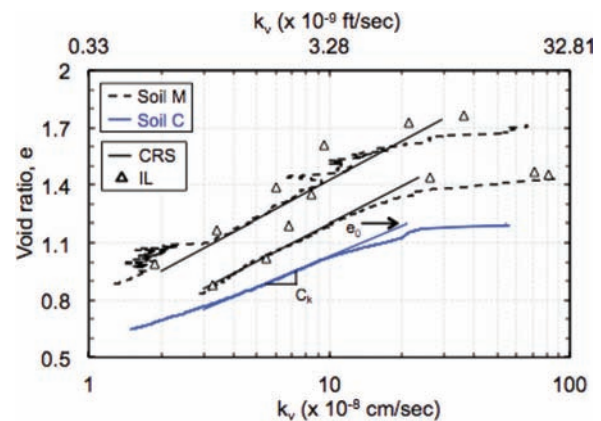


Figure A.4.8 Void ratio versus permeability from CRS and IL consolidation tests.

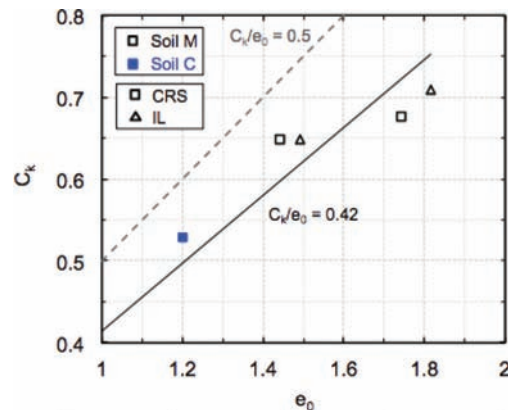


Figure A.4.9 C_k versus initial void ratio from CRS and IL consolidation tests.

A.4.4. UNDRAINED SHEAR BEHAVIOR

A.4.4.1 Introduction

This section provides a detailed evaluation of results from SHANSEP triaxial tests conducted on undisturbed samples of marl (soil M and soil C). The evaluation includes derivation of the undrained shear strength profiles and the soil's SHANSEP parameters for the marl deposit. One-dimensional compression data from the consolidation phase of SHANSEP triaxial tests were also used to determine the stress history profile, the compressibility properties, and the in situ lateral stress ratio (K_0) for the marl deposit as discussed in Section A.4.3. This section is organized in three major sub-sections: the general undrained shear behavior is summarized first, followed by a discussion of the undrained strength ratio and the effective stress failure envelope.

A total of eleven K_0 -consolidated SHANSEP triaxial compression tests (CK₀UTC(L)) were performed on marl samples obtained from different boreholes at various depths. Six of these tests were sheared normally consolidated, and five were sheared at OCR values varying between approximately 2 and 6. The data from these tests are summarized in Table A.4.10 and Table A.4.11 for soil M and soil C, respectively. The tables present a summary of the tests location; the in situ phase data (w_n , e_0 , S_i , and σ'_{v0}); the pre-shear conditions; the shear parameters at peak and at maximum obliquity; as well as the normalized undrained modulus at 0.1% axial strain ($E_{0.1}/\sigma'_{vc}$) and at peak ($E_{u, max}/\sigma'_{vc}$).

Table A.4.12 presents a summary of all shear properties for soil M and soil C. The following subsections will discuss the results of the various shear properties in greater detail.

A.4.4.2 General Undrained Shear Behavior

Figure A.4.14 and Figure A.4.15 show the results of the SHANSEP triaxial compression tests carried out on marl at OCRs of 1.0, 2.1, 4.2, and 6.0. The dashed black lines represent soil M and the continuous blue lines represent soil C. Figure A.4.14(a–c) show the normalized shear stress (q/σ'_{vc}), the normalized excess pore pressure ($u_e/\sigma'_{vc} = [\Delta u - \Delta \sigma_h] / \sigma'_{vc}$), and the obliquity ($R = \sigma'_h/\sigma'_v$) versus axial strain (ϵ_a). The same results are presented in Figure A.4.15(a–b) for smaller axial strain values (up to strain at failure, ϵ_{af}), this is important to evaluate the soil response prior to failure, especially the complex behavior observed at low strains for the pore pressure response. The following general observations were made from these curves:

- For both soil M and soil C, increasing OCR results in:
 - transition from a ductile behavior to a strain-softening behavior;

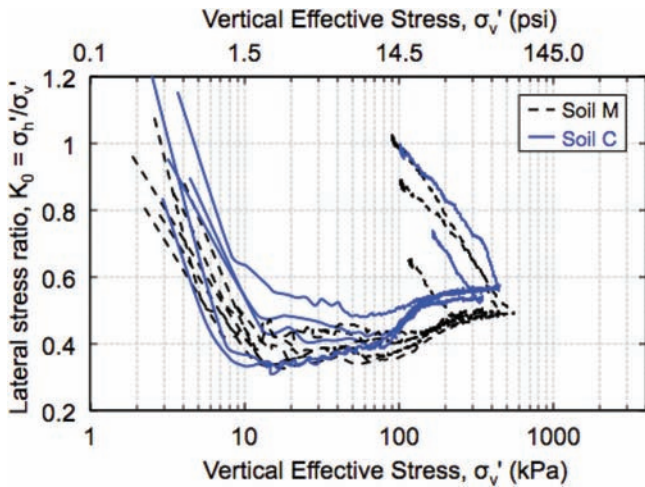


Figure A.4.10 Lateral stress ratio versus vertical effective stress from consolidation phase of SHANSEP CK₀UTC(L) tests.

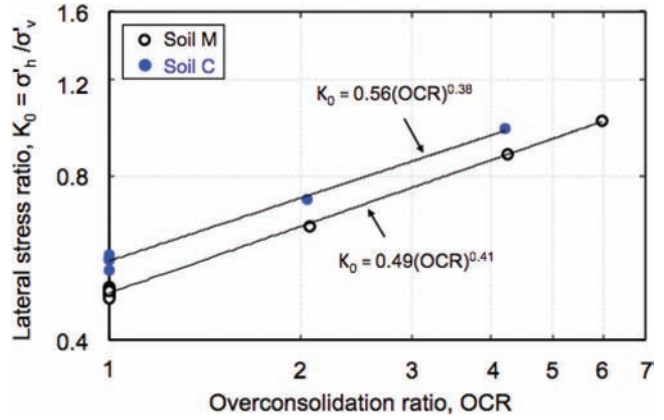


Figure A.4.11 Lateral stress ratio versus overconsolidation ratio from consolidation phase of SHANSEP CK₀UTC(L) tests.

TABLE A.4.9
Values of C_{ae}/C_c for natural soils (modified after Mesri & Godlewski, 1977)

Soil	C_{ae}/C_c
Peat	0.075 to 0.085
San Francisco Bay Mud	0.04 to 0.06
Calcareous organic silts	0.035 to 0.06
Leda clay (Canada)	0.03 to 0.06
Mexico City clay	0.03 to 0.035
Soft blue clay (Victoria, B.C.)	0.026

- an increase in the peak value of the normalized shear stress (q/σ'_{vc});
 - an increase in the axial strain at failure (ϵ_{af}). This is also illustrated in Figure A.4.16, which shows that ϵ_{af} increases linearly with increasing OCR on a log-log plot from about 0.5% for OCR of 1 to about 3.6% for OCR equal to 6 ($r^2 = 0.84$ on collective data). No clear difference was identified between soil M and soil C.
- For the same value of OCR, the marl with higher CaCO₃ content (soil M) has higher normalized undrained shear strength than the marl with lower CaCO₃ content (e.g., for OCR = 1, $q/\sigma'_{vc} \sim 0.34$ vs. 0.28). This might be attributed to the shear reinforcement provided by the shells as well as the

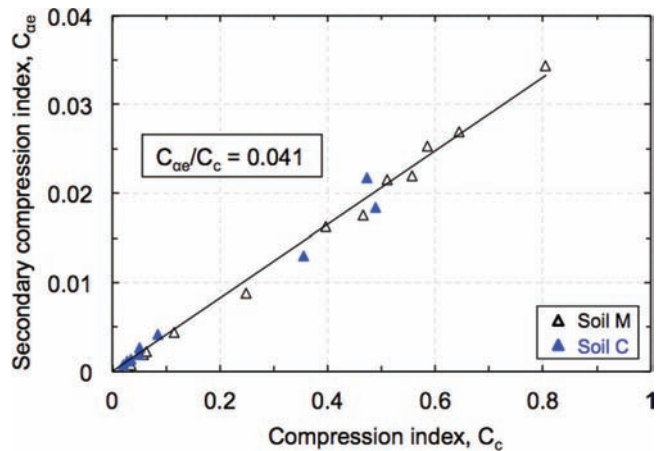


Figure A.4.12 Relationship between secondary compression index and compression index for marl.

cementation caused by the higher carbonate content present in soil M (Section A.3.4).

- In all normally consolidated tests, the normalized excess pore pressure (u_e/σ'_{vc}) increases with increasing axial strain. However, in overconsolidated tests, the u_e/σ'_{vc} initially increases then gradually decreases when q_f is approached, but directly after peak large positive excess pore pressures start to develop. This behavior was also observed for Boston blue clay BBC (Berman, 1993), resedimented Boston blue clay RBBC (Santagata, 1998), and Avezzano (AZ) silt in the Fucino basin (Burghignoli, Miliziano, & Soccodato, 2010). In general, at small strains ($\epsilon_a < 0.5\%$), u_e/σ'_{vc} increases with increasing OCR, but at large strains, u_e/σ'_{vc} decreases with increasing OCR. For NC marl, no clear difference was observed between soil M and soil C. However, for OC marl, Soil M has slightly higher u_e/σ'_{vc} than soil C.

The pore pressure parameter ($A = [\Delta u - \Delta \sigma_h] / [\Delta \sigma_v - \Delta \sigma_h]$) is plotted in Figure A.4.15(c). It can be observed that for $OCR = 1$, A-parameter increases with increasing axial strain until reaching failure. For $OCR > 1$, however A-parameter decreases with axial strain, this is typical for a wide range of clay reported in the literature (e.g., BBC (Sheahan, 1991); Taipei clay (Chin, Chen, Hu, Yao, & Chao, 2007)). The figure also shows that the pore pressure parameter at failure (A_f) decreases with OCR. This is also illustrated in Figure A.4.17, which shows that A_f decreases linearly with increasing OCR on a log-log plot from about 0.72 for OCR of 1 to about 0.04 for OCR equal to 6 ($r^2 = 0.97$ on collective data). No clear difference was identified between soil M and soil C.

Figure A.4.14(c) plots the obliquity ($R = \sigma'_v/\sigma'_h$) versus axial strain (ϵ_a). Despite the initial heterogeneity (e.g., void ratio, water content, plasticity index) of the different specimens, the obliquity R (Figure A.4.14(c)) at large strain appears to converge to a certain value (with minor scattering), which may be identified as the critical state condition. Soil M has an average value equal to 3.82, corresponding to a friction angle of 36 degrees. This value is lower for soil C (2.68), corresponding to a friction angle of 27 degrees.

A.4.4.3 Young's Modulus

The normalized undrained secant Young's modulus (E_u/σ'_{vc}) are plotted versus the axial strain in Figure A.4.18. The degradation of modulus with increasing axial strain is apparent. In general, soil M has slightly higher values of E_u/σ'_{vc} compared

with soil C. The figure also shows that the values of E_u/σ'_{vc} increases with OCR at the same level of ϵ_a . The E_u/σ'_{vc} for NC soil is consistently smaller than the OC soil at all strain levels.

A.4.4.4 Undrained Strength Ratio

Ladd and Foott (1974) suggested that for a large range of natural clays the undrained shear strength (S_u) of soil at any depth can be directly related to its in situ vertical effective stress (σ'_{v0}) and OCR via the SHANSEP (Stress History and Normalized Soil Engineering Properties) equation:

$$S_u/\sigma'_{v0} = S (OCR)^m$$

where S (= the normally consolidated value of S_u/σ'_{v0}) and m (= the strength increase exponent) are the two SHANSEP parameters. This concept has significant practical value as it provides a useful framework for comparing and relating the behavioral characteristics of different cohesive soils and allows estimation of the undrained shear strength profile as the vertical effective stress and stress history profiles of the site change. Thus, the SHANSEP design method is ideally suited for the design of staged construction/preloading procedures (Ladd, 1991), which are commonly employed in marl deposits.

The SHANSEP testing program carried out in this study shows that marl exhibits normalized behavior and can be described by the SHANSEP equation. Figure A.4.19 presents the undrained shear strength ratio versus OCR on a log-log plot for six NC tests and five OC tests. Overall, the data lie on two straight lines that can be represented by $S = 0.34$; $m = 0.85$; $r^2 = 1.00$ for soil M; and $S = 0.28$; $m = 0.72$; and $r^2 = 0.99$ for soil C.

A.4.4.5 Effective Stress Failure Envelope

Figure A.4.20 and Figure A.4.21 present the effective stress paths and the effective stress paths normalized to the maximum vertical consolidation stress (σ'_{vm}), respectively for SHANSEP $CK_0UTC(L)$ tests conducted on NC and OC marl. The MIT stress path convention was used where the shear stress is calculated as $q = (\sigma'_v - \sigma'_h) / 2$ and the average effective stress is calculated as $p' = (\sigma'_v + \sigma'_h) / 2$. The results show that the effective stress paths approach a common failure envelope at large strains. The p' - q effective stress failure envelope (ESFE) is defined by a linear regression through the shear stress and

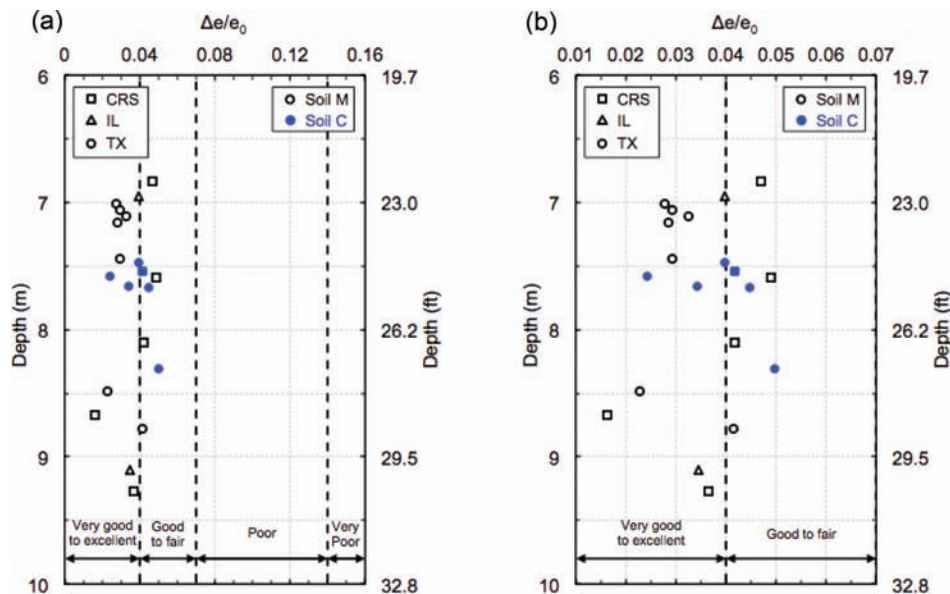


Figure A.4.13 Evaluation of sample quality for marl specimens according to the criterion proposed by Lunne et al. (1997).

TABLE A.4.10
Summary of shear data from SHANSEP CK₀UTC(L) tests for soil M

Test #/Depth	In situ		Pre shear			At peak			At maximum obliquity		$E_{0.1}/\sigma'_{vc}E_{u, max}/\sigma'_{vc}$
	$w_n e_0$	$S_i \sigma'_{v0}$	$K_c e_c$	$\sigma'_{vm} \sigma'_{vc}$	$OCR \varepsilon_v$	$q/\sigma'_{vc} p'/\sigma'_{vc}$	$\varepsilon_{af} \phi'$	A_f	$q/\sigma'_{vc} p'/\sigma'_{vc}$	$\varepsilon_a \phi'$	
TX107	58.4	98	0.499	342.9	1.00	0.323	0.305	0.590	0.241	10.53	134.2
8.48	1.63	84.1	1.277	342.9	13.10	0.712	27.0		0.395	37.7	53.2
TX108	65.7	99	0.483	244.1	1.00	0.343	0.736	0.801	0.273	10.65	131.7
7.01	1.80	74.3	1.447	244.1	12.47	0.662	31.2		0.419	40.7	26.2
TX109	65.9	99	0.486	440.8	1.00	0.332	0.543	0.772	0.261	10.07	123.8
7.11	1.81	75.0	1.277	440.8	18.91	0.679	29.3		0.420	38.5	30.2
TX111	68.5	98	0.646	245.1	2.07	0.649	1.298	0.173	0.522	10.26	435.8
7.06	1.89	74.6	1.556	118.4	11.23	1.124	35.3		0.808	40.3	78.1
TX112	68.5	99	0.877	442.4	4.25	1.145	2.460	0.084	1.070	7.17	493.1
7.16	1.86	75.3	1.382	104.1	16.84	1.842	38.4		1.692	39.2	91.9
TX114	62.2	97	1.011	549.6	5.98	1.521	2.092	0.027	1.306	1.11	548.3
7.44	1.74	77.2	1.275	92.0	16.84	2.462	38.1		2.025	40.2	148.4

Note: Depth in m; stresses in kPa; w_n , S_i , and ε in %; ϕ' in $^\circ$.

TABLE A.4.11
Summary of shear data from SHANSEP CK₀UTC(L) tests for soil C

Test #/Depth	In situ		Pre shear			At peak			At maximum obliquity		$E_{0.1}/\sigma'_{vc}E_{u, max}/\sigma'_{vc}$
	$w_n e_0$	$S_i \sigma'_{v0}$	$K_c e_c$	$\sigma'_{vm} \sigma'_{vc}$	$OCR \varepsilon_v$	$q/\sigma'_{vc} p'/\sigma'_{vc}$	$\varepsilon_{af} \phi'$	A_f	$q/\sigma'_{vc} p'/\sigma'_{vc}$	$\varepsilon_a \phi'$	
TX102	36.6	93	0.563	345.6	1.00	0.277	0.332	0.782	0.196	11.18	112.5
8.31	1.11	82.9	0.859	345.6	11.31	0.731	22.3		0.392	30.0	40.2
TX103	39.7	98	0.560	293.7	1.00	0.271	0.339	0.682	0.200	12.11	101.1
7.47	1.14	77.3	0.883	293.7	11.56	0.743	21.4		0.416	28.8	35.4
TX105	52.2	99	0.573	444.6	1.00	0.278	0.512	0.824	0.209	11.83	109.4
7.67	1.46	78.7	0.983	444.6	18.62	0.720	22.7		0.413	30.4	27.2
TX115	47.0	99	0.976	441.6	4.21	0.757	4.217	0.091	0.738	6.45	443.8
7.58	1.32	78.1	0.956	104.8	15.75	1.611	28.0		1.562	28.2	37.3
TX116	37.3	98	0.725	343.7	2.05	0.509	1.005	0.178	0.394	8.81	418.9
7.66	1.08	78.6	0.813	167.4	12.56	1.109	27.3		0.783	30.2	79.6

Note: Depth in m; stresses in kPa; w_n , S_i , and ε in %; ϕ' in $^\circ$.

TABLE A.4.12
Summary of shear properties

OCR	Soil M				Soil C			
	1.0*	2.1	4.2	6.0	1.0*	2.1	4.2	
At peak	q/σ'_{vc}	0.333	0.649	1.145	1.521	0.275	0.509	0.757
	p'/σ'_{vc}	0.684	1.124	1.842	2.462	0.731	1.109	1.611
	ε_{af}	0.528	1.298	2.46	2.092	0.394	1.005	4.217
	ϕ'	29.2	35.3	38.4	38.1	22.13	27.3	28
	A_f	0.721	0.173	0.084	0.027	0.763	0.178	0.091
At maximum obliquity	q/σ'_{vc}	0.258	0.522	1.070	1.306	0.202	0.394	0.738
	p'/σ'_{vc}	0.411	0.808	1.692	2.025	0.407	0.783	1.562
	ε_a	10.42	10.26	7.17	1.11	11.71	8.81	6.45
	ϕ'	39.0	40.3	39.2	40.2	29.73	30.2	28.2
$E_{0.1}/\sigma'_{vc}$		129.9	435.8	493.1	548.3	107.7	418.9	443.8
$E_{u, max}/\sigma'_{vc}$		36.5	78.1	91.9	148.4	34.3	79.6	37.3
$S_u/\sigma'_{v0} = S (OCR)^m$			S = 0.34; m = 0.85				S = 0.28; m = 0.72	
ϕ'_{mo}			39 $^\circ$				30 $^\circ$	

*The data corresponds to the average of three NC tests.

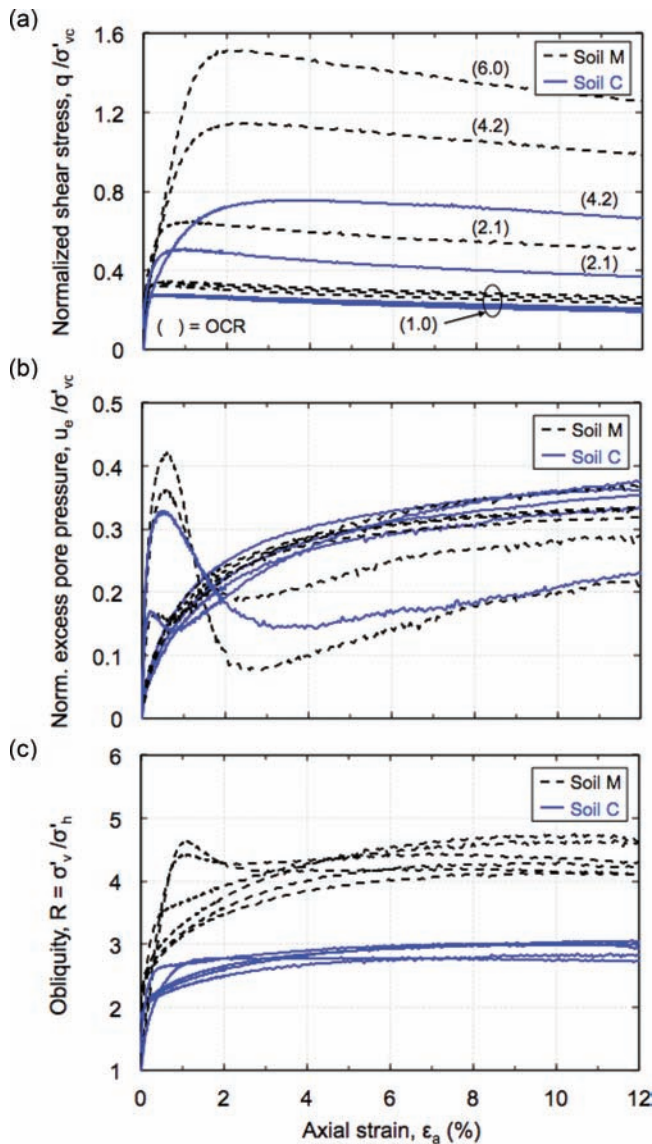


Figure A.4.14 Results for SHANSEP CK₀UTC(L) tests of marl: (a) normalized shear stress, (b) norm. excess pore pressure, and (c) obliquity vs. axial strain.

average effective stress at maximum obliquity represented with hollow black diamonds for soil M and solid blue diamonds for soil C. The linear regression on the data yields a friction angle at maximum obliquity (ϕ'_{mo}) of 39° for soil M and 30° for soil C and a negligible cohesion ($c' \sim 0$) for both types of soils. As mentioned earlier, this higher friction angle might be attributed to the shear reinforcement provided by the shells as well as the

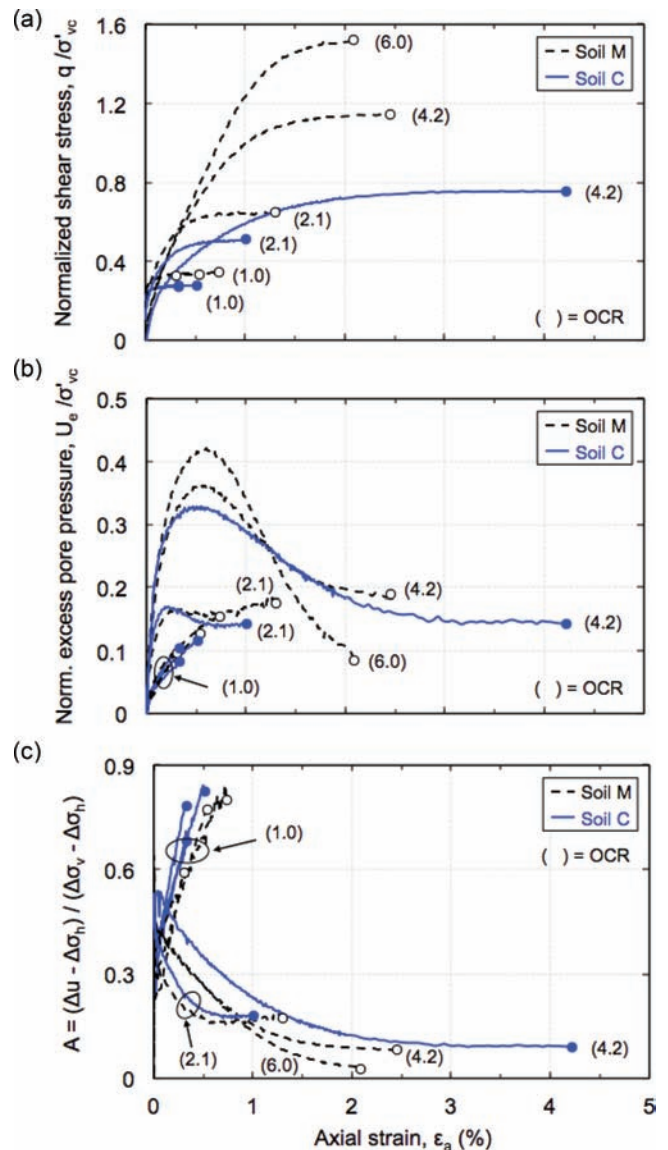


Figure A.4.15 Results for SHANSEP CK₀UTC(L) tests of marl: (a) normalized shear stress, (b) norm. excess pore pressure, and (c) A-parameter vs. axial strain.

cementation caused by the higher carbonate content present in soil M.

Note that the higher the OCR, the lower the strain at which the maximum obliquity failure envelope is mobilized ($\epsilon_a > 10\%$ for NC marl) and that only for OCR equal 6 does the soil reach the maximum obliquity envelope before reaching the peak undrained strength (see Figure A.4.14(c)).

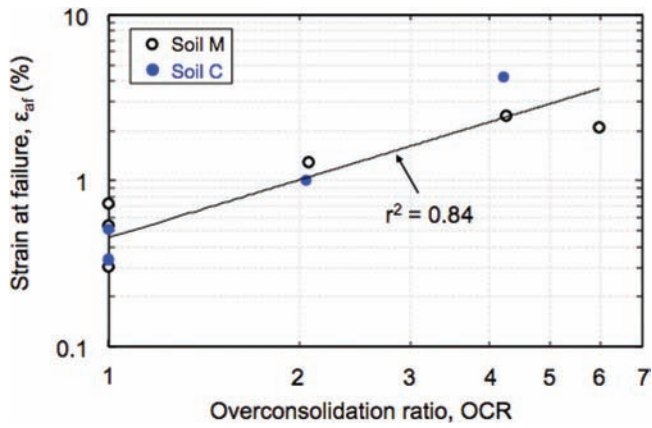


Figure A.4.16 Strain at failure versus OCR for marl.

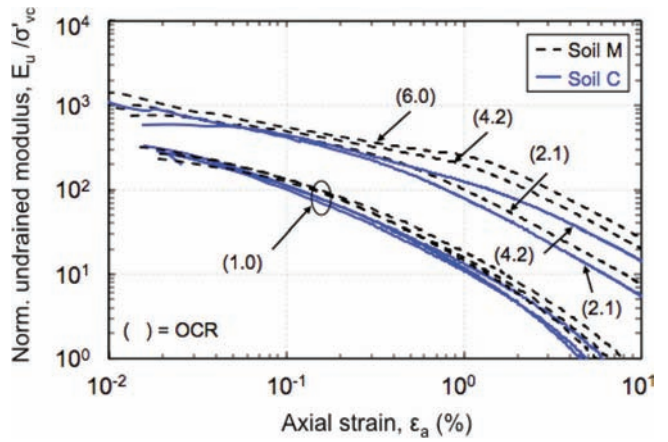


Figure A.4.18 Normalized undrained modulus degradation for SHANSEP.

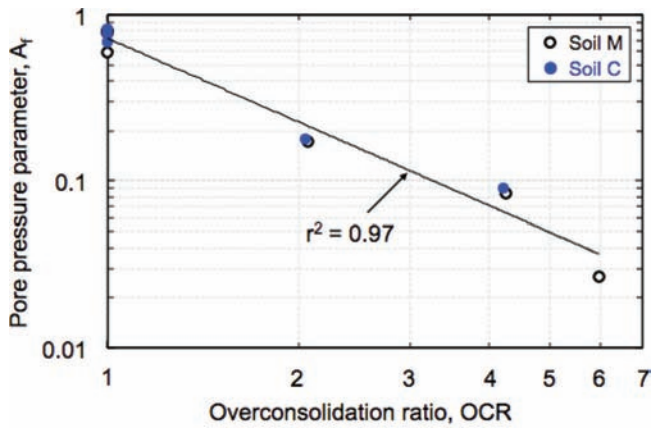


Figure A.4.17 Pore pressure parameter at failure versus OCR

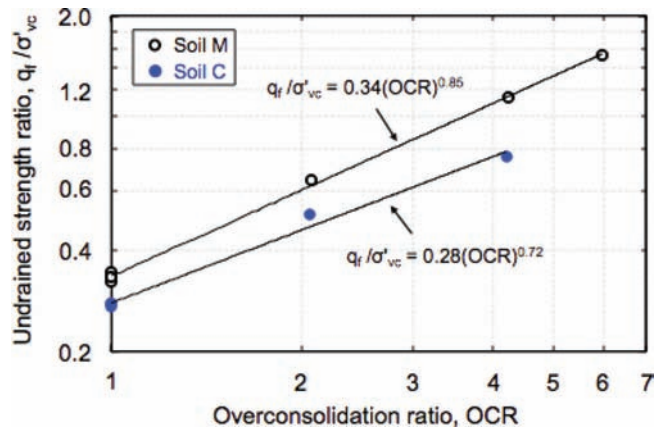


Figure A.4.19 Undrained strength ratio vs. OCR for SHANSEP CK₀UTC(L) tests of marl.

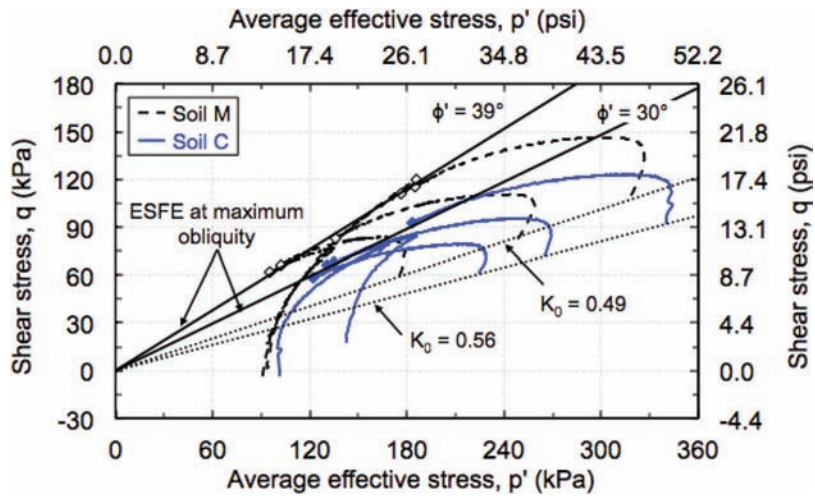


Figure A.4.20 Effective stress paths for SHANSEP CK₀UTC(L) tests of marl.

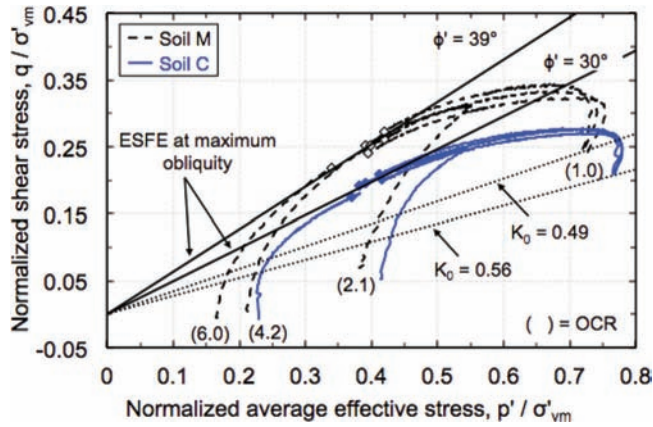


Figure A.4.21 Normalized effective stress paths for SHANSEP CK₀UTC(L) tests of marl.

APPENDIX 5: INTEGRATION OF LABORATORY AND FIELD DATA

A.5.1. INTRODUCTION

This appendix presents a detailed evaluation of the results from the field tests described in Section A.2.5. The evaluation includes further analysis of the basic results summarized in Section A.2.6 as well as integration of laboratory and field data. The appendix is organized in two sections: (i) field vane tests and (ii) piezocone tests. Section A.5.2 discusses the field vane tests results and provides a comparison between the corrected field vane undrained shear strength and the reference strength obtained from laboratory SHANSEP CK₀UTC(L) tests. Section A.5.3 analyzes the piezocone tests results and provides marl specific correlations to estimate shear wave velocity, stress history, and undrained strength from the Piezocone penetration measurements.

Figure A.5.1 shows the soil profile and index properties at the site. The figures include the results of index tests conducted on undisturbed samples of marl (described earlier in Section A.3.3) as well as additional tests performed on undisturbed samples collected from the split spoons retrieved from the soil above and below the marl layer. The data presented in Figure A.5.1 show the elevated natural water content, Atterberg limits and CaCO₃ content in the marl layer compared with the soil above and below.

A.5.2. FIELD VANE (FV) TEST

Field vane tests were performed in this study in order to obtain the in-situ undrained shear strength profile for marl and compare it to the one measured in the laboratory using SHANSEP triaxial program. The equipment and testing procedures are summarized in Section A.2.5.3 and the measured peak and remolded strengths are presented in Section A.2.6.3. It is well established that the measured field vane strengths should be corrected for use in undrained stability analyses due to installation disturbances, mode of failure, strain rate, and anisotropy effects. Bjerrum (1972) studied a number of excavation and embankment failures for which field vane data were available and derived an empirical correction factor (μ) versus plasticity index (PI); this correlation as well as more recent case histories are shown in Figure A.5.2. For a plasticity index of 20%, the Bjerrum's factor μ equals to 1.0.

The plasticity index of marl is higher than 20%, but is not uniform across the deposit. As reported earlier, the marl layer is not homogenous and is composed of two types of soils (i.e., soil M and soil C) that are repeated in horizontal thin layers. These layers are shown in the soil profile column on the left side of Figure A.5.3, where soil M is represented in gray and soil C is represented in blue. It can be seen that soil M is prominent.

The total vane height including the taper ends is about 0.3 m (1 ft); hence it can be assumed that the soil sheared by the vane is about 0.3 m (1 ft). The Bjerrum's factor for each FV test was determined based on a weighted average PI, with PI equals to 33.1 and 25.9 for soil M and soil C respectively. Figure A.5.3(a) shows the measured peak and remolded FV strengths, as well as the undrained strength corrected using Bjerrum's factor μ . As can be seen, there is no appreciable difference between the corrected and uncorrected peak FV strength for this deposit ($\mu > 0.9$). For reference, the undrained shear strength profiles obtained from the SHANSEP CK₀UTC(L) tests for both soil M and soil C are also plotted in Figure A.5.3(a). The SHANSEP equations presented in Section A.4.4.4 were used with OCR equals to 1.9 and 1.3 for soil M and soil C, respectively. On Figure A.5.3(b), the comparison is made in terms of profiles of normalized shear strength.

The different types of soils (M and C) were carefully examined in the laboratory, and special effort has been made to conduct tests on specimens with only one type of soil. However, this is not the case for the field vane test where $S_u(FV)$ represents the shear behavior of about 0.3 m (1 ft) of soil and the result is influenced by the relative abundance of each type of soil. This can be seen by examining the two FV tests FV4 and FV5. The $S_u(FV)$ obtained from test FV4 conducted at depth ~7.2 m (23.5 ft) is close to the $S_u(TX)$ for soil M, which is consistent with the fact that only soil M is found at that depth (see the soil profile column in Figure A.5.3). On the other hand, relatively high concentration of soil C is found at a depth of ~7.8 m (25.5 ft), where test FV5 is conducted resulting in much lower $S_u(FV)$ ~ 18 kPa, which is close to the $S_u(TX)$ for soil C. The higher sensitivity (~10) observed at this depth (see Figure a.2.23) is in good agreement with the fact that soil C has higher sensitivity (depicted by the strong S-shape compression curves) compared with soil M (see Figure A.4.1).

Despite this difference between soil M and soil C, $S_u(FV)$ is generally lower than the weighted average peak strength in triaxial compression $S_u(TX)$ of soil M and soil C, which is also reported by Lefebvre, Ladd, and Paré (1988). The authors reported that the measured $S_u(FV)$ is close to the undrained shear strength determined

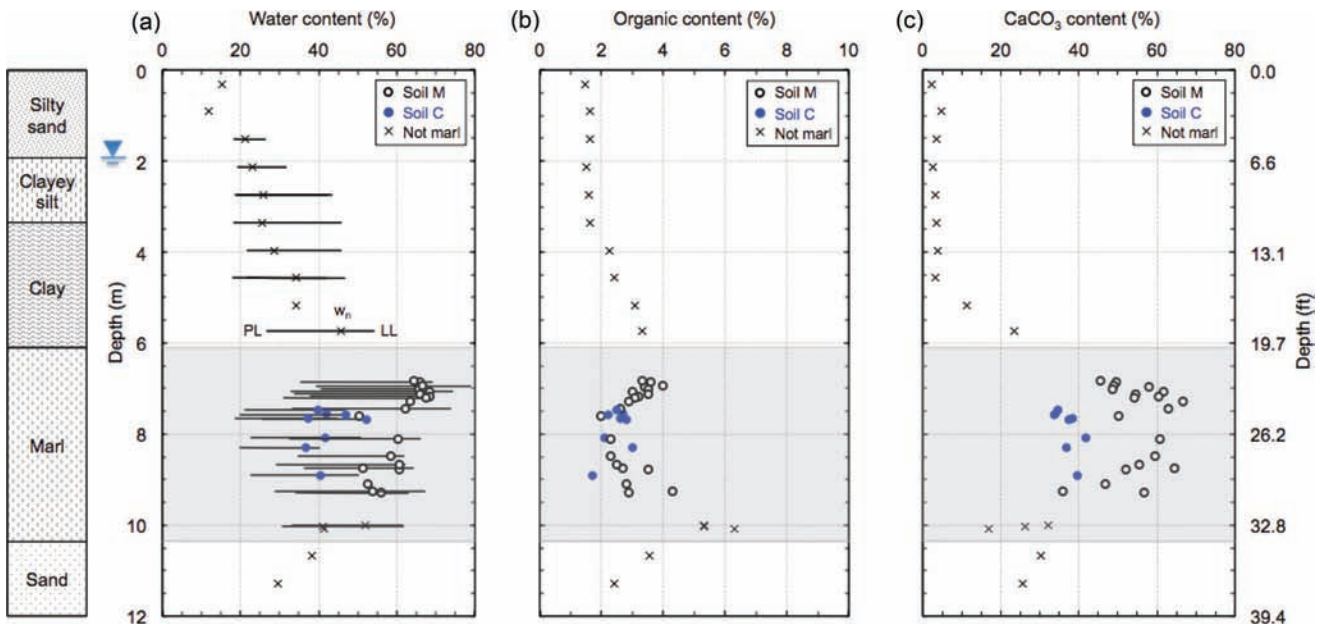


Figure A.5.1 Index properties: (a) water content, (b) organic content, and (c) CaCO₃ content versus depth.

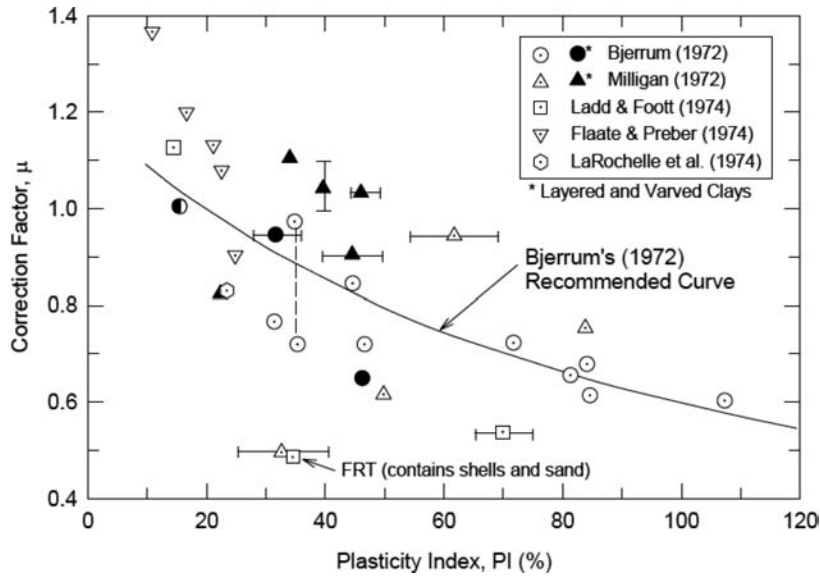


Figure A.5.2 Field vane correction factor versus plasticity index derived from embankment failures (Ladd, Foott, Ishihara, Schlosser, & Poulos, 1977).

in direct simple shear (DSS) tests, which is intermediate between the peak triaxial compression (TC) and triaxial extension (TE) strengths.

A.5.3. PIEZOCONE TEST (CPT_u)

Due to its numerous advantages over other in-situ tests, the CPT has been increasingly used for conducting highway site investigations for exploring soft soils to support pavement subgrades, embankments, and bridge foundations. Extensive work has been conducted to correlate soil parameters from CPT results. The main objective of the Piezocone testing program in this research was to investigate the current correlations reported in literature and provide site-specific correlations for marls that can be used as preliminary design tool on these soft soils.

Seven different CPTs were performed in the field, as shown in Figure A.2.3. At all seven locations records of tip resistance, excess pore pressure, and sleeve friction as a function of depth were obtained. Additionally, CPT#4 and CPT#5 were used to obtain profiles of the shear wave velocity with depth, whereas measurements of the excess pore pressure dissipation were conducted at CPT#3A and CPT#6. The CPT field data were examined to derive correlations for three major soil parameters: the shear wave velocity (V_s), the preconsolidation stress (σ'_p), and the undrained shear strength (S_u).

A.5.3.1 Shear Wave Velocity

Various researchers have studied relationships between CPT data and V_s . The studies explored correlation relationships between V_s

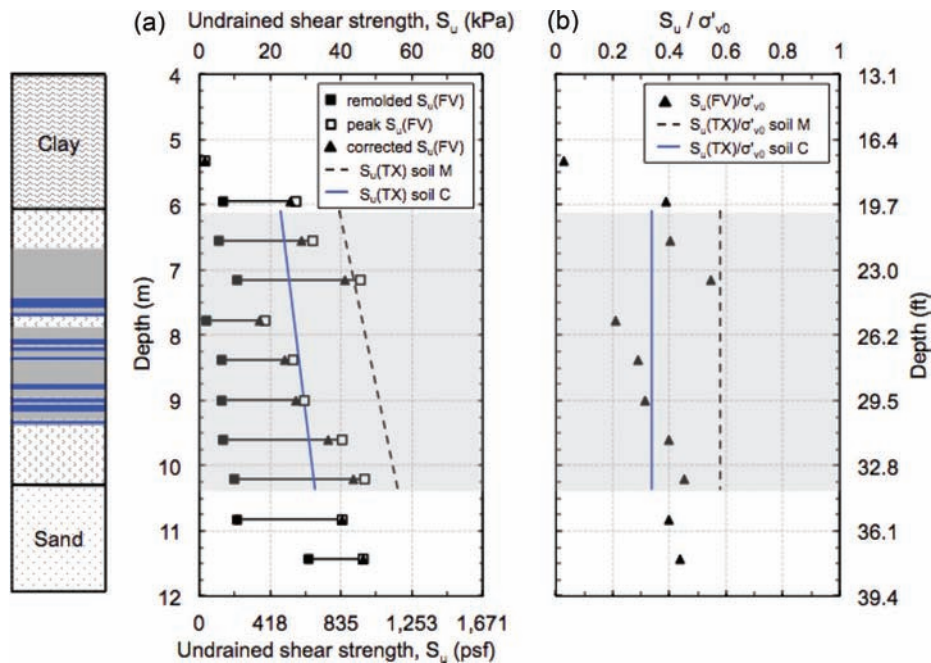


Figure A.5.3 (a) Undrained shear strength and (b) normalized undrained shear strength as obtained from field vane and laboratory SHANSEP CK₀UTC(L) tests.

TABLE A.5.1
CPT- V_s correlation equations

Soil Type	V_s (m/s)	Geologic Age	Reference
All soils	$(10.1 \log(q_t) - 11.4)^{1.67} (100 f_s / q_t)^{0.3}$	Quaternary	Hegazy & Mayne (1995)
	$32.3 q_t^{0.089} f_s^{0.121} D^{0.215}$	Holocene	Piratheepan (2002)
	$118.8 \log(f_s) + 18.5$	Quaternary	Mayne (2006)
	$2.62 q_t^{0.395} I_c^{0.912} D^{0.124} SF^*$	Holocene & Pleistocene	Andrus et al. (2007)
	$[(10^{(0.55I_c + 1.68)}) (q_t - \sigma_v) / p_a]^{0.5}$	Quaternary	Robertson (2009)
Sand	$134.1 + 0.0052 q_t$	—	Sykora & Stokoe (1983)
	$17.48 q_t^{0.13} \sigma_v'^{0.27}$	Holocene	Baldi, Bellotti, Ghionna, Jamiolkowski, & LoPresti (1989)
	$13.18 q_t^{0.192} \sigma_v'^{0.179}$	Quaternary	Hegazy & Mayne (1995)
	$12.02 q_t^{0.319} f_s^{-0.0466}$	Quaternary	Hegazy & Mayne (1995)
	$25.3 q_t^{0.163} f_s^{0.029} D^{0.155}$	Holocene	Piratheepan (2002)
Clay	$3.18 q_t^{0.549} f_s^{0.025}$	Quaternary	Hegazy & Mayne (1995)
	$1.75 q_t^{0.627}$	Quaternary	Mayne & Rix (1995)
	$11.9 q_t^{0.269} f_s^{0.108} D^{0.127}$	Holocene	Piratheepan (2002)

Units: q_t , f_s , σ_v , and σ_v' are in kPa, depth (D) in meters, $p_a = 100$ kPa.
*SF = 0.92 for Holocene and 1.12 for Pleistocene.

and different parameters such as: q_t , f_s , soil behavior type index (I_c), σ_v' , and depth (D). Correlation equations that were reviewed for this study are summarized in Table A.5.1. The equations are grouped in three different categories depending on the soil types (i.e., all soils, sand, and clay). The correlation equations presented in Table A.5.1 were analyzed for the seven CPTs and the derived V_s values were compared with the field seismic measurements of V_s at CPT#4 and CPT#5 presented in Figure A.2.20. This investigation shows that the V_s of the soil above and below the marl layer can be best estimated using the correlation provided by Mayne (2006) for “all soils” type, whereas for the marl layer, the correlation developed by Andrus, Mohanan, Piratheepan, Ellis, & Holzer (2007) for all soils with a Pleistocene geologic age should be used.

Figure A.5.4(a) compares the field seismic measurements of V_s with the values correlated from the seven CPTs. The values derived using Mayne (2006) are represented by dashed lines, while the ones derived using Andrus et al. (2007) are represented by continuous lines. Hollow squares and solid black triangles are used to represent the field measurements of V_s obtained from the seismic measurements conducted at both CPT#4 and CPT#5, respectively.

Figure A.5.4(b) shows the same measurements of V_s (square and triangle symbols) along with the estimates of V_s obtained applying the above-cited correlations to the data obtained from CPT#4 and CPT#5 only. The following conclusions can be drawn from Figure A.5.4:

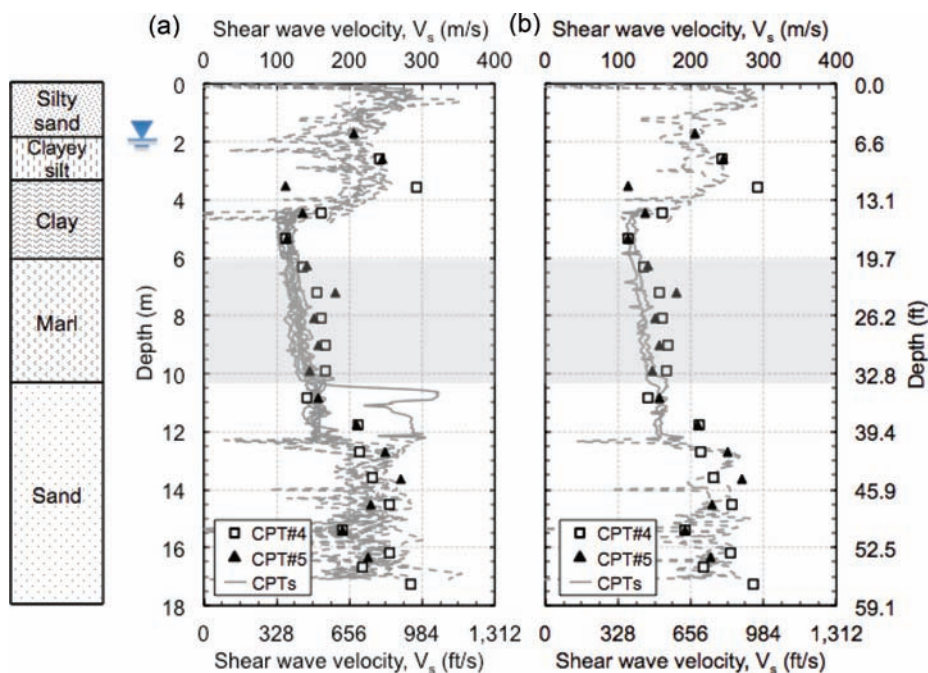


Figure A.5.4 Shear wave velocity as obtained from CPT correlations and seismic measurements from (a) all CPTs and (b) from CPT#4 and CPT#5.

1. The estimates of V_s from the CPT data form a band that reflects the variability in tip resistance and sleeve friction measured in the field.
2. The values of V_s obtained from the seismic measurements at CPT#4 and CPT#5 are generally consistent with each other over the entire deposit.
3. In general, the estimates of V_s obtained from the correlations with the CPT data are in a good agreement with the values of V_s derived from the seismic measurements over the entire deposit.
4. The correlation by Andrus et al. (2007) is effective in predicting the V_s of marl deposits.
5. The correlation by Mayne (2006) is effective in predicting the V_s of soil above and below the marl layer, but is not applicable for marl.

A.5.3.2 Preconsolidation Stress

The preconsolidation stress can be estimated from: (i) the net tip resistance, $q_t - \sigma_{v0}$, using the equation proposed by Mayne (1995) ($\sigma'_p = 0.33 [q_t - \sigma_{v0}]$); (ii) the effective tip resistance, $q_t - u_2$, using the equation proposed by Mayne (2005) ($\sigma'_p = 0.60 [q_t - u_2]$); and the excess pore pressure, $u_2 - u_0$, using the equation proposed by Chen and Mayne (1996) ($\sigma'_p = 0.53 [u_2 - u_0]$).

These three relations were used to examine the ability to predict the preconsolidation stress of the marl deposit investigated in this research from the CPT results by comparing the derived σ'_p values with the laboratory measurements of σ'_p presented in Figure A.4.2. This investigation shows that the σ'_p of marl can be best estimated using the correlation provided by Mayne (1995). The values of σ'_p obtained applying this correlation to the traces of each of the seven CPTs performed are shown in Figure A.5.5(a). The curve highlighted in black corresponds to CPT#1, the sounding closest to the locations of the borings (MR#1, #2, #3 and #4) from which the soil used for the laboratory consolidation tests was obtained (see Figure A.2.3). The symbols shown in Figure A.5.5(a) pertain to the laboratory values for soil M (white symbols) and soil C (blue symbols). Figure A.5.5(b) shows the corresponding values of the overconsolidation ratio (OCR). It is

found that the correlation by Mayne (1995) is effective in capturing the values of the preconsolidation stress for soil M, while slightly overestimating σ'_p for soil C. This might be due to the fact that soil M is more prominent, and thus controls the measured tip resistance.

A.5.3.3 Undrained Shear Strength

The undrained shear strength, S_u , can be estimated from the net tip resistance, $q_t - \sigma_{v0}$, by substituting the cone tip resistance, q_t , the total overburden stress, σ_{v0} , and the empirical cone factor, N_{kt} , at given depths into the following equation:

$$S_u = (q_t - \sigma_{v0}) / N_{kt}$$

The value of N_{kt} was backcalculated using the cone resistance measurements obtained at all seven CPTs, and the CK₀UTC(L) SHANSEP profile as the reference undrained shear strength. Figure A.5.6(a) and Figure A.5.6(b) present the N_{kt} profiles calculated from all seven CPTs for soil M and soil C respectively, using the two SHANSEP equations resulting from the CK₀UTC(L) testing program (Soil M: $S_u = \sigma'_{v0} \times 0.34 (1.9)^{0.85}$; and soil C: $S_u = \sigma'_{v0} \times 0.28 (1.3)^{0.72}$) to calculate the reference strength. The curves highlighted in black and dark blue correspond to CPT#1, the sounding closest to the locations of the borings (MR#1, #2, #3 and #4) from which the soil used for the laboratory consolidation tests was obtained (see Figure A.2.3). As shown in both figures, no clear variation in N_{kt} was observed with depth. The mean values of N_{kt} derived from all CPTs for soil M and soil C are 10 and 17, respectively. Similar mean values were obtained when considering CPT#1 only. For soil M, the lower values of N_{kt} values are due to the higher $S_{u(TC)}$ derived from the SHANSEP program.

The TC undrained strength profiles at the locations of boreholes CPT#1 to CPT#7 were calculated using $N_{kt} = 10$ assuming the deposit is composed of soil M only, and $N_{kt} = 17$ assuming the deposit is composed of soil C only. Note that when building on a marl deposits, the value of N_{kt} selected for deriving the TC undrained strength profile should consider the presence of both types of soils (M and C) and a representative value should be selected depending on the prevalence of each.

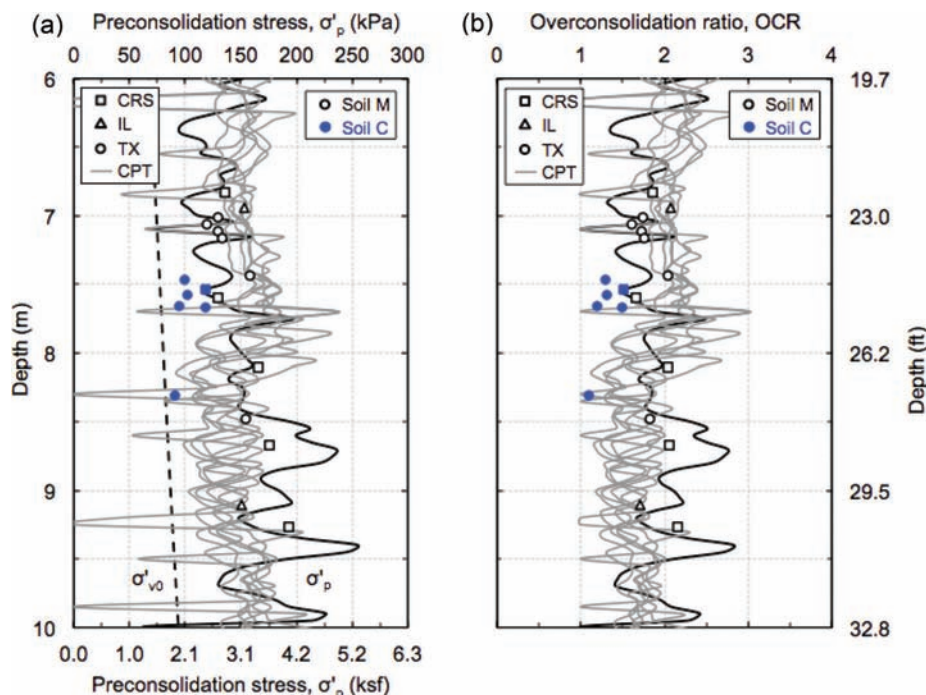


Figure A.5.5 (a) Preconsolidation stress and (b) overconsolidation ratio as obtained from CPT correlations and laboratory tests.

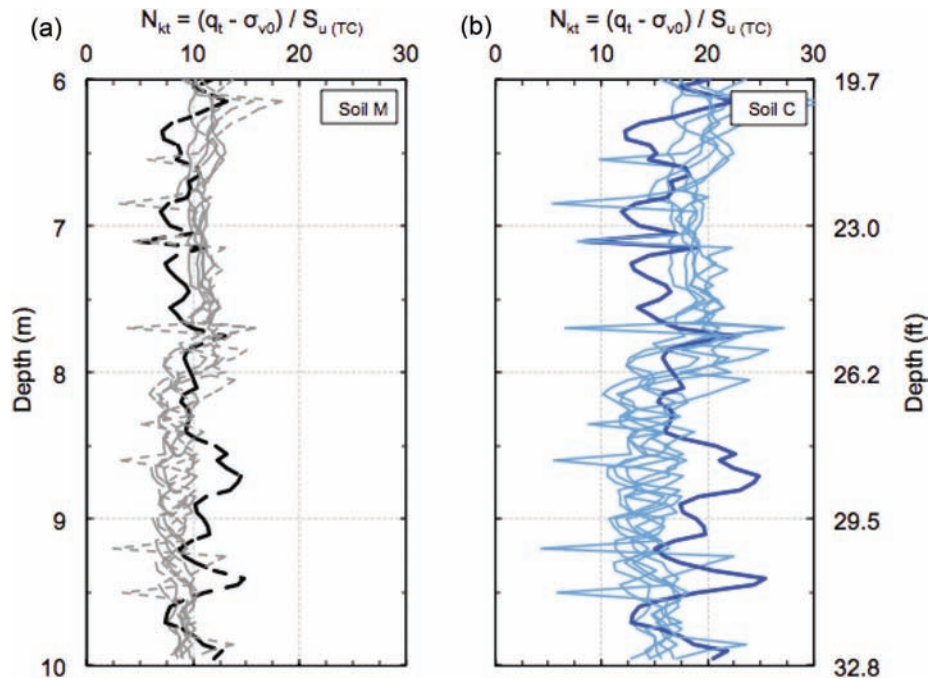


Figure A.5.6 Empirical cone factor $N_{kt(TC)}$ derived from all CPTs for (a) soil M and (b) soil C.

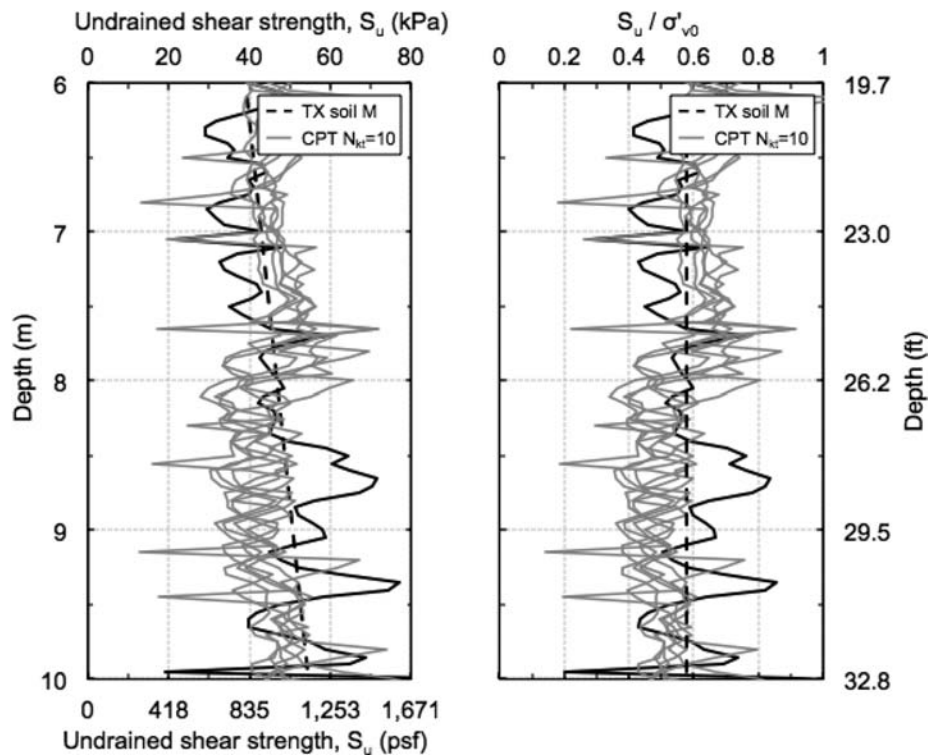


Figure A.5.7 (a) Undrained shear strength and (b) normalized undrained shear strength as obtained from CPT (using $N_{kt} = 10$) and laboratory SHANSEP $CK_0UTC(L)$ tests for soil M.

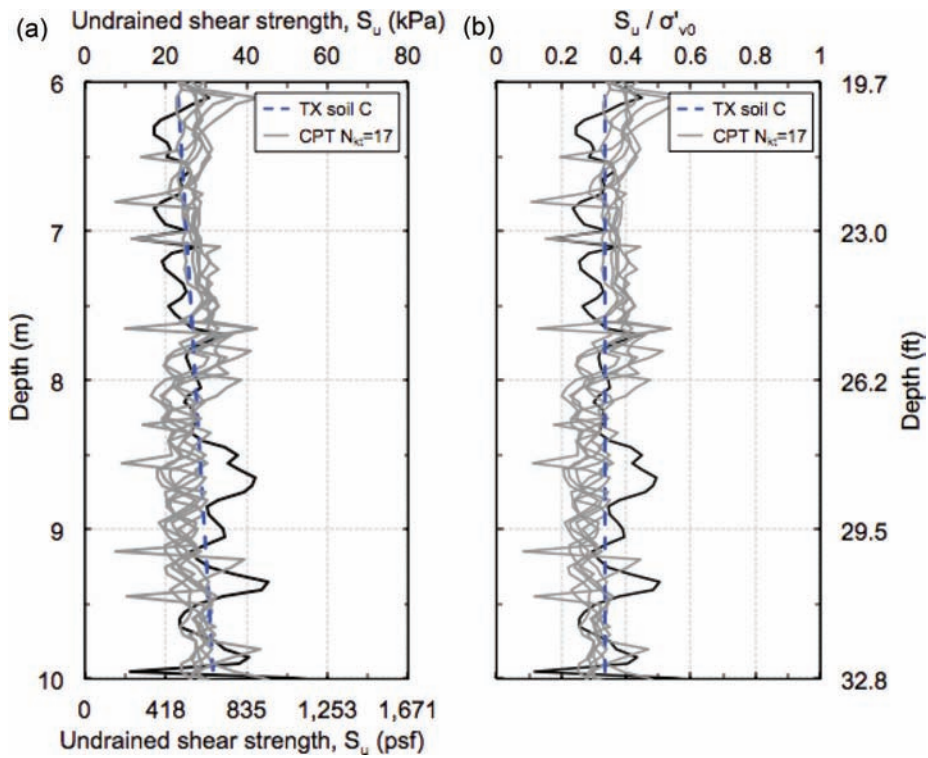


Figure A.5.8 (a) Undrained shear strength and (b) normalized undrained shear strength as obtained from CPT (using $N_{kt} = 17$) and laboratory SHANSEP CK₀UTC(L) tests for soil C.

The undrained shear strength profiles and the normalized undrained shear strength profiles as obtained from CPT (using $N_{kt} = 10$) and laboratory SHANSEP CK₀UTC(L) tests for

soil M are shown in Figure A.5.7(a) and Figure A.5.7(b), respectively. Figure A.5.8 shows the profiles as obtained from CPT (using $N_{kt} = 17$) and laboratory SHANSEP CK₀UTC(L) tests for soil C.

APPENDIX 6: SUMMARY OF BORING LOGS

This appendix summarizes the boring logs for the six boreholes (MR#1, MR#2, MR#3, MR#4, HAS#1, and FV#1) that were drilled as part of the field program.

				LOG OF TEST BORING Boring No. : MR#1 Location: Madison, Daviess, IN Date: Monday 10/31/2011			Latitude: 38.898745 Longitude: -86.990570 Elevation: 150.84m (494.88ft) Sheet 1 of 3		
SAMPLE				DEPTH	DESCRIPTION/CLASSIFICATION	SOIL PROPERTIES			
No.	Rec.		SPT			Pen.	HCl reaction	Observations	
	(in)	(%)		(m)	(ft)				
SS1	13	54	2-4-6-7	0	0	Silty Sand , yellow, moist, loose			
SS2	8	33	5-4-3-5	0.6	2				
SS3	12	50	2-1-3-2	1.2	4				
				1.8	6	1.7m (5.5ft)			
				2.4	8	Clayey Silt , brown, moist, medium stiff			Could not retrieve because the centerbid was not used
				3	10				
SS4	18	75	2-3-4-5				1.5		
SS5	24	100	2-2-2-3			3.5m (11.5ft)	0.5		
				3.7	12		2		
SS6	16	67	1-2-2-2			Clay , blue, moist, very soft	1.5		
				4.3	14				
SS7	23	96	WOH- WOH- 1-1			4.9m (16ft)	0.25		
				4.9	16				
(ST1)						↓ Shelby tubes with fixed piston (drilling using mud rotary $\phi = 82.55\text{mm} = 3.25\text{in}$	0.5	None	
				5.5	18				
(ST2)						Blue, soft		Medium	
				6.1	20				

GENERAL OBSERVATIONS: SS = split spoon
 ST = shelly tube
 WOH = weight of hammer

SCHOOL OF CIVIL ENGINEERING PURDUE UNIVERSITY.				LOG OF TEST BORING		Latitude: 38.898745 Longitude: -86.990570 Elevation: 150.84m (494.88ft) Sheet 2 of 3		
				Boring No. : MR#1 Location: Madison, Daviess, IN Date: Tuesday 11/01/2011				
SAMPLE				DESCRIPTION/CLASSIFICATION	SOIL PROPERTIES			
No.	Rec. (in) (%)		SPT		Depth (m) (ft)	Pen.	HCl reaction	Observations
ST3				6.1	20		Low	Lost 4 in from bottom
				6.7	22	Drilling to deeper depth by mistake		
				7.3	24			
ST4				7.9	26	0.75	Medium	
ST5				8.5	28	1	Medium	
ST6				9.1	30	0.25	Medium	
ST7				9.8	32	1	Low	
ST8				10.4	34	1.25	Low	Stiff soil
SS8				11.0	36	0.75	Split spoons (top, middle, bottom in ziplock). Driller thinks it's hard to push ST	
ST9				11.6	38	0.75		
SS9	24	100	2-9-13-15	11.7	38.5	0.75		
				12.2	40			
GENERAL OBSERVATIONS:				SS = split spoon ST = shelby tube				

SCHOOL OF CIVIL ENGINEERING PURDUE UNIVERSITY.				LOG OF TEST BORING		Latitude: 38.898745 Longitude: -86.990570 Elevation: 150.84m (494.88ft) Sheet 3 of 3			
				Boring No. : MR#1 Location: Madison, Daviess, IN Date: Tuesday 11/01/2011					
SAMPLE					DESCRIPTION/CLASSIFICATION	SOIL PROPERTIES			
No.	Rec. (in) (%)		SPT	Depth (m) (ft)		Pen.	HCl reaction	Observations	
SS10	20	83	3-9-9-8	12.2	40	Sand, brown, loose	1		<i>Note that penecrometer is not applicable for sand (it was found for illustration purpose only)</i>
SS11	19	79	3-4-4-5	12.8	42		0.25		
SS12	22	92	1-2-2-1	13.4	44		0		
SS13	15	63	2-6-7-9	14.0	46		0		
SS14	14	58	3-2-2-2	14.6	48		0		
				15.2	50	14.9m (49ft)	0.75	V. Low	
						Silty sand			

GENERAL OBSERVATIONS: SS = split spoon
ST = shelby tube

				LOG OF TEST BORING		Latitude: 38.898745 Longitude: -86.990615 Elevation: 150.84m (494.88ft) Sheet 1 of 3		
				Boring No. : MR#2 Location: Madison, Daviess, IN Date: Tuesday 11/01/2011				
SAMPLE				DESCRIPTION/CLASSIFICATION		SOIL PROPERTIES		
No.	Rec.		SPT	Depth		Pen.	HCI reaction	Observations
	(in)	(%)		(m)	(ft)			
SS1	9	38	2-6-7-8	0	0	1.5		
				0.6	2			
SS2	8	33	2-6-7-8	1.2	4	0.75		
				1.2	4	1.2m (4ft)		
SS3	22	92	2-2-2-3	1.8	6	0.75		
SS4	22	92	1-1-3-3	2.4	8	0.75		Some gravel
				2.4	8	1.25		
SS5	20	83	1-3-3-4	3	10	1.5		Very hard to cut
				3	10	2		
SS6	18	75	1-2-2-4	3.7	12	1		
				3.7	12	3.5m (11.5ft)		
SS7	16	67	1-2-2-3	4.3	14	1.5		
				4.3	14	0.75		
SS8	22	92	WOH- WOH- WOH- WOH	4.9	16	0.25		
				4.9	16	4.9m (16ft)		
ST1				5.5	18			Not good! almost empty! only 4in recovered
				5.5	18			
ST2				6.1	20	0.5	Low	
				6.1	20			

GENERAL OBSERVATIONS: SS = split spoon
 ST = shelly tube
 WOH = weight of hammer

SCHOOL OF CIVIL ENGINEERING PURDUE UNIVERSITY.				LOG OF TEST BORING		Latitude: 38.898745 Longitude: -86.990615 Elevation: 150.84m (494.88ft) Sheet 2 of 3		
				Boring No. : MR#2 Location: Madison, Daviess, IN Date: Wednesday 11/02/2011				
SAMPLE				DESCRIPTION/CLASSIFICATION	SOIL PROPERTIES			
No.	Rec. (in) (%)		SPT		Depth (m) (ft)	Pen.	HCl reaction	Observations
ST3				6.1	20	0.25	Medium	
ST4				6.7	22	0.75	Medium	
ST5				7.3	24	0.25	Medium	Lost 4 in from bottom
ST6				7.9	26	0.75	Strong	Lost 4 in from bottom
ST7				8.5	28	0.5	Medium	
ST8				9.1	30	0.5	Medium	
ST9				9.8	32	0.5	Medium	Stiff soil
ST10				10.4	34	0.5	Medium	Stiff soil
X				11.0	36	Forgot the piston below the tube edge		
ST11				11.6	38	0		
				12.2	40	11.9m (39ft) Sand, brown, loose		

GENERAL OBSERVATIONS: ST = shelly tube

LOG OF TEST BORING

Boring No. : MR#2
 Location: Madison, Daviess, IN
 Date: Wednesday 11/02/2011

Latitude: 38.898745
 Longitude: -86.990615
 Elevation: 150.84m (494.88ft)
 Sheet 3 of 3

SAMPLE				DESCRIPTION/CLASSIFICATION	SOIL PROPERTIES		
No.	Rec.		SPT		Pen.	HCl reaction	Observations
	(in)	(%)		Depth (m)	(ft)		
SS9	14	58	2-2-2-3	12.2	40	0	Note that penetrometer is not applicable for sand (it was found for illustration purpose only)
SS10	21	88	4-3-2-2	12.8	42	0	
SS11	15	63	2-3-2-3	13.4	44	0	
SS12	18	75	2-6-12-16	14.0	46	0.25	Some gravel
SS13	15	63	5-5-3-2	14.6	48	0	Some gravel
				15.1m (49.5ft)		0.25	
							Silty sand
				15.2	50		

GENERAL OBSERVATIONS: SS = split spoon
 ST = shelly tube

SCHOOL OF CIVIL ENGINEERING PURDUE UNIVERSITY.				LOG OF TEST BORING		Latitude: 38.898770 Longitude: -86.990570 Elevation: 150.84m (494.88ft) Sheet 1 of 2			
Boring No. : FV#1 (+piezometer) Location: Madison, Daviess, IN Date: Wednesday 11/02/2011									
SAMPLE				DESCRIPTION/CLASSIFICATION	SOIL PROPERTIES				
No.	Rec. (in)	(%)	SPT		Depth (m)	(ft)	Pen.	HCl reaction	Observations
SS1	18	75	2-2-5-5	0	0	Silty Sand, yellow, moist, loose	2.75		
SS2	13	54	3-5-6-7	0.6	2		2.5		
SS3	18	75	1-3-3-3	1.2	4	1.5m (5ft)	1.5		
SS4	23	96	WOH-2-4-4	1.8	6	Clayey Silt, brown & yellow, moist, medium stiff to stiff	0.75		
SS5			1-2-3-4	2.4	8		0.25		
SS6			1-2-2-2	3	10	Clay, blue & yellow, moist, very soft	1.25		
SS7	20	83	1-1-2-2	3.7	12		1.5		
				4.3	14	3m (10ft)	1		
				4.9	16	4.3m (14ft)	1.25		
				5.5	18	↓ Vane shear test (drilling using hollow stem auger $\phi = 107.95\text{mm} = 4.25\text{in}$) → undisturbed test → remolded test → collection of disturbed soil using SS → installed piezometer when done			Very soft
				6.1	20				

GENERAL OBSERVATIONS: SS = split spoon
 FV = field vane shear test
 WOH = weight of hammer

SCHOOL OF CIVIL ENGINEERING PURDUE UNIVERSITY.				LOG OF TEST BORING		Latitude: 38.898770 Longitude: -86.990570 Elevation: 150.84m (494.88ft) Sheet 2 of 2	
Boring No. : FV#1 (+piezometer) Location: Madison, Daviess, IN Date: Friday 11/04/2011							
SAMPLE				DESCRIPTION/CLASSIFICATION	OPEN PIPE PIEZOMETER		
No.	Rec. (in) (%)	SPT	Depth (m) (ft)				
FV3			6.1 - 20				
FV4			6.7 - 22				
FV5	V. low remolded strength (~1 div) High sensitivity		7.3 - 24				
FV6			7.9 - 26	8.2m (27ft)			
FV7			8.5 - 28	8.8m (29ft)			
FV8			9.1 - 30	9.1m (30ft)			
FV9	Disturbed but good! Tested only top 6in. then push 1.5ft & test		9.8 - 32				
FV10			10.4 - 34	10.7m (35ft)			
FV11			11.0 - 36				
			11.6 - 38	11.6m (38ft)			
			12.2 - 40				
GENERAL OBSERVATIONS:				FV = field vane shear test			
				Piezometer was installed on Monday 11/07/2011			

SCHOOL OF CIVIL ENGINEERING PURDUE UNIVERSITY.				LOG OF TEST BORING		Latitude: 38.898795 Longitude: -86.990570 Elevation: 150.84m (494.88ft) Sheet 1 of 2		
				Boring No. : HSA#1 Location: Madison, Daviess, IN Date: Monday 11/07/2011				
SAMPLE				DESCRIPTION/CLASSIFICATION	SOIL PROPERTIES			
No.	Rec. (in) (%)	SPT	Depth (m) (ft)		Pen.	HCl reaction	Observations	
SS1	12	50	2-4-4-5	0	Silty Sand , yellow, moist, loose	2.5		
SS2	10	42	4-3-3-3	0.6		2.5		bottom 6in: more silt compared with previous borings
SS3	18	75	2-3-3-4	1.2		2.5		more silt compared with previous borings
				1.8	1.7m (5.5ft)	1.5		more silt compared with previous borings
SS4	19	79	2-3-3-5	2.4	Clayey Silt , brown to blue, moist, medium stiff to stiff	2		
SS5	20	83	2-2-3-3	3		1.75		some roots
SS6	24	100	2-3-4-4	3.7		1		some roots very hard to cut
				4.3	3.7m (12ft)	1.75		
SS7	18	75	1-1-2-2	4.9	Clay , blue, moist, very soft	1		
SS8	24	100	WOH- WOH- WOH- WOH-	4.9		0.25	None	
				4.9	4.9m (16ft)	0.25	None	
(ST1)				5.5	Shelby tubes with fixed piston (drilling using hollow stem auger $\phi = 82.55\text{mm} = 3.25\text{in}$)	0.25	None	Missing 3in from top
(ST2)				6.1		0.5	Medium	Good

GENERAL OBSERVATIONS: SS = split spoon
ST = shelly tube
WOH = weight of hammer

SCHOOL OF CIVIL ENGINEERING PURDUE UNIVERSITY.				LOG OF TEST BORING		Latitude: 38.898795 Longitude: -86.990570 Elevation: 150.84m (494.88ft) Sheet 2 of 2			
				Boring No. : HSA#1 Location: Madison, Daviess, IN Date: Tuesday 11/08/2011					
SAMPLE					DESCRIPTION/CLASSIFICATION	SOIL PROPERTIES			
No.	Rec. (in) (%)		SPT	Depth (m) (ft)		Pen.	HCl reaction	Observations	
ST3				6.1	20		0.5	Strong	Not good! Lost 6in top coz piston stuck (using wrong spring)
ST4				6.7	22		0.5	Strong	Good
ST5				7.3	24		0.5	Strong	Missing 2in from bottom
X				7.9	26		Fixed piston stucked because he used the wrong spring fot the piston		
ST6				8.5	28		0.5	Medium	Good
ST7				9.1	30		0.5	Medium	Good
ST8				9.8	32		0.75	Medium	Good
ST9				10.4	34		0.75	Low	Good
ST10				11.0	36		0.5	Low	Missing 2in from top (no vacuum)
				11.6	38		11.6m (38ft)		
				12.2	40				

GENERAL OBSERVATIONS: ST = shelby tube

SCHOOL OF CIVIL ENGINEERING PURDUE UNIVERSITY.				LOG OF TEST BORING		Latitude: 38.898770 Longitude: -86.990610 Elevation: 150.84m (494.88ft) Sheet 1 of 2		
				Boring No. : MR#3 Location: Madison, Daviess, IN Date: Thursday 11/10/2011				
SAMPLE				DESCRIPTION/CLASSIFICATION	SOIL PROPERTIES			
No.	Rec. (in) (%)		SPT		Depth (m) (ft)	Pen.	HCl reaction	Observations
				0	0			
				0.6	2			
				1.2	4			
				1.8	6			
				2.4	8			
				3	10			
				3.7	12			
				4.3	14			
				4.3m (14ft)				
ST1	Not machined		U U	4.9	16	0.5	Low	Not good! half empty!
ST2	Very soft			5.5	18	0	None	Not good! almost empty! only 4in recovered
ST3				6.1	20	0.5	Medium	Not good! Missing 9in top & 4in bottom
GENERAL OBSERVATIONS:				ST = shelby tube		Machined ST (ICR = 0) U U		
						Not machined ST (ICR > 0) U U		

LOG OF TEST BORING

Boring No. : MR#3
 Location: Madison, Daviess, IN
 Date: Thursday 11/10/2011

Latitude: 38.898770
 Longitude: -86.990610
 Elevation: 150.84m (494.88ft)
 Sheet 2 of 2

SAMPLE				DESCRIPTION/CLASSIFICATION	SOIL PROPERTIES			
No.	Rec. (in) (%)		SPT		Depth (m) (ft)	Pen.	HCl reaction	Observations
ST4				6.1	20	0.25	Medium	Good
ST5				6.7	22	0.25	Strong	Good
X				7.3	24	<i>Drilling to deeper depth by mistake</i>		
ST6				7.9	26	0.75	Strong	Good
ST7				8.5	28	0.25	Medium	Good
ST8				9.1	30	0.25	Medium	Good
ST9				9.8	32	0.5	Medium	Missing 2in from top
ST10				10.4	34	0.25	Medium	missing 4in from top
ST11				11.0	36	0.5	None	Good
				11.6	38	<i>Sand at bottom of ST 11.6m (38ft)</i>		
				12.2	40			

GENERAL OBSERVATIONS: ST = shelly tube

SCHOOL OF CIVIL ENGINEERING PURDUE UNIVERSITY.				LOG OF TEST BORING		Latitude: 38.898785 Longitude: -86.990600 Elevation: 150.84m (494.88ft) Sheet 1 of 3		
				Boring No. : MR#4 Location: Madison, Daviess, IN Date: Thursday 11/10/2011				
SAMPLE				DESCRIPTION/CLASSIFICATION	SOIL PROPERTIES			
No.	Rec. (in) (%)		SPT		Depth (m) (ft)	Pen.	HCl reaction	Observations
				0	0			
				0.6	2			
				1.2	4			
				1.8	6			
				2.4	8			
				3	10			
				3.7	12			
				4.3	14			
				4.9	16			
(ST1)	Very soft			4.9	16			
				5.5	18			
(ST2)				6.1	20			
				4.9m (16ft)				
				↓ Shelby tubes with fixed piston (drilling using mud rotary $\phi = 82.55\text{mm} = 3.25\text{in}$)		0	None	Not good! Empty ST (with vacuum & waited 15 min)
						0.25		missing 1in from top & 1in from bottom (with vacuum)
GENERAL OBSERVATIONS: ST = shelly tube								

				LOG OF TEST BORING		Latitude: 38.898785 Longitude: -86.990600 Elevation: 150.84m (494.88ft) Sheet 2 of 3		
SAMPLE				DESCRIPTION/CLASSIFICATION		SOIL PROPERTIES		
No.	Rec.		SPT	Depth		Pen.	HCI reaction	Observations
	(in)	(%)		(m)	(ft)			
ST3				6.1	20	0.25	Medium	Good
ST4				6.7	22	0.5	Medium	Good
ST5				7.3	24	0.75	Strong	Good (not too much vacuum)
ST6				7.9	26	0.75	Medium	missing 2.5in bottom (no vacuum)
ST7	Fixed piston was not used			8.5	28	Nothing was recovered. Use not machined ST with fixed piston again to recover the disturbed soil		
ST8	Not machined ∩∩			9.1	30		Strong	Highly disturbed! Do not use for eng. Properties. Only for classification (missing 4in top & 4 in bottom)
ST9				9.8	32	0.75	Medium	Good
ST10				10.4	34	0.5	Low	missing 3in top
ST11				11.0	36		None (bottom of ST)	Good
ST12				11.6	38	1		11.6m (38ft)
				12.2	40	0.5	None	Sand at top & bottom of ST

GENERAL OBSERVATIONS: ST = shelby tube
ICR = inside clearance ratio

Machined ST (ICR = 0) ∩∩
Not machined ST (ICR > 0) ∩∩

SCHOOL OF CIVIL ENGINEERING PURDUE UNIVERSITY.				LOG OF TEST BORING		Latitude: 38.898785 Longitude: -86.990600 Elevation: 150.84m (494.88ft) Sheet 3 of 3			
				Boring No. : MR#4 Location: Madison, Daviess, IN Date: Friday 11/11/2011					
SAMPLE					DESCRIPTION/CLASSIFICATION	SOIL PROPERTIES			
No.	Rec. (in) (%)		SPT	Depth (m) (ft)		Pen.	HCl reaction	Observations	
SS1	17	71	1-1-2-2	12.2	40	<i>Sand, brown, wet, loose</i>			
SS2	17	71	4-5-3-2	12.8	42				
SS3	20	83	2-3-4-5	13.4	44				
SS4	16	67	8-11-14-16	14.0	46				
SS5	16	67	5-9-3-7	14.6	48				
				15.2	50	15.1m (49.5ft) <i>Silty sand</i>	None	Some gravel	
GENERAL OBSERVATIONS: SS = split spoon ST = shelby tube									

APPENDIX 7: PIEZOCONE PENETRATION PROFILES

This appendix summarizes the Piezocone penetration profiles for the seven Piezocone penetration tests (CPT#1, CPT#2, CPT#3A, CPT#4, CPT#5, CPT#6, and CPT#7) that were conducted as part of the field program.

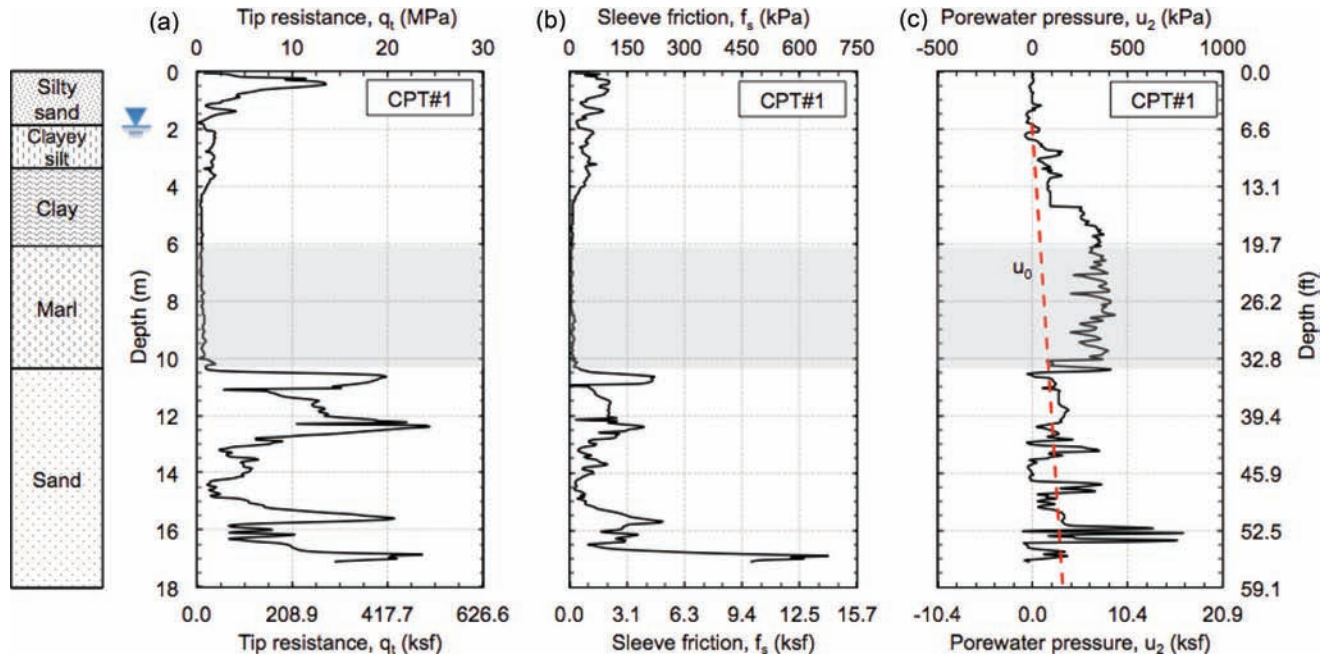


Figure A.7.1 CPT#1 results: (a) tip resistance, (b) skin friction, and (c) porewater pressure versus depth.

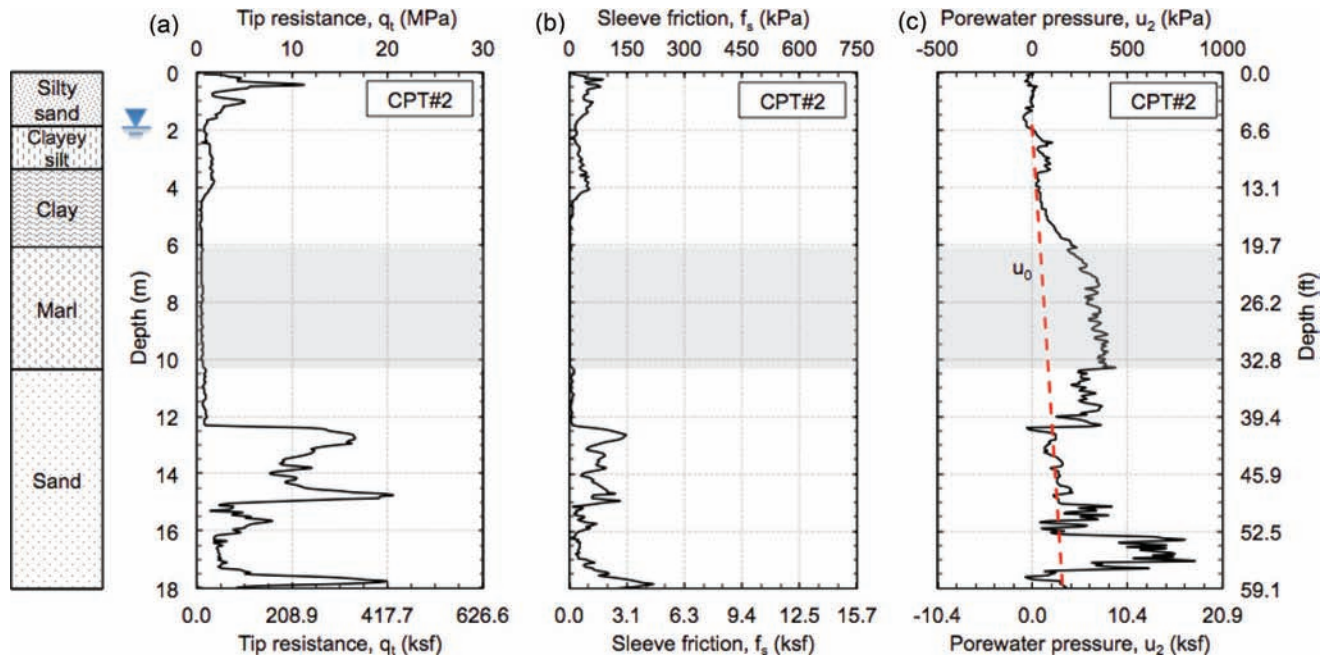


Figure A.7.2 CPT#2 results: (a) tip resistance, (b) skin friction, and (c) porewater pressure versus depth.

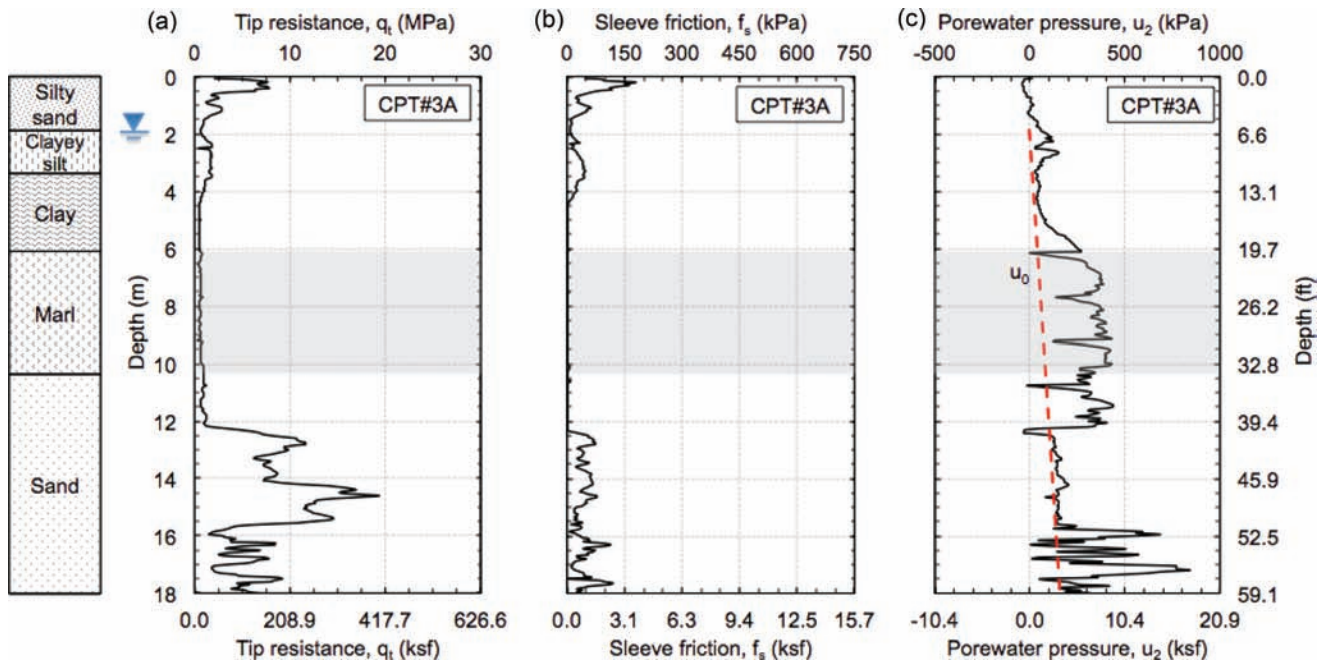


Figure A.7.3 CPT#3A results: (a) tip resistance, (b) skin friction, and (c) porewater pressure versus depth.

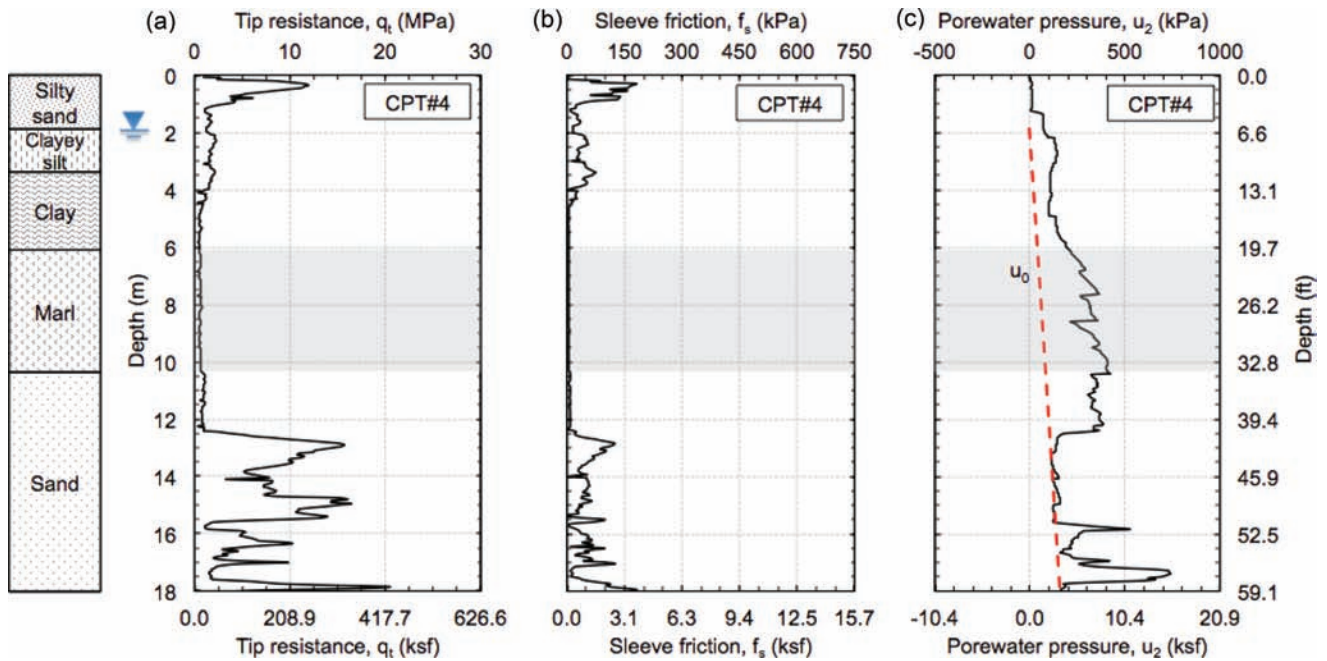


Figure A.7.4 CPT#4 results: (a) tip resistance, (b) skin friction, and (c) porewater pressure versus depth.

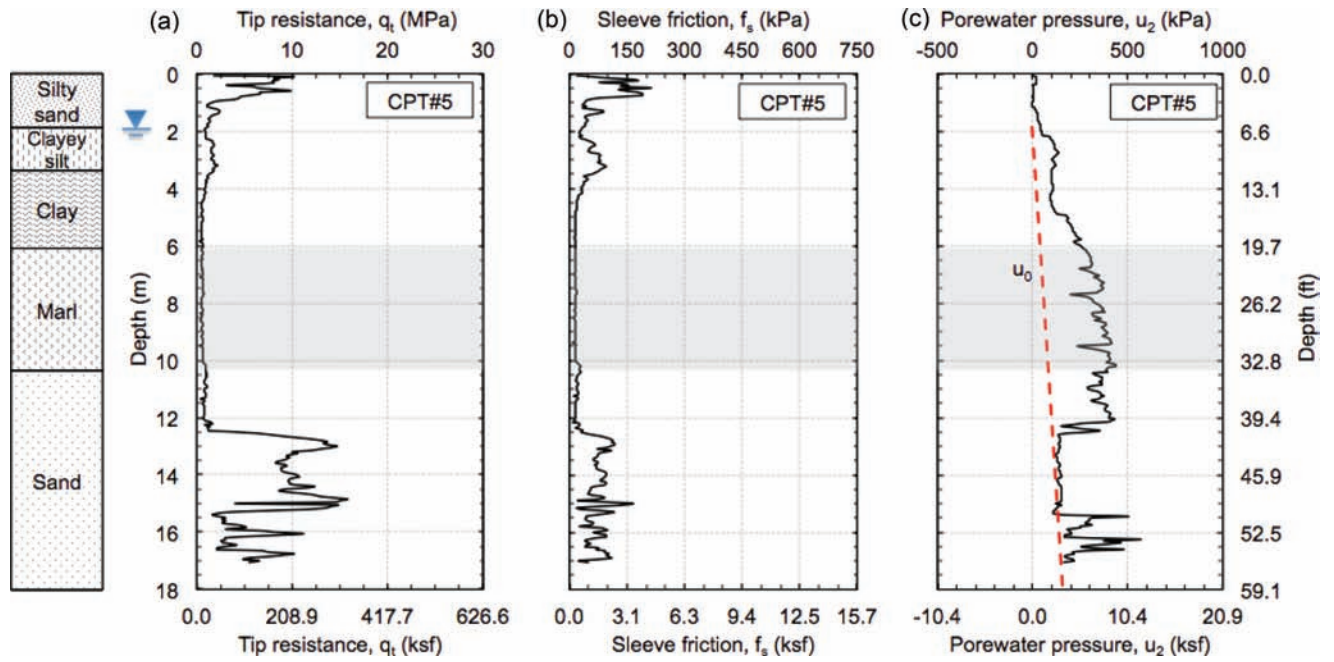


Figure A.7.5 CPT#5 results: (a) tip resistance, (b) skin friction, and (c) porewater pressure versus depth.

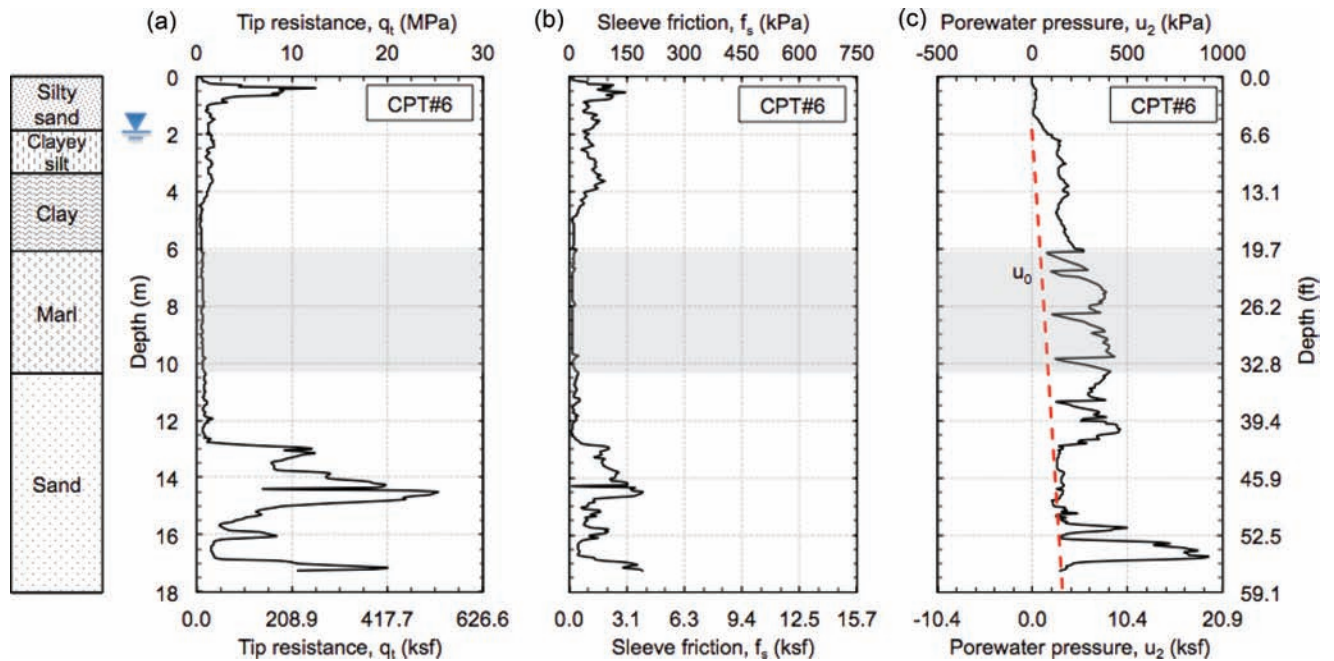


Figure A.7.6 CPT#6 results: (a) tip resistance, (b) skin friction, and (c) porewater pressure versus depth.

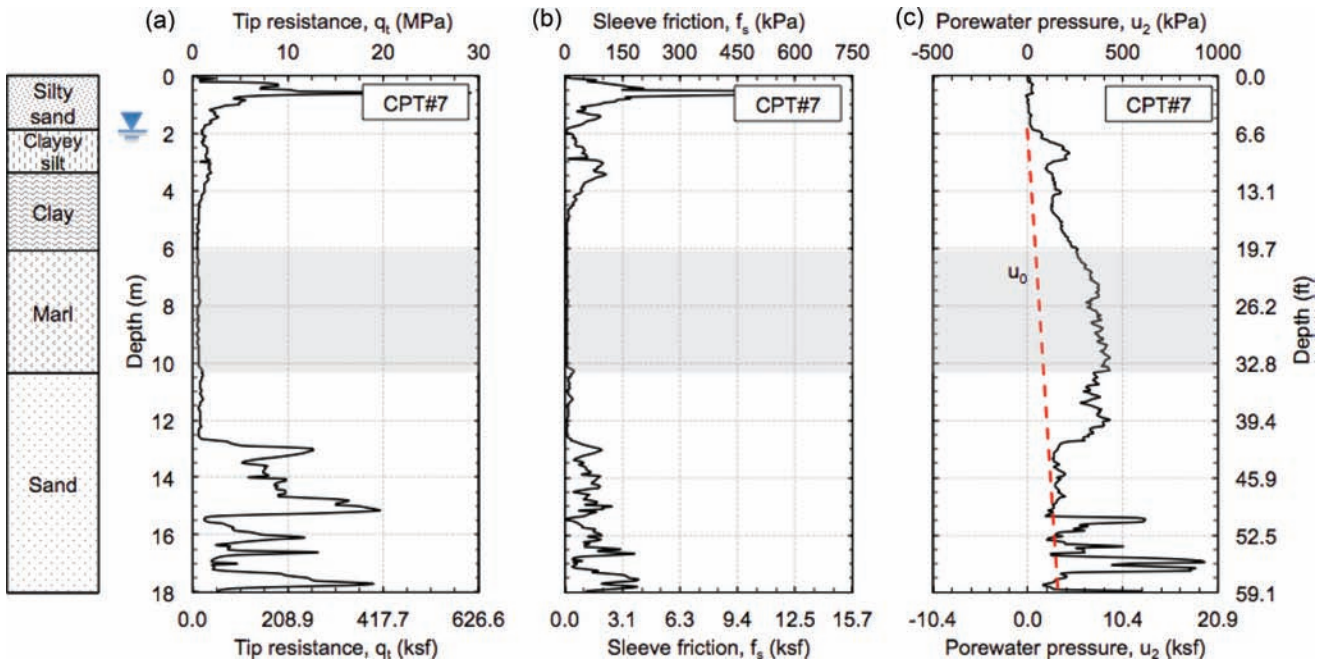


Figure A.7.7 CPT#7 results: (a) tip resistance, (b) skin friction, and (c) porewater pressure versus depth.

APPENDIX 8: FIELD VANE SHEAR TESTS

This appendix summarizes the results of the eleven field vane shear tests conducted at various depths as part of the field program.

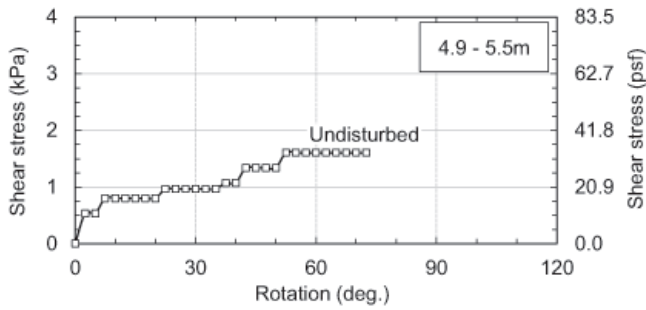


Figure A.8.1 Results of field vane shear test (FV1) conducted at ~5.3 m (17.5 ft).

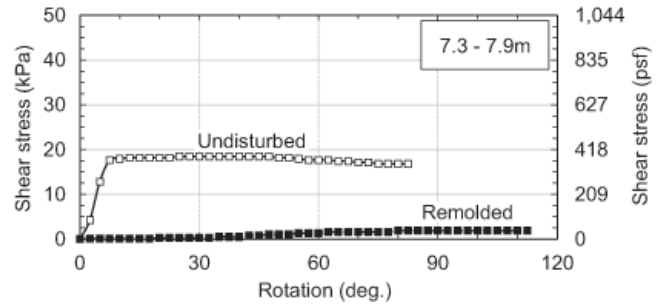


Figure A.8.5 Results of field vane shear test (FV5) conducted at ~7.8 m (25.5 ft).

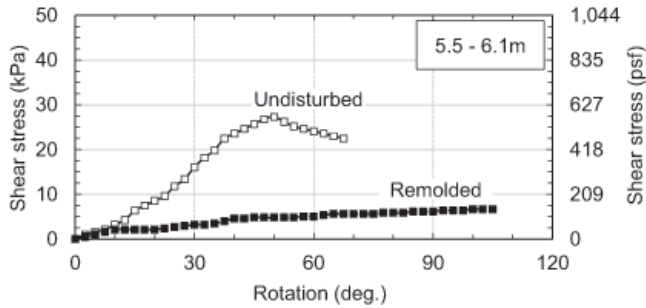


Figure A.8.2 Results of field vane shear test (FV2) conducted at ~5.9 m (19.5 ft).

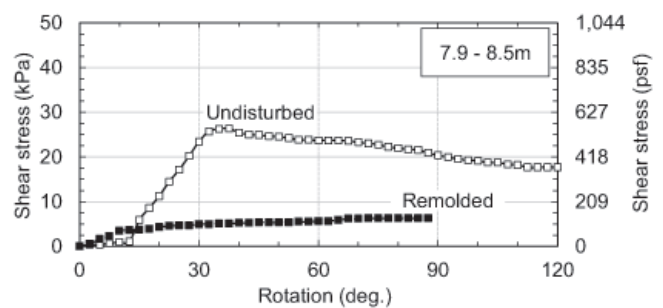


Figure A.8.6 Results of field vane shear test (FV6) conducted at ~8.4 m (27.5 ft).

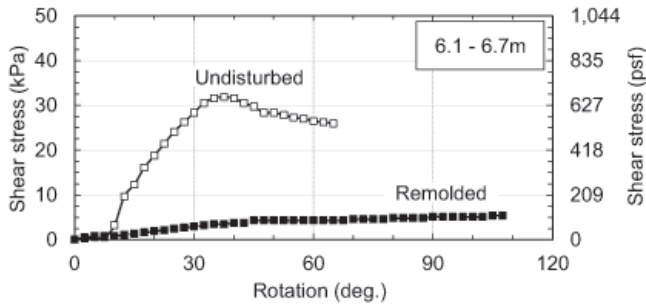


Figure A.8.3 Results of field vane shear test (FV3) conducted at ~6.7 m (22.0 ft).

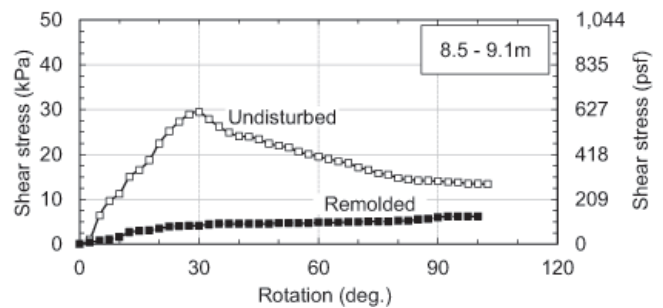


Figure A.8.7 Results of field vane shear test (FV7) conducted at ~9.0 m (29.5 ft).

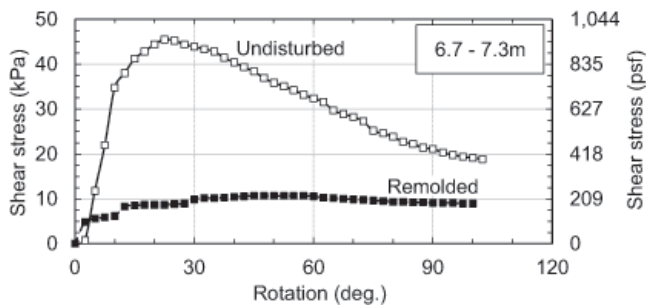


Figure A.8.4 Results of field vane shear test (FV4) conducted at ~7.0 m (22.8 ft).

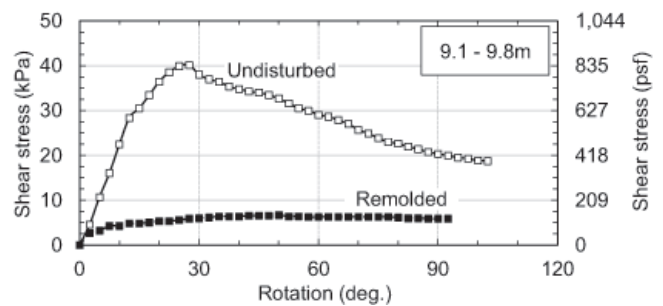


Figure A.8.8 Results of field vane shear test (FV8) conducted at ~9.5 m (31.2 ft).

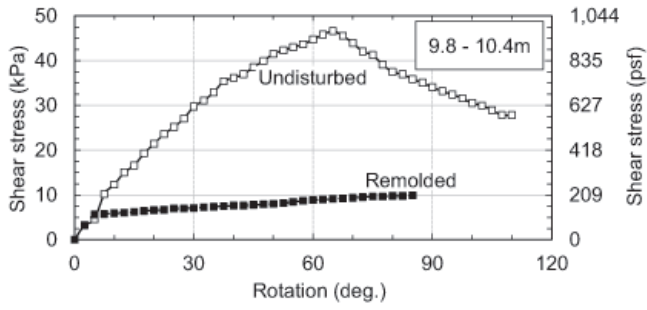


Figure A.8.9 Results of field vane shear test (FV9) conducted at ~10.2 m (33.5 ft).

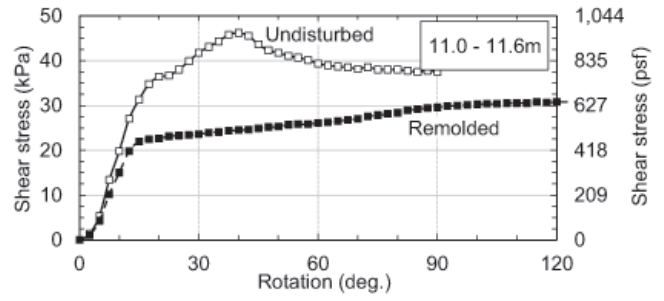


Figure A.8.11 Results of field vane shear test (FV11) conducted at 11.4 m (37.5 ft).

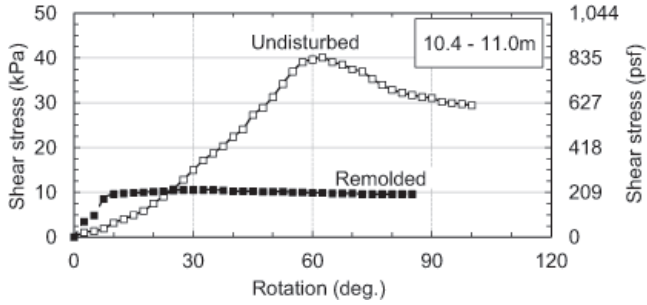


Figure A.8.10 Results of field vane shear test (FV10) conducted at 10.8 m (35.5 ft).

About the Joint Transportation Research Program (JTRP)

On March 11, 1937, the Indiana Legislature passed an act which authorized the Indiana State Highway Commission to cooperate with and assist Purdue University in developing the best methods of improving and maintaining the highways of the state and the respective counties thereof. That collaborative effort was called the Joint Highway Research Project (JHRP). In 1997 the collaborative venture was renamed as the Joint Transportation Research Program (JTRP) to reflect the state and national efforts to integrate the management and operation of various transportation modes.

The first studies of JHRP were concerned with Test Road No. 1—evaluation of the weathering characteristics of stabilized materials. After World War II, the JHRP program grew substantially and was regularly producing technical reports. Over 1,500 technical reports are now available, published as part of the JHRP and subsequently JTRP collaborative venture between Purdue University and what is now the Indiana Department of Transportation.

Free online access to all reports is provided through a unique collaboration between JTRP and Purdue Libraries. These are available at: <http://docs.lib.purdue.edu/jtrp>

Further information about JTRP and its current research program is available at: <http://www.purdue.edu/jtrp>

About This Report

An open access version of this publication is available online. This can be most easily located using the Digital Object Identifier (doi) listed below. Pre-2011 publications that include color illustrations are available online in color but are printed only in grayscale.

The recommended citation for this publication is:

El Howayek, A., Santagata, M., Bobet, A., & Siddiki, N. Z. (2015). *Engineering properties of marls* (Joint Transportation Research Program Publication No. FHWA/IN/JTRP-2015/11). West Lafayette, IN: Purdue University. <http://dx.doi.org/10.5703/1288284315533>